160 years of oceanic variability of the greater Caribbean reconstructed from two coral cores

Dissertation for the Doctoral Degree in Natural Sciences

Dr. rer. nat.

Within the faculty of Geosciences
At the University of Bremen

Submitted by
Marie Harbott

Table of Contents

Abbreviation	Term
AMO	Atlantic Multidecadal Oscillation
AMOC	Atlantic Meridional Overturning Circulation
AWP	Atlantic Warm Pool
B/Ca	Boron to Calcium ratio
Ca	Calcium
CC	Caribbean Current
CF	calcifying fluid
CO2	Carbon dioxide
DIC	Dissolved Inorganic Carbon
ECM	Extracellular Medium
ENSO	El Niño Southern Oscillation
GOM	Gulf of Mexico
ICP-MS	Inductively Coupled Plasma-Mass Spectrometer
IPCC	Intergovernmental Panel on Climate Change
LA-MC-ICP-MS	Laser Ablation- Multicollector-ICPMS
LC	Loop Current
NAO	North Atlantic Oscillation
NOAA	National Oceanic and Atmospheric Administration
SLP	Sea Level Pressure
SODA	Simple Ocean Data Assimilation
Sr	Strontium
Sr/Ca	Ratio of Strontium to Calcium
SSS	Sea Surface Salinity
SST	Sea Surface Temperature
SW	Seawater
TA	Total Alkalinity
VPDB	Vienna-Pee Bee Belemnite
WOA	World Ocean Atlas
yr	year(s)
$\delta 11B$	stable boron isotope ratio composition
$\delta 18O$	stable oxygen isotope ratio composition
$\delta 18OSW$	stable oxygen isotope ratio composition of seawater
Ω	Aragonite saturation state

Units	Measurement
°C	degree Celsius
‰	per mill
μm	micrometer
cm	centimeter
km	kilometer
m	meter
ppb	parts per billion
ppm	parts per million
psu	practical salinity unit
mmol	millimole
kg	kilogram

List of Figures

Introduction

Manuscript I

Manuscript II

Manuscript III

List of Tables

Manuscript I

Manuscript II

Abstract

Instrumental in-situ observations of climate and environmental parameter changes are sparse and only date back until the mid 20th century for the most part. Multidecadal variability cannot be well reflected in a short record like this. To truly separate the anthropogenic impact from natural variability in the climate system, longer time series, giving us a basis to go off of, are needed. Only then can we evaluate the impact of ongoing environmental changes in the ocean on marine organisms.

Climate sensitive proxies have been largely used on land and in the ocean to extend the environmental record beyond the instrumental one. One organism group that incorporates the environmental information of the ocean into its skeleton are massive tropical corals. Their extension rate of a few millimeters to centimeters per year makes it possible to retrieve ultra-high resolution of sub-seasonal records. Trace elements and stable isotope measurements can reveal changes in sea surface temperature (SST), sea surface salinity (SSS), and the carbonate chemistry of the ocean. The latter has so far been largely restricted to the reconstruction of pH from corals. While there are a few studies on the northern Gulf of Mexico (GOM) in the Atlantic, the southern part has been mostly neglected for SST, SSS, and carbonate chemistry reconstructions. For each proxy reconstruction, a species-specific calibration is need, which is however mostly constricted to the *Porites* species that are common in the Pacific, but not frequently used in the Atlantic. Additionally, in-situ measurements for such calibrations are sparse, and coverage is less extensive in this region.

The objective of this thesis is to test whether the coral core taken from the northern Cuban coast is recording environmental changes in its skeletal material reliably and whether reconstructions of carbonate chemistry of seawater parameters can be based on coral skeletal materials. Furthermore, this thesis aims to establish a new species-specific pH- δ^{11}B calibration for the coral *Orbicella annularis*, taken from La Parguera, Puerto Rico, and looks at the impact of secondary diagenesis on pH reconstructions.

For these purposes a multi-proxy record from a *Siderastrea siderea* coral core was generated for the southern GOM. The coral records show seasonal cycles that agree well with gridded SST. Oxygen isotopes, Sr/Ca and Sr-U as SST proxies present an increase in temperature over 160 years, spanning from 1845 to 2005. In the late 1980s, all proxies show a stagnation in the warming trend that can be linked to the decreasing strength of the Loop Current (LC), passing

Abstract

though the GOM. This trend is confirmed by coral cores in the northern GOM, that show a potential slow-down of the LC. Reconstructing $\delta^{18}O$ of seawater ($\delta^{18}O_{SW}$) makes it possible to gain insights into the hydroclimatology of the southern GOM. Although seasonal variabilities are not picked up by the $\delta^{18}O_{SW}$ signal, long terms trends such as the Atlantic Multidecadal Oscillation (AMO) pattern and the teleconnection between the Atlantic and Pacific are reflected in the data. Several El Niño years can be identified in the $\delta^{18}O_{SW}$ record as years of very low salinity. A shift to lower salinity values as a long-term trend in the 1980s indicates a shift in the AMO phase, from a negative to a positive one.

As the coral is recording changes in SST and SSS, it is also presenting variability in pH and other carbonate chemistry parameters. The coral recovered from Cuba shows a clear decline in pH in its extracellular calcification center (ECM) and the values reconstructed for seawater (SW). While total alkalinity (TA) is constant in SW, dissolved inorganic carbon (DIC) are increasing over time, which marks the carbonate chemistry of ocean acidification (OA). Simultaneously, in the ECM TA and DIC are decreasing. Although, the *S. siderea* coral is known to have a high temperature and low pH threshold the carbonate chemistry of the ECM indicates an already suffering coral, by showing a declining aragonite saturation state, and decreasing DIC and TA in its ECM.

Ongoing OA makes corals vulnerable to macro- and microboring organisms, thereby changing the geochemical signal extracted from the coral skeletal material to reconstruct environmental changes. An ultra-high resolution record was generated for the Caribbean coral *Orbicella annularis* with Laser Ablation Inductively Coupled Plasma Mass Spectrometry (LA-ICP-MS), from Puerto Rico, to compare to high resolution in-situ measurements from a buoy nearby between 2014 and 2020. The record shows seasonal cycles in pH with a significant change to higher pH values after 2015. Secondary aragonite in boreholes from different organisms of the coral's microbiome might be responsible for a shift to higher pH values. Fungi, cyanobacteria, and green algae infested the coral and have bored through the skeletal material. Secondary aragonite was able to precipitate in the empty boreholes and the LA method picked up the changes in the signal. The pristine material prior to 2015 yielded a species-specific pH-$\delta^{11}B$ calibration.

In summary, different coral records presented in this thesis capture climate variabilities in the wider Caribbean and are a valuable tool for extending the instrumental record further to the past.

Zusammenfassung

Zusammenfassung

Instrumentelle Aufzeichnungen des Klimawandels und schwankende Umweltparameter sind spärlich und reichen größtenteils nur bis zur Mitte des 20. Jahrhunderts zurück. Natürliche Schwankungen über mehrere Jahrzehnte können in einem so kurzen Zeitraum nicht gut wiedergegeben werden, um den anthropogenen Einfluss von der natürlichen Variabilität des Klimasystems zu trennen. Längere Zeitreihen sind von Nöten, die uns eine Referenz liefern können. Nur dann können wir die Auswirkungen von Umweltveränderungen im Ozean auf Meeresorganismen beurteilen.

An Land und im Ozean wurden in großem Umfang Klimaanzeiger verwendet, um die Umweltdaten über die instrumentellen Daten hinaus zu erweitern. Ein Organismus, der die Umweltinformationen des Ozeans in sein Skelett integriert hat, sind die massiven tropischen Korallen. Ihre Wachstumsraten von einigen Millimetern bis Zentimetern pro Jahr ermöglicht es, sub-saisonale Aufzeichnungen mit ultrahoher Auflösung zu erhalten. Messungen von Spurenelementen und stabilen Isotopen können Veränderungen der Meeresoberflächentemperatur (SST), des Salzgehalts der Meeresoberfläche (SSS) und der Karbonatchemie des Ozeans aufzeigen. Letzteres war bisher auf die Rekonstruktion des pH-Werts aus Korallen beschränkt. Während es einige wenige Studien über den nördlichen Golf von Mexiko (GOM) im Atlantik gibt, wurde der südliche Teil für die Rekonstruktion von SST, SSS und Karbonatchemie weitgehend vernachlässigt.

Für jede Proxy-Rekonstruktion ist eine artenspezifische Kalibrierung erforderlich, die sich jedoch meist auf die im Pazifik verbreitete, im Atlantik jedoch nicht häufig verwendete *Porites*-Spezies beschränkt. Darüber hinaus gibt es nur wenige In-situ-Messungen für solche Kalibrierungen und die Abdeckung ist in dieser Region weniger umfangreich.

Ziel dieser Arbeit ist es, zu zeigen, dass der an der nordkubanischen Küste entnommene Korallenkern Umweltveränderungen in seinem Skelettmaterial zuverlässig aufzeichnet und dass Rekonstruktionen der Karbonatchemie von Meerwasserparametern auf Korallenskelettmaterial basieren können. Darüber hinaus zielt diese Arbeit darauf ab, eine neue artenspezifische pH-δ^{11}B-Kalibrierung für die Koralle *Orbicella annularis* aus La Parguera, Puerto Rico, zu erstellen und die Auswirkungen der sekundären Diagenese auf pH-Rekonstruktionen zu untersuchen.

Zusammenfassung

Für den südlichen GOM wurde ein Multi-Proxy-Datensatz aus einem Korallenkern der Spezies *Siderastrea siderea* erstellt. Die Korallenaufzeichnungen zeigen saisonale Zyklen, die gut mit den gerasterten SST Daten übereinstimmen. Sauerstoffisotope, Sr/Ca und Sr-U als SST-Proxies weisen einen Temperaturanstieg über 160 Jahre auf, von 1845 bis 2005. In den späten 1980er Jahren zeigen alle Proxies eine Stagnation des Erwärmungstrends, die mit der abnehmenden Stärke der Loop Current (LC), die durch den GOM fließt, in Verbindung gebracht werden kann. Dieser Trend wird durch Korallenbohrkerne im nördlichen GOM bestätigt, die eine mögliche Verlangsamung des LC zeigen. Die Rekonstruktion von $\delta^{18}O_{SW}$ ermöglicht es, Einblicke in die Hydroklimatologie des südlichen GOM zu gewinnen. Obwohl saisonale Schwankungen vom $\delta^{18}O_{SW}$ -Signal nicht erfasst werden, spiegeln sich in den Daten langfristige Trends wie das Muster der Atlantischen Multidekadischen Oszillation (AMO) und die Telekonnektion zwischen dem Atlantik und dem Pazifik wider. Mehrere El-Niño-Jahre lassen sich in der $\delta^{18}O_{SW}$ -Aufzeichnung als Jahre mit sehr niedrigem Salzgehalt identifizieren. Eine Verschiebung zu niedrigeren Salzgehaltswerten als langfristiger Trend in den 1980er Jahren deutet auf eine Verschiebung von einer negativen zu einer positiven AMO-Phase hin.

Die Koralle zeichnet neben SST und SSS Schwankungen auch Veränderungen der Karbonatchemie auf. Die kubanische Koralle zeigt einen deutlichen Rückgang des pH-Wertes in ihrem extrazellulären Kalzifizierungszentrum (ECM) und den für das Meerwasser (SW) rekonstruierten Werten. Während die Gesamtalkalinität (TA) im SW konstant ist, steigt der gelöste anorganische Kohlenstoff (DIC) im Laufe der Zeit an, was die Karbonatchemie der Ozeanversauerung (OA) kennzeichnet. Gleichzeitig nehmen in der ECM TA und DIC ab.

Während der fortschreitenden Versauerung des Ozeans zeigt die Koralle einen Rückgang der Aragonitsättigung in der ECM, aber auch im SW, während ihre lineare Ausdehnungsrate konstant bleibt. Obwohl die Koralle in einer sich verändernden Umwelt lebt, scheint sie noch nicht von OA betroffen zu sein. Ihre Anpassungsmechanismen haben dazu beigetragen, dass diese Art bis zum Jahr 2005, als der Korallenkern entnommen wurde, unter wärmeren Temperaturen und OA gedeihen konnte.

Für die karibische Koralle *Orbicella annularis* wurde eine ultrahochauflösende Aufzeichnung mit der Laserablation (Inductively Coupled Plasma Mass Spectrometry, LA-ICP-MS) aus Puerto Rico erstellt, um sie mit hochauflösenden In-situ-Messungen von einer nahe gelegenen Boje zwischen 2014 und 2020 zu vergleichen. Die Aufzeichnungen zeigen saisonale Zyklen

Zusammenfassung

des pH-Werts mit einer deutlichen Veränderung zu höheren pH-Werten nach 2015. Sekundäres Aragonit in Bohrlöchern von verschiedenen Organismen des Mikrobioms der Korallen könnte für die Verschiebung zu höheren pH-Werten verantwortlich sein. Pilze, Cyanobakterien und Grünalgen haben die Koralle befallen und sich durch das Skelettmaterial gebohrt. In den leeren Bohrlöchern konnte sich sekundäres Aragonit ablagern. Durch die hochauflösende LA-Methode, konnten die Veränderungen im Signal erfasst werden. Das unberührte Material vor 2015 lieferte eine artspezifische pH-δ^{11}B-Kalibrierung.

Zusammenfassend lässt sich sagen, dass die verschiedenen in dieser Arbeit vorgestellten Korallenaufzeichnungen Klimavariabilitäten in der Karibik im weiteren Sinne erfassen und ein wertvolles Instrument sind, um die instrumentelle Aufzeichnung weiter in die Vergangenheit zu verlängern.

Personal Acknowledgement

I would like to thank Prof. Hildegard Westphal for stepping in as my Doctor-mutter, providing me with advise and a female role model in the world of academia.

This endeavor would not have been possible without my other Doctor-parent Henry Wu, who-not only came up with the idea of this project- but provided me with endless advice, reassurance and encouragements to finish this thesis. Thank you, Henry.

I would also like to thank my research committee made up by Tim Rixen, and Henning Kuhnert, who did not only provide advice and guidance during the meetings but helped make sense of the data and helped the manuscripts make sense as well. Thanks also go to the committee members that supported the defense by joining the committee.

The Glomar graduate school and ZMT academy offered me many opportunities for my development as a PhD student and gave me tools to make it to the end of this dissertation.

My research stay at LDEO of Columbia University, NY, was a unique opportunity to get to know the academic world abroad and exchange with experts. Many thanks go to Braddock Linsley for hosting us and answering our coral questions.

Thanks, should also go to Steve Doo, for getting me through tough times and always being ready to give advice and help out. The same goes for my dear friend and college Gary Murphy, who I miss dearly. I wish you could be here and celebrate this moment with me, as I am sure you would. You always listened to me and my concerns, and I am grateful for the advice and friendship you offered.

For always cheering us up in the lab and trying everything possible to make the ICP-MS work for us special thanks go to Jule Mawick and Donata Monien from the Laboratory Team, as well as to our research assistants Sahra Greve, Sharon Dbritto, and Annalise Povolo.

I could not have undertaken this journey without my PhD partner in crime Sara Todorovic. Where would I be without our common struggle finishing up this dissertation? Thank you for always listening, giving me a different perspective and just being my friend! Of course, there were also other PhD candidate accompanying me throughout this journey, that need to be thanked: Claire Siddiqui, for helping me conquer Python and Agustin and Dani, for showing me, how it is done.

Words cannot describe my gratitude to my partner Hugo Tiraby, who never ceased in believing in me and telling me so; who always found encouraging words and supported me in our busy parental life so that I could finish this work.

1 Introduction

In a united effort to quantify the anthropogenic global climate change that has been underway due to enhanced CO_2 emissions and land use changes, a large group of international scientists have worked together since 1988 to create a report on climate change. More than 200 researchers worldwide have participated on the latest, the 6th Climate Assessment report of the Intergovernmental Panel on Climate Change (IPCC). The global CO_2 concentration in the atmosphere has been rising from ca. 280 ppm to over 400 ppm today (fig. 1.1) (Intergouvernemental panel on climate change, 2007; Lan et al., 2023). The Panel concluded that global heat content has increased since 1971 for the upper surface (0-700m) layer of the ocean and that ocean pH has declined globally at the surface over the last 40 years (Gulev et al., 2021). The global ocean temperature has increased by 0.88°C from 1850-1900 to 2010-2020 and is projected to increase even further by 0.86°C (in SSP1-2.6) and by 2.89 (in SSP5-8.5) from 1995-204 to 2081-2100 (Fox-Kemper et al., 2021).
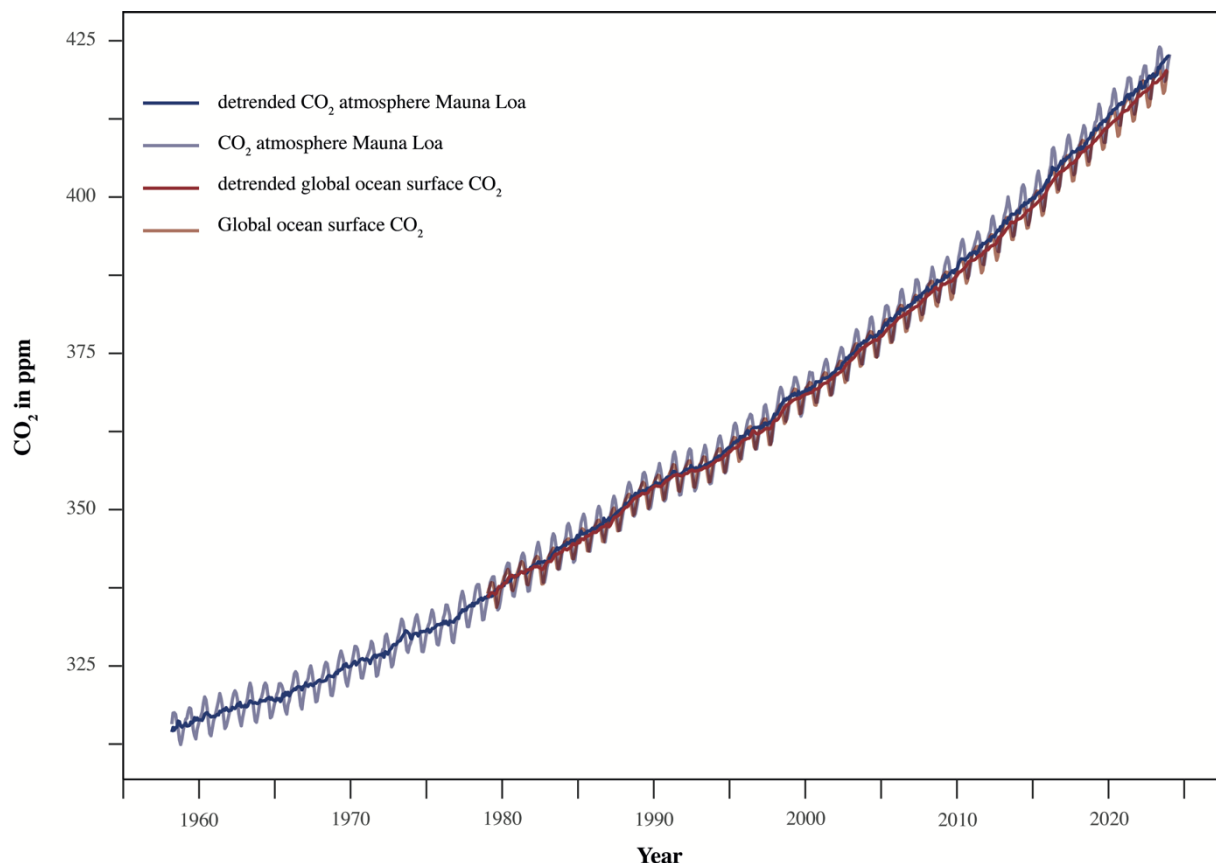
Figure 1.1: Global ocean surface CO_2 (red) and CO_2 measured at Mauna Loa, Hawaii, in the atmosphere (blue). Due to CO_2 emission and land use change CO_2 has been rising constantly in the atmosphere leading to global climate change such as rising numbers of marine heatwaves, ocean acidification and numerous other effects (Gulev et al., 2021; Lan et al., 2023).

Introduction

A consequence of increased CO_2 emission in the atmosphere is the increase in the frequency, intensity, and duration of marine heatwaves since the 1980s (Fox-Kemper et al., 2021). Heat waves in the ocean expose marine organisms to longer periods of extreme warm temperature to which they might not be adapted (Fox-Kemper et al., 2021).

Among the risks of ongoing alterations of climate patterns due to increased CO_2, are that climate regulating components, such as the Atlantic Meridional Overturning circulation (AMOC) are at risk to reach a tipping point and have so far experienced a slowdown. The tipping point of the AMOC has been a major player in the past and has had a quasi-global impact in past abrupt climate change (Dima et al., 2021). However, projections about the AMOC have a low confidence level since simulated climate models and observations result in significantly different hindcast (Dima et al., 2021; Fox-Kemper et al., 2021). A key knowledge gap is that the span of observation for a natural variability of the AMOC is highly limited and therefore key processes of the AMOC are not well understood (Dima et al., 2021; Fox-Kemper et al., 2021).

Tropical, reef building corals can help shed light onto unknown past climatic changes, as well as help predict future developments. During their long live, that can last centuries, they incorporate changes in the ocean's chemistry into their aragonite skeleton. Trace elements and stable isotopes provide useful proxy records of the past (Montagna et al., 2014a; Ross et al., 2019; Thompson, 2022). Regular annual density banding of corals facilitate tracking their ages as well as pin pointing the exact year, season, month of change.

Tropical corals grow between 30°N and 30°S of the equator in an environment of 23°C and 29°C (Spalding & Brown, 2015). Ca. 275 million people live in the vicinity of coral reefs that is providing food, generate jobs and act as a defense against storm and land erosion (Spalding & Brown, 2015). As aragonite forming marine organisms they are not only an important archive for climatic and environmental change but also highly affected by those changes.

Introduction

1.1.1   Ocean warming and its impact of coral reefs
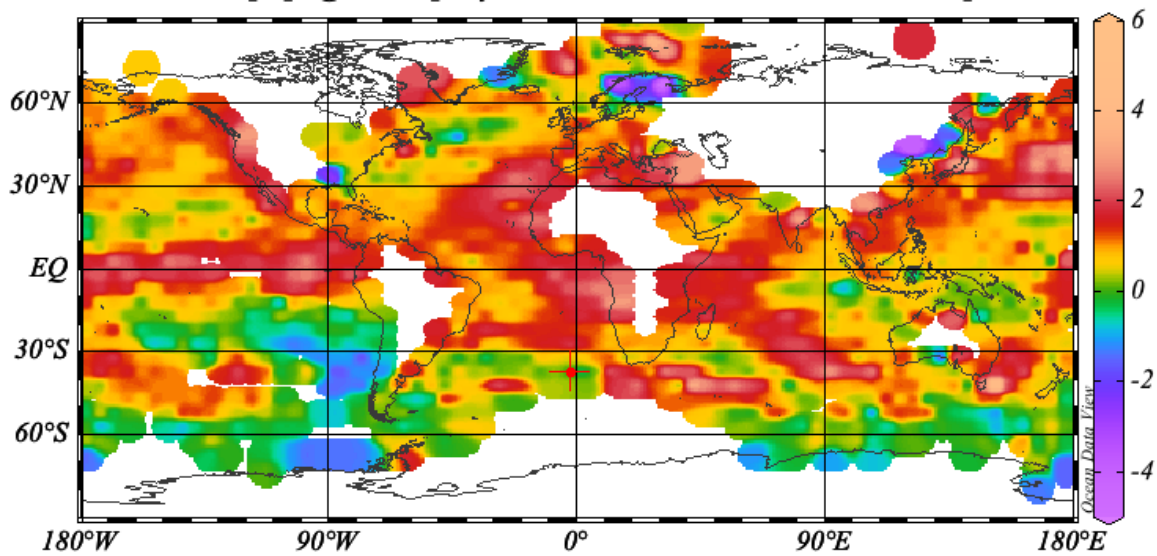
Figure 1.2: HadSST.4.0.0.0 SST anomalies (°C) for December 2023 relative to 1961 – 1990 average (Kennedy et al., 2019, https://crudata.uea.ac.uk/cru/data/temperature/#datdow; accessed on 14.02.2024).

One major stressing factor for coral reefs is the warming of the ocean. It is predicted that at least 83% of the ocean will warm in the course of the 21st century (Fox-Kemper et al., 2021). So far the ocean has stored 91% of the total energy gained from 1971-2018 (Gulev et al., 2021). In the tropics, temperature is rising faster than in other parts of the ocean (Figure 1.2) (Collins et al., 2019; Kennedy et al., 2019). However, some corals benefit from higher temperatures, by showing increasing calcification rates. An increase in metabolism and enhanced photosynthesis due to warmer temperatures might be a cause for this. Until a certain threshold is reached, corals thus might benefit from warming oceans (Buddemeier, 2004; Castillo et al., 2014a).

Marine heatwaves, where corals are exposed to extreme water temperatures over several weeks are causing severe damage to coral reefs such as bleaching. Since the 1980s, heatwave occurrences have doubled in frequency (Fox-Kemper et al., 2021). During marine heatwaves coral reefs are exposed to higher than usual temperature over prolonged time.

Corals are hosts to photosymbionts of the genus *Symbiodiniaceae*. *Symbiodiniacceae* provide their hosts with photosynthate, helping accelerate calcification. In cases of prolonged anomalously warm ocean temperatures, symbionts overproduce oxygen radicals which lead to an expulsion of the symbionts by the coral. The symbionts pigmentation are, what gives the coral their colorful appearance. When most of the symbionts have been expelled, the white

Introduction

skeleton shines through the transparent tissue, leading to the term coral bleaching (Baker et al., 2008; Hoegh-Guldberg, 1999).

Prolonged marine heatwaves can lead to the death of the coral, since the symbionts are providing the coral with nutrients (Spalding & Brown, 2015). During the expulsion of their symbionts, coral lose up to 95% of their energy supply, inhibiting calcification or reproduction (Leder et al., 1991; Szmant & Gassman, 1990)

Another threat to coral reefs that might intensify with warming SSTs are tropical storm surges (Grinsted et al., 2013; Seneviratne et al., 2021). Due to limited data availability on storm surges (satellite data only going back about 40 years (Seneviratne et al., 2021)), observed trends are not robust, and statements about trends have to be handled with caution (Grinsted et al., 2013; Seneviratne et al., 2021). The USA have one of the longest and reliable record of landfall events of hurricanes and shows no change in frequency of landfall events since 1900 (Seneviratne et al., 2021). What has changed is the velocity of tropical storms with which they move across the earth surface. Tropical storms have slowed down, thereby causing increased local rainfall amounts, and an overall longer duration of storm events (Seneviratne et al., 2021). The global increase in SST might lead to an increase in storm intensity(Knutson et al., 2010), as well as prolonged storm season, since the temperature threshold for hurricanes in the Atlantic for example, will be exceeded over longer periods (Seneviratne et al., 2021). A longer lasting storm season, slower moving velocity, and more intense storms are posing a major threat to coral reefs. Coral reefs are not only being physically destroyed, but are stressing the marine organisms living in it, be it fish or corals, as well.

When the coral is stressed, fungi, algae and bacteria have an easier access to the corals' interior. As part of every coral's microbiome, algae, bacteria and fungi are most likely already present inside the coral's skeleton. However, when the coral is stressed its defense mechanism might be reduced, and fungi can attack the corals polyps more easily (Ricci et al., 2019). The holobiont of a coral harbors a multitude of organisms that form the microbiome of a coral. Some microorganisms can be beneficial to the coral by providing an alternative carbon source (the green algae Ostreobium), when the symbionts leave the coral, due to high SSTs. The provision with carbon can potentially help the coral to survive stress events such as bleaching (Galindo-Martínez et al., 2022; Ricci et al., 2019). However, those stress events can also lead to a shift in the microbiome towards potentially harmful fungi, bacteria, and pathogens population. Even

Introduction

an increase in algae biomass during a bleaching event can cause lesions that make the corals more susceptible to pathogens (Ricci et al., 2019).

In 2014 a major bleaching event affected coral reefs all around the world and lasted until 2016. Models suggest, if temperatures continue to increase coral reefs might experience annual bleaching until 2050 (van Hooidonk et al., 2016). The effects of bleaching might potentially weaken the coral reefs' ecosystem engineer (Alvarez-Filip et al., 2011; Doney et al., 2009; Pandolfi et al., 2011).

1.1.2 Ocean acidification and its impact on coral reefs

The second change coral reefs are currently facing is ocean acidification, a reduction of pH in the ocean. Continuous CO_2 emission and land use change, due to anthropogenic activity, have altered the atmosphere and oceans chemistry. The open surface water pH ranges between 7.9 and 8.2. The subtropical oceans vary between 8.05 in warmer months and 8.15 during winter months (Takahashi et al., 2014). Ambient water of coral reefs show an even wider range in pH of 7.65 to 8.4 (Manzello, 2010; Santos et al., 2011; Shaw et al., 2012), due to biological processes, such as photosynthesis and respiration, manipulating the carbon cycle in a reef (Manzello, 2010; Shaw et al., 2012).

Since preindustrial times ($\sim$ 1750) the oceans pH has dropped by approx. 0.11 pH units which is equal to an acidification of 30% (L. Jiang et al., 2023). So far, the oceans have absorbed one quarter of the anthropogenically added CO_2 (Gulev et al., 2021). The additional CO_2 leads to a shift in the carbonate chemistry of the ocean towards lower pH values. The added CO_2 reacts with the water and carbonic acid forms. This will lead to a release of hydrogen ions, hence a drop in pH (Hoegh-Guldberg et al., 2017; Orr et al., 2005; Zeebe & Wolf-Gladrow, 2001). Following equation describes the formation of carbonic acid in seawater:

$$CO_2 + H_2O \leftrightarrow HCO_3^- + H^+ \leftrightarrow CO_3^{2-} + 2H^+ \qquad [1.1]$$
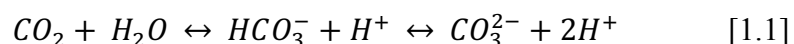
The more available hydrogen ions will bind to available carbonate ions forming hydrocarbonate [HCO_3^-]. The formation of hydrocarbonate decreases the carbonate saturation state of the ocean, since its occupying the carbonate ion [CO_3^{2-}] to form bicarbonate ions [HCO_3^-] (Cao et al., 2007). Marine organisms incorporate the carbonate ion to form their skeleton or shell that is made of either calcite or aragonite $CaCO_3$. Although the tropics and subtropics will remain

supersaturated, models still predict a decline in calcifying rates for corals and other carbonate building organisms (L. Jiang et al., 2023; Orr et al., 2005). However, the lack of carbonate chemistry observations and the interactions between the different carbonate chemistry components (TA, DIC, pH, pCO_2, SST, SSS) are complicating the predictions for future developments (Hönisch et al., 2012; Orr et al., 2005). Long-term continuous measurements for pCO_2 and pH have been put in place in 1988 in different locations of the world. At Bermuda Atlantic Time Series (BATS), Hawaii Ocean Time Series (HOT) station ALOHA, and European Station for Time Series in the Ocean Canary Islands (ESTOC) are measuring carbonate chemistry components such as pH, pCO_2, TA, and DIC (fig. 1.3C). In addition to these continuously measuring stations there are data products providing collections of observational ocean data. Surface Ocean CO_2 Atlas Database (SOCATv2023, fig 1.3B) is a database for fCO_2 measurements obtained from ships, moorings, and autonomous drifting surface platforms from 1957 to 2023 in the latest version from 2023 (Bakker et al., 2016, 2023). Global Ocean Data Analysis Project (GLODAPv2 2023, fig 1.3A) (Lauvset et al., 2022) contains as a data product, data from discrete bottle-based measurements. The most recent release is from 2022. The Coastal Data Analysis Project for North America (CODAP-NA) (L.-Q. Jiang et al., 2021) contains carbon data from North American margins. The data of all products is managed and accessible in the Ocean Carbon and Acidification Data System (L.-Q. Jiang et al., 2023). Even though, there are many different projects assembling carbon data there are still many areas with no data at all.

Introduction

GLODAPv2 2023

SOCATv2023

Station Location
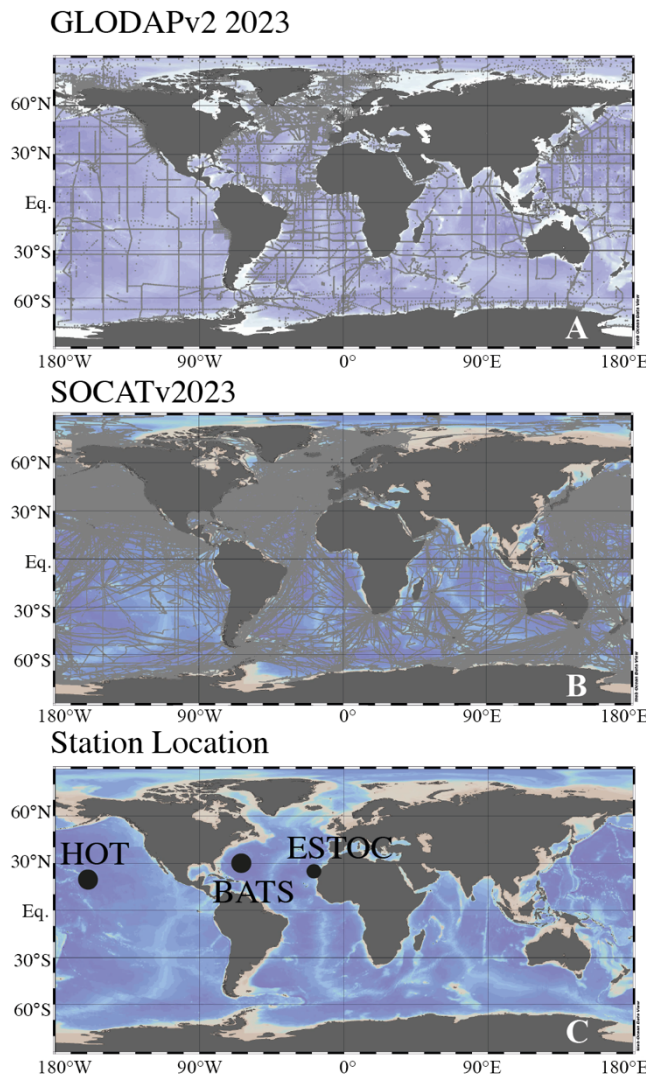
Figure 1.3: Global maps of GLODAPv2 2023 (Lauvset et al., 2022), SOCATv2023 (Bakker et al., 2023), and the Stations HOT , BATS, and ESTOC that measure some of the carbonate chemistry parameters in the Pacific and Atlantic.

As with warming SST, higher CO_2 concentration affects the coral reefs organisms in different and complex ways. Depending on the species, some corals increase their calcification rate with increased CO_2 in the water due to more DIC available (Castillo et al., 2014a; Pandolfi, John M. et al., 2011). The massive reef building coral *Siderastrea siderea*, for example, exhibits a parabolic response to warming temperatures and moderate alterations of pCO_2. However, when pCO_2 is elevated to extremes (in their study to above 500 ppm), calcification starts to decline as well (Castillo et al., 2014a). Experiments that combined an increase in temperature with an increase in pCO_2 have shown, that the change in temperature affects the coral before increased pCO_2 content in SW, resulting in a decline in pH_{CF}. This might be due to the enhanced stress posed on the symbionts, which may divert energy to towards tissue repair instead of the upregulation of internal pH (Cameron et al., 2022; Castillo et al., 2014a).

1.2 The Caribbean climate

The Caribbean is an important supplier of warm surface water masses for the Gulf Stream. Therefore, variabilities in SST and SSS of the Caribbean waters have an impact on the Atlantic Meridional Overturning Circulation as part of the climate system, hence, changes in its constitution will have a direct effect on the climate system (DeLong et al., 2014; H. Liu et al., 2012). Only a few reconstructions stem from the northern part of the Caribbean; the Gulf of Mexico (Castillo et al., 2014a; DeLong et al., 2014). To add to the proxy records of the GOM

Introduction

we chose a coral from the northern Cuban coast in addition to a coral from Puerto Rico, in the Caribbean Sea.

The rainfall season in the Caribbean Sea is mostly controlled by the Intertropical Convergence Zone (ITCZ), trade winds, Hadley Cell circulation, and interactions between land masses and atmosphere (Poveda et al., 2006). The ITCZ is a region close to the equator, with ascending air, deep convective clouds high precipitation rates, and converging trade winds (Henderson-Sellers and Robinson, 1986). The seasonal insolation cycle determines the position of the ITCZ, lagging the zenithal position by one month (Poveda et al., 2006). In boreal summer the ITCZ reaches as far north as the northern border of Costa Rica, while in boreal winter the ITCZ is situated over the Amazon basin, southern Columbia and Ecuador (Poveda et al., 2006). As a result of the meridional movement of the ITCZ the south eastern part of the Caribbean Sea (Jamaica, Dominican Republic, and Puerto Rico) experiences bi-modal annual rainfall cycle with the ITCZ passing two times over those regions. Cuba is situated on the edge of the rainfall belt and shows an uni-modal precipitation pattern with increased rainfall from May to July and a lower contribution from November to December (Jury et al., 2007). The islands to the south experience higher rainfall from May to December with a small drop from August to October (Jury et al., 2007).

1.2.1   Interannual to decadal oscillation

The Caribbean rainfall is furthermore influenced by atmospheric forcing such as the North Atlantic Oscillation (NAO), the Atlantic Multidecadal Oscillation (AMO) as well as an El Niño Southern Oscillation (ENSO) teleconnection between the Pacific and Atlantic Ocean (fig. 1.4 and 1.5).

The NAO is an index given for when the sea level pressures over North and Central Atlantic are below (North Atlantic) and above (central) average in wintertime (Hurrell, 1995). This phenomenon leads to changes in in the mean wind speed and direction over the Atlantic as well as changes in the transportation patterns of heat and moisture, intensity of storms and their tracks. In positive NAO years the increase in SLP in boreal winter leads to stronger northerly winds over north eastern Canada and Greenland flowing southward and thereby cooling land temperature and SSTs (Hurrell et al., 2003). While the extratropical atmosphere does not show long-term memory effects for persistence in regards to NAO, the stronger winds over the north

wester Atlantic lead to a cooling of the ocean's surface temperature and a vertical mixing of the water column.

This NAO signal will reach the Caribbean by May – June with negative SST and negative rainfall anomalies (Giannini et al., 2000b). This low frequency anomaly of the North Atlantic has a timescale of about 10 days (Feldstein, 2000). The predictability of the NAO remains to this day unresolved and even resulted in a "signal-noise-paradox". The "paradox" describes the ratio of predictability components in hindcast of a model that is bigger than 1, leading to the model being less predictable than what is observed in nature (Strommen and Palmer, 2018). However, this Decadal Prediction System 3 (DePreSys3) conducted by the UK Met office remains the closest to predicting the NAO (Dunstone et al, 2016). Some climate models suggest a slight displacement of the NAO center towards the North East (Ulbrich and Christoph, 1999), others show a weak trend towards a positive NAO phase (Hurrell et al., 2003; Hanna and Cropper, 2017). Nevertheless, due to our limited understanding of NAO and a reliable prediction, projections for the future have to be treated with caution (Hanna and Cropper, 2017).

1.2.2 Multidecadal Oscillation in the Atlantic basin

The Atlantic Multidecadal Oscillation (AMO) index is describing Atlantic SST patterns persisting over multiple decades. It is established by averaging SSTs over the whole North Atlantic (0° - 70°N) and detrending them with a 10-year running mean (fig. 1.4) (Talley et al., 2011). A positive AMO index or warm AMO describes warm SST in the North Atlantic and cool southern Atlantic (Talley et al., 2011). These warm SSTs are associated with a northward shift of the ITCZ north of its climatological March to May position. This leads to changes in the trade winds and an increase of precipitation in the Sahel while precipitation decreases in North East Brazil. During the opposite phase (negative index or a cold AMO) the ITCZ is shifted southward leading to decreasing rainfall in the Sahel zone and increased precipitation over North East Brazil (Knight et al., 2006). The time scale of positive and negative AMO phase is between 60 to 80 years (Knight et al., 2005).

However, SST observations for the North Atlantic only date back approximately 160 years, making only 1.5 to 2 AMO cycles for observation possible. If the AMO is reoccurring with a set periodicity remains to be proven (Alexander et al., 2014). The same is true for NAO.

Introduction

So far, we know very little about the workings of the AMO due to limited observations and inconclusive or contradictory modelling of the AMO. A continuous observation of changing SST in AMO areas has only started in 2004 and does not yield sufficient data to describe the driving mechanisms of the AMO.
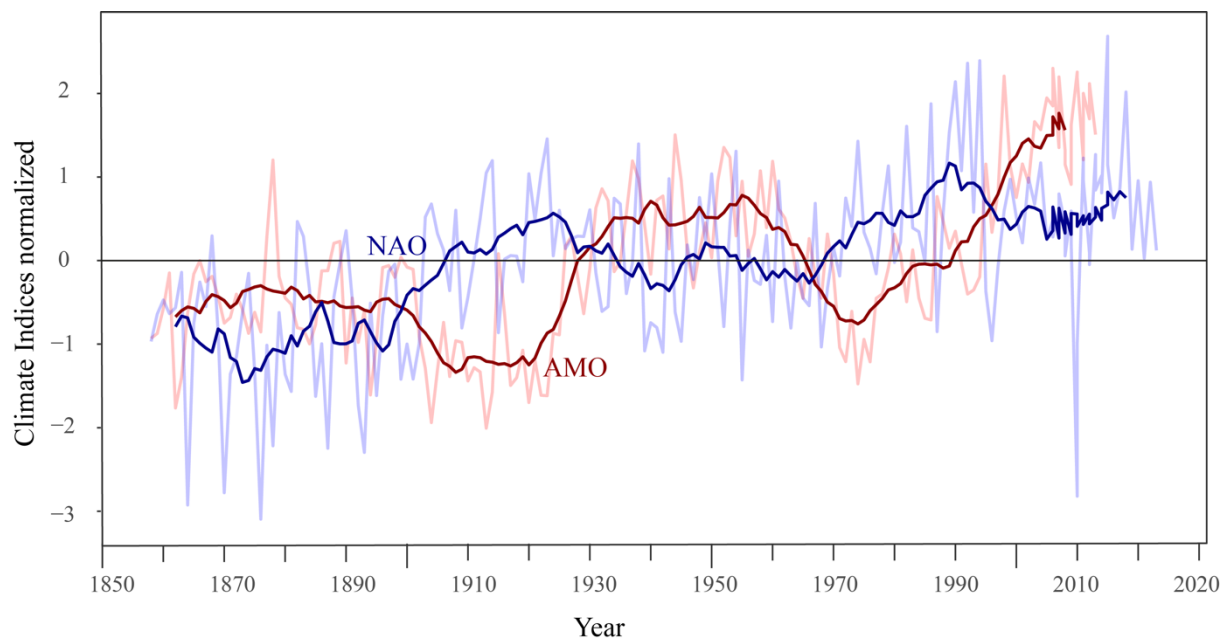
Figure 1.4: Times series with 10 year running mean and normalize. AMO from the Kaplan SST dataset (Enfield et al., 2001, https://psl.noaa.gov/data/timeseries/AMO/, accessed on 15.02.2024). NAO index is the difference of SLP between Lisbon, Portugal and Stykkisholm Iceland (Compo et al., 2011; Hurrell, 1995, https://psl.noaa.gov/data/20thC_Rean/timeseries/monthly/NAO/, accessed on 15.02.2024, and https://www.cpc.ncep.noaa.gov/products/precip/CWlink/pna/nao.shtml, accessed on 15.02.2024)

The AMO has its impacts on the Atlantic Warm Pool (AWP) as well. The AMW is defined as a large body of water with temperatures above 28.5 °C and situated in the Gulf of Mexico, the Caribbean Sea, and the western tropical North Atlantic (fig. 1.5) (Wang and Enfield 2001,2003). It starts developing in June and decays after October (Liu et al, 2012). Variabilities of the AWP are due to forcings from NAO. Increased trade winds due to a positive NAO index could lead to changes in latent heat flux and SST anomalies of the tropical North Atlantic and with that, the AWP (Liu, 2012). The AWP varies interannually, multidecadal, and secularly. The secular trend is the increased size of the AWP due to global warming. Multidecadal variabilities of the AWP are in phase with AMO. In an AMO warm phase the AWP extends,

while in an AMO cold phase colder SST in the North Atlantic lead a smaller AWP (Zhang et al., 2012).

Those warm SSTs in the North Atlantic in a warm AMO phase and a larger AWP have furthermore, an effect on the tropical cyclone formation. In warm AMO years the AWP extends towards the east Atlantic. The warming SSTs in the main development region (MDR) or hurricanes lead to a decrease in the vertical wind shear and favors hurricane formation. The AWP is thereby, acting as a link between the AMO and Atlantic tropical cyclones (Wang et al., 2008).

A better understanding of the different forcings on the AMO and NAO is needed for their predictability as well as for understanding future scenario especially in times of anthropogenic climate change.

1.2.3   The Pacific-Atlantic Teleconnection

Even though, separated by North and South America the Pacific and Atlantic have their pull due to their teleconnection. This is especially noticeable through the El Niño Southern Oscillation (ENSO). A preceding of the ENSO starting in December can already be observed in July – August before the ENSO event. While in the eastern Pacific a weak SLP develops, SLP over the equatorial Atlantic is strong. The SLP gradient between the ITCZ and the North Atlantic high is lower, leading to a decreased strength in trade winds and with that less heat loss from the ocean and negative rainfall anomalies. Once the ENSO dies down the atmospheric anomalies disappear. However, SST anomalies are still present in spring of after the ENSO event in the Caribbean and peak between May and June (Giannini et al., 2000).

Depending on the location in the Caribbean sea the impact of the ENSO on the basin will differ. While Cuba experiences excessive rainfalls and flooding during January and February of an El Niño year (when El Niño started the previous December), the southern part of the Caribbean basin is more likely to be drier from July to March (A. (Lamont-doherty E. O. Giannini et al., 2000). The lagged ocean response will lead to a warming of the ocean approximately one season after the warming of the Pacific Ocean. This is due to the development of the SLPs over the different ocean basins (A. (Lamont-doherty E. O. Giannini et al., 2000). The effect of ENSO

on the tropical Atlantic will further be influenced by Multidecadal Oscillations (AMO) and the North Atlantic Oscillation (NAO) that have impacts on SST as well as rainfall pattern in the Caribbean Sea (Giannini et al., 2001; Giry et al., 2010).

A positive NAO index will have the opposite effect of the effect a warm ENSO has on the Caribbean basin. During winter of a NAO positive year the trade winds over the tropical North Atlantic will be stronger, a warm ENSO phase will have the opposite effect, thereby cancelling out the cooling effect of a positive NAO (A. (Lamont-doherty E. O. Giannini et al., 2000). A negative NAO and a cold phase ENSO can likewise enhance each other's effects on SST of the Caribbean Sea (Giannini et al., 2001).
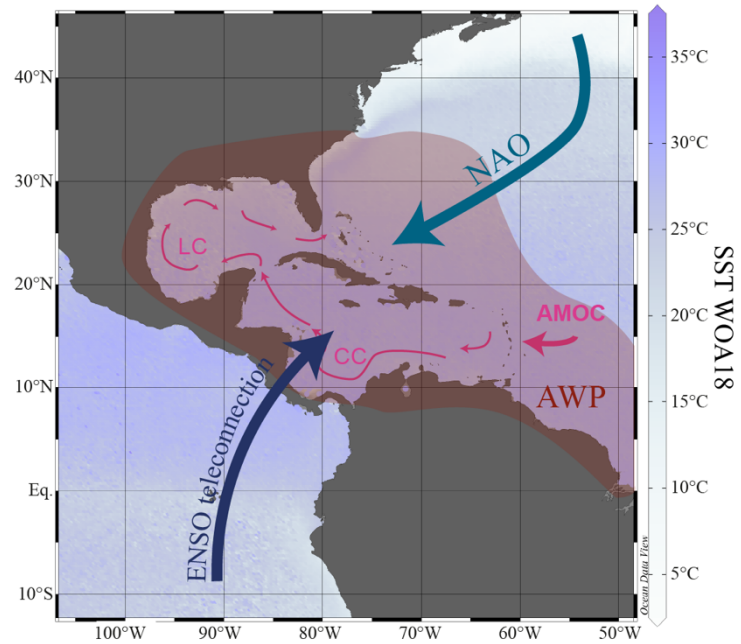
Figure 1.5: Map of SST from the World Ocean Atlas 2018 (WOA18, Locarnini et al., 2019) Schematic representation of ENSO teleconnection and NAO as influencing interannual and multidecadal oscillations on Caribbean climate. The Atlantic Warm Pool (AWP) in light red as an example of a large AWP extension (Lopez et al., 2022). Pink arrows represent the part of the AMOC entering the Caribbean basin as the Caribbean Current and transforming into the Loop Current in the Gulf of Mexico.

1.3 Paleo proxies

To track changes in SST, SSS, and other environmental changes prior to instrumental measurements, geochemical analysis of the coral skeleton can be used. While growing, corals will incorporate the chemistry of the surrounding seawater into their aragonite skeleton. Elements such as Strontium, Barium, Manganese, and (Sr^{2+}, Ba^{2+}, Mn^{2+}) are chemically similar to Calcium (Ca^{2+}) and can therefore replace Calcium and can be found in traces in the coral skeleton (Bradley & Elias, 2015). Relative abundances compared to Calcium act as relative indicators for the ocean SST, SSS, river runoff, upwelling, etc. Depending on environmental changes, the trace elements are more or less likely incorporated into the skeleton of the coral.

Introduction

In relatively colder environments corals prefer Sr to Ca and therefore the ratio will increase (S. V. Smith et al., 1979b), while the Mg/Ca ratio decreases with decreasing temperatures (Bradley & Elias, 2015; Hillaire-Marcel & de Vernal, 2007). (Mitsuguchi et al., 1996)) suggested the use of U/Ca ratio since it correlated with Sr/Ca, the most widely used and reliable SST proxy so far (Kilbourne et al., 2008; DeLong et al., 2013; Wu et al., 2014). Nevertheless, the process of substitution of trace elements for Calcium is not well understood, yet variation in those records are depending on multiple factors.

Trace element content in coral aragonite may vary due to changes in growth rate light intensity, sea level, turbidity, and nutrient supply (Villiers et al., 1994). Following the principal of Rayleigh fractioning the fluid in the space will change its trace element composition with progressing accretion of the skeleton. The trace element – Calcium ratio will decrease at a given temperature with proceeding precipitation and changing the resulting TE/Ca in the skeleton (DeCarlo et al., 2015a, DeCarlo et al., 2016).

However, biominerals such as aragonite coral skeleton are dependent on physiological, biological as well as chemical processes. While Rayleigh fractioning might lead to a signal similar to global equilibrium, environmental changes, and growth kinetics may change the signal. In addition, the incorporation changes from species to species, and might even change in one single colony depending on its position in the colony. It remains of the utmost importance to understand the skeletal accretion in corals to make better statements for the environmental implications (Vielzeuf et al., 2018). In order to use trace elements and isotopic ratios as environmental proxies a calibration with in situ measured SST or satellite data with each data set is indispensable.

1.3.1 Coral Biomineralization

Skeletal aragonite is accreted between the skeleton and the calicoblastic ectoderm, in a semi-enclosed extracellular calcifying medium (ECM), also termed calcifying fluid (CF) (Allemand et al., 2004; Drake et al., 2020; Thompson, 2022). The ECM or CF is separated from the seawater by the coral tissue, that is composed of the oral tissue, facing the seawater and the aboral issue, facing the skeleton (Allemand et al., 2004). Seawater is passively transported to the ECM via the calicoblastic ectoderm through paracellular diffusion. For the skeletal accretion selected ions, reach the ECM, via a transcellular metabolic pathway, thereby increasing the concentration of these ions compared to seawater. The coral is capable of

Introduction

regulating the concentration of Calcium, but also carbonate ions in its ECM to establish supersaturation, so that aragonite precipitation is facilitated (Allemand et al., 2004; Comeau, Tambutté, et al., 2017; Falini et al., 2015; M. McCulloch, Falter, et al., 2012a; Ross et al., 2017; Thompson, 2022). The transcellular or 'active' pathway can selectively transport Ca^{2+} to the ECM. Ca^{2+} is exchanged via the $Ca^+ATPase$ for two hydrogen ions. This process in increasing the pH in the ECM and shifts the DIC equilibrium towards $[CO_3^{2-}]$ by removing the $[H^+]$ from the $[HCO_3^-]$ (Allemand et al., 2004; Comeau, Cornwall, et al., 2017; D'Olivo et al., 2019; M. McCulloch, Falter, et al., 2012a; M. T. McCulloch et al., 2017a; Ross et al., 2017; Zoccola et al., 2015). A heightened aragonite saturation state favors skeletal accretion. With advancing skeletal formation Rayleigh like fractioning processes modify the geochemistry of the ECM. Impacts of Rayleigh fractioning are thought to be most important during rapid skeletal accretion (Marchitto et al., 2018; Thompson, 2022). The active pumping of ions is thereby regulated by energy supply through metabolic processes (M. T. McCulloch et al., 2017a; Thompson, 2022). A simplified biomineralization model in figure 1.6 illustrates the ion transport mechanisms and accretion.
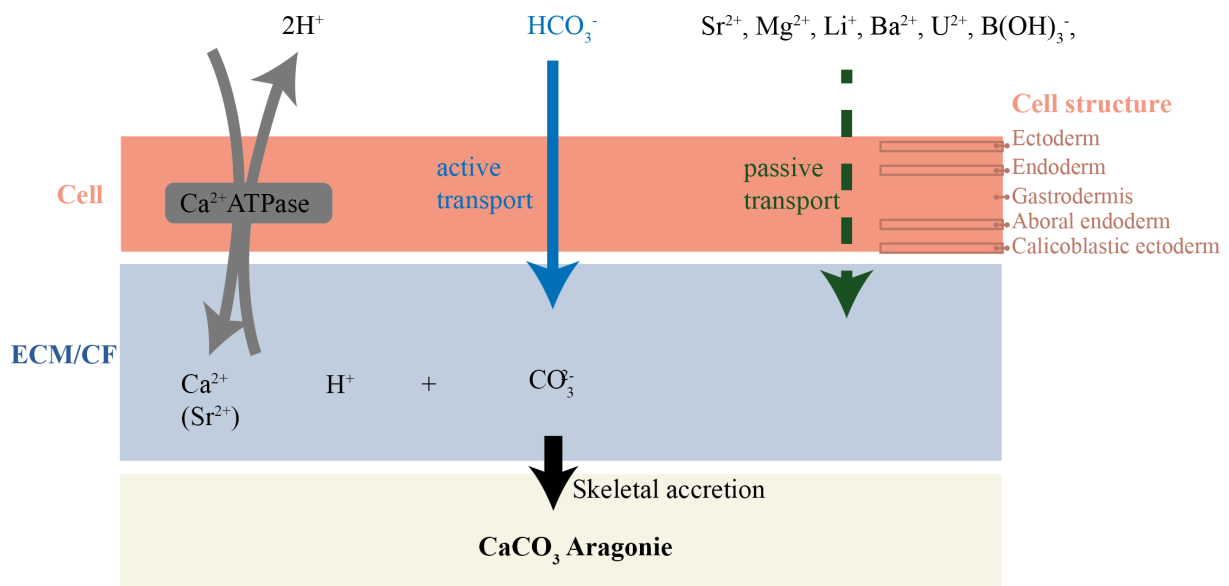
Figure 1.6: Simplified biomineralization model for scleractinian corals inspired by McCulloch et al. (2017) and Thompson (2022). Through a passive pathway (dashed green arrow) seawater with its geochemical signal is transported to the ECM. The coral actively transports (blue arrow) bicarbonate and carbonate ions to the ECM where it separates the hydrogen ion and exchanges it via a $Ca^+ATPase$ with Ca^{2+} (grey arrows). This increases the pH, DIC, aragonite saturation state and TA in the ECM compared to seawater. The heightened aragonite saturation state favors skeletal accretion, whereby certain ions are favorably incorporated (e.g. Sr^{2+}, Ba^{2+}) over others (e.g. Mg^{2+}, Li) (Thompson, 2022).

Introduction

1.3.2 Sea surface temperature

As part of the climate system keeping track of oceans temperature is vital to understanding future climate variability. SST observations go back centuries, are however neither continuous nor do they cover the entire ocean. Different measuring methods (such as shipboard sensors, buckets, floating buoy, and satellites) have led to biases in the multitude of SST products. Differentiating correctly natural variability from anthropogenic influences is therefore made more complicated. The AMO variability is re-occurring with a frequency of 60-80 years (Knight et al., 2006). Even though Atlantic SST observations go back to 1908 (Chan et al., 2019), this would still only cover one change in period. Climate reconstructions using geochemical records, obtained from foraminifera or corals can help to improve our knowledge of temperature variability prior to in-situ observations and potentially fill gaps, where there are no records available. Corals incorporate a multitude of geochemical components into their skeleton recording environmental changes. Oxygen isotopes and Sr/Ca have been the most commonly used temperatures proxies for tropical (e.g.: de Villiers et al., 1994, 1994, 1995; DeLong et al., 2014; Gagan et al., 2012; Ren et al., 2003; Swart et al., 2002; Wu et al., 2014).

1.3.2.1 Oxygen isotopes

Another proxy often used for SST reconstruction is $\delta^{18}O$, the ratio of the isotopically heavier O^{18} and the lighter O^{16}. The $\delta^{18}O$ ratio in seawater and with that in the coral skeleton is controlled by SST as well as SSS. In combination with another proxy for SST such as Sr/Ca the SST control on $\delta^{18}O$ can be removed from the signal for the reconstruction of past changes in SSS (T. Chen et al., 2015). SST reconstruction from oxygen isotope ratios goes back to 1972 when it was shown that coralline oxygen isotopes depended on SST, although an offset to SW oxygen isotope signature is present (Evans et al., 2000; Fairbanks & Dodge, 1979; Weber & Woodhead, 1972). The offset stems from fractioning due to photosynthetic activity of the symbionts providing the coral with the necessary components to accrete their skeleton. The $\delta^{18}O$ value might therefore vary depending on the position of where the coral core was taken from (from the side of the coral or the top), how much light reached the coral, depending on the depth etc. (Fairbanks & Dodge, 1979; Linsley et al., 1999). However, $\delta^{18}O$ is not always affected by light and growth rate. Only when growth rate is very slow, for example under bleaching conditions or with very little light available, is $\delta^{18}O$ actually affected in healthy corals (Grottoli & Eakin, 2007).

Introduction

1.3.2.2 Sr/Ca

The longest and most widely used paleotemperature proxy for corals is Sr/Ca (e.g. (DeLong et al., 2011; Finch & Allison, 2003; Harbott et al., 2023; Nurhati et al., 2011; S. V. Smith et al., 1979a; Watanabe et al., 2020; Y. Wu et al., 2021; Xu et al., 2015). Sr/Ca is negatively correlated to temperature, showing warmer temperatures with lower Sr/Ca values and vice versa. Sr^{2+} substitutes, for Ca^{2+} in coral aragonite $CaCO_3$. It has a similar ionic radius than Ca^{2+} and can therefore be substituted for Calcium ions. Sr had a long residence time in the ocean, the incorporation of Sr is hence reflecting and the variability is hence assumed to reflect SST variability (Grove et al., 2013). However, Strontium concentration in the coral can also depend on growth rate and are coral species specific. Following the principal of Rayleigh fractioning the fluid in the space will change its trace element composition with progressing accretion of the skeleton. In times of rapid growth certain cations (e.g. Sr) are preferentially incorporated into the skeleton than others (e.g. Mg, Li), therefore depleting the accretion fluid in Sr (Thompson, 2022).

1.3.2.3 New approaches

The search for a reliable, robust, and universal SST proxy that is valid for one or even more coral species is still well underway. From this, several new approaches for SST calibrations have been proposed, such as Li/Mg and Sr-U.

Li/Mg seems unaffected by Rayleigh fractioning and extension rate of a coral (Fowell et al., 2016). Although Mg/Ca is not a promising paleothermometer, when put into relation with Lithium Li/Mg show a strong correlation to temperature. Both elements Li and Mg are not substituted for Ca like Sr. Their ionic radius differs from the ionic radius of Calcium and therefore cannot occupy the Ca^{2+} site in aragonite. It is more likely that Mg^{2+} and Li^{2+} are absorbed onto crystal discontinuities, this leads to Mg/Ca and Li/Ca showing strong variations (Montagna et al., 2014b). However, when comparing Li/Mg to the measured temperature the biological effect is reduced and SST remains as the primary control (Montagna et al., 2014b). The Li/Mg-SST calibration showed a direct relationship between ambient seawater temperature and Li/Mg, independent of coral species and in temperature range from 0-75-28°C, so cold and warm water corals (Cuny-Guirriec et al., 2019; Hathorne et al., 2013; Montagna et al., 2014a). Corals that show algae green bands and /or diagenetic calcite have to be treated with care when measuring Li/Mg. Organic matter is enriched in Mg and will therefore overestimate reconstructed temperature for Li/Mg-SST calibration by 15-30°C. Furthermore, the Atlantic coral *Siderastrea siderea* does not necessarily fall onto the calibration curve suggested by

Introduction

Montagna et al. (2014), but needs a species and location specific SST calibration, as do other more common SST proxies, such as Sr/Ca (Fowell et al., 2016). Nevertheless, when used in combination with other SST proxies or as part of a multiproxy approach Li/Mg remains a good option and addition to temperature reconstruction proxies.

The Sr-U thermometer is based on the relationship between Sr/Ca, which is temperature dependent and but highly influenced by Rayleigh fractioning, and U/Ca which is dependent on the DIC concentration, hence Rayleigh fractioning in the ECM, but not on temperature (DeCarlo et al., 2016; Galochkina et al., 2023). Uranium is incorporated into the aragonite lattice by the substitution of $[CO_3^{2-}]$ with an uranyl complex (DeCarlo et al., 2015, 2016). The dependence of U/Ca to the carbonate ion concentration could account for the Rayleigh fractioning Sr/Ca is affected by (DeCarlo et al., 2016; Galochkina et al., 2023). In the original development of this new proxy, multiple Sr/CA and U/CA pairs were regressed over a 1 year record calculating a single value for 1 year (DeCarlo et al., 2016; Mollica et al., 2023). This requires fast growing corals that yields enough yearly samples to result in an annual resolution when using bulk analysis. The most recent approach increased the sampling rate with Laser ablation inductively couples mass spectrometry (LA-ICP-MS) and a multiple regression method. This method yielded a robust calibration to temperature and reliable recording even during ENSO events (Mollica et al., 2023). Slower growing corals and different species still need to be tested to validate Sr-U as a universal SST proxy. Results so far however, look promising.

1.3.3   Sea surface salinity

Sea surface salinity records are rather sparse and do not cover more than a few decades (Kilbourne et al., 2004). Sea surface salinity can be an important indicator for water mass movement as well as precipitation. Due to the lack of SSS observations oxygen isotope records from foraminifera but also coral cores are used, to reconstruct the hydrological balance of seawater and extend the records (e.g.: Dassié et al., 2018; Dissard et al., 2021; Kilbourne et al., 2004; Ren et al., 2003). Oxygen isotope ratios incorporated is primarily controlled by SST and SSS. The temperature component should be removed from $\delta^{18}O$ to get $\delta^{18}O_{SW}$ (Gagan et al., 1998; Kilbourne et al., 2004; M. T. McCulloch et al., 1994; Ren et al., 2003). Once the $\delta18OSW$ has been calculated a regression to local SSS is necessary to reconstruct SSS prior to observations available. A first approach to $\delta18OSW$ is to remove the monthly means from $\delta^{18}O$ to obtain anomaly values for $\delta^{18}O$. Where SSS interannual variability exceeds seasonal

variability, this first method can effectively remove the SST component as was demonstrated in Vanuatu and Fiji (Kilbourne et al., 2004; Le Bec et al., 2000). Two additional methods use reconstructed SST provided by the Sr/Ca-SST regression to reconstruct SSS changes. By solving an empirical δ^{18}O- SST equation and removing SST obtained from the Sr/Ca-SST calibration the resulting residuals reflect the δ^{18}O$_{SW}$ variations (Gagan et al., 1998; M. T. McCulloch et al., 1994; Ren et al., 2003). In a second attempt, Ren et al. (2000) calculated the instantaneous changes for δ18OSW, by solving two equations derived from partial derivates of the calibration for Sr/Ca-SST and δ^{18}O - SST simultaneously. The results are relative changes over time in δ^{18}O that can be added to an arbitrary reference to have absolute values instead of relative change.

1.3.4 Carbonate chemistry

The addition of CO_2 will change the carbonate chemistry of the ocean. More Co2 will not only from carbonic acid, thereby decreasing pH in the seawater, but also decrease the aragonite/calcite saturation state in the oceans, a measure of available carbonate ions for calcification. In water, carbon dioxide exists in three forms: as CO_2 (aq.), as bicarbonate ion [HCO_3^-], and as carbonate ion [CO_3^{2-}]. Carbonite acid is formed by water and CO_2 and is in constant dissociation to form bicarbonate and carbonate ions :

$$CO_2 + H_2O \leftrightarrow H_2CO_3 \leftrightarrow H^+ + HCO_3^- \leftrightarrow 2H^+ + CO_3^{2-} \qquad [1.2]$$

The total dissolved inorganic carbon content is called DIC or TCO2 for total CO_2 and expressed as the sum of the carbon forms (Zeebe, 2012; Zeebe & Wolf-Gladrow, 2001):

$$DIC = [CO_2] + [HCO_3^-] + [CO_3^-] \qquad [1.3]$$

The total alkalinity (TA) keeps track of the charge balance in the seawater (Zeebe, 2012; Zeebe & Wolf-Gladrow, 2001):

$$TA = [HCO_3^-] + 2[CO_3^{2-}] + [B(OH)_4^-] + [OH^-] - [H^+] + minor\ components \qquad [1.4]$$

In total the carbonate chemistry of the ocean can be described by 6 components: TA, DIC, [CO_2], [CO_3^-], [HCO_3^-], and [H^+] (also expressed as pH) (fig. 1.7). With any two components the rest can be calculated (Zeebe & Wolf-Gladrow, 2001). By adding CO_2 to the ocean, as is part of the ocean acidification process, we are augmenting DIC, while TA does not change. The

formation of $CaCO_3$ binds CO_2, thereby decreasing DIC and TA. AS a consequence CO_2 levels rise and pH decreases (fig. 1.7) (Zeebe & Wolf-Gladrow, 2001).

1.3.4.1   *Reef Carbonate chemistry*

Organic carbon metabolism and inorganic metabolism are the two drivers of the carbon cycle on a reef. Photosynthetic fixation and respiration are performed by marine organisms as part of the organic metabolism, whereas calcification and dissolution is an inorganic process. During the day CO_2 is used by photosynthetic organisms and is therefore drawn down to preform photosynthesis. The consumption of carbon-dioxide will decrease the dissolved organic carbon content (DIC, or TCO_2 for total CO_2) while the total alkalinity does not change. The production of organic matter: calcification, will decrease DIC that is bound into CaCO3 and also decrease TA. The oxidation of organic matter, or dissolution of CaCO3 through respiration, that happens at night, will increase DIC and TA (J. P. Gattuso et al., 1995; Manzello, 2010). The precipitation of CaCO3 is actually a source of CO_2 by following equation (Bates, 2002; Manzello, 2010; Shaw et al., 2012):

$$Ca^{2+} + 2HCO_3^- \leftrightarrow CaCO_3 + CO_2 + H_2O \qquad [1.5]$$
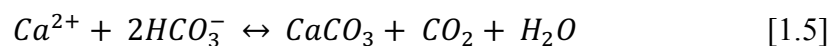
Available hydrogen ions might therefore bind to the available carbonate ions forming bicarbonate, therefore increasing the pH of the reef water (Shaw et al., 2012). During the night the process of respiration and dissolution releases Calcium and bicarbonate ions, leading to an increase in DIC and a decrease in pH. The aragonite saturation state will therefore rise during the day and fall at night (Bates, 2002; Manzello, 2010; Shaw et al., 2012).

1.3.4.2   *$\delta^{11}B$ as a paleo proxy for pH and carbonate chemistry of the ocean*

The boron isotope ratio is frequently used in coral studies to reconstruct paleo pH variations due to its dependence of pH and the incorporation of Boron into the corals skeleton (e. g. DeCarlo et al., 2018; Foster & Rae, 2016; Fowell et al., 2018; Hönisch et al., 2004; Marschall & Foster, 2018; Wu et al., 2018).

Boric acid [$B(OH)_3$] and borate anion [B(OH)4-] are the two most abundant boron species in seawater (Hemming & Hanson, 1992). Boric acid is predominant at lower pH of seawater and the borate anion at higher pH in seawater as is demonstrated in figure 1.8.

Introduction
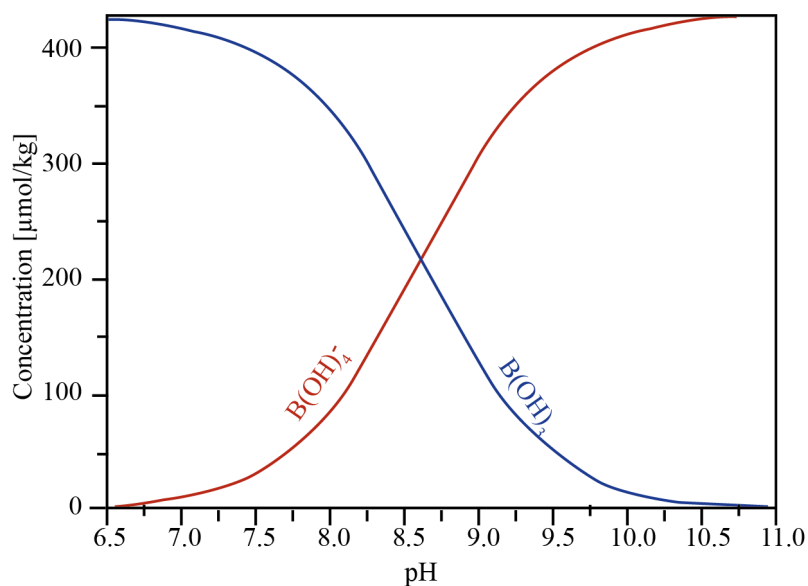
Figure 1. 7: Relationship of boron species to pH in seawater.

Their dissociation constant pkB is temperature and salinity dependent and is 8.6 at 25°C and 35 salinity (Dickson, 1990; Marschall & Foster, 2018).

Boron is found in marine carbonates as a trace element. Aragonite incorporates 3 to 5 times more Boron than calcite. While aragonite prefers to incorporate the borate anion, calcite is more likely to have boric acid (Marschall & Foster, 2018). Boric acid has a trigonal shape and is slightly smaller than the tetrahedral borate anion (Hershey et al., 1986). The isotopically heavier [11]B prefers the trigonal shape of boric acid, while the isotopically lighter [10]B prefers the borate anion (Marschall & Foster, 2018). In aragonite the Ca^{2+} cation is bonded to nine $[CO]_3^{2-}$ anions, which leads to a looser arrangement than in Calcite, where the cation is bonded to eight anions. Therefore, in aragonite larger cations than Ca^{2+} will more easily bond to the anions. Borate, due to its size, shape and charge is most likely to substitute for $[CO]_3^{2-}$ as $[BO]_3^{-}$ (Marschall & Foster, 2018) and is more easily incorporated into aragonite than calcite (Marschall & Foster, 2018)

Studies investigating the growth of synthetic aragonite show that Boron is incorporated straight from the surrounding solution without fractioning. Hence, $\delta^{11}B$ values from the aragonite correspond to $\delta^{11}B_{[B(OH)4-]}$ values from the solution (Holcomb et al., 2016; Mavromatis et al., 2015; Noireaux et al., 2015). In experiments under controlled conditions aragonite appears to only incorporate the tetrahedral boric acid (Marschall & Foster, 2018) with a very small percentage (<15 %) of the trigonal boric acid, probably transformed in a post crystallization process (Marschall & Foster, 2018). Tropical corals live in a pH environment of typically 8.0 to 8.1 and have a $\delta^{11}B$ composition of ca. 22% to 25%.

Introduction

The incorporation of boron into the coral skeleton offers therefore a great opportunity to reconstruct past pH changes. The δ^{11}B ratio is expressed as follows (Marschall & Foster, 2018):

$$\delta^{11}B_{coral} = \left(\left[\frac{\left[\frac{^{11}B}{^{10}B_{Coral}}\right]}{\left[\frac{^{11}B}{^{10}B_{NIST}}\right]}\right] - 1\right) \times 1000 \qquad [1.6]$$

The measured isotopic ratio from the skeletal material is expressed as $1\,^{11}B/^{10}B_{Coral}$ and compared to the isotopically ratio of the standard material $^{11}B/^{10}B_{NIST951}$.

The boron isotope ratios translates into pH of the calcifying fluid with following equation (Zeebe & Wolf-Gladrow, 2001):

$$pH_{CF} = log\left[\frac{\delta^{11}B_{SW} - \delta^{11}B_{Coral}}{\alpha_{B3-B4} * \delta^{11}B_{Coral} - \delta^{11}B_{SW} + 1000(\alpha_{B3-B4}) - 1}\right] \qquad [1.7]$$

$\delta^{11}B_{SW}$ is the isotopical ratio of seawater (39.61 ‰) (Foster et al., 2010) and αB3-B4 defines the isotopic fractioning factor 1.0272 (Klochko et al., 2006), while $\delta^{11}B_{Coral}$ is the measured boron isotopic ration of the coral skeleton.

The most frequently used fractioning factor for the isotope fractionation was defined by Klochko et al. (2016) through experiments and is α(B3-B4) = 1.0272 (Klochko et al., 2006, 2009). Other fractioning factors have been reported in a range of 1.024 to 1.030 and demonstrate that the fractioning factor defined by Klochko et al. (2006) cannot describe fractioning for all marine species. For a conversion of the pH$_{CF}$ to values of seawater, species specific calibration curves have to be applied to pH$_{CF}$.

1.4 Motivation

High resolution, continuous climate records of the surface ocean are sparse, especially prior to the 1950s. Long-term climate variabilities such as the AMO, AMOC variability, and NAO but also short-term changes like ENSO need longer records to truly capture their frequency and feedback to environmental changes. Reconstructions of climate parameters have helped shed light onto past changes and have been fed to numerical climate models as calibration and validation for those models. Tropical corals serve as an excellent climate archive, recording environmental changes in their skeleton. Today, we are able to reconstruct past climatic changes

continuously and with an ultra-high resolution. Although climate reconstruction with corals as climate archives have been performed since the 1970s (e.g. Livingston & Thompson, 1971; Smith et al., 1979), there are still gaps in spatial coverage but also records ending before a baseline climate signal starting before the industrial revolution could be established. Gridded SST and SSS analysis products, such as OISST and ERSST (Banzon et al., 2014; Huang et al., 2021a, 2021b; Reynolds et al., 2007) are good tools to visualize and analyze large scale environmental changes. They do not, however, capture local, coastal near processes. Reconstructions from coral skeleton material can prolong the climate and environmental record into the past. Some environmental parameters have had even less attention on them for the longest time. The carbonate chemistry of the ocean including TA, DIC, calcite and aragonite saturation state, as well as pH are more complicated to measure, therefore continuous records are limited to certain regions and do not show a long-term coverage. Fortunately, boron isotope ratios are dependent on the pH on the water column and are incorporated into calcite and aragonite of marine skeletal building organisms such as corals. This makes it possible to not only reconstruct past pH changes but also changes in the carbonate chemistry if SSS and SST as well as another component of the carbonate chemistry is known (Hönisch et al., 2004; Zeebe & Wolf-Gladrow, 2001). To reconstruct pH from a coral core, a species specific pH- δ^{11}B calibration is needed but is not always available. Therefore, more calibration studies need to be done, to include a bigger variety of coral species.

1.5   Research hypothesis

The tropical reef building coral *Siderastrea siderea* is recording past climate change accurately for the north-western Cuban coast. The first aim is to establish if the coral core taken from the north-western coast of Cuba from a *Siderastrea siderea* is a good climate archive and has recorded environmental changes robustly. Accordingly, ca. bimonthly samples have been taken from the corals thecal wall to allow measurements of multiple proxies such as Sr/Ca, δ^{18}O, Sr-U, and Li/Mg for sea surface temperature and sea surface salinity reconstructions.

The Cuban *S. siderea* is showing ocean acidification for the Gulf of Mexico and shows changes in the carbonate chemistry accordingly. If the coral from Cuba is a reliable archive for SST and SSS, it might also be recording changes in pH, recorded by boron isotopes incorporated into the coral skeleton. From SSS and pH carbonate chemistry can be reconstructed. Ocean acidification will not only change pH in the ocean and thereby change the carbonate chemistry but will also be noticeably in the corals calcifying fluid. Using SSS

reconstructed from δ^{18}OSW, SST and pH from δ^{11}B, long term changes in carbonate chemistry of the ocean can be reconstructed for the first time only using coral proxies as well as the changes in the CF of the coral.

The *S. siderea* is adapting to OA. If long term changes in the carbonate chemistry are visible from the reconstructions, indicating ocean acidification (by an increase in DIC, while TA stays constant) the coral might show a mechanism of adaption by regulating its calcifying fluid. For calcification corals are actively modifying their CF by exporting hydrogen ions against calcium ions, thereby increasing the pH of the calcifying fluid compared to the pH of SW. DIC is also heightened to ensure increased aragonite saturation rates for better skeletal accretion. The control over the CF might therefore help the coral to adapt to environmental long-term changes.

The reef building coral *Orbicella annularis* from the La Parguera National Park is recording pH in its δ^{11}B values and we can offer a new δ^{11}B – pH calibration for this species. The aim for this hypothesis is to establish the coral *Orbicella annularis* as a reliable environmental archive for pH. In the vicinity of the coral a buoy is recording pH, pCO$_2$, SST, and SSS since 2009, offering a unique opportunity to calibrate the coral with local in-situ measurements and thereby, establishing a new coral calibration for pH. To compare the high resolution buoy measurements to values from the coral, high resolution Laser Ablation MC-ICP-MS can be used to measure boron isotope ratios.

1.6 Thesis outline

Chapter 1 describes scientific context for the three following chapter by outlining the current status of climate change research and identifying the relevance of the study area. Furthermore, the chapter discusses the current status of paleo proxy research, especially using corals as climate archives and presents the motivation and hypothesis of this thesis.

In **Chapter 2** the three main manuscripts are listed that have been either prepared for, submitted or published in peer reviewed international journals. Each chapter described in more detail the current status of the research and expands thereby on chapter one. The specific methodology for each Manuscript is included in the individual chapter.

Chapter 2.1 established the age model as well as SST and SSS reconstructions from a Siderastrea siderea coral taken from the north- western Cuban coast in the Gulf of Mexico. The

Introduction

reconstructed record spans 160 years from 1845 to 2005, when the coral core was taken. The coral record shows seasonal SST fluctuations and is validated and compared to reanalysis SST products and another coral record approx. 250 km north of the *S. siderea.* The coral SST record shows a warming of the southern GOM that came to a halt in the 1980s, as is also shown by the coral core from the northern GOM. Both indicate a possible slow-down of the Loop current, passing through the GOM. A long-term freshening of the southern GOM cannot be observed, although a slight freshening of the GOM in the 1980s and 1990s might show the change to a positive AMO phase.

Chapter 2.2 uses the age model set in chapter 2.1 as well as reconstructed SST and SSS to reconstruct the carbonate chemistry of the CF of the coral and the ambient SW. Since there are no in-situ measurements and only large scale gridded SST, SSS and carbonate chemistry products available, coral skeletal B/Ca and δ^{11}B make it possible to reconstruct ocean acidification and changes in the oceans carbonate chemistry. The coral skeletal material shows a clear OA signal by increasing DIC values while TA stays stable over the 160 years the coral grew. The record also shows that the coral manipulated its CF against SW to ensure skeletal accretion. Although the aragonite saturation state is decreasing in CF and SW together with a decreasing pH the coral still manages to show a stable liner extension rate. The coral records reveal that the coral is adapting to a changing ocean chemistry. Furthermore, declining δ^{13}C ratios and exceedingly high pCO_2 values of SW from the coral indicate the anthropogenic Suess-Effect influencing the ratio as well as enhanced diffusion of pCO_2 from SW into the coral.

Chapter 2.3 established a new age model for a new coral core taken from the La Parguera National Parc in Puerto Rico. The massive coral *Orbicella annularis* was cored in 2020 and δ11B was measured at a bi-weekly resolution with LA-MC-ICP-MS. The boron isotope record was compared to in-situ pH, SST, and SSS measurements from a buoy close by, that has been recording since 2009. The ultra-high resolution record goes back to 2013. The coral skeleton has been changes by boring organisms such as green algae, fungi, and cyanobacteria, thereby altering the skeletal δ^{11}B signal from 2015 on, when the skeleton shows very heavy boring and some secondary aragonite in certain boreholes. The boron isotope ratio is changes to heavier values that become evident in a pronounced change in mean of δ^{11}B values in the coral record. Nevertheless, the pristine part of the coral could still be used to establish a pH-δ^{11}B calibration for *Orbicella annularis*.

Chapter 3 summarizes the findings described in the manuscripts from the previous chapter and draws parallels between each Manuscript. Final conclusions are drawn circling back to the research hypothesis made in chapter one.

2 Manuscripts

Manuscript I

A warming southern Gulf of Mexico: Reconstruction of anthropogenic environmental changes from a *Siderastrea siderea* coral on the northern coast of Cuba

Authors: **Marie Habott**, Henry C. Wu, Henning Kuhnert, Carlos Jimenez, Patricia González-Díaz, Tim Rixen

Status: Published in Paleoceanography and Paleoclimatology'

Citation: Harbott, M., Wu, H. C., Kuhnert, H., Jimenez, C., González-Díaz, P., & Rixen, T. (2023). A warming southern Gulf of Mexico: Reconstruction of anthropogenic environmental changes from a Siderastrea siderea coral on the northern coast of Cuba. Paleoceanography and Paleoclimatology, 38, e2023PA004717. https://doi.org/10.1029/2023PA004717

Data citation: Harbott, Marie; Wu, Henry C; Kuhnert, Henning; Jimenez, Carlos; González-Díaz, Patricia; Rixen, Tim (2023): Stable isotope and trace element data for a Siderastrea siderea coral core CIM_C_2-2-1/CIM_C_2-2-2 from the Gulf of Mexico. *PANGAEA*, https://doi.org/10.1594/PANGAEA.963278

Manuscript II

Carbonate chemistry of seawater and calcifying fluid reconstructed from Cuban *Siderastrea siderea* from the Gulf of Mexico

Authors: **Marie Harbott**, Tim Rixen, Henning Kuhnert, Simone Kasemann, Anette Meixner, Carlos Jimenez, Patricia González-Díaz, Henry C. Wu

Status: Submitted to 'Scientific Reports' (second round of reviews)

Manuscript III

pH-δ^{11}B calibration from a pristine vs. infested *Orbicella annularis* from Puerto Rico compared to in-situ pH measurements

Authors: **Marie Harbott,** Sara Todorovic, Henry C. Wu, Grit Steinhöfel-Sasgen, Albert Bentin, Sherman Clark, Amos Winter

Status: Drafted and ready for submission to 'Geochimica and Cosmochimica Acta'

Authors Contribution

Manuscript I

1) Assessments of X-ray images for sampling
2) Sampling with Micro-drill and preparation of ca. 1000 samples from the Cuban coral core for Stable isotope measurements and trace element measurements
3) Measuring of trace elements in the facilities of ZMT with the Analytik Jena PlasmaQuant MS
4) Developments of 2 agemodels based on oxygen isotopes and Sr/Ca,
5) interpreted SST records
6) reconstructed $\delta^{18}O_{SW}$, $\delta^{18}O_{pseudo}$ and interpreted record, performed spectral analysis
7) Wrote manuscript and successfully published in 'Paleoceanography and Paleoclimatology'

Manuscript II

1) Microdrilled 160 annual samples and prepared ca 50 samples or $\delta^{11}B$ analysis at the Marum facilities
2) Measured boron isotopes with Laboratory Head Anette Meixner
3) Reconstructed pH and calculated DIC, TA, pCO2, and aragonite saturation state for seawater and calcifying fluid
4) Interpreted reconstructed records
5) Wrote the manuscript and leading the submission process to 'Scientific Reports'

Manuscript III

1) Evaluated best sampling path with Laser Ablation method
2) Prepared samples to thick slides for Laser Ablation chamber and mapped out sampling path on slides at the facilities of the Alfred Wegener Institute in Bremerhaven.
3) Interpreted results for changes in pH and boring activities of microorganisms
4) Wrote and prepared the manuscript for submission to 'Geochimica and Cosmochimica Acta'

2.1 A warming southern Gulf of Mexico: Reconstruction of anthropogenic environmental changes from a *Siderastrea siderea* coral on the northern coast of Cuba

M. Harbott[1*], H. C. Wu[1*], H. Kuhnert[2], C. Jimenez[3, 4], P. González-Díaz[5], and T. Rixen[1, 6]

[1] Leibniz Centre for Tropical Marine Research (ZMT) GmbH, Fahrenheitstraße 6, 28359 Bremen, Germany

[2] MARUM – Center for Marine Environmental Sciences, University of Bremen, Leobener Str. 8, 28359 Bremen, Germany

[3] Enalia Physis Environmental Research Centre, Acropoleos 2, Aglantzia 2101, Nicosia, Cyprus

[4] The Cyprus Institute. 20 Konstantinou Kavafi St, 2121 Aglantzia. Nicosia, Cyprus

[5] Centro de Investigaciones Marinas Universidad de La Habana, Calle 16 no.114 e/ 1ra y 3ra, Miramar. Playa, Ciudad de La Habana, Cuba

[6] Institute of Geology, University of Hamburg, Bundesstrasse 55, 20148 Hamburg, Germany

Corresponding author: Marie Harbott (marie.harbott@leibniz-zmt.de)

Henry C. Wu (henry.wu@leibniz-zmt.de)

Key Points:

- A massive coral was used as a paleoclimatic and -environmental archive for the reconstruction of SST and $\delta^{18}O_{SW}$
- Reconstruction reaches back 160 years from 1845 to 2005 and shows a warming south eastern GOM of 2.6 to 3.3°C
- A freshening of the southern GOM starting in the 1990s shows the onset of a phase shift to a positive AMO

Abstract

The Gulf of Mexico is a vital region for the Atlantic Meridional Overturning Circulation (AMOC), that fuels the exchange of heat between the tropics and the polar regions. A weakening of the AMOC would have dire consequences for the planet. First observations and ocean models show that this process has already started. Very limited knowledge on the components that are part of the AMOC such as the Loop Current (LC) make it difficult to understand its dynamics as well as changes in strength or temperature since the onset of the industrial revolution. Currently there are no continuous *in-situ* sea surface temperature or salinity measurements for the south-eastern Gulf of Mexico or reconstruction attempts for this region, showing the necessity for high resolution climate archives. A *Siderastrea siderea* coral core was retrieved from the north-western Cuban coast and used as a sub-seasonally resolved sea surface temperature and hydroclimate archive. The approach is based on skeletal $\delta^{18}O$ and trace and minor element contents shows an increase in temperature over 160 years since 1845 of 2.6°C to 3.3°C. A possible stagnation of the warming trend set in after the 1980s, indicating a potential weakening of the Loop Current. Impacts in SSS such as El Niño events in the Pacific region can still be detected in the Gulf of Mexico as decreases in salinity in 1998 from the reconstructed $\delta^{18}O_{SW}$ coral record. In-situ measurements remain crucial to understand the dynamics in the LC and its influence on the AMOC.

Plain Language Summary

The Atlantic Meridional Overturning Circulation (AMOC) is an important part of our climate system by exchanging heat between the northern and southern hemisphere. Changes in its strength, could have severe consequences for our climate system, like changes in rain patterns leading to droughts in Europe. The Gulf of Mexico (GOM) is supplying the AMOC with heat, it transports to the north. Due to the anthropogenic climate change, sea surface temperature and salinity of the GOM changed since the industrial revolution. However, measurements of these changes are rare. Paleoclimate and environmental archives such as coral cores can help to reconstruct those changes and better understand the anthropogenic climate change. Coral cores from massive corals act as archives and yield bi-monthly resolution, making it possible to reconstruct changes in seasonality as well as long term trends. The coral core used in this study shows an increase in sea surface temperature of 2.6 to 3.3°C from 1845 to 2005. In the 1980s we observe a halt in this increase in

temperature pointing towards a weakening of the part of the AMOC in the GOM. It is important to understand the first signs of a weakening AMOC and its consequences for our climate system.

2.1.1 Introduction

The Atlantic Meridional Overturning Circulation (AMOC) is a crucial component of global ocean circulation (Boeres et al., 2021; Dima et al., 2021). A projected decrease in the strength of AMOC will have profound impacts on global climate including a very likely AMOC strength decline in the 21st century. A rise in extreme event occurrences or abrupt climate change on human time scales are further alarming consequences of a weaker AMOC. The reason for the weakening AMOC can be found in the enhanced anthropogenic emission of CO_2 to the atmosphere and with that the warming of the ocean (Cheng et al., 2017; Roemmich et al., 2012). However, key information and understanding of the processes in the development of the AMOC since the 20th century remain unknown and impair our ability for more accurate predictions leading to larger uncertainties (IPCC AR6, 2021). A continuous direct measurement of the AMOC started only in 2004, yet decadal and interdecadal fluctuations need a higher time span to be accurately represented (Ceasar et al., 2021). Longer term reconstructions of the AMOC have to be based on proxy data reconstructions (Ceasar et al., 2021). Recent studies observed the first onsets of declining stability of the AMOC by changes in sea surface temperature (SST) and sea surface salinity (SSS) in the northern Atlantic Ocean (Boers, 2021; Ceasar et al., 2021; Dima et al., 2021; Smeed et al., 2018).

One important component of the AMOC is the Caribbean Current that transforms into the Loop Current (LC) once it reaches the Gulf of Mexico (GOM; Fig. 2.1.1). The LC enters the GOM via the Yucatan channel from the Caribbean Sea and joins the Florida Current, thereby providing the GOM with warm surface water (fig. 2.1.1) (Gordon, 1967). A decreased heat transport of the LC will result in reduced warming in the GOM (Liu et al., 2012). Thus, an overall weakening of the AMOC will lead to a weakened LC. However, the spatial and temporal distribution of SST and SSS for the GOM are not homogenous in its latitudinal distribution. Recent satellite-derived SST observations indicate a warming of the LC in the central GOM since 1985, whereas the shelf areas of Florida and Cuba indicate a cooling trend between 1985 and 2009 (Chollett et al., 2012).

2.1.1.1 Interannual and interdecadal oscillation

The tropical western Atlantic, the Caribbean basin, and the Gulf of Mexico are also influenced by competing forcings influencing SST and SSS records, notably the El Niño Southern Oscillation (ENSO), the North Atlantic Oscillation (NAO), and the Atlantic Multidecadal Oscillation (AMO) (Enfield and Mayer, 1997, Giannini et al, 2000 & 2001, Wang et al., 2008).
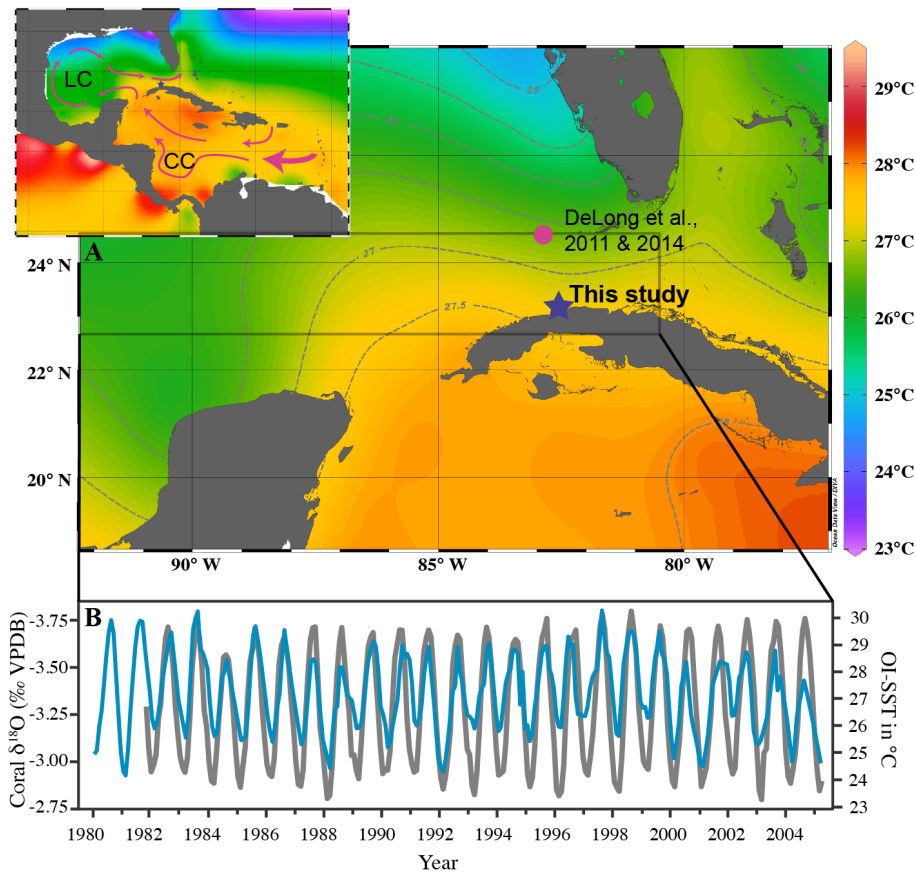
Figure 2.1.1: A-Interpolated SST (annual average from 1955-2017) temperature from the World Ocean Atlas 2018 1° x 1° grid in Ocean Data View. Red Arrows representing the Caribbean Current (CC) entering the GOM via the Yucatan channel and transporting warm surface water to the GOM. The Loop Current (LC) exits the GOM and joins the Florida Stream (Gordon, 1967, Liu et al., 2012). B –Light grey line representing OI-SSTv2.1 for the southern GOM from 80.5°W to 96.5°W and 22.5°N to 24.5°N compared to coral δ^{18}O from this study.

The ENSO teleconnection between the Pacific and Atlantic has different effects on different parts of the tropical Atlantic. During the mature phase of an ENSO event, a seesaw pattern between the Sea Level Pressure (SLP) over the eastern Pacific and equatorial Atlantic forms. This SLP pattern leads to a divergent atmospheric flow over the Caribbean on a southwest-northeast axes from the convergent eastern Pacific during the mature phase of the ENSO (Giannini et al., 2000). While the ITCZ shifts further south in January and February of the following year of an ENSO event a negative SLP anomaly forms south of the eastern coast of the US, leading to intensified precipitation over the GOM (Giannini et al., 2000). The formation of the low SLP over the southern USA leads to weaker meridional atmospheric flow and an increase in SST over the Caribbean basin (Giannini et al., 2000). It has been shown that teleconnections across Central America induced precipitation changes in the Atlantic Ocean during EN years reacting to changes in the Pacific Ocean with a delay of one season (Giannini et al., 2000). While the ITCZ shifts further south in January and February of the following year of an ENSO event, a negative SLP anomaly forms off the south eastern Coast of North America over the GOM, leading to intensified precipitation over the GOM. Cuba in the southern GOM will therefore be more likely to experience an increase in precipitation in the spring and summer after a severe EN event (Giannini et al., 2000). A clear signal of the ENSO teleconnection is not always visible in proxy data since counteracting forces such as the NAO might reduce the effect of ENSO on Caribbean precipitation.

During a positive NAO phase, the North Atlantic High is relatively strong during the winter leading to stronger trade winds in the equatorial Atlantic and with that to a cooling of the ocean's surface, counteracting the warming effect of a warm ENSO event (Giannini et al., 2001). A strengthening of a warm ENSO effect is observed when NAO is in a negative phase (Giannini et al., 2001).

The AMO is defined by oscillatory SST anomalies in the North Atlantic with coherent natural variability at 30-80 years. The positive (negative) phase of the AMO is associated with positive (negative) SST anomalies in the Atlantic Warm Pool (AWP), a large body of warm water including the GOM, the Caribbean Sea, and the western tropical North Atlantic (Wang et al., 2008). A warm phase of the AMO will lead to a larger AWP, which favors the formation of Atlantic tropical cyclones (Enfield, 2008). Over the GOM the warm phase of the AMO is characterized by more

precipitation compared to the cold phase (Goly et al., 2014). Cold AMO periods were registered approximately from 1900-1925, 1965-1994, while warm phases occurred from 1875-1899, 1926-1965, and 1995 to present (Alexander et al., 2014).

2.1.1.2   Current best practice

In-situ continuous SST and SSS measurements are relatively sparse in the tropical oceans and especially in the southern GOM (Chollett et al., 2012). Moreover, the lack of long-term in-situ measurements impedes the understanding of regional changes of the LC to project future trends of the region. Without such records, potential cooling or warming and weakening or strengthening of the LC in the GOM cannot be properly assessed and forecasted (DeLong et al., 2014; Liu et al., 2012). Additionally, extreme temperature changes due to the current anthropogenic climate change are already taking its toll on marine organisms, leading to mass coral bleaching events and thereby destroying entire coral reef ecosystems (Hughes et al., 2018). Besides providing the foundation of coral reef ecosystems, corals are also an important archive for reconstructing climate and environmental changes. By recording environmental factors such as SST and SSS in their skeletal materials, corals have been shown to be effective for the understanding of regional to large-scale ocean and climate variabilities.

Currently, several studies have published SST and SSS reconstruction from planktonic foraminifers in the GOM (Flower and Kennett, 1990; Lund and Curry, 2004; Poore et al., 2003; Richey et al., 2007; Richey et al., 2009; Schmidt et al., 2012). However, these sediment core-based records are only able to resolve climate at a low-resolution limiting our knowledge of seasonality, interannual, and interdecadal variability. The previously published high-resolution climate reconstructions from coral archives are also limited to the Dry Tortugas Island in the northern GOM (DeLong et al., 2011, 2014; Maupin et al., 2008). Furthermore, none of these studies attempted to reconstruct hydrological influences such as SSS, an important indicator for the strength of the AMOC (Boers, 2021; Dima et al., 2021). The studies conducted in the Dry Tortugas region point towards a stagnating warming after 1985, confirming a weakened warming in the GOM and with that a possible slowdown of the LC (Delong et al., 2014). However, other studies and climate models indicate a warming of the southern GOM, including north of Cuba, only a few

hundred kilometers away from Dry Tortugas (Chollett et al., 2012). To understand how large-scale and local climate phenomena influence these regions, local high-resolution climate reconstructions are necessary.

2.1.1.3 Scleractinian corals as climate archives

Sr/Ca and $\delta^{18}O$ records of *S. siderea* have been verified as accurate and reliable climate archives in previous studies (Guzman and Tudhope, 1998; Delong et al., 2011, 2014; Maupin et al., 2008; Rodriguez et al., 2019). The coral-based proxy records have been shown to be in coherence with regional climate variability allowing for the development of long continuous records of reconstructed SST in the GOM region (Delong et al., 2011, 2014; Maupin et al., 2008). Coral skeletal Sr/Ca and $\delta^{18}O$ ratios are the most widely used proxies for SST and hydroclimate (i.e., a mixture of freshwater and evaporation, and hence SSS). Coral skeletal $\delta^{18}O$ is dependent on SST and the $\delta^{18}O$ of seawater. By using Sr/Ca that is primarily temperature-driven, the temperature component in $\delta^{18}O_{coral}$ can be subtracted, yielding $\delta^{18}O_{SW}$ (Ren et al., 2002).

While growing, corals reflect the chemistry of the surrounding seawater in their aragonite skeletal composition. Cations in the ambient seawater, particularly those chemically similar to calcium (Ca^{2+}) such as strontium (Sr^{2+}), are incorporated in trace to minor amounts in the coral skeleton (Bradley & Elias, 2015). In relatively colder environments corals increasingly incorporate Sr and therefore the Sr/Ca ratio will increase (S. V. Smith et al., 1979b). The Sr/Ca ratio of seawater is spatially homogenous with only minor depth gradients, and it is stable on the time-scale considered here (de Villiers et al., 1994).

2.1.1.4 Aim of the study

This study uses a multi-proxy approach of a *S. siderea* coral to reconstruct changes in SST and $\delta^{18}O_{sw}$-SSS from the northern coast of Cuba. The coral archive and reconstructed climate variability span the period from 1845 to 2005. High-resolution reconstructions of climate variabilities have been scarce in this region. This study will calibrate and apply different coral-based proxy reconstructions of SST using the $\delta^{18}O$ values, and Sr/Ca relationship to assess

reliability of each proxy. Moreover, coral-based $\delta^{18}O_{sw}$ based on paired coral skeletal $\delta^{18}O$ and Sr/Ca is compared to gridded instrumental SSS. Finally, we aim to establish possible evidence of anthropogenic climate change imprint and the weakening signal of the AMOC in this region.

2.1.2 Materials and Methods

2.1.2.1 Coral retrieval and sampling

In July 2005, a 53 cm long coral core was collected from the center growth axis of a *S. siderea* colony off the northern coast of Havana, Cuba (82.4239W, 23.1277N; Fig. 2.1.1) at 6 m depth. The sample was cored along the maximum growth axis of the coral to secure a continuous record and transported to the Leibniz Centre for Tropical Marine Research (ZMT) in Bremen, Germany. Slabs measuring 5 mm were removed from the coral core half with x-radiograph imaging completed at the Zentrum für moderne Diagnostik (ZEMODI, Bremen, Germany) to reveal internal growth structure to guide sampling transect selection (Fig. 2.1.2)(DeLong et al., 2013). The x-radiograph positive images revealed the density banding couplets of the coral as well as the orientation of the individual polyps. Prior to microsampling, the individual slabs were cleaned in an ultrasonic bath with 18.2 Ω milliQ water. Each individual wash lasted 5 minutes and the process was repeated for 3 wash cycles on each slab. The slabs were dried for at least 24 hours at room temperature. A continuous theca wall of an individual coral polyp identified on the x-ray images was microsampled by milling for skeletal powder material (Fig. 2.1.2). The vertical linear extension rate of the *S. siderea* used in this study was 3-8 mm year^{-1}. The sampling intervals of 0.5 mm on the vertical growth axis yielded up to 1.5 mg of skeletal aragonite powder for bimonthly-resolved geochemical analysis. The powder samples were collected with a Proxxon drill fitted with a 0.4 mm diameter diamond tipped drill bit operated at low speed on an independent x-y-z directional stage. The sampling path is 1 mm in depth and 2 mm wide consisting of theca wall material. Although great care was taken to avoid admixtures from other skeletal elements, we cannot rule out that powder from the columella may have occasionally been included in minor amounts.
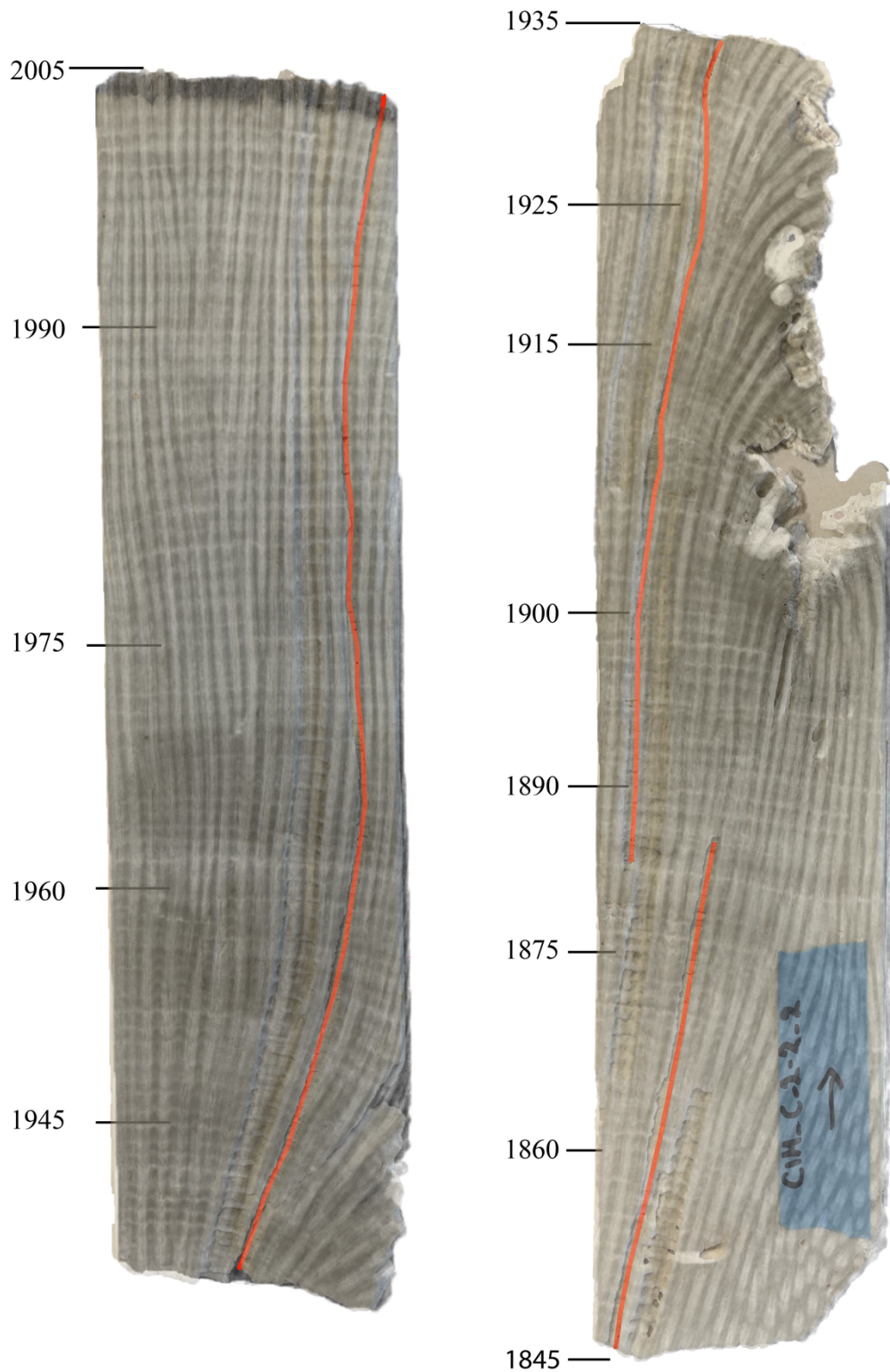
Figure 2.1.2: X-ray positive image over a photo of the sampled coral (wider sampling paths were sampled for yearly resolution and sampled over 2 polyps and are not included in this study) of the Cuban Siderastrea siderea coral core slabs with optimized sampling transects

indicated in red following a single polyp thecal wall for most of the core across multiple slabs.

2.1.2.2 Stable isotope analysis

Stable isotope measurements were analyzed individually at 0.5 mm intervals at the MARUM-Centre for Marine Environmental Sciences of the University of Bremen, Bremen, Germany. For each coral skeletal powder sample, approximately 60-120 μg of powder was dissolved in ~105% H_3PO_4 at 75 ºC in an automated carbonate preparation device (Finnigan Kiel I or ThermoFisher Kiel IV), generating CO_2 gas that was then analyzed on a Finnigan MAT 251 or ThermoFisher MAT 253plus isotope-ratio mass spectrometer. Calibration and correction of offsets due to inter-machine differences were based on measurements of the Solnhofen limestone 2008 in-house standard, which itself was calibrated against NBS 19. The isotopic values are reported in ‰ versus the Vienna Peedee Belemnite (VPDB) reference scale. Repeat analyses of the house standard yielded a standard deviation of ±0.05‰ for $\delta^{18}O$. Following common practice, no correction was applied to account for the constant offset when measuring aragonite on a system calibrated with calcite.

2.1.2.3 Trace elements analysis

The elemental composition was measured on an Analytik Jena Plasma Quant MS Elite Inductively Coupled Plasma - Mass Spectrometer (ICP-MS) at ZMT from splits of the same coral skeletal powder as were the stable isotopes. Ultrapure 2% HNO_3 (2 mL) was added to digest 500 μg of coral skeletal powder, shaken and dissolved for at least 24 hours. An aliquot of 0.6 mL from the initial solution was diluted further with 0.6 mL of 2% ultrapure HNO_3 to reach a calcium concentration of approximately 50 ppm. An in-house internal coral standard (dissolved coral *S. siderea* skeleton from the north Cuban coast) as well as JCp-1 were diluted to reach a similar concentration in Ca of 50 ppm to be measured alongside the coral samples. To reduce interferences, we applied the internal gas mode for the isotopes ^{88}Strontium, ^{24}Magnesium, $^{43/44}$Calcium, ^{137}Barium, and ^{238}Uranium (Tech Note v1.17, Analytik Jena). The collision gas mixture of H_2 and He decreases the interferences and increases the signal to noise ratio. For the isotopes ^{7}Lithium and $^{10/11}$Boron, the application of the gas mode would lead to a loss of sensitivity, therefore the gas mode was not used for these two elements (Tech Note v1.17, Analytik Jena).

Certified single element stock solutions from Inorganic Ventures were used for the calibration of each individual element. Five calibration solutions of different concentrations for the different elements except Ca were prepared from one stock solution that was used over one week. Ca concentration remained the same for all calibration solutions and was added after diluting the stock solution to the different concentrations. After every fifth sample measurement on the ICP-MS, brackets of laboratory standards (a JCp-1, an in-house coral standard, and a consistency standard similar in concentration to our average value calibration solution) were measured to correct for instrumental drift (Schrag, 1999). Instrumental precision is ±0.35% relative standard deviation for Sr/Ca, 1.23% for Li/Mg, 0.36% for Mg/Ca and, 1.83 % for U/Ca. For outliers, the measurement was repeated and the average of all repetitions was calculated. Our average JCP-1 Sr/Ca value is 8.84 ±0.03 mmol/mol (1σ, n = 273), 4.19 ± 0.015 mmol/mol for Mg/Ca (1σ, n = 273), 1.19 ± 0.02 µmol/mol for U/Ca (1σ, n = 273), and 1.6 ± 0.02 mmol/mol for Li/Mg (1σ, n = 273).

2.1.2.4 Chronology

We established an initial age model based on the clear annual density banding revealed by the x-radiograph positive image with the top of the colony corresponding to 2005, the year of collection (Fig. 2.1.2). By comparing the estimated age to the seasonal variations in $\delta^{18}O$ and Sr/Ca, the depth to age relationship was confirmed. The highest $\delta^{18}O$ and Sr/Ca values correspond to the winter growing season and were assigned to February, the coldest month on average, and the lowest $\delta^{18}O$ and Sr/Ca values were assigned to August corresponding to the peak summer month. For the most recent record beginning in November 1981, the highest and lowest $\delta^{18}O$ and Sr/Ca values were assigned to the coldest and warmest month respectively of the gridded OISSTv2.1 (Huang et al., 2020) (Fig. 2.1.3 A); the same was done for intermediate points in spring and autumn, provided the growth rate of the coral gave the necessary temporal resolution. For each year 2 to 4 points were assigned to corresponding months from the OISSTv2.1 gridded data product (Huang et al., 2020).

The ages for the remaining samples were linearly interpolated based on spatial distances between age tie points, and x-radiograph imaging. Since both annual banding pattern, $\delta^{18}O$ and Sr/Ca seasonality are clear and regular, we do not consider the possibility of age errors on the time scale

of years. However, the assumption that SST extremes always fall onto the same months introduces a non-cumulative error of ±1 month for each sample.

For comparison with instrumental data and further statistical analyses we interpolated our time series to equidistant, monthly, resolution using the Arand software Ager and Timer (Howell et al., 2006). Annual averages were calculated from these interpolated values. For anomaly calculations, the time interval from 1950 to 2000 was used as the reference period.

Outliers were identified through the outlier detection method provided by Chen and Liu (1993) on the by Arand interpolated geochemical data. The time series is described by a fitted general autoregressive moving average model. Outliers are identified in 3 steps: first, all potential outliers are identified based on preliminary model parameters , second, joint estimates of model parameters and outliers are detected and significant (threshold 0.001) outliers are removed and the parameter estimates are adjusted after removal of outliers. In the third step the original series is filtered based on the adjusted parameters from step two and with the new residuals go through steps 1 to 2. The linear regression methods were then used on the outlier corrected data

The geochemical and isotopic time series of this *S. siderea* coral span from 1845 to 2005 for a total of 160 years.

2.1.2.5   Calibration to SST

Coral $\delta^{18}O$ and Sr to Ca ratios were calibrated to the 0.25º by 0.25º gridded OI-SST (Reynolds et al., 2007; Huang et al., 2020, NOAA High Resolution SST data provided by the NOAA/OAR/ESRL PSL, Boulder, Colorado, USA, from their Web site at https://www.ncei.noaa.gov/data/sea-surface-temperature-optimum-interpolation/v2.1/access/avhrr/) centered at 82.375 °W and 23.125 °N. The calibration period is 1981 to 2005 (Fig. 2.1.3). We chose to only display $\delta^{18}O$ and Sr/Ca results for their robust regressions to OI-SST 2.1 (Reynolds et al., 2007; Huang et al., 2020). Additional element to Ca ratios calibrated to OI-SST based on the $\delta^{18}O$ and Sr/Ca age models can be seen in the supplementary materials tables S1 A and B.

Outlier detection was based on the iterative outlier detection and adjustment procedure of Chen and Liu (1993) and incorporated into the R package "*Forecast*" (Hyndman and Athanasopoulos, 2018). It was applied to the time series generated by Arand (further explanation how Arand was used, can be found in section 2.5) (Howell et al., 2006). The ordinary least square (OLS) regression method has been one of the most commonly used regression techniques for the development of the reconstruction of SST from element to Ca ratios and δ^{18}O. This regression technique only assumes an error for the dependent variable and an error of zero for the independent variable, while other regression methods such as weighed least square, reduced major axis (RMA), and bootstrapped weighed least square (BWLS) developed by Xu et al. (2015) account for errors on both axes. Unfortunately, there is still no common approach for the coral-based paleoceanography community on which technique to use thus leading to differences in regressions for the same species and regions (Xu et al., 2015). After testing the data for homoscedasticity, the OLS method was chosen.

Error assessment for the Sr/Ca and δ^{18}O to SST calibration can be reviewed in supplementary materials. The analytical errors of Sr/Ca and δ^{18}O were propagated with the in table 2.1.2 (in supplementary materials) reported regression errors and yielded the overall errors of ±0.05°C for δ^{18}O and 0.21°C for Sa/Ca.

2.1.2.6   Reconstructed $\delta^{18}O_{SW}$

δ^{18}O of seawater ($\delta^{18}O_{SW}$) reconstruction from coral skeletal δ^{18}O ($\delta^{18}O_C$) assumes that $\delta^{18}O_{Coral}$ is a function of both SST and $\delta^{18}O_{SW}$, while variations in Sr/Ca depend on SST primarily. Thus, the reconstruction method as described by Ren et al. (2002) is important to note that instantaneous changes in $\delta^{18}O_C$ are the sum of two components, where one component describes the changes in SST, whereas the other contribution influences instantaneous changes in $\delta^{18}O_{SW}$ (Ren et al., 2002).

$$\Delta\delta^{18}O_C = \Delta\delta^{18}O_{(SST\ contribution)} + \Delta\delta^{18}O_{(SW\ contribution)}$$
$$= \Delta(\partial\delta^{18}O_{(C)}/\partial SST)*\Delta SST$$
$$+ (\Delta\partial\delta^{18}O_{(C)}/\Delta\partial\delta^{18}O_{(SW)})*\Delta\delta^{18}O_{SW}, \qquad [2.2.1]$$

$\triangle \partial$ $\delta^{18}O_{(C)}$ /∂SST is the rate of change of -0.22‰ per °C for the formation temperature of carbonates and the oxygen isotopic equilibrium, a mean based on 19 coral calibrations (Lough, 2004). For Siderastrea coral a slope of -0.043 mmol/ mol per °C was applied, following the master coral regression of DeLong et al. (2014) for the rate of change $\triangle \partial$ $\delta^{18}O_{(C)}$/ $\triangle \partial$ $\delta^{18}O_{(sw)}$. Eq. (1) only yields relative changes instead of absolute values. By adding up the changes gained by Eq. (1) to the $\delta^{18}O_{SW}$ reference value from the GOM of 1.84‰, it is possible to reconstruct the variation for this region (Lowenstam and Epstein, 1957). Error propagation can be found in the supplementary materials. The error for $\delta^{18}O_{SW}$ is ±0.2 ‰ and was calculated from the combined error of the analytical errors of $\delta^{18}O$ and Sr/Ca as well as the calibration errors from the OLS regressions.

2.1.2.7 Pseudo Coral forward modeling

Variations in $\delta^{18}O_C$ depend on both local SST and $\delta^{18}O_{SW}$ at the time of growth. In order to estimate the influence of both environmental factors on coral skeletal $\delta^{18}O$ ratios, a forward modelling exercise was applied by generating a pseudo-coral model. A pseudo-coral proxy or pseudo coral forward model is a bivariate model comparing observed $\delta^{18}O_C$ with predicted $\delta^{18}O_C$ from a linear model driven by instrumental data of the 20th century (Thompson et al., 2011). This bivariate model yields the following equation (Thompson et al., 2011):

$$\delta^{18}O_{Pseudocoral} = a_1 \, SST + a_2 \, SSS \qquad [2.2.2]$$

where a_1 = -0.22 ‰ °C^{-1}, describing the effect of formation temperature on carbonate oxygen isotopic composition (Lough, 2004), and a_2 is the empirical slope of $\delta^{18}O_{SW}$ versus SSS (0.15 ‰ per salinity unit) for the tropical Atlantic reported by LeGrande and Schmidt (2006). The SST and SSS used for this model are from the following instrumental data products: SST, OI-SST v2.1 (Huang et a., 2021; Reynolds et al., 2007); SSS, SODA v2.1.6 (Carton and Giese, 2007).

2.1.3 Results and Discussion

2.1.3.1 Age model comparison of $\delta^{18}O$ and Sr/Ca with instrumental SST

In this study we developed two different age models based on $\delta^{18}O$ and the more established Sr/Ca (Figure 2.1.3) (Maupin et al., 2008; DeLong et al., 2011;2014, Fowell et al., 2016, Weerabaddana et al., 2021). In addition, the Sr/Ca-OI-SST slope (for the Sr/Ca age model) fits into the slope range reported by DeLong et al. (2011) with a rate of change of 0.045 mmol/mol per °C (±0.006°C) (Figure 2.1.3 C). Both reconstruction attempts (based on the $\delta^{18}O$; Figure 2.1.3 A and B; and Sr/Ca-age models; Figure 2.1.3 C and D) show an increase in temperature from 1845 to 2005. Although Sr/Ca is the more established proxy for temperature reconstruction for this region, $\delta^{18}O$ shows a more promising fit for the OI-SST regression (Tables S1 and S3) (Maupin et al., 2008; Delong et al., 2011;2014; Fowell et al., 2016; Weerabaddana et al., 2021) (all results for both age models can be found in the supplementary materials). The better fit to OI-SSTv2.1 might be due to the highest temperature occurring during the same month as the maximum precipitation rate (Jury et al., 2007), since $\delta^{18}O$ is both, a proxy for temperature and $\delta^{18}O_{SW}$ (Rend et al., 2002). The pseudo coral model shows a correlation coefficient between the model and OI-SST2.1 of 0.98, indicating a stronger influence of SST on the corals $\delta^{18}O$. Therefore, we have decided to base our analysis on the $\delta^{18}O$ age model. All results based on the Sr/Ca age model can be found in the supplementary materials.
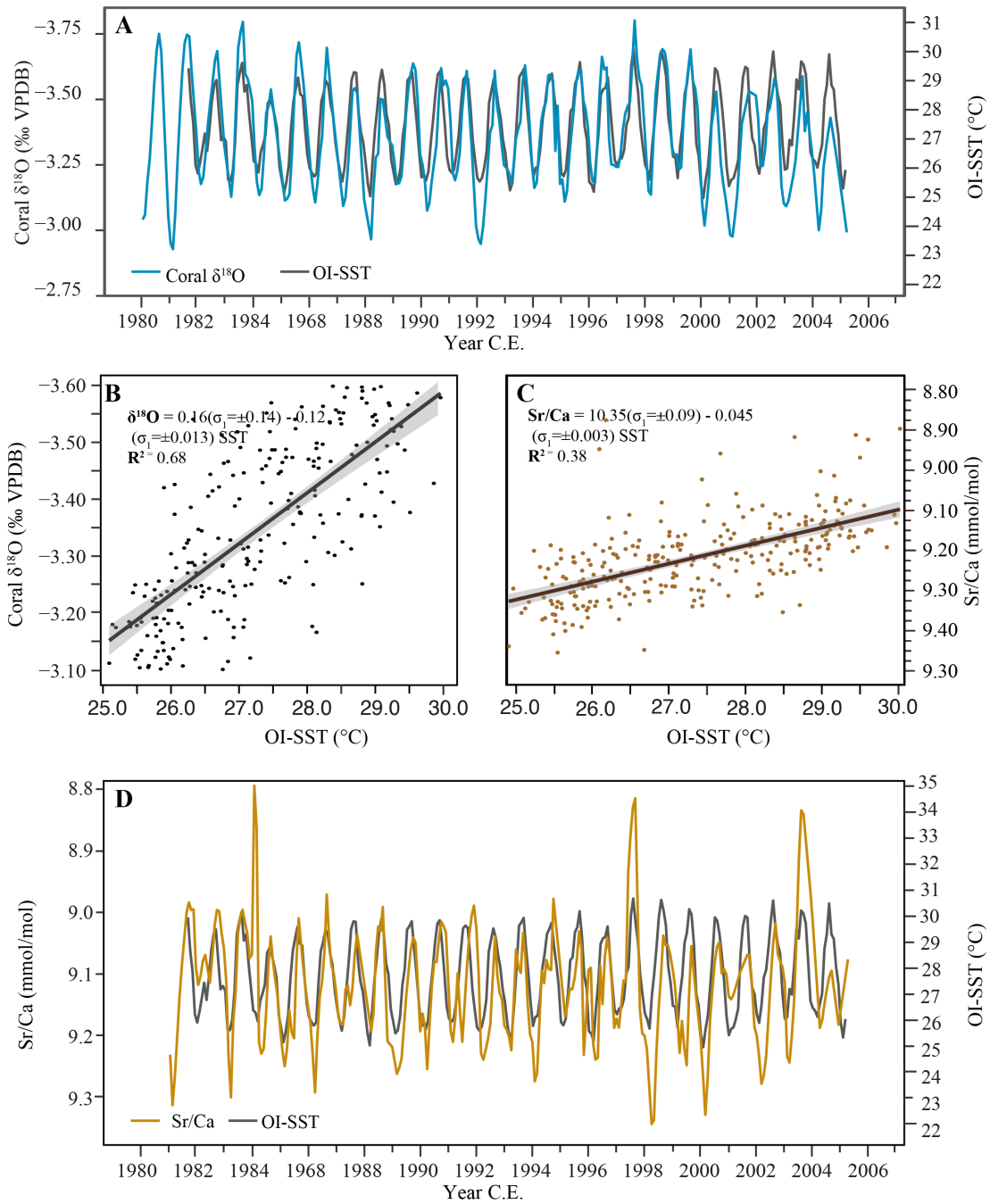
Figure 2.1.3: Coral $\delta^{18}O$ ratios transformed to age domain, based on $\delta^{18}O$ age model, plotted with the gridded OI-SSTv2.1 product from the grid cell centered at 82.375 °W and 23.125 °N (Huan et al., 2021; Reynolds et al., 2007). B-Regression of Coral $\delta^{18}O$ and OI-SST (Huang et al., 2020). C- Regression of Coral Sr/Ca, based on Sr/Ca age model, and OI-SST (Huang et al., 2020). The Pearson correlation coefficients as well as the regression equation are summed up in Table 2.1.2 /in supplementary materials). The gridded product OI-SSTv2.1 was used for the calibration of the proxy due to the lack of instrumental records for this

region. D- Sr/Ca ratios transformed to age domain, based on Sr/Ca age model, plotted with the gridded OI-SSTv2.1 product (Huan et al., 2021; Reynolds et al., 2007).

Table 2.1.1: Trend of temperature and hydroclimate proxies over time and their significance and change per decade in °C for each proxy reconstructed SST. The year variable refers to the year and decimal month. R is the Pearson correlation coefficient.

Proxy	r	p-value	Trend over time	Total temperature increase from linear regression °C
$\delta^{18}O_{coral}$	-0.4	**<0.001**	$\delta^{18}O = -0.002\ (\pm0.0001)\ yr + 0.52\ (\pm0.19)$	0.16
$\delta^{18}O_{SW}$	0.18	**<0.001**	$\delta^{18}O_{SW} = -0.0014\ (\pm0.0002)\ yr\ -1.12\ (\pm0.40)$	
$\delta^{18}O_{pseudo}$	-0.05	0.09	$\delta^{18}O_{pseudo} = -0.003\ (\pm0.004)\ yr + 8.05\ (\pm7.23)$	0.20
Sr/Ca	-0.28	**<0.001**	$Sr/Ca = -0.0007\ (\pm0.00004)\ yr + 10.51\ (\pm0.94)$	0.21
Li/Mg	0.03	0.19	$Li/Mg = 0.00009\ (\pm0.00007)\ yr + 1.63\ (\pm0.01)$	-0.03
U/Ca	-0.24	**<0.001**	$U/Ca = -0.0004\ (\pm0.00003)\ yr + 2.00\ (\pm0.06)$	0.15
Mg/Ca	0.33	**<0.001**	$Mg/Ca = 0.002\ (\pm0.0001)\ yr + 0.06\ (\pm0.23)$	0.30
Sr-U	-0.24	**<0.001**	$Sr-U = -0.0004\ (\pm0.00004)\ yr + 9.95\ (\pm0.07)$	0.04
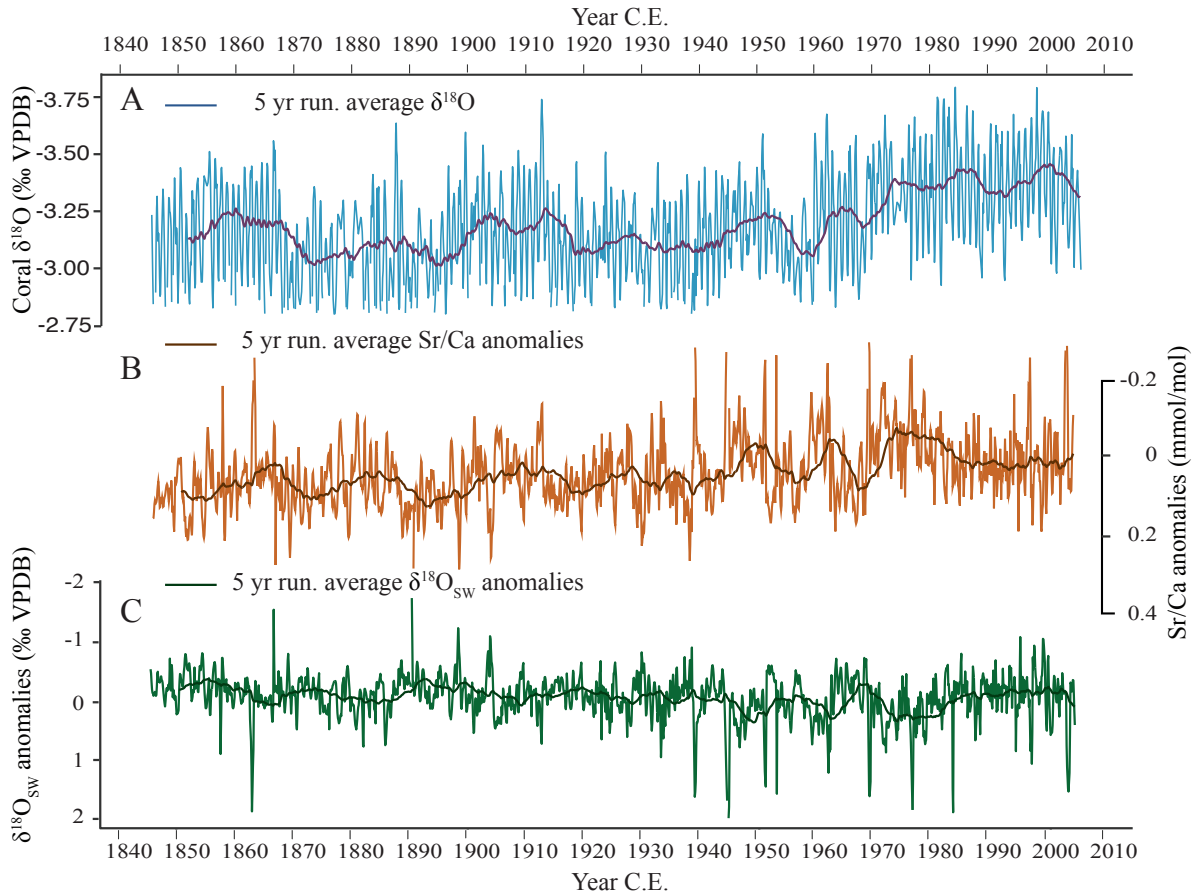
Figure 2.1.4: A-$\delta^{18}O$ inversely plotted and transformed into the age domain with a 5 year running average plotted at the end of the respective 5 year period. Total temperature increase from linear regression in Table 2.1.1 is 2.6 °C over 160 years. B-Sr/Ca anomalies with 5 year running averages plotted at the end of the respective 5 year period. Anomalies were calculated with the climatological mean from 1950-2000. A temperature increase of 3.3°C from the regression in Table 2.1.1 over 160 years was calculated. C- $\delta^{18}O_{SW}$ ratios calculated with $\delta^{18}O$ and Sr/Ca (equation 2). Anomalies were calculated with the climatological mean from 1950-2000.

The two age models developed for this study based on $\delta^{18}O$ and Sr/Ca agree on an increase in temperature over the 160 year time span from 1845 to 2005. For the respective grid cells encompassing our location, both OI-SST (1988-2005) and ERSST (1854-2005) indicate no significant increase in SST (Reynolds et al., 2002; Smith and Reynolds, 2004). This disagreement between coral-based SST and gridded SST products has been previously observed in the Caribbean and across many other regions in the Pacific (Evans et al., 2000, Kilbourne et al., 2008, Vásquez-

Bedoya et al., 2012). The discrepancy between coral SST reconstructions and the gridded SST data of OI-SST and Extended Reconstructed Sea Surface Temperature version 4 (ERSST; Huang et al., 2017) may be due to the spatial averaging of the SST values across the grid cell. By using gridded SST products instead of *in situ* measurements, local SST signals are suppressed by averaging over 2º by 2° (ERSST) or 0.25° by 0.25° (OI-SST). Furthermore, we would not recommend using annually averaged data for the calibration of temperature proxies since this would lead to a loss of information for the extreme values. Unfortunately, *in situ* measurements are not available for the northern Cuban coast. Despite the lack of similar secular trends, verification of our coral-based δ^{18}O-SST reconstruction with the gridded ERSST yields a correlation coefficient of (r) = 0.54 for the period 1854-2005. Another significant correlation (r = 0.36; p < 0.001) was also recorded between Sr/Ca-SST and ERSST.

2.1.3.2   *Warming of the southern GOM*

Illustrating the quality of the massive coral's ability to record SST, the environmental proxies derived from this northern Cuba *S. siderea* coral skeletal δ^{18}O, Sr/Ca, U/Ca, Mg/Ca, and Sr-U all indicate strong correlations to SST (Table 2.1.3 in supplementary materials). SSTs reconstructed over the period 1845 to 2005 differ between proxies, with the overall warming ranging from 0.7 to 3.32 °C (±0.21°C), equivalent to 0.04 to 0.21 °C per decade (Figs. 2.1.4 and 2.1.5).

The magnitude of SST change reconstructed from Sr/Ca and δ^{18}O from the southern GOM (Fig. 2.1.4 A and B) in this study appear relatively larger compared to previous studies conducted in the northern GOM at Dry Tortugas (DeLong et al., 2014, Maupin et al., 2008). Taking the more conservative regression equations of previous studies from the northern GOM and the data of this study yields a temperature increase of 0.95-2.38 °C from 1845-2005 (DeLong et al., 2014; Maupin et al., 2008). In the western Caribbean Sea on the Mesoamerican Barrier Reef of Belize, the temperature increase based on Sr/Ca-SST was similarly consistent with only a warming of 0.05-0.14°C per decade over the past 160 years (Fowell et al., 2016). The most extreme temperature increase in the southern GOM is found from the δ^{18}O- and Sr/Ca-SST of this study with a rate of warming equaling 2.62 (±0.05°C)to 3.32 (±0.21)°C (3.32 °C for Sr/Ca) or 0.21 ºC per decade.

Although coral $\delta^{18}O$ is reflecting the combined changes in SST and $\delta^{18}O_{SW}$, the magnitudes of the SST increases reconstructed from $\delta^{18}O$ and Sr/Ca agree.

To further verify coral $\delta^{18}O$ sensitivity to SST at this location, a forward modelling approach using a pseudo-coral model (Dee et al., 2017; Thompson et al., 2011) was tested and confirmed that local SST can explain up to 98% of the variability in coral skeletal $\delta^{18}O$. This validates the fidelity of *S. siderea* coral skeletal $\delta^{18}O$ as a stronger recorder for SST at this location than for $\delta^{18}O_{SW}$ and parallel salinity changes. However, a difference in the temperature trend can be observed between $\delta^{18}O_{coral}$ and $\delta^{18}O_{pseudocoral}$. The pseudo coral forward model exhibits no significant ($p = 0.09$) temperature trend over the 160 years of reconstructed record.

At Dry Tortugas in the northern GOM, DeLong et al. (2014) reported a significant temperature increase of 0.7 °C from 1952 until 1985 based on a reconstruction from a *S. siderea* coral core. This late 20th century trend is in agreement with our data from the southern GOM of Cuba with a contemporaneous warming between 0.49 °C based on Sr-U-SST up to 0.68 °C from Sr/Ca-SST (Table 2.1.3).

A visual shift (Figure 2.1.4 and 2.1.5) in reconstructed SST can be observed after 1980 where the reconstructed $\delta^{18}O$-SST reached a plateau equating to a pause in warming. Reconstructed Sr/Ca-SST and Sr-U SST even suggest a slight decrease in SST up to the year 2005. Quantifying the significance of this change is difficult due to the shortness of this trend at the end of the record. However, the results are consistent with the findings of DeLong et al. (2014) that described a discontinuation of warming SST after 1985 and attributed it to the possible slowdown of the LC.
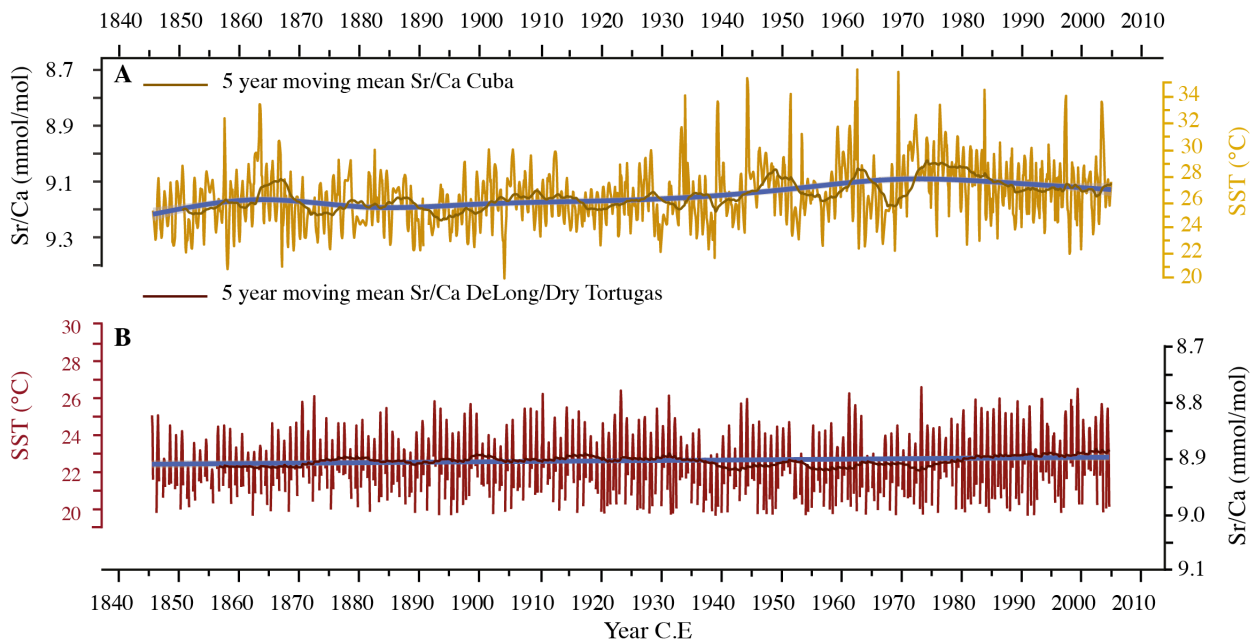
Figure 2.1.5: A-Sr/Ca (based on the $\delta^{18}O$ age mode) and reconstructed temperatures from Sr/Ca regression. B – Master Coral record from DeLong et al. (2014), averaged of Sr/Ca time series of 3 different corals from the Dry Tortugas National Park.

2.1.3.3 Long-term SST trend linked to LC and AMOC

Ocean models show a weakening of the LC that is consistent with the 20-25% reduction of the AMOC strength from the late 20st century to the late 21st century (Liu et al., 2012). Multiple proxy records produced by Caesar et al. (2021) based on changes in the heat transport reconstructed from a variety of ocean and land-based proxies (sortable silt data, coral, foraminifera, tree rings, ice cores), suggest an unprecedented decline in the last 2000 years of AMOC strength since the 20th century. Evidence indicating a weakening of the AMOC such as the Florida Current and the Gulf of Mexico transport have declined the fastest during the last 2 decades (Piecuch, 2020). While the LC still warms the southern GOM, it does not reach the northern GOM due to the weakening. The longer-term trend for the northern GOM is confirmed by 25 years of satellite data. The warm Caribbean basin water still reaches the southern GOM leading to a warming in that region (Chollett et al., 2012). It is possible that a lack of in-situ measurements in the southern GOM as well as the averaging of SSTs in gridded data biased towards a loss of warming trend of the southern GOM.

Summer warming has increased more than winter warming leading to a larger seasonality as observed by satellite data for the Caribbean Sea and the GOM (Chollett et al., 2012). This is in

agreement with the reconstructed SST observed from our coral colony. While the seasonal amplitude before a calculated change point in 1968 was 2.49 °C, it increased to 3.26 °C after 1968 (based on the seasonality means of all proxies and a change point analysis based on a detection algorithm provided in the R package Strucchange)(Otto et al., 2019, Zeileis et al., 2002). The observed hiatus of the warming trend may be indicating a slowdown of the LC, in agreement to the observations of DeLong et al. (2014) from the northern GOM due to a possible weakening of the AMOC (Boers et al., 2021, Dima et al., 2021). However, the extended OI-SST record for this northern Cuba location indicate the resumption of a significant increase in SST ($p < 0.05$) after 2005 for the period 1981-2019 (Reynolds et al., 2002). A similar significant warming trend ($p < 0.05$) can be observed in another gridded SST product between 1981-2021 (ERSST v5; Huang et al., 2017). While other regions, such as the Caribbean Sea, exhibit increasing temperatures of up to 0.5°C per decade (Chollett et al., 2012), the southeastern as well as the northern GOM indicate no warming from the 1980s onward. Other studies have linked such a stop in warming with a decline in the strength of the LC and with that of the AMOC (DeLong et al., 2014; Liu et al., 2012). However, such a decline, as hypothesized by DeLong et al. (2014) needs to be verified with instrumental records and cannot solely be based in reconstruction efforts. Our coral-based reconstructed SST records may possibly be indicating the slowdown of the LC and with it a decline in the warming of the GOM. The noteworthy global warming trend continues unimpeded in other regions of the Caribbean and the western Atlantic (Ceasar et al., 2018).

2.1.3.4 Interannual, Interdecadal, and multidecadal variability

Other coral-based proxy records from the Caribbean region have revealed significant interannual variability following signal processing with Singular Spectrum Analysis (SSA) (Giry et al., 2012, Kilbourne et al., 2008). However, the proxy records from this study did not reveal significant frequencies from SSA. Although no significant spectral peaks could be identified, component analysis revealed interannual variabilities in all proxy records. All SST indicators in this study show a 3-7 year interannual variability pointing towards the ENSO teleconnection between the Pacific and Atlantic Ocean (Giry et al 2012). 11% of the variability can be attributed to the 3-7 year band for $\delta^{18}O$ and 22% for Sr/Ca.

SSA (Vautard and Ghil, 1989) does not identify significant interdecadal to multidecadal components in the proxy time series. . However, component analysis shows that 11% of the variability in δ^{18}O can be explained by a 33-year cycle, while Sr/Ca shows a 16-year variability (17%). Multidecadal variabilities between 30- and 70-years in the Atlantic are often connected to the AMO. Recent studies however, have suggested that multidecadal oscillations could be an artefact of volcanic eruptions (Mann et al., 2021). Furthermore, anthropogenic warming might overprint warming effects of warm or cool phases during the last century of the AMO, thereby producing the differences in observed and reconstructed AMO oscillation patterns (Mann et al., 2021). The length of our coral record (160 years) limits detection of variance in the AMO band to the short-period end (~30 years).

2.1.3.5   Hydroclimatology

By removing the temperature effect from $\delta^{18}O_{coral}$ using paired $\delta^{18}O_{coral}$ and Sr/Ca- data, we have reconstructed $\delta^{18}O_{SW}$ (Fig. 2.1.4 C). In previously published paired coral δ^{18}O and Sr/Ca records, $\delta^{18}O_{SW}$ has been shown to be a reliable proxy for SSS in regions dominated by changes in SST and $\delta^{18}O_{SW}$ due to changes in SSS (Gagan et al., 1998, 2000; Ren et al., 2002). Over the 47-year period between 1958-2005, reconstructed $\delta^{18}O_{SW}$ indicate a reduction by 0.016 ‰ that translates into a freshening of the surface water of -0.081 g/kg. Qualitatively, this agrees with the SODA SSS (Carton and Giese, 2007), but under-estimates the change of –0.311 g/kg indicated by the latter (Fig. 2.1.6). This discrepancy might again be due to the size of the SSS grid taking a bigger region into account than what is represented by our coral.

However, correlation between reconstructed monthly $\delta^{18}O_{SW}$ and SODA SSS v.2.1.6 (Carton and Giese, 2007) is not as robust as the coherence between coral δ^{18}O-SST and ERSST, with SSS explaining less than 1 % of the variability in the results. To reduce the influence of high- frequency noise, we also compared the 5-year moving means of SODA SSS and $\delta^{18}O_{SW}$. Filtering out the noise by comparing the smoothed $\delta^{18}O_{SW}$ data to the SSS-SODA dataset shows better correlation (e.g. 10 year smoothing correlated well to the SSS dataset with a Pearson correlation coefficient of 0.66, p<0.001, table 2.1.8). While monthly variability is not captured by the coral, long term trends are well reflected in the $\delta^{18}O_{SW}$ data. Over ENSO timescales, the gridded SSS dataset shows

a minimum of 35.13 g/kg in late autumn of 1992 while the reconstructed $\delta^{18}O_{SW}$ shows a minimum of 0.85 ‰ (equivalent to 32.32 g/kg) for the summer of 1999. In January 1992 and December 1998, two of the more severe El Niño (EN) events categorized by the extended Multivariate ENSO index were documented in the Pacific Ocean (Wolter and Timlin, 2011). The low SODA SSS as well as the low $\delta^{18}O_{SW}$ values in late 1992 and 1999 were likely induced respectively by the central and eastern Pacific EN event and atmospheric teleconnection to the Atlantic altering the precipitation pattern in the following months (Fig. 2.1.6). Due to the 0.5° by 0.5° grid size of the SODA SSS gridded product, a wider region is taken into account for the SSS values, leading to lower salinity values in 1992 when the coral did not record its lowest values. The Caribbean Sea experiences high precipitation later in the year than the GOM, thereby potentially influencing the SSS dataset (Giannini et al., 2000).

The running mean in figure 2.1.6B as well as binned $\delta^{18}O_{SW}$ data over the entire time span in figure S7 indicate significant differences in means (p<0.001) for the late 20th century. A change point analysis revealed a significant (p < 0.05) change in mean in 1980 to lower values (Otto, 2019; Zeileis et al., 2002). A shift to lower salinity values corresponds to lower $\delta^{18}O_{SW}$ ratios reaching its peak in the early 1990s, which also coincides with a change in phase of the Atlantic Multidecadal Oscillation (AMO) index (Fig. 2.1.6) (Enfield et al., 2001) and an increased tendency to more biennial Central Pacific ENSO events (Cai et al., 2019). The time period in the early 1990s also witnessed a shift to more central Pacific EN events with SST warming located in the central equatorial Pacific compared to the conventional canonical EN with SST warming in the eastern Pacific (Goly et al., 2014; Yu et al., 2014). Thus, the combination of a strong EN event in 1992 and 1998 as well as the shift in AMO could possibly explain the increase in precipitation and associated change in salinity in the southern GOM during this time (Fig. 2.1.6). The decrease we observe in $\delta^{18}O_{SW}$ especially in the 1990s as well as in the gridded SSS data might therefore partly be explained by a shift in the phase of the AMO. The change point analysis for $\delta^{18}O_{SW}$ shows a shift in $\delta^{18}O_{SW}$ mean before the AMO index changes. Under the aspect that the correlation between AMO indices and paleoclimate records show no correlation for the preindustrial period and correlation since (Kilbourne et al., 2008), longer records for the southern GOM are needed to verify this link between the AMO and coral SST records.
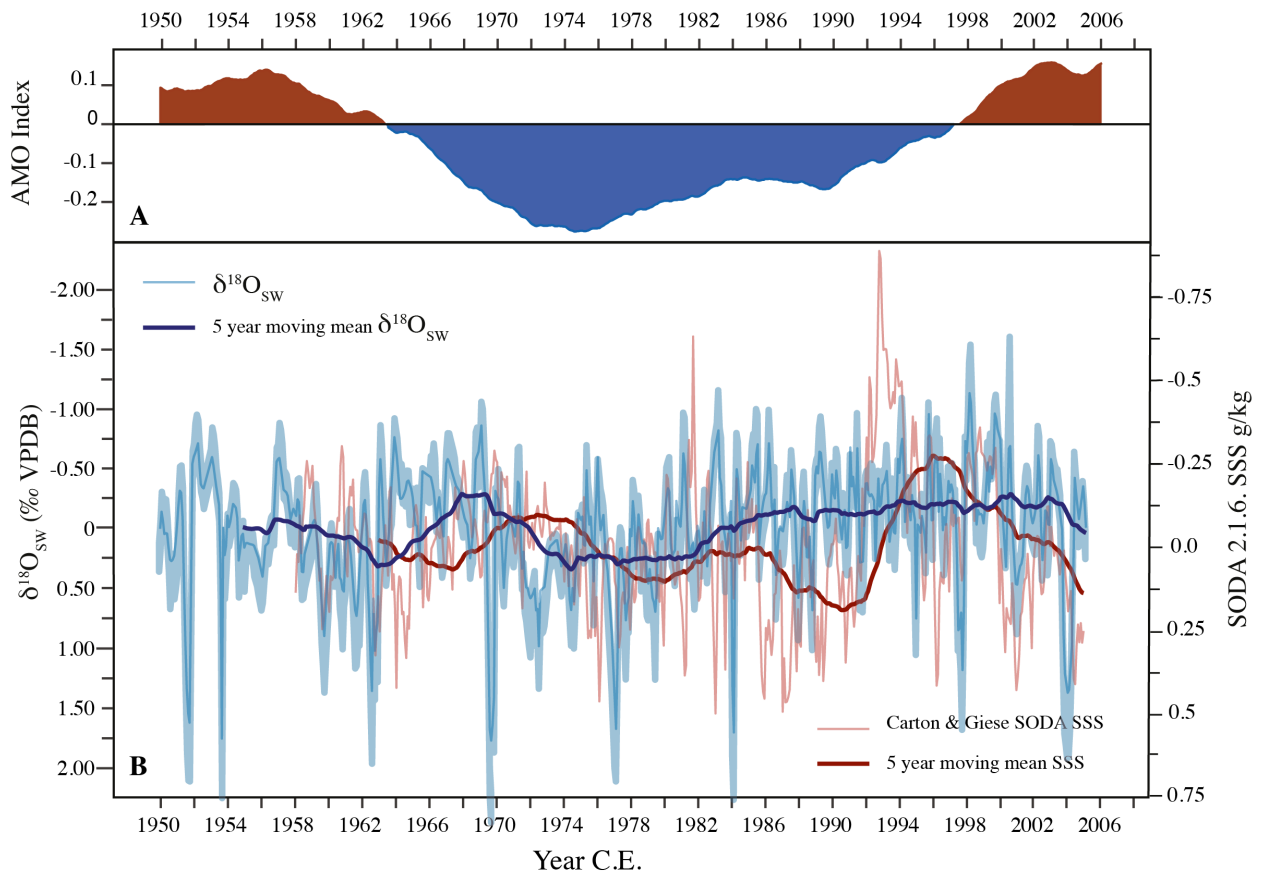
Figure 2.1.6: A- AMO index (Enfield et al., 2001). The positive AMO index is colored red and represents the warm AMO phases. The blue negative AMO part is the cold AMO period. B-Reconstructed detrended $\delta^{18}OSW$ in light blue. The dark blue line represents the 5 year smoothed $\delta^{18}O_{SW}$ (±0.2‰ in blue shading) ratios. Seasonal detrended SSS values from Carton and Giese (2007) are shown by the light red line, while the dark red line is the 5 year smoothed SSS signal.

Due to the oscillatory character of AMO with periodicities of 30-80 years, the comparison of the 40-year running averages of the AMO index and $\delta^{18}O_{SW}$ detailed a significant relationship of 0.5 ($p < 0.001$) (Kilbourne et al., 2008; Wang et al., 2008). Other studies from the Caribbean found the AMO signature in their reconstructed $\delta^{18}O_{SW}$ with strong 60-year cycle (Kilbourne et al., 2008). Time-series analysis with the Singular Spectrum Analysis (Vautard and Ghil, 1989) of our reconstructed $\delta^{18}O_{SW}$ yielded no components in the decadal-interdecadal band that would show a periodicity in the time domain of the AMO even though the correlation between the 40-year moving mean of the AMO index and reconstructed $\delta^{18}O_{SW}$ ratios indicate a robust connection (Fig. 2.1.6, Figures 2.1.8 to 2.1.12 in supplementary materials). Previous studies conducted in the Dry

Tortugas have remarked similar results, showing no periodic variation within the record (DeLong et al., 2014). Studies from the Caribbean basin show the AMO cyclicity in $\delta^{18}O_{SW}$ data (Kilbourne et al., 2008). However, recent studies show that those multidecadal oscillations in proxy and instrumental data might actually be artefacts of volcanic activity or other natural and anthropogenic forcings acting together (Mann et al., 2020, Mann et al., 2021). The AMO remains a multi-decadal climate mode that is not well understood and might not even be definable by its periodicity. Although no proxy time series in this study shows a significance ($p < 0.05$) in the decadal and interdecadal domain, 25.9% of the variability in the data can be explained by 3-7 years periodicities, as well as 16 years (20.2% of variability in the data is explained by this component) can be observed in the reconstructed $\delta^{18}O_{SW}$. The masking of this signal due to external forcings as described by Mann et al. (2020 and 2021) might lead to false periodicities in the 40-70 years band and even near 16 years, so the AMO signal in our proxy records might even be impossible to distinguish from other forcings.

In 1997-98, a very strong EN event manifested in the eastern Pacific with regional precipitation reaching record levels compared to the 1992 EN event (Xie and Arkin, 1996). There is no corresponding salinity anomaly in the SODA SSS dataset for the 1998 EN in our study region, however, reconstructed $\delta^{18}O_{SW}$ indicates a salinity minimum for the northeastern Cuban coast most probably reflecting increased precipitation (Carton and Giese, 2007). A strong positive phase of the North Atlantic Oscillation started in the early 1990s (Giannini et al., 2001, Visbeck et al., 2001). A positive phase of the NAO counteracts the ENSO-linked precipitation in the GOM due to an increased sea level pressure and a subsequent cooling of the ocean's surface waters (Giannini et al., 2001). The onset of a strong positive NAO phase in 1990 with its climax in 1996 (Visbeck et al., 2001) may have led to a subsequent enhanced winter cooling and therefore less precipitation in the southwestern GOM. Various El Niño (1968, 1983, 1987, 1992,1997/98) and La Niña years (1971, 1975, 1985, 1995) show contradictory $\delta^{18}O_{sw}$ values with certain La Niña years showing a minima in the $\delta^{18}O_{SW}$ record in contrast to what we would expect.

Changes in AMO, ENSO, and NAO are multiple contributing factors affecting SST, SSS, and $\delta^{18}O_{SW}$ values in the GOM. This makes identification of ENSO years in coral $\delta^{18}O_{SW}$ records a challenge for further research.

2.1.4 Conclusion

New coral records from the northern coast of Cuba revealed a warming trend in the southeastern GOM from 1845-2005. However, the onset of the stagnating trend after the 1980s suggests a reduction in LC strength. This observation was also noted by similar coral studies conducted in the Dry Tortugas in the northern GOM, in addition to model simulations and recent satellite observations (Chollett et al., 2012; DeLong et al., 2014; Lui et al., 2012). The extended gridded SST products of OI-SST and ER-SST suggests a further warming after this pause in warming trend between 1980 and 2005 (Reynolds et al., 2002; Huang et al., 2017). Through our coupled coral Sr/Ca and δ^{18}O records, the first high-resolution hydroclimate record from the southeastern GOM revealed the onset of a warm AMO phase in the early 1990s. Additionally, two strong EN events of 1992 and 1998 led to an increase in precipitation in the GOM and to freshening conditions. This freshening was observed as strongly depleted coral-based reconstructed $\delta^{18}O_{SW}$ ratios and is in coherence to the gridded SODA SSS (Carton and Giese, 2007). Furthermore, a decrease in salinity coincided with depleted reconstructed $\delta^{18}O_{SW}$ demonstrating the *S. siderea* coral's fidelity as an excellent recorder for hydroclimatology. Due to the scarcity of long-term in-situ salinity, precipitation, and temperature records, the reconstructions completed provide additional understanding to the possible teleconnection dynamics in this region due to changes in atmospheric modes of the NAO and AMO.

2.1.5 Acknowledgments

2.1.6   Open Research

All data reported in this study (trace and minor element ratios and stable isotope ratios have been deposited at the information system PANGAEA (Data Publisher for Earth and Environmental Science), [DOI Link will be updated here, archiving the Datasets in PANGEA is underway]. The ERSST data set is publicly available (Huang et al., 2017) and was obtained from the IRI/LDEO Climate Data Library (http://iridl.ldeo.columbia.edu/SOURCES/.NOAA/.NCDC/.ERSST/.version5/?sem=iridl%3AAir-Sea-Interface, accessed 01.04.2022). OISSTv2.1 is also publicly available (Huang et al., 2020, Huang et al., 2020b) and was retrieved from U.S. National Oceanic and Atmospheric Association (NOAA) National Centers for Environmental Information (NCEI, https://www.ncei.noaa.gov/products/optimum-interpolation-sst, accessed 01.04.2022). The SODA SSS v2.1.6 (Carton and Giese, 2008) dataset was accessed through the IRI/LDEO Climate Library, and is publicly available (http://iridl.ldeo.columbia.edu/SOURCES/.CARTON-GIESE/.SODA/.v2p1p6/, accessed 01.04.2022). The publicly available AMO index times series is based on the Kaplan SST dataset (Enfield et al., 2001) and was retrieved from NOAA Physical Science Laboratory (https://psl.noaa.gov/data/timeseries/AMO/, accessed 04.04.2022).

2.1.7   Supplementary Information

The supplementary materials include an error propagation for temperature reconstructions based on the δ18O age model as well as the Sr/Ca age model. Error propagation for the reconstruction of δ18OSW is also documented. Additional figures and result tables are also included. The new temperature proxies Li/Mg and Sr-U are included as a figure, do not however, correlate well with OI-SSTv2.1 and do not add important information to the study (Huang et al., 2020b; Reynolds et al., 2007). Single spectrum analysis did not yield any significant results and are therefore also

included in the supplementary information. Listed tables show the regressions and results for all paleothermometer proxies analysed for this study.

Error Propagation

We follow the error propagation as presented by Nurhati et al. (2011). The error for the $\delta^{18}O$ SST reconstruction is compounded from 1) the analytical precision 2) the slope of the σ of the $\delta^{18}O$-OISST calibration curve and 3) the σ for the intercept.

$$SST = \delta^{18}O * m + b$$

$$SST \pm \sigma = (\delta^{18}O \pm \sigma_{\delta^{18}O}) * (m \pm \sigma_m) + (b \pm \sigma_b)$$

$$\pm \sigma_{Slope} = |m * \delta^{18}O| * \sqrt{\left(\frac{\sigma_m}{m}\right)^2 + \left(\frac{\sigma_{\delta^{18}O}}{\delta^{18}O}\right)^2}$$

$$\pm \sigma_{SST} = \sqrt{\sigma_b^2 + (m * \delta^{18}O)^2 * \left(\frac{\sigma_m}{m}\right)^2 + \left(\frac{\sigma_{\delta^{18}O}}{\delta^{18}O}\right)^2}$$

$$\pm \sigma_{SST} = 7.71 \ °C$$

The analytical error was reported as 0.05‰. The slope and error are -5.84 (± 0.24) and the intercept and error are 7.7078 (± 0.8).

The overall temperature trend for $\delta^{18}O$ for 160 years is +2.62 °C with a trend slope error of $\sigma_1 = 0.003$ °C.

The calibration slope error is 0.05°C making the overall error +2.62 °C ($\pm$ 0.05 °C).

For Sr/Ca SST reconstruction based on the δ18O age model the slope and slope error are -6.56 $\pm$ 0.73and for the intercept and error 87.10 ± 6.66. The analytical error for Sr/Ca reported as 0.03 together with the trend slope error and calibration slope error yield an overall error of ± 0.21°C, which makes Sr/Ca SST and δ18O-SST not fall within the error of each other.

However, when calculating the error for Sr/Ca based on Sr/Ca age model the temperature increases by +2.62°C $\pm 0. 26$°C while the combined error (including the analytical error, trend slope

error and calibration slope error) yields an error of ±0.26°C, showing a similar increase in SST and error for SST. For these values the δ18O-SSTs fall into the error of Sr/Ca-SST.

The error for δ18OSW calculated as follows after Nurhati et al (2011):

$$\Delta\delta18OCoral = \Delta\delta18OSST + \Delta\delta18OSW$$

$$\Delta\delta18OCoral \pm \sigma\Delta\delta18OCoral = \Delta\delta18OSST \pm\sigma\Delta\delta18OSST + \Delta\delta18OSW \pm \sigma\Delta\delta18OSW$$

$$\sigma\ \Delta\delta18OCoral = \sqrt{(\sigma_{\Delta\delta18OCoral})^2 + (\sigma_{\Delta\delta18OCoral})^2}$$

$$\sigma\ \Delta\delta18OCoral = 0.07\ ‰$$

$$\sigma\Delta Sr/Ca = \sqrt{\sigma_{Sr/Ca}{}^2 + \sigma_{Sr/Ca}{}^2}$$

The analytical error for Sr/Ca is 0.03 mmol/mol.

$$\sigma\Delta Sr/Ca = 0.04\ mmol/mol$$

$$\Delta\delta18OSST = \left[\Delta Sr/Ca\ \frac{\partial SST}{\partial Sr/Ca}\ \frac{\partial \delta^{18}O_{Coral}}{\partial SST}\right]$$

$$\sigma\quad \Delta\delta18OSST\quad =\quad \left|\Delta Sr/Ca\ \frac{\partial SST}{\partial Sr/Ca}\ \frac{\partial \delta^{18}O_{Coral}}{\partial SST}\right| \sqrt{\left(\frac{\sigma_{\frac{\Delta Sr}{Ca}}}{\frac{\Delta Sr}{Ca}}\right)^2 + \left(\frac{\sigma_{SST-SrCa\ Slope}}{SST-SrCa\ Slope}\right) + }$$

$$\left(\frac{\sigma_{coral\ \delta18O-SST\ slope}}{coral\delta^{18}O-SST\ slope}\right.$$

$$\sigma\ \Delta\delta18OSST = 0.002‰$$

$$\sigma\ \Delta\delta18OSW = \sqrt{\sigma^2_{\Delta\delta18OSST} + \sigma^2_{\Delta\delta18OCoral}}$$

$$\sigma \, \Delta\delta18OSW = \sqrt{0.07^2} + \, 0.002^2$$

$$\sigma \, \Delta\delta18OSW = 0.07$$

$$\sigma \, \Delta\delta18OSW = \sqrt{\sigma^2_{\Delta\delta18OSW} + \, \sigma^2_{\Delta\delta18OSW}} = \sigma \, \delta18OSW * \sqrt{2}$$

$$\sigma \, \delta18OSW = 0.1‰$$
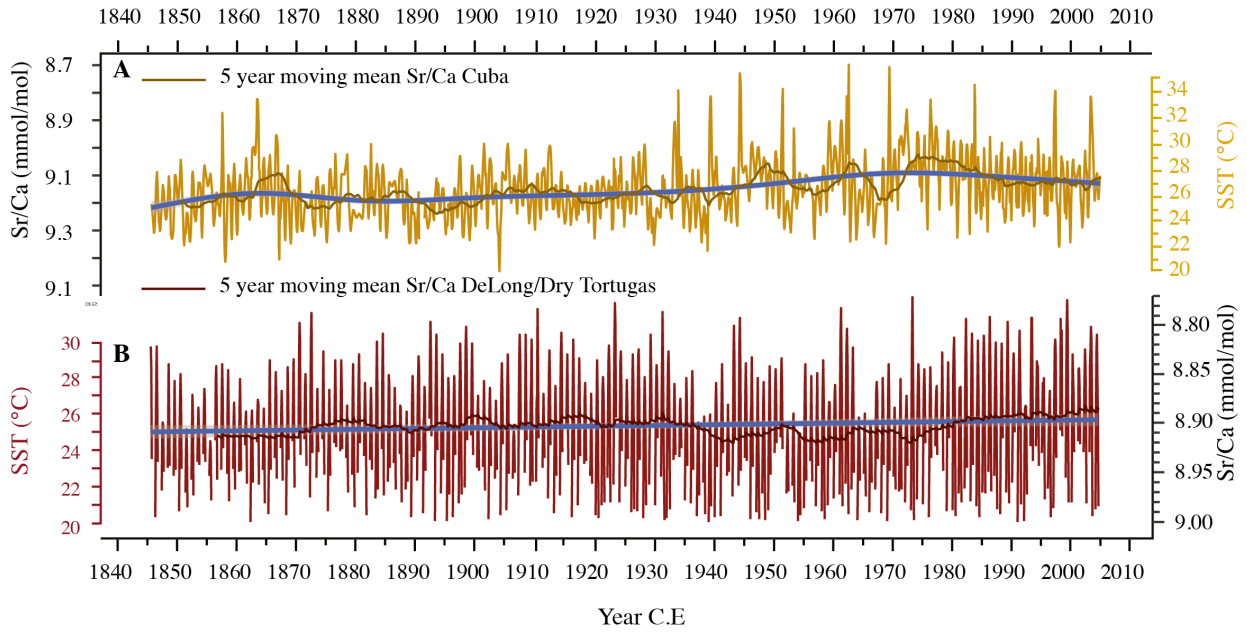
Figure 2.1.7: A- shows Li/Mg in mmol/mol and reconstructed SST in °C with its 5 year running average plotted at the end of the respective 5 years. Li/Mg is one of the only temperature indicators for the coral core showing no noteworthy warming in the southeastern GOM. B- Sr-U in mmol/mol and its reconstruction to SST in °C. The overall increase in reconstructed SST is 2.4°C over 160 years. Sr-U shows a stagnation in the warming trend starting in the 1980s as shown by δ^{18}O and Sr/Ca (see Fig. 2.1.4). The temperature reconstructions are based on the δ^{18}O age model.
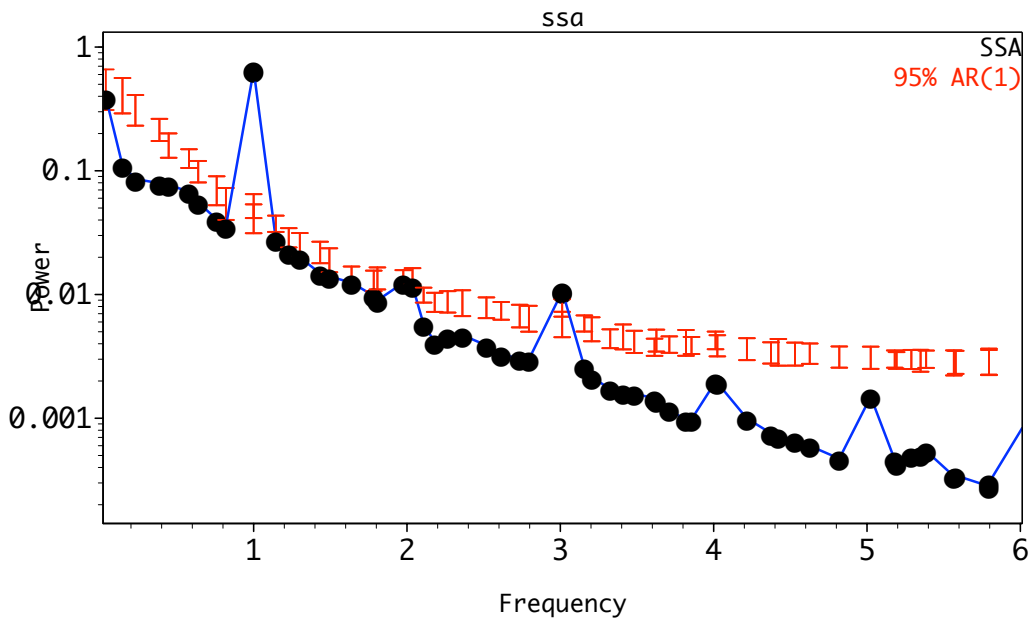
Figure 2.1.8: SSA δ^{18}O detrended (linear trend removed, δ^{18}O age model data). Frequency 1 = seasonal variability. Frequency 3,4,5 = 3-5 years probably ENSO variability. SSA was performed with kSpectra.
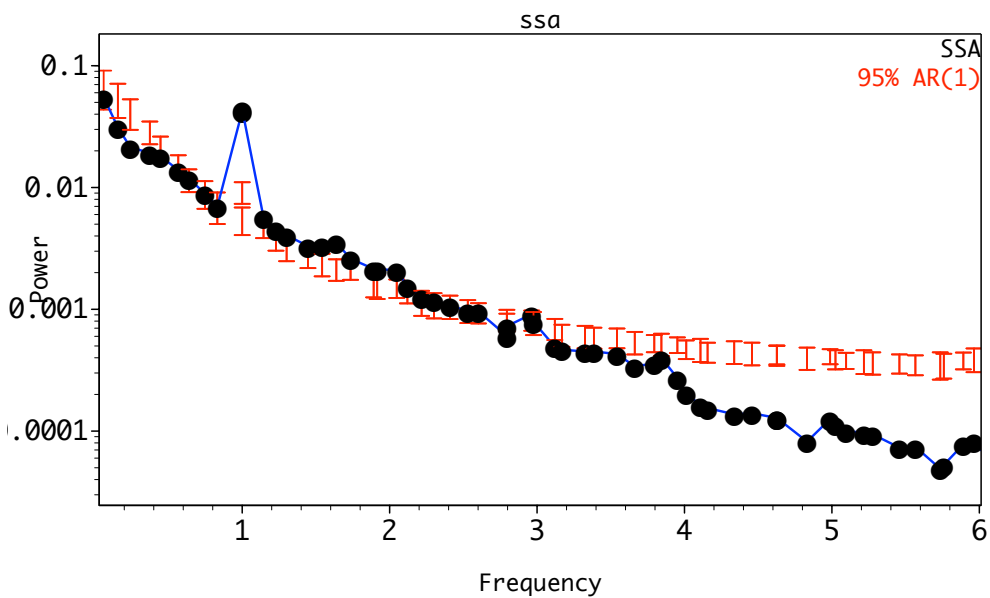
Figure 2.1.9: SSA Sr/Ca detrended (linear trend removed, δ^{18}O-OI-SST age model). Frequency 1 = seasonal variability. SSA was performed with kSpectra.
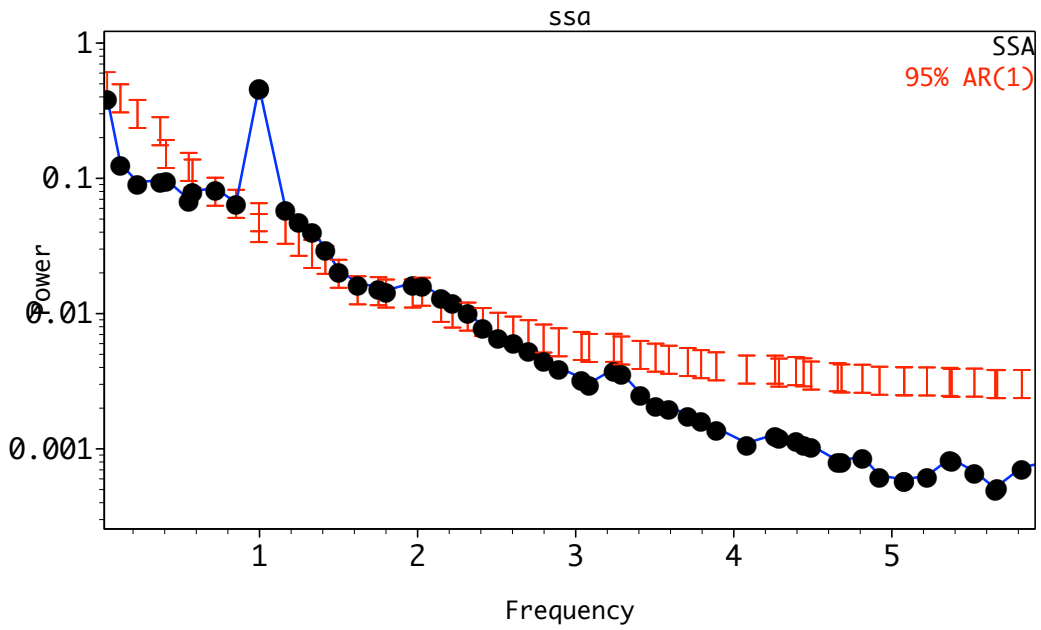
Figure 2.1.10: SSA $\delta^{18}O$ detrended (Sr/Ca-OI-SST age model based). SSA was performed with kSpectra.
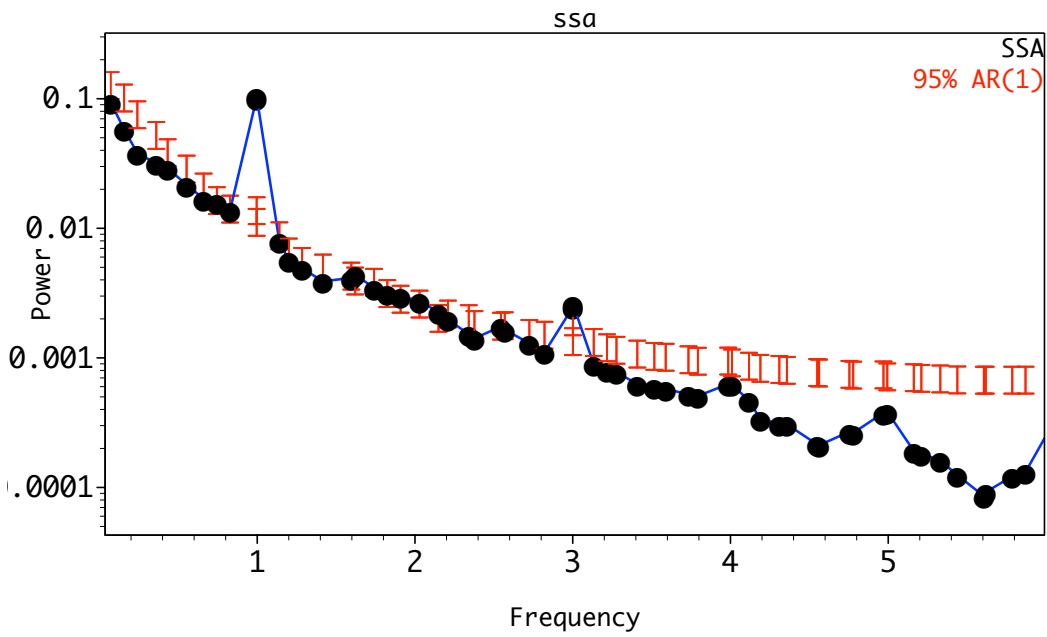
Figure 2.1.11: SSA Sr/Ca detrended (Sr/Ca-OI-SST age model). SSA was performed with kSpectra.
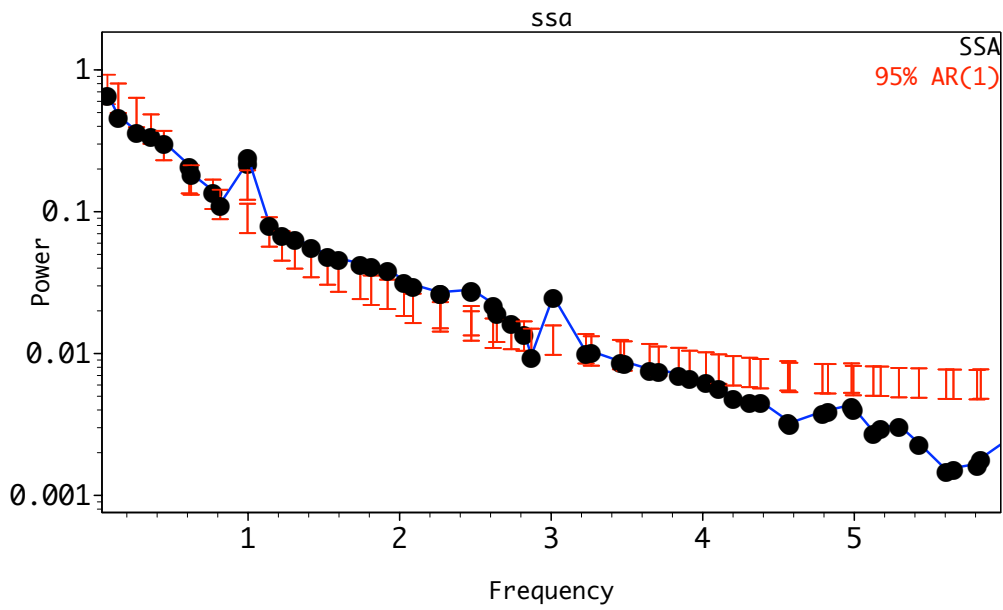
Figure 2.1.12: SSA of $\delta^{18}O_{SW}$ (Sr/Ca -OISST age mode based). A significant peak for yearly and every 3 years. SSA was performed with kSpectra.
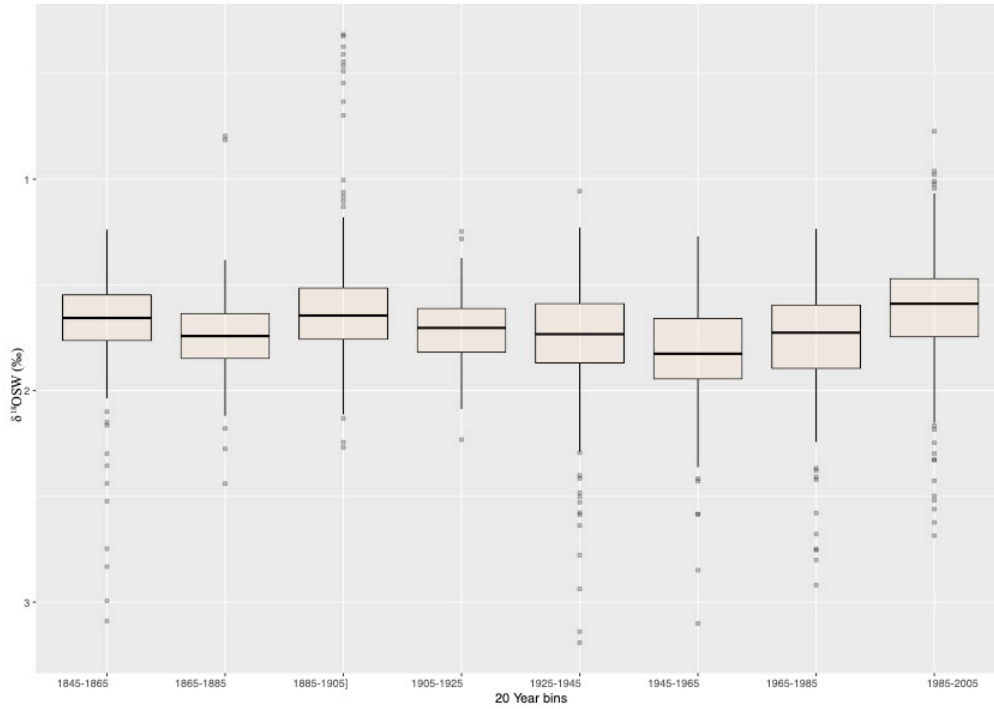
Figure 2.1.13: 20 year binned $\delta^{18}O_{SW}$ values and their mean. The Tukey test (multiple pairwise comparison test) revealed significant (p<0.001) changes in mean between the bins 1925 - 1945 and 1945-1965.

Table 2.1.2: Regression equations for Temperature indicators and OI-SST based on $\delta^{18}O$ age model. The error reported here is 1σ (Huang et al., 2020b ; Reynolds et al., 2007).

Proxy	r	p-value	Proxy regressed onto SST	Change per decade in °C
$\delta^{18}O$	0.83	<0.001	$\delta^{18}O$ =-0.16 (±0.14) - 0.12 (±0.013) SST	0.16
Sr/Ca	0.47	<0.001	Sr/Ca = 10.04 (±0.8) - 0.03 (±0.003) SST	0.21
Li/Mg	0.35	<0.001	Li/Mg = 2.67 (±0.32) - 0.03 (±0.004) SST	-0.03
$\delta^{18}O_{pseudo}$	0.99	<0.001	$\delta^{18}O_{pseudo}$=5.44 (±0.21) - 0.22 (±0.009) SST	0.20
U/Ca	0.50	<0.001	U/Ca= 1.94 (±0.12) - 0.02 (±0.001) SST	0.15
Mg/Ca	0.30	<0.001	Mg/Ca= 2.17 (±0.56) + 0.06 (±0.02) SST	0.30
Sr-U	0.47	<0.001	Sr-U=9.88 (±0.59)-0.03 (±0.002) SST	0.04

Table 2.1.3: Results from different proxy time series, calculates on the basis of the $\delta^{18}O$ age mode, interpolated with Arand. Anomalies calculated with the mean 1950-2000.

A	$\delta^{18}O$ (in ‰VPDB)	Sr/Ca (in mmol/mol)	Li/Mg (in mmol/mol)	U/Ca (in mmol/mol)	Mg/Ca (in mmol/mol)	Sr-U (in mmol/mol)	$\delta^{18}O_{pseudo}$ (in ‰)	$\delta^{18}O_{SW}$ (in ‰)
Mean	-3.17 (±0.001)	9.15 (±0.032)	1.82 (±0.022)	1.30 (±0.014)	3.69 (±0.014)	9.15 (±0.167)	-0.56	1.58
Maximum value	-2.54 (±0.001)	9.63 (±0.034)	2.54 (±0.031)	1.51 (±0.028)	4.84 (±0.017)	9.38 (±0.172)	0.19	2.93
Minimum value	-3.80 (±0.002)	8.71 (±0.03)	1.32 (±0.016)	1.08 (±0.019)	3.08 (±0.01)	8.91 (±0.163)	-1.31	0.18
B								
Winter (JFM) mean	-2.97 (±0.001)	9.21 (±0.032)	1.90 (±0.023)	1.34 (±0.024)	3.58 (±0.013)	9.20 (±0.168)	-0.27	1.60
Winter (JFM) max	-2.63 (±0.001)	9.36 (±0.033)	2.36 (±0.029)	1.46 (±0.027)	4.74 (±0.016)	9.34 (±0.171)	0.15	2.73
Winter (JFM) min	-3.37 (±0.001)	8.84 (±0.031)	1.61 (±0.019)	1.20 (±0.022)	3.18 (±0.01)	9.04 (±0.165)	-0.38	1.00
C								
Summer (JAS) mean	-3.35 (±0.001)	9.09 (±0.032)	1.75 (±0.022)	1.26 (±0.023)	3.78 (±0.014)	9.11 (±0.167)	-0.99	1.58
Summer (JAS) max	-2.92 (±0.001)	9.43 (±0.033)	2.20 (±0.025)	1.41 (±0.026)	4.67 (±0.017)	9.27 (±0.169)	-0.79	2.66
Summer (JAS) min	-3.73 (±0.002)	8.76 (±0.031)	1.47 (±0.017)	1.09 (±0.020)	3.37 (±0.012)	8.92 (±0.163)	-1.16	0.78
D								
Mean anomaliy	0.12 (±0.0001)	0.04 (±0.0001)	-0.01 (±0.001)	0.02 (±0.0004)	-0.09 (±0.0003)	0.02 (±0.004)	-0.01	0.0012
Max anomaly	0.60 (±0.0004)	0.59 (±0.005)	0.72 (±0.038)	0.20 (±0.004)	1.26 (±0.02)	0.23 (±0.042)	0.22	1.42
Min anomaly	-0.33 (±0.0003)	-0.43 (±0.002)	-0.60 (±0.011)	-0.20 (±0.004)	-0.70 (±0.003)	-0.23 (±0.042)	-0.29	-1.49

Table 2.1.4: Regression equations for temperature indicators and OI-SST based on Sr/Ca age model (Reynolds et al., 2007; Huang et al., 2020b). Change per ‰ per °C for $\delta^{18}O$ and $\delta^{18}O_{pseudo}$. For other proxies: change per mmol/mol per °C. The error reported in brackets are 1σ for the regression, r is the Pearson correlation coefficient for the reconstructed SST and OI-SSTv2.1 (Huang et al., 2020b, Reynolds et al., 2007).

Proxy	r	p-value	SST-Proxy	Change per decade in °C
$\delta^{18}O$	0.54	<0.001	$\delta^{18}O$ = -1.24 (±0.19) - 0.08 (±0.007) SST	0.24
Sr/Ca	0.62	<0.001	Sr/Ca = 10.35 (±0.09) - 0.045 (±0.003) SST	0.15
Li/Mg	0.38	<0.001	Li/Mg = 2.80 (±0.15) - 0.037 (±0.006) SST	-0.13
$\delta^{18}O_{pseudo}$	0.999	<0.001	$\delta^{18}O_{pseudo}$ = 5.44 (±0.05) - 0.22 (±0.002) SST	0.21
U/Ca	0.59	<0.001	U/Ca = 2.11 (±0.07) - 0.031 (±0.003) SST	0.12
Mg/Ca	0.43	<0.001	Mg/Ca = 1.51 (±0.29) + 0.09 (±0.01) SST	0.21
Sr-U	0.59	<0.001	Sr-U = 10.04 (±0.08)-0.03 (±0.003) SST	0.04

Table 2.1.5: Linear regression over the entire period from 1845 to 2005 for each proxy based on Sr/Ca age model. Change per ‰ per month for $\delta^{18}O$, $\delta^{18}O_{pseudo}$, and $\delta^{18}O_{SW}$. For other proxies: change per mmol/mol per month (yr = YYYY,MM).

Proxy	r	p-value	Trend over time	Change per decade in °C
δ18O	-0.4	<0.001	δ18O = -0.002 (±0.0001) yr + 0.56 (±0.19)	0.24
			δ18OSW = -0.0003 (±0.0001) yr + 0.94	
δ18OSW	-0.01	0.61	(±0.02)	
δ18Opseu			δ18Opseudo = -0.005 (±0.003) yr + 8.74	
do	-0.05	0.41	(±5.19)	0.21
			Sr/Ca = -0.0007 (±0.00005) yr + 10.49	
Sr/Ca	-0.28	<0.001	(±0.05)	0.15
Li/Mg	0.03	0.12	Li/Mg =0.0005 (±0.00009) yr + 0.84 (±0.17)	-0.13
U/Ca	-0.24	<0.001	U/Ca = -0.0004 (±0.00003) yr + 2.04 (±0.07)	0.12
Mg/Ca	0.33	<0.001	Mg/Ca= 0.002 (±0.0001) yr + 0.15 (±0.25)	0.21
Sr-U	-0.24	<0.001	Sr-U = -0.0004 (±0.00004) yr + 9.94 (±0.07)	0.21

1 **Table 2.1.6:** Results from different proxy time series, calculates on the basis of the Sr/Ca age mode, interpolated with Arand.
2 Anomalies calculated with the mean from the time interval of 1950-2000.

A	δ¹⁸O (in ‰VPDB)	Sr/Ca (in mmol/mol)	Li/Mg (in mmol/mol)	U/Ca (in mmol/mol)	Mg/Ca (in mmol/mol)	Sr-U (in mmol/mol)	δ¹⁸O$_{pseud}$O (in ‰)	δ¹⁸O$_{SW}$ (in ‰)
Mean	-3.17 (±0.001)	9.15 (±0.032)	1.82 (±0.022)	1.30 (±0.014)	3.69 (±0.014)	9.15 (±0.167)	-0.56	1.58
Maximum value	-2.54 (±0.001)	9.63 (±0.034)	2.54 (±0.031)	1.51 (±0.028)	4.84 (±0.017)	9.38 (±0.172)	0.19	2.93
Minimum value	-3.80 (±0.002)	8.71 (±0.03)	1.32 (±0.016)	1.08 (±0.019)	3.08 (±0.01)	8.91 (±0.163)	-1.31	0.18
B								
Winter (JFM) mean	-2.97 (±0.001)	9.21 (±0.032)	1.90 (±0.023)	1.34 (±0.024)	3.58 (±0.013)	9.20 (±0.168)	-0.27	1.60
Winter (JFM) max	-2.63 (±0.001)	9.36 (±0.033)	2.36 (±0.029)	1.46 (±0.027)	4.74 (±0.016)	9.34 (±0.171)	0.15	2.73
Winter (JFM) min	-3.37 (±0.001)	8.84 (±0.031)	1.61 (±0.019)	1.20 (±0.022)	3.18 (±0.01)	9.04 (±0.165)	-0.38	1.00
C								
Summer (JAS) mean	-3.35 (±0.001)	9.09 (±0.032)	1.75 (±0.022)	1.26 (±0.023)	3.78 (±0.014)	9.11 (±0.167)	-0.99	1.58
Summer (JAS) max	-2.92 (±0.001)	9.43 (±0.033)	2.20 (±0.025)	1.41 (±0.026)	4.67 (±0.017)	9.27 (±0.169)	-0.79	2.66
Summer (JAS) min	-3.73 (±0.002)	8.76 (±0.031)	1.47 (±0.017)	1.09 (±0.020)	3.37 (±0.012)	8.92 (±0.163)	-1.16	0.78
D								
Mean anomaliy	0.12 (±0.0001)	0.04 (±0.0001)	-0.01 (±0.001)	0.02 (±0.0004)	-0.09 (±0.0003)	0.02 (±0.004)	-0.01	0.0012
Max anomaly	0.60 (±0.0004)	0.59 (±0.005)	0.72 (±0.038)	0.20 (±0.004)	1.26 (±0.02)	0.23 (±0.042)	0.22	1.42
Min anomaly	-0.33 (±0.0003)	-0.43 (±0.002)	-0.60 (±0.011)	-0.20 (±0.004)	-0.70 (±0.003)	-0.23 (±0.042)	-0.29	-1.49

3
4

Table 2.1.7: Correlations of detrended $\delta^{18}O_{SW}$ to AMO, CMAP, SODA SSS (Carton and Giese 2007), and SSS SODA detrended based on $\delta^{18}O$ age model.

Dataset correlation of $\delta^{18}O_{SW}$ det	r monthly	p-value	r 10 years	p-value	r 40 years	p-value
AMO	0.02259136	0.3477	0.1262652	<0.001	0.5211067	<0.001
CMAP	-0.0347978	0.539	-0.3599832	<0.001	-	-
SSS	0.1290201	0.002101	0.6982651	<0.001	0.8445079	<0.001
SSS_det	0.05428354	0.1972	0.44064	<0.001	-0.5428755	<0.001
Dataset $\delta^{18}O_{SW}$ vs	r monthly	p-value	r 10 years	p-value	r 40 years	p-value
AMO	-0.0119956	0.6181	-0.0347558	0.1632	0.217746	<0.001
CMAP	-0.0350396	0.5362	-0.4062348	<0.001	-	-
SSS	0.113818	0.006715	0.6586492	<0.001	0.806984	<0.001
SSS_det	0.05457149	0.1948	0.4376748	<0.001	-0.513564	<0.001

Table 2.1.8: Correlations of detrended $\delta^{18}O_{SW}$ to AMO, CMAP, SODA SSS (Carton and Giese 2007), and SSS SODA detrended based on Sr/Ca age model.

Dataset correlation of $\delta^{18}O_{SW}$ detrended vs	r monthly	p-value	r 10 years	p-value	r 40 years	p-value
AMO	0.1635645	<0.001	0.5888825	<0.001	0.7035854	<0.001
CMAP	-0.1854888	0.0009584	0.4392297	<0.001	-	-
SSS	0.08964512	0.03298	0.5214904	<0.001	0.8551333	<0.001
SSS_detrended	0.03372473	0.4233	0.04501677	0.3423	0.3317896	<0.001
Dataset $\delta^{18}O_{SW}$ vs	r monthly	p-value	r 10 years	p-value	r 40 years	p-value
AMO	0.2337218	<0.001	0.5375493	<0.001	0.5068187	<0.001
CMAP	-0.1856836	0.0009464	0.3927468	<0.001	-	-
SSS	0.1357022	0.001211	0.6606709	<0.001	0.9449549	<0.001
SSS_detrended	0.0331992	0.4305	0.1514733	<0.001	0.4913378	<0.001

2.2   Carbonate chemistry of seawater and calcifying fluid reconstructed from Cuban *Siderastrea siderea* from the Gulf of Mexico

M. Harbott[1*], T. Rixen[1, 2] , H. Kuhnert[3], S. Kasemann[3], A. Meixner[3], C. Jimenez[4, 5], P. González-Díaz[6], and H. C. Wu[1]

[1] Leibniz Centre for Tropical Marine Research (ZMT) GmbH, Fahrenheitstraße 6, 28359 Bremen, Germany

[2] Institute of Geology, University of Hamburg, Bundesstrasse 55, 20148 Hamburg, Germany

[3] MARUM – Center for Marine Environmental Sciences, University of Bremen, Leobener Str. 8, 28359 Bremen, Germany

[4] Enalia Physis Environmental Research Centre, Acropoleos 2, Aglantzia 2101, Nicosia, Cyprus

[5] The Cyprus Institute. 20 Konstantinou Kavafi St, 2121 Aglantzia. Nicosia, Cyprus

[6] Centro de Investigaciones Marinas Universidad de La Habana, Calle 16 no.114 e/ 1ra y 3ra, Miramar. Playa, Ciudad de La Habana, Cuba

Corresponding author: Marie Harbott (marie.harbott@leibniz-zmt.de)

Abstract

Ocean acidification (OA) is affecting one of our most species-rich ecosystems on Earth: coral reefs. By absorbing atmospheric CO_2, the ocean is not only acidifying but also decreasing its aragonite saturation state. Less carbonate ions lead to less accretion of coral skeletal material and is endangering skeletal forming corals and calcifying marine organisms. Corals are not only affected by OA but are also our window into the past, by serving as an archive for the carbonate chemistry of the ocean. We reconstruct the carbonate chemistry of seawater and of the calcifying fluid of coral skeletal material from the southern Gulf of Mexico and the $\delta^{13}C$ skeletal ratios. It was found that the coral is upregulating Total Alkalinity, Dissolved Inorganic Carbonate (DIC), pH, and the aragonite saturation state compared to the seawater (SW) to facilitate calcification. While TA is relatively constant, DIC is increasing and pH decreasing in seawater, showing an acidifying Gulf of Mexico. This correlates with data from the Ocean Carbonate Data System, showing that the coral is recording long term trends in OA and carbonate chemistry of seawater. Decreasing skeletal $\delta^{13}C$ values confirm enhanced diffusion of pCO_2 into the coral as well as the Suess Effect in the ambient water.

2.2.1 Introduction

The continuous emission of anthropogenic CO_2 from burning fossil fuels and land use change is changing our ocean's chemistry since the industrial revolution. The ocean has absorbed one quarter of the anthropogenically emitted CO_2 so far (Gulev et al., 2021). Adding CO_2 to the ocean shifts the equilibrium of the carbonate system: Dissociation of carbonic acid releases hydrogen ions and hence decreases the seawater pH(Hoegh-Guldberg et al., 2017; Orr et al., 2015; Zeebe & Wolf-Gladrow, 2001) [1].

$$CO_2 + H_2O \leftrightarrow H_2CO_3 \leftrightarrow HCO_3^- + H^+ \leftrightarrow CO_3^{2-} + 2H^+ \qquad [1]$$
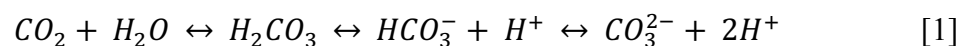
With increasing H^+ concentration, hydrogen ions bind to carbonate ions, forming hydrocarbonate, thereby decreasing the availability of carbonate ions to calcifying organisms. Alongside changes in pH, Dissolved Inorganic Carbon (DIC), and total alkalinity (TA) are impacted by ocean acidification (OA). With more CO_2 in the surface ocean, DIC will increase, while the charge balance of the carbonate ion species and other components does not change. Other carbonate chemistry parameters such as the aragonite saturation state, measuring the availability of the carbonate ion for marine organisms to form their skeleton, will decrease over

time with progressing acidifying oceans. OA is alongside other stressors, such as ocean warming, a major threat to coral reefs.

Reduced competitiveness of stony coral species most sensitive to OA, as indicated in their declining growth rates (Comeau et al., 2018; Cooper et al., 2008; Marubini et al., 2008; H. C. Wu, Dissard, et al., 2017), favors more resilient and opportunistic species and generally affects species composition and diversity of coral reef ecosystems (Alvarez-Filip et al., 2011; Doney et al., 2009; Pandolfi, John M. et al., 2011).

The Gulf of Mexico (GOM) harbors extensive reef formations and also plays a vital role in the global water mass circulation. It supplies the Atlantic meridional overturning circulation with warm and saline water masses, feeding the Gulfstream (H. Liu et al., 2012; Turner & Rabalais, 2019).

Only a few long-term observation projects have measured OA over longer term periods since 1988 CE: Bermuda Atlantic Time Series (BATS), Hawaii Ocean Time Series (HOT) Station ALOHA, and the European Station for Time Series in the Ocean Canary Islands (ESTOC). Two buoys have been collecting ocean carbon data and measuring pH in the GOM since 2014 CE. One is located on the continental shelf off the coast of Louisiana and the other in the Florida Keys, USA. The ocean carbonate data system (OCADS) is a carbon data repository, collecting data on ocean carbon cycling and OA(L.-Q. Jiang et al., 2023) (https://www.ncei.noaa.gov/products/ocean-carbon-acidification-data-system, accessed 30.06.2023). New insights into past pH variability over time can be gained by pH reconstruction through climate archives such as foraminifera(Foster & Rae, 2016; Hönisch et al., 2012; Sanyal et al., 2001) or coral cores (Fowell, Foster, Ries, Castillo, De La Vega, et al., 2018; Hönisch et al., 2004; Pelejero et al., 2005; H. C. Wu et al., 2018). For the North Atlantic, there are reconstructions based on $\delta^{11}B$ from the Sargasso Sea near Bermuda using the coral *Diploria* as the archive (Goodkin et al., 2015). Fowell et al. (2018) used $\delta^{11}B$ in the coral species *Siderastrea siderea* to reconstruct pH in a back and forereef environment. Both studies showed, that corals can record changes in pH of seawater (pH$_{SW}$) due to atmospheric changes in pCO$_2$, but that the corals respond not only to changes in pH, but also to alterations of the carbonate chemistry of seawater (Comeau, Tambutté, et al., 2017).

Manuscript II: Carbonate Chemistry changes in SW and CF

Two epithelial tissues are covering the skeleton of the coral, oral tissue, towards the seawater and aboral tissue facing the skeleton (Allemand et al., 2004). The calicoblastic cells in the aboral ectoderm, closest to the skeleton, control the ion flux for the formation of the aragonite skeleton (Falini et al., 2015). Seawater provides the ions used for calcification. Seawater reaches the calcification site via a transcellular pathway or paracellular pathway or both(Allemand et al., 2004). The transcellular pathway controls the calcifying space by regulating pH and DIC via the Ca^+ ATPase removing H^+ ions and importing Ca^{2+} ions (Allemand et al., 2004; Comeau, Tambutté, et al., 2017; Falini et al., 2015; M. McCulloch, Falter, et al., 2012a; M. T. McCulloch et al., 2017b; Ross et al., 2017). CO_2 is mainly of metabolic origin from the calicoblastic cells, although can also originate from seawater (Allemand et al., 2004; Falini et al., 2015). Carbonic anhydrase is localized in the calicoblasitc epithelium and responsible for a speedy transformation from CO_2 to HCO_3^-. CO_2 and HCO_3^- might be transported via diffusion and/or pumping of HCO_3^- via bicarbonate anion transporters into calcifying space (Allemand et al., 2004; M. T. McCulloch et al., 2017b; Zoccola et al., 2015).

The removal of protons via the Ca^+ATPase increases the pH of the calcifying fluid (pH_{cf}) and shifts the dissolved inorganic carbon (DIC) equilibrium in favor of CO_3^{2-}, increasing the aragonite saturation (Ω) in the calcifying space and promoting calcification (Allemand et al., 2004; Comeau, Cornwall, et al., 2017; D'Olivo et al., 2019; M. McCulloch, Falter, et al., 2012a; M. T. McCulloch et al., 2017b; Ross et al., 2017; Zoccola et al., 2015).

Several studies show the upregulation of DIC, pH, and Ω in the calcifying fluid (CF) for shorter time spans (8 weeks to 2 years)(Comeau, Tambutté, et al., 2017; M. McCulloch, Falter, et al., 2012a; M. T. McCulloch et al., 2017b; Ross et al., 2017). OA will lead to an increase in DIC in seawater while the charge balance, also expressed as TA does not change(Zeebe, 2012). With a decreasing pH in ambient seawater the coral has to lower the pH even further to maintain a pH gradient with the seawater, which is energetically more challenging for the coral(Comeau, Cornwall, et al., 2017; Hohn & Merico, 2012) .

Another effect of anthropogenic CO_2 uptake by the oceans is known as the Suess Effect(Keeling, 1979), where the depletion of $\delta^{13}C$ isotopic ratio in seawater due to the lighter ^{12}C increasingly reaching the atmosphere from burning of fossil fuels and due to air-sea gas exchange in the oceans. The incorporation of carbon isotopes into the coral skeleton is

controlled by changes in light intensity, photosynthesis, and growth rate(Grottoli, 1999, 2000; Swart et al., 2010). The strong impact of the Suess Effect on the atmosphere and the ocean, has reached the coral skeleton as well. A similar continuous decreasing isotope ratio can be seen in corals all over the world in coherence to the Law Dome Ice core record.(Rubino et al., 2013; Swart et al., 2010; H. C. Wu et al., 2018).

Long-term change in the carbonate chemistry of the CF under ongoing OA have so far been investigated by D'Olivo et al. (2019) from 1939 to 2013 CE. A majority of coral studies have focused solely on the pH component and are mostly situated in the Pacific(Tarique & Rahaman, 2022) with limited reconstruction records from the Atlantic(Chalk et al., 2019; Coadic et al., 2013; Foster & Rae, 2016; Fowell, Foster, Ries, Castillo, De La Vega, et al., 2018; Goodkin et al., 2015). Currently, there has neither been pH reconstructions nor continuous measurements of pH from the southern GOM since preindustrial times. Since 1996 CE, *in situ* pH measurements have been collected mostly from the northern GOM(Osborne et al., 2022). Coral $\delta^{11}B$ and B/Ca have been used in combination to reconstruct coral CF carbonate chemistry as well as the pH of the CF and surrounding seawater in the Indian Ocean close to Australia (X. Chen et al., 2021; Comeau, Cornwall, et al., 2017; Comeau, Tambutté, et al., 2017; DeCarlo et al., 2018; M. McCulloch, Falter, et al., 2012a; Ross et al., 2017).

Long-term pH, DIC, and TA measurements are non-existent and is yet urgently needed as key parameters for crucial ocean monitoring systems on boundary conditions. Due to this fact, there has so far been no comparison of changes in pH in the CF with other carbonate chemistry parameters in seawater. With limited availability based on reconstructions and non-existent *in situ* measurements of pH and carbonate chemistry for the Gulf of Mexico, we carefully reconstructed DIC, TA, and pH time series of seawater using geochemical techniques based on coral skeletal material accounting for error propagations. In order to calculate the seawater carbonate chemistry, sea surface temperature, salinity, and two additional components of the carbonate system parameters are required (e.g. TA, DIC, $pCO_{2\ (aq)}$, pH) (Zeebe & Wolf-Gladrow, 2001).

Here we present reconstructed seawater carbonate chemistry from the $\delta^{18}O_{SW}$-sea surface salinity (SSS) and TA relationship as the first component of the carbonate chemistry (Takahashi et al., 2014) and pH_{SW} reconstructed from measured $\delta^{11}B$ from the coral skeleton as the second

component. To compare the reconstructed carbonate chemistry values of seawater to those of the coral CF, we used the coral skeletal ratio B/Ca for DIC and the stable isotopic signature of $\delta^{11}B$ for the pH of the CF. The results show an upregulation of the coral of its DIC, TA, pH, and Ω in the CF versus seawater, as was observed by several previous studies (Comeau, Cornwall, et al., 2017; Comeau, Tambutté, et al., 2017; DeCarlo et al., 2018; M. McCulloch, Falter, et al., 2012a; Ross et al., 2017). We examined how southern GOM carbonate chemistry is changing with increased anthropogenic atmospheric CO_2, water pollution, and how corals are reacting and adapting. We will show that reconstructed acidification of the GOM and the accompanying decrease in Ω agree with the trends for the tropical oceans [38]. Furthermore, the $\delta^{13}C$ signature of the coral is a product of a combination of increased diffusion of pCO_2 as well as the Suess Effect(Keeling, 1979).
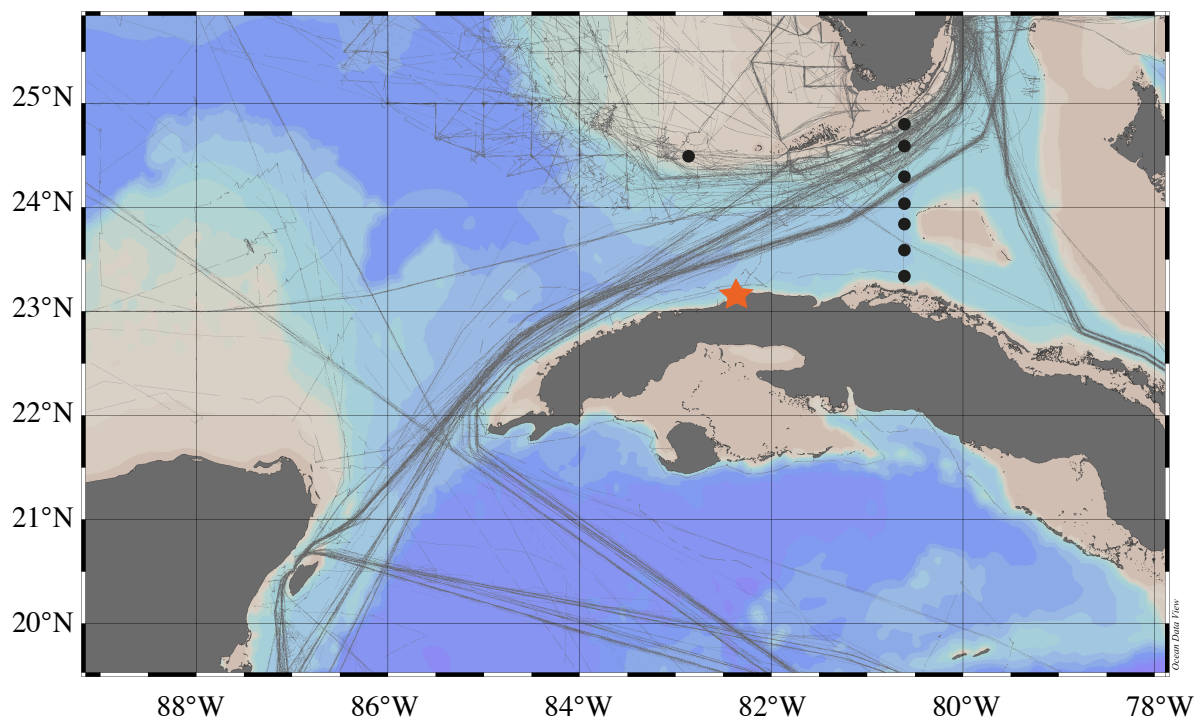
Figure 2.2.1: Map of the Gulf of Mexico with the position of the coral core (sp. Siderastrea siderea, 82.4239W, 23.1277N) in front of Havana marked with a red star. Grey lines indicate SOCAT(Bakker et al., 2023) measurement positions. Black dots are measurements from GLODAPv2 2019(Olsen et al., 2019). Map made with Ocean Data View 5.1.7

2.2.2 Results

2.2.2.1 Carbonate Chemistry reconstruction in seawater
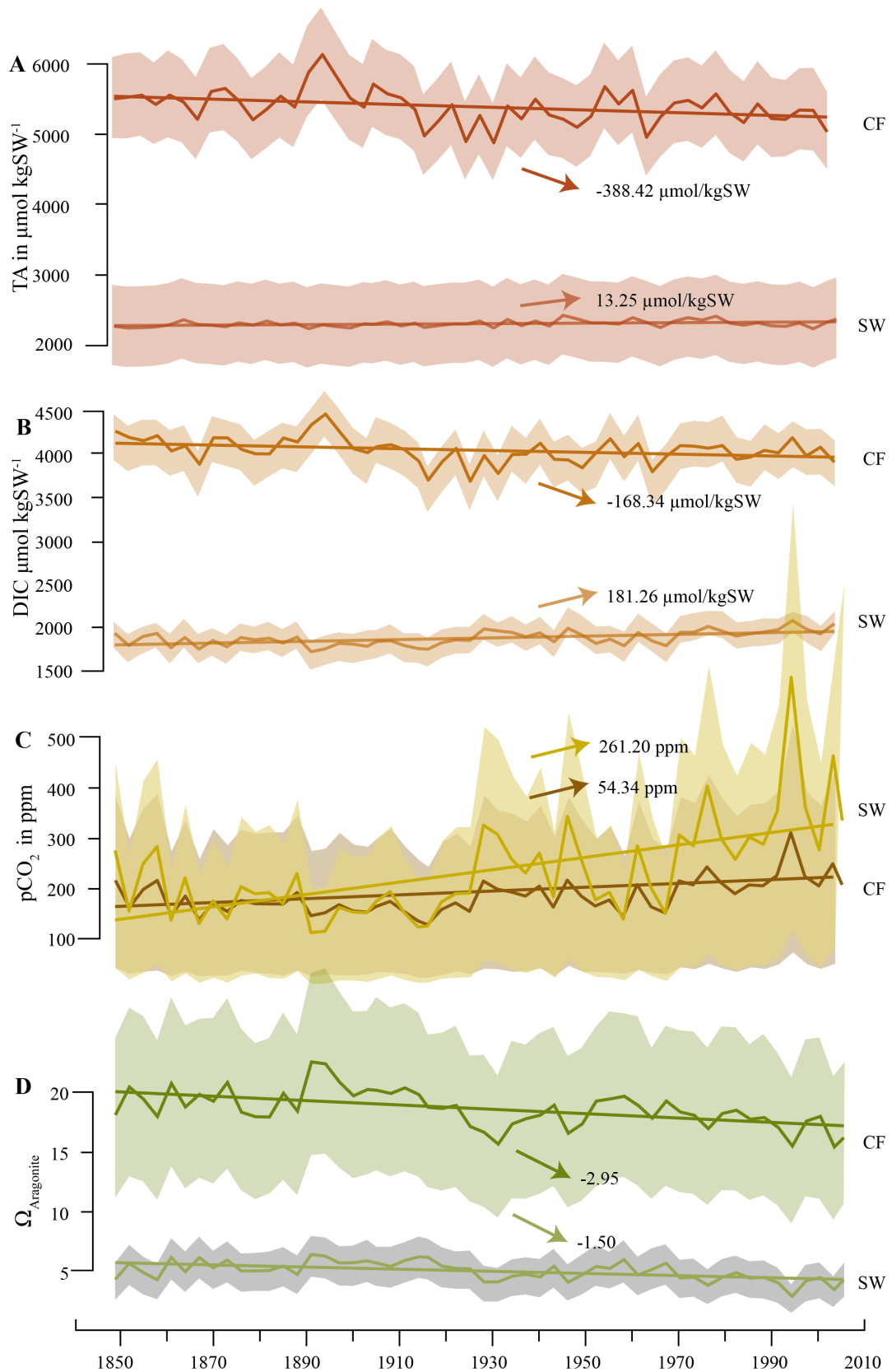
Figure 2.2.2: Carbonate chemistry reconstructed for SW and CF. The coral is upregulating its internal carbonate chemistry compared to the ambient SW carbonate chemistry to facilitate skeletal accretion(M. T. McCulloch et al., 2017b; Ross et al.,

2017). A- TA in CF dark brown and in SW in light brown. TA in CF decreased significantly (p<0.001), while the increase in SW is not robust (p=0.02, for a confidence interval of 99%). B- DIC in CF (dark orange) is dropping significantly (p<0.001) and rising in SW (light orange, p<0.001). C- pCO_2 in SW (yellow) is in agreement with pCO_2 in CF until ca. 1925, when pCO_2 in SW starts exceeding pCO_2 in CF. Both show a robust rise in values (p<0.001). D- Aragonite saturation state in SW (dark green) and CF (light green). The aragonite saturation state is decreasing twice as much in the CF (p<0.001) as the aragonite saturation state in SW (<0.001). Error margins as reported in 6.7 Error Estimation.

Annual $\delta^{18}O_{SW}$ varies from 0.88-2.58‰, corresponding to 33.94–37.56 in salinity, with a mean salinity value of 35.80 reconstructed form eq.6 and a long-term trend of 1.06 over 160 years from 1845 to 2005 CE (p=0.02, Fig. 2.2.4). The mean salinity reconstructed from this study is approaching the lower salinity ranges of the World Ocean Atlas 2018 (WOA18)(Boyer et al., 2018), which fluctuates from 35.89 to 36.94 around a mean of 36.09 (2018, 1955-2017 CE) (Boyer et al., 2018; Zweng et al., 2019). The Global Data Analysis Project (GLODAPv2.2019)(Olsen et al., 2019) dataset includes in-situ measurements relatively close to the coral along a transect across the Florida straight including 7 sampling sites and one sampling site west of Key West with a mean of 36.20 (measured in August 2017, fig. 2.2.2, red dots). The interannual variability in reconstructed SSS is larger than the measured and gridded data show. A higher variability in the SSS data from the Cuban coast is to be expected due a shallower reef environment. WOA18 is a gridded product, consolidating the SSS values as an average over a 1°x1° grid, which is not fully representing local coastal variabilities, while GLODAP only reflects SSS values measured in August 2017. The confidence interval for trends and correlations reported here is 99%.

The reconstructed pH_{SW} of the coral ranges between 7.88 and 8.45 and has a mean of 8.24. The pH_{SW} decreases by 0.3 (p<0.001) over 160 years from 1845 to 2005 CE (Fig. 2.2.2). There are currently no in-situ measurements available for northern eastern Cuban coast, to verify the reconstructed pH. The GLODAP dataset has determined pH value from across the Florida Strait. This data show a mean pH of 8.02 (σ_1=0.02) in surface waters (water-depth < 25 m) (Olsen et al., 2019) which appear to be offset from the reconstructed pHsw but in agreement with the long-term secular trend as recorded in the reconstructed values (Fig. 2.2.3).

TA is mainly controlled by changes in salinity (i.e. evaporation, sea ice formation/melting, precipitation) in the subtropical and tropical ocean and can therefore be expressed with a linear relationship to salinity (Lee et al., 2006; Millero et al., 1998; Takahashi et al., 2014). Coastal near processes such as riverine inputs, upwelling of groundwater, biological activity e.g. precipitation and dissolution of $CaCO_3$ can also alter TA. The southern GOM is most likely impacted by water masses coming from the Caribbean Sea but unlikely influenced by riverine discharges from large river systems (e.g. Mississippi – Atchafalaya)(Cai et al., 2010; Z.-P. Jiang et al., 2014). A correlation from the Caribbean Sea shows close resemblance to the open ocean North Atlantic presented by Takahashi et a. (2014). Due to a lack of research in this area, we cautiously went ahead with the use of the linear relationship between SSS and TA displayed in Takahashi et al. (2014) taken across the broad central Atlantic (40°N-40°S). Over the last 160 years (1845-2005 CE) an insignificant decrease in TA_{SW} can be seen of about 13.25 µmol kgSW^{-1} (p=0.02). Maximum and minimum values are 2,245 µmol kgSW^{-1} and 2,435 µmol kgSW^{-1}, respectively. Reconstructed DIC in SW (derived from TA_{SW} and pH_{SW})(Zeebe & Wolf-Gladrow, 2001) increased by 181.26 µmol kgSW^{-1} (p<0.001) over the same period, ranging from 1,653 µmol kg^{-1} to 2,057 µmol kg^{-1}. The GLODAP dataset also includes TA and DIC values that confirm the range of the reconstructed TA_{SW} and DIC_{SW} data (Fig. 2.2.3) as well as the trend in the reconstructed coral data (location of GLODAP and SOCAT measurements can be found in Fig. 2.2.1).

pCO_2 in SW derived from SSS-TA_{SW} and pH_{SW}, increases by 261.2 ppm from 1845 to 2005 CE and varies from 104 ppm to 588 ppm. Figure 2.2.4A shows reconstructed $pCO_{2\,SW}$ compared to SOCAT data, a database with *in situ* pCO_2 measurements from 1996 to 2022 CE (Bakker et al., 2023). The trend in reconstructed $pCO_{2\,SW}$ values (p<0.001) is in agreement with the SOCAT data (Fig. 2.2.4). Derived from SSS-TA_{SW} and pH_{SW}, the aragonite saturation state in SW has a minimum of 2.8 and maximum of 6.3 over the 160-year period, while exhibiting a decline in aragonite saturation state by 1.5 (p<0.001). Overall, the reconstructed coral carbonate chemistry data reflects the available instrumental measurements, although with some constrains. One possible constraint is that the variability of carbonate chemistry components is much higher in a reef environment than in the open ocean, due to net community calcification and net dissolution in a reef community. The drawdown of pCO_2 during the day from net photosynthesis will lead to an increase in DIC and pH during the day, while net respiration

during the night will have the opposite effect on the carbonate chemistry components(Shaw et al., 2012).

In addition to *in situ* data, there are also several reanalysis or in essence reconstructed products. We have extrapolated these data for the grid from where our coral is located. Monthly coral-based reconstructed SSS data do not correlate well neither with gridded SSS from the Simple Ocean Data Assimilation (SODA) v2.1.6 (r = 0.12, p = 0.002 [Ref.](Carton & Giese, 2008), Table S1)(Harbott et al., 2023) nor with ORA20c (Ocean Reanalysis 20c) (Boisseson & Alonso-Balmaseda, 2016) (r= 0.05, p=0.6). These two gridded reanalysis products, SODA2.6.1 and ORA20c, are also not consistent with each other showing poor coherence (r=0.34, p=0.02). However, applying smoothing filters to the coral-based $\delta^{18}O_{SW}$ record and (Table S1) to the SODA data, correlation ameliorates (for 10 year running average r=0.70, p<0.001, for 40 year running average r = 0.84, p<0.001), but not for ORA (r=0.04, p=0.7). While short term variability is not well represented in the $\delta^{18}O_{SW}$-SSS data, long-term trends are likely to have been recorded by the corals.

Historical reconstructed carbonate chemistry data can be accessed from the reconstructed historical OCADS data repository, based on SOCAT, GLODAP, Coastal Ocean Data Analysis Product (CODAP-NA version 2021(L.-Q. Jiang et al., 2021)), and several Earth system models (Fig. 2.2.3). For all carbonate chemistry components, the reconstructed SW trends agree well with the OCADS trends for the most recent time period (from 1970s to 2005 CE). Significant correlation coefficients for OCADS data and the coral reconstructed data can be found in table S2.

2.2.2.2 Carbonate chemistry reconstruction of the calcifying fluid

$\delta^{11}B$ measurements yielded values in the range of 24.6-26.2‰ corresponding to 8.39 and 8.66 for pH_{CF}. Over the past 160 years, $\delta^{11}B$ decreases by 0.6, equivalent to declines in pH_{CF} by 0.14 (p<0.001). Annual B/Ca values of the coral are increasing significantly by 20.17 µmol mol^{-1} (p<0.001) over 160 years and ranges from 447.55 µmol mol^{-1} to 610.64 µmol mol^{-1}.

pH_{CF} and B/Ca derived DIC in the calcifying fluid declined by 168 µmol kg^{-1} (p = 0.02). DIC of CF ranges between 3,573-4442 µmol kg^{-1} and is approximately 2 times higher than DIC_{SW}. In the CF, pCO_2 is rising in the 160 years by 54.34 ppm with a minimum value of 133 ppm and

a maximum value of 314 ppm. The minimum TA value in the CF is 4,886 µmol kg^{-1} while the maximum is 6,138 µmol kg^{-1}. Both values are approximately 2.5 times higher than in the surrounding seawater. Over the 160 years reconstruction period, the overall decrease in TA$_{CF}$ is 388 µmol kg^{-1}.

The maximum aragonite saturation state value in the CF is 22.95, while the minimum is 15.04, or 3 to 5 times higher than in seawater. The values of CF and SW are well within the values suggested in the growth model by McCulloch et al. (2017) and agreed in coherence to other coral species such as *Poritie s*(M. McCulloch, Trotter, et al., 2012; M. T. McCulloch et al., 2017b). This indicates that the previously agreed pH$_{CF}$ to pH$_{SW}$ equation (eq. 4) considered to be species-specific only for *Porites cylindric*(Fowell, Foster, Ries, Castillo, Vega, et al., 2018; M. McCulloch, Falter, et al., 2012b; Trotter et al., 2011) remains constant and even applicable for the species, *Siderastrea siderea*, of this study. Aragonite saturation is found to be decreasing in the CF by 2.95 over the 160-year record of the coral.

2.2.3 Discussion

Reconstructed carbonate chemistry of the GOM

Qualitatively, reconstructed trends of pH, DIC, pCO$_2$ and Ω are in coherence with those from observations and modeling (OCADS repository, https://www.ncei.noaa.gov/data/oceans/ncei/ocads/metadata/0259391.html, accessed on March 15, 2023) (Fig. 2.2.3). However, there are notable differences: Trends in the latter are continuous over the past 160 years and have been accelerating in the most recent 50 years. In contrast, reconstructed carbonate system parameters only indicate trends since the 1920s. The magnitudes of change are also different, with coral reconstructed changes being about 1.4 (for TA$_{SW}$) to 3.5 (for pH$_{SW}$) times larger in magnitude when compared to the changes observed in the OCADS reconstruction (change over time can be found in Table S2). There is a noticeable offset between the OCADS reconstructed carbonate chemistry data and the coral reconstructed data between 1850 until 1920 CE. From the 1980s to the most recent recorded year, the carbonate chemistry values of both OCADS and coral are in full agreement.

The propagated error estimate (see Materials and Methods) described important error margins for the reconstructed carbonate chemistry values for seawater and calcifying fluid. The error margins for the reconstructed pCO$_2$ of seawater and the calcifying fluid appear to be wide due

to the propagation of analytical and non-systematic errors (Fig. 2.2.4A). All reconstructions are based on reconstructed SST and SSS, that have themselves propagated errors from the analytical and calibrated error. It is a given that combining these errors makes the absolute value rather large. Thus, results are viewed with caution. A reproduction of the method with more reliable SSS and SST data would be highly encouraged. It is noteworthy that the low-resolution OCADS modeled data is represented only every 10-years, while our reconstructed carbonate chemistry components were calculated at a much higher resolution of every 3-years from the coral. The high variability in the coral data is likely a mix of the environmental signal and internal reactions of the coral to changing environmental factors. Therefore, we mainly looked at the reconstructed long-term changes reflected by the coral data similar to the only available low-resolution results of OCADS.

Ocean acidification caused by the anthropogenic increase of CO_2 in the atmosphere leads to an increase in DIC while the charge balance, expressed as TA, stays constant (Schulz, 2009). This is reflected in the OCADS data, where TA increases by only 9 µmol kgSW^{-1}, whereas DIC rises by 60 µmol kg^{-1}. Similarly, the change in coral reconstructed TA is small (54 µmol kgSW^{-1}) and not significant (Table S2) compared with DIC (189 µmol kgSW^{-1}), although both values exceed the observed values (Fig. 2.2.3).

The rise of pCO$_2$ in seawater reconstructed from coral proxies is consistently lower than the OCADS pCO$_2$, which is in direct coherence with atmospheric pCO$_2$ values (Figs. 2.2.3D and 2.2.4). Only in the late 1920s, 1950, and 1970s do the coral reconstructed seawater pCO$_2$ values match the atmospheric pCO$_2$ values. In the 1990s, seawater pCO$_2$ values exceed the atmospheric values and rise up to 552 ppm. One possibility for the incoherence between pCO$_2$ of reef water and atmospheric CO_2 on short timescales is likely because the pCO$_2$ of reef water is not in equilibrium with the atmosphere.

At the reef scale, community metabolism is consistently manipulating the diurnal pCO$_2$ concentrations in ambient seawater. pCO$_2$ values can range from below pre-industrial atmospheric values (< 285 µatm) to more than 1,000 µatm (Shaw et al., 2012). Higher ranges are especially observed in summer, as are higher growth rates, leading to a stronger influence of summer conditions in measurements and adding to the measuring error, that seems to be important especially in the 1990s (Figs. 2.2.4 and 2.2.5).(Falter et al., 2013; Kline et al., 2015)

It is noteworthy that the pCO_2 of the CF follows the pCO_2 of the seawater until the late 1920s, where the pCO_2 of CF diverges from the pCO_2 of seawater with peaks in the 1950s and 1970s, after which the two time-series finally separate as independent datasets.

The historical OCADS dataset (Fig. 2.2.3) is based on GLODAPv2, SOCAT (2022), and CODAP-NA (2021) observations as well as Earth System Models for historical estimations(L. Jiang et al., 2023). The OCADS output as historical projections are a gridded estimation of the carbonate chemistry for an $1°x1°$ area based on limited measurements, which are not necessarily reflecting the real carbonate chemistry history for the northern Cuban coast(L. Jiang et al., 2023). For the more recent time period the historical projections from OCADS and the reconstructed values from the coral are in agreement and diverge mostly from 1850 to 1920s (correlation coefficients can be seen in Table S2).

Carbonate Chemistry of the calcifying fluid. While DIC and TA in seawater increase with seawater pCO_2, both DIC and TA notably decreased in the CF by 168 and 388, respectively (Fig. 2.2.2). Energetically, it is more challenging for the coral to keep up with a high buffering capacity (TA) while DIC is decreasing under a decreasing pH_{CF} (Comeau, Tambutté, et al., 2017). The decrease in Ω_{CF} (Fig. 2.2.2) is therefore consistent with the decrease in DIC. The linear extension of the coral is thereby neither increasing nor decreasing. Overall, the region is experiencing rising SST(Chollett et al., 2012),(Harbott et al., 2023). With warmer temperatures, less energy is necessary for the coral to import DIC and keeping internal Ω_{CF} high to secrete aragonite.(D'Olivo et al., 2019) Overall, the reconstructed CF carbonate chemistry is well within the range of published values (Comeau, Tambutté, et al., 2017; M. McCulloch, Falter, et al., 2012b; M. T. McCulloch et al., 2017b).

Coral calcifying Fluid comparison to seawater. The observations from this coral show a manipulation of the carbonate components in the CF within the range of previous findings. In contrast, the DIC in CF is 2 to 3 times higher than that in seawater with the Ω_{CF} between 15 and 20 (Comeau, Cornwall, et al., 2017; Comeau, Tambutté, et al., 2017; M. T. McCulloch et al., 2017b; Ross et al., 2017). While DIC in the seawater is increasing with increasing pCO_2, DIC of CF decreases. Keeping a high DIC_{CF} and TA_{CF} at high pH_{CF} is energetically challenging for the coral (Comeau, Cornwall, et al., 2017). At the same time, warmer temperature facilitate photosynthesis for the symbionts that deliver more energy to the coral. Therefore, we would

expect rising DIC contents in the CF. The depletion of DIC in the CF may be the initial indication of a physically struggling coral that is unable to maintain high DIC levels while carrying a high pH_{CF} and TA_{CF} either in spite of more energy being delivered to the coral or from the affected symbionts (Castillo et al., 2014a; Comeau, Cornwall, et al., 2017; M. T. McCulloch et al., 2017b).

The pCO_2 concentrations of the CF and seawater track each other closely from 1845 until the late 1920s, when pCO_2 in seawater starts exceeding pCO_2 in the CF. It appears that up until the late 1920s, corals have kept their CF pCO_2 in equilibrium with that of seawater (Fig. 2.2.4A and B). When pCO_2 started rising in the water column, due to anthropogenic CO_2 emission, corals needed to manipulate their pCO_2 in the CF to remain low to favor carbonate precipitation(Allemand et al., 2004). CO_2 and its ion species enter the corals calcifying space through multiply pathways. One CO_2 pathway of entering the coral is via metabolic CO_2 pathway provided by the symbionts. The corals in turn derive their CO_2 directly from SW. Additionally, carbonate and bicarbonate ion are actively transported to the CF and can therefore be regulated by the coral as the second pathway. With an increase in pCO_2 in SW and CF, the bicarbonate ion concentration increases as well, thus lowering the aragonite saturation state. By maintaining a constant pCO_2 in the CF, the coral can sustain its skeletal accretion for survival (Langdon & Atkinson, 2005). However, as the pressure of the rising pCO_2 in the atmosphere increases, the pCO_2 in the CF also increases over time by 54 ppm most likely manifesting from coral animal's energy requirements.

Comparing reconstructed seawater pCO_2 data with $\delta^{13}C$ (Fig. 2.2.4B), our results found a decrease in the $\delta^{13}C$ signature replicating many studies as explained by enhanced burning of fossil fuel and land use changes (Keeling, 1979; H. C. Wu et al., 2018). The depletion of $\delta^{13}C$ values started around 1900 CE, preceding the rapid rise of pCO_2 in seawater. There is a e depletion in coral $\delta^{13}C$ values, indicating a change in the carbon isotope pool and an evident anthropogenic influence. From 1850 to 2005 CE, the isotopic values of $\delta^{13}C$ became depleted by -1.5‰. This depletion is in good agreement with the Law Dome Ice Core Record of -1.6‰ and many other coral reconstruction studies across other tropical regions (Rubino et al., 2013; H. C. Wu et al., 2018). The ocean carbon cycle model (HAMOCC) indicate a depletion in $\delta^{13}C$ isotopic ratio for the coastal waters of Cuba of around -0.8‰ since 1850 CE, correcting for the regionally varying surface dissolved CO_2 concentration (B. Liu et al., 2021; Popp et al., 1989).

The depletion of the coral $\delta^{13}C$ signature would therefore partially arise from the changed atmospheric $\delta^{13}C$ signal known as the Suess Effect and an enhanced diffusion of pCO_2 into the coral from the late 1920s onward (Fig. 2.2.4) (Popp et al., 1989; Zeebe & Wolf-Gladrow, 2001).

The rate of decline in aragonite saturation in the CF over the past 160 years is proportionally less subtle than in seawater (-3 for CF compared to -1.5 in seawater, Fig. 2.2.2.) and in good agreement with a declining DIC_{CF}. Nevertheless, the coral shows no significant change in linear extension. Density data from this coral was not available to us, therefore conclusions can only be based on vertical linear extension(Castillo et al., 2014a; Rippe et al., 2018). Previous experiments provided evidence of a parabolic growth response to higher SST and seawater pCO_2, showing that after *S. siderea* reached its optimal growth temperature and pCO_2 level, calcification rates declined(Castillo et al., 2014a; Ross et al., 2017). Additional studies showed a decline in density while linear extension remained stable in a *S. siderea* (Rippe et al., 2018). We postulate that the critical threshold has not yet been reached which would have also impacted vertical linear extension (Castillo et al., 2014b; Rippe et al., 2018). Density measurements would be a necessity in the future for support. As skeletal density may be decreasing due to increased SST and/or OA while the linear extension rate remains stable. It appears that the symbionts profit from higher seawater pCO_2, thereby providing the coral with more energy to keep up growth (Castillo et al., 2014b; Martinez et al., 2019).

Several experiments on corals have shown that neither pH_{SW} nor DIC_{SW} are the drivers in coral calcification (Comeau et al., 2018; Marubini et al., 2008). Due to the coral's ability to control their DIC and pH in the CF, corals can adapt to changing environments. Experiments in controlled environments have also shown that DIC_{CF} increases with DIC_{SW}, which is not the case for our study(Comeau, Cornwall, et al., 2017). DIC_{CF} is negatively correlated to pH_{CF}, showing the corals ability to counterbalance low pH by upregulating DIC and thereby facilitating the accretions of skeletal material (Comeau, Cornwall, et al., 2017). In our study the DIC_{CF} is decreasing while DIC_{SW} is increasing (Fig. 2.2.2). Previous studies have shown a negative correlation between DIC_{CF} and pH_{CF}. These modulations in the calcifying space have been explained by a possible strategy of the coral to keep the DIC/proton ratio constant for a stable skeletal precipitation(Comeau, Cornwall, et al., 2017; M. McCulloch, Falter, et al., 2012b). Nevertheless, an increase in DIC in SW still means that the coral has to upregulate its internal DIC compared to that in SW, against decreasing pH. This demands more energy of the

coral. A warming GOM and OA in the region might have stressed the coral already to a degree where it cannot keep a constant upregulation between DIC_{CF} and DIC_{SW}. The decrease in DIC_{CF} is affecting Ω in the CF, which has dropped by almost 3 compared to 1.5 in SW (Castillo et al., 2014b).
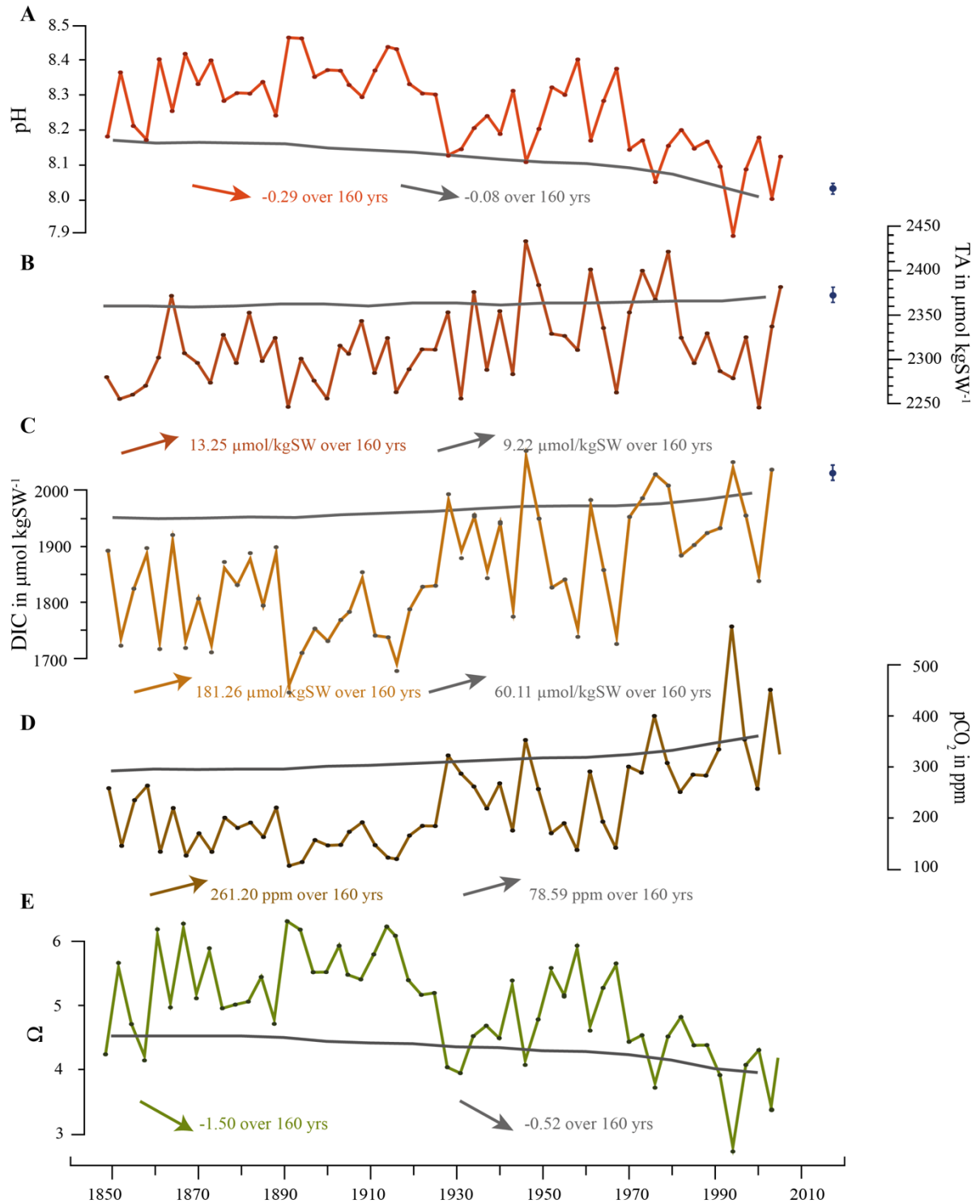
Figure 2.2.3: Carbonate Chemistry of seawater and OCADS data. pH_{SW}, TA_{SW}, DIC_{SW}, $pCO_{2\ SW}$, and Ω_{SW} reconstructed from the coral species *S. siderea* plotted with a 3 year resolution (except for TA, which is annual), compared to OCADS (Jiang et al., 2023, https://www.ncei.noaa.gov/products/ocean-carbon-acidification-data-system, accessed 30.06.2023) time series, 10 year averages, in each panel in gray. **A**- pH_{SW} (red) reconstructed form the coral core and pH from OCADS (grey) compared to GLODAP measurements (blue dot with error bar) is 0.8 (p-value <0.001); **B**- TA_{SW} plotted with an offset of +120µmol/kgSW and measurements from GLODAPv2 (blue dot in 2017)(Olsen et al., 2019). TA_{SW} reconstructed from $\delta^{18}O_{SW}$-SSS and TA from OCADS (grey) is 0.3 (p-value = 0.27); **C**- DIC_{SW} plotted with an offset of 100 µmol/kgSW and plotted with data point from GLODAP (blue dot measured in 2017). Reconstructed DIC_{SW} and DIC from OCADS (grey) with 0.7 (p-value <0.001); **D**- reconstructed $pCO_{2\ SW}$ (dark brown) and pCO_2 from OCADS (grey) is 0.8 (p-value <0.001); **E**- reconstructed Ω_{SW} (green) and Ω from OCADS (grey) is 0.5 (p-value = 0.04). Number of degrees of freedom in correlations $v = 14$. Trends for the whole coral core period are marked for each panel in corresponding colors.

The decrease in Ω_{SW} is consistent with the OA scenario. Although still supersaturated the subtropical Ω_{SW} is declining due to OA as can be seen in the data (Fig. 2.2.3E). The coral is again over-estimating the decline in Ω_{SW} compared to the OCADS data. Takahashi et al. (2014) described a decline of 0.1 per decade for the subtropical oceans that is well reflected in the decline of 0.09 per decade for Ω_{SW} reconstructed from the coral.
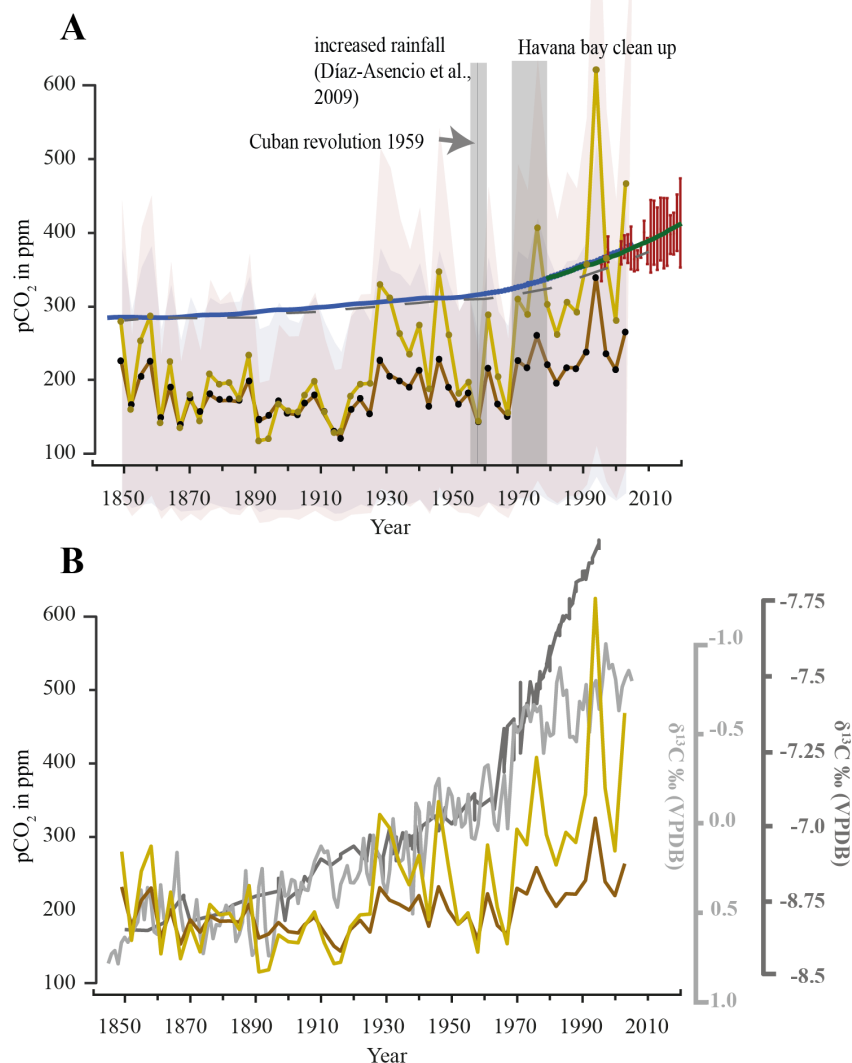
Figure 2.2.4: pCO₂ of SW and CF, and δ¹³C. **A**-pCO₂ in the calcifying fluid in dark brown plotted against pCO₂ in SW in yellow both reconstructed from the coral skeletal material. The light blue and light yellow shades indicate the error range for pCO₂ CF and pCO₂ SW respectively. In blue reconstructed pCO₂ values for the atmosphere(Rixen, 2023). The dashed blue lines are reconstructed pCO₂ values from the OCADS data set(L.-Q. Jiang et al., 2023). Red dots and corresponding error bars are SOCAT data points(Bakker et al., 2023). Dark green line represents the trend in the globally averaged yearly atmospheric carbon dioxide from the Global monitoring laboratory measurements(Lan et al., 2023). The dark grey line marks the timing of the Cuban revolution in 1959. Light grey shading marks a period of increased rainfall in the early 1960s (Goldstein & Galbally, n.d.). In the 1970s a clean-up program started, with the intention of cleaning the Havana Bay area

(Díaz-Asencio et al., 2011). **B**-pCO$_2$ trends reconstructed from Corals TA, B/Ca and δ^{11}B in SW (yellow) and in the CF (brown), every 3rd year, compared to δ^{13}C (annual, light grey) and Law Dome Ice Core(Rubino et al., 2013) δ^{13}C values in dark grey.

Potential influence of environmental pollution. While seawater pCO$_2$ is lower than atmospheric values until the late 1920s, seawater pCO$_2$ and the atmospheric values become consistently more in locked-step in the late 1920s and 1950s and again from the 1970s to today (Fig. 2.2.4B). These phases of coherence coincides with political turmoil and important development in Havana, Cuba. Up until 1959, Havana experienced a phase of rapid urban expansion due to capital inflow from the United States. Cuba's economic and industrial center was concentrated in Havana. Thus, this development was accompanied by increased values of seawater pCO$_2$ that matched the atmospheric pCO$_2$ values (Colantonio & Potter, 2006). The onset of the Cuban revolution in the late 1950s halted the funding for urbanization of Havana and the regime aimed to ruralize the city and urbanize the countryside. Pollution in Havana's bay steadily increased from 1930s to 1961 (Díaz-Asencio et al., 2011), due to the rapid urban expansion with untreated wastewater being disposed directly into the sea. This was followed by consequential clean-up efforts in the 1970s(Colantonio & Potter, 2006). The peak of seawater pCO$_2$ in the beginning of the 1960s takes place during a period of high precipitation and therefore an extra source of CO$_2$ input to the surface waters because precipitation removes CO$_2$ from the atmosphere(Goldstein & Galbally, 2007). We speculate that the trend in reconstructed seawater pCO$_2$ is partially caused by regional environmental pollution. The increase in pCO$_2$ in the atmosphere but also SST increase of the GOM, making CO$_2$ less soluble(Schulz, 2009) and hence increase fugacity might have contributed to the trend in seawater pCO$_2$. Additional water quality data of the most recent 70 years would be required to test our hypothesis.

2.2.4   Conclusion

The approach to reconstruct the carbonate chemistry of seawater from the $\delta^{18}O_{SW}$-SSS relationship and for CF from B/Ca and δ^{11}B show promising results, especially, when there is a dearth of data available from the Gulf of Mexico and Cuba. While seasonal changes are not well reflected in the data, long-term changes are faithfully recorded. For the most recent time period (the last 20 years), coral reconstructed values are coherent and set in the range of measured values from GLODAPv2 and SOCAT, indicating the rich potential of massive corals as a carbonate chemistry archive.(Bakker et al., 2023; Olsen et al., 2019)

The coral from the GOM is recording carbonate chemistry changes of CF and seawater with an offset comparable to that of previously published studies (Comeau, Tambutté, et al., 2017; M. T. McCulloch et al., 2017b; Ross et al., 2017). Coral $\delta^{11}B$ confirms the ongoing OA, which is reflected in the DIC and TA values of seawater. Previous studies indicate that *S. siderea* has a high temperature and CO_2 optimum(Castillo et al., 2014a; Ross et al., 2017). Decreasing DIC levels in the CF contrary to DIC in SW indicate a physically stressed coral, that might already be unable to keep up its vertical linear extension rate. While linear extension remains stable, without the accompanying density records, predictions of the health of the corals can only be assumed with caution. However, the species *S. siderea* is known to be more resilient and remains the dominant species close to Havana, being less affected by bleaching events and OA(Duran et al., 2017). If the threshold values for SST and pH of this coral have not been reached, this might soon be the case in the very near future. This would ultimately reduce the competitiveness and threaten the survivability of even this hardy species in the GOM.

2.2.5   Materials and Methods

2.2.5.1   Coral retrieval and sampling

The *Siderastrea siderea* coral core was retrieved in July 2005 from the northern Cuban coast (82.4239W, 23.1277N) at a water depth of 6 m (fig. 2.2.1). The coral was cored along the maximum growth axis and arrived at the Leibniz Centre for Tropical Marine Research in Bremen, Germany, where the coral core was cut and a slab of 5 mm was removed for sampling. The slab was examined with X-radiograph images (Zemodi - Zentrum für modern Diagnostik, Bremen, Germany) to identify the growth bands of the coral. Cleaning and microsampling procedures have previously been reported elsewhere (Harbott et al., 2023).

For trace element and stable isotope analysis the coral slab was sampled every 0.5 mm with a Proxxon Drill fitted with a 0.4 mm diameter diamond coated drill bit. This sampling procedure yielded approximately 1.5 mg of aragonite powder for a bimonthly resolution. Boron isotope measurements need a higher quantity of aragonite powder, therefore annual samples were taken based on a combination of growth banding and established age-depth relationship of the core based on stable isotope data. Annual samples were taken from 2 entire polyps to assure enough sample for analysis, which yielded approximately 30 mg of sample powder.

2.2.5.2 Boron isotope measurements

Boron isotope ratios were analyzed in the Isotope Geochemistry Laboratory at the MARUM - Center for Marine Environmental Sciences, University of Bremen. Prior to digestion, the samples were cleaned using a cleaning procedure modified after (Barker et al., 2003). Approximately 15 mg of the annual sample powder was first washed in 1 mL ultrapure Milli-Q water and sonicated for 30 seconds before the water was removed and the samples were oxidized with 1% H_2O_2 (buffered with 0.1 M NH_4OH). After an additional sonication step, the solution was removed and the oxidizing step was repeated two more times. The samples were washed again with 1 mL Milli-Q water and finally digested in 300 µL 1N HNO_3.

Boron separation was performed by sublimation experiments as described in Hüpers et al. (2016)2/18/25 9:12:00 PM2/18/25 9:12:00 PM. For this, 45 µL of the sample solution was placed together with 5 µl of 7N HNO_3 in the center of a screw top of conical 5 mL Savillex beaker, which was sealed and placed with the lid on a hot plate at 98°C for 18 hours. The condensate was diluted with 2% HNO_3, adjusted to 50 µg L^{-1} of B (± 10%) and measured with a Thermo Scientific Neptune Plus Multicollector-Inductively Coupled Plasma-Mass Spectrometer (MC-ICP-MS) using the stable introduction system and a X-cone. Samples and reference material (RM) were analyzed repeatedly in the standard-sample bracketing mode using unprocessed NIST SRM 951 with 50 µg L^{-1} of B as reference standard. A 2% HNO_3 solvent was measured before and after each standard or sample, and the average of both analyses was used as the analytical baseline for correction.

The B isotope data were expressed in the delta notation relative to unprocessed SRM NIST 951 (figure 2.2.6), with the uncertainty of sample measurements reported as 2σ. The quality of the purification method and isotope measurements was controlled by NIST SRM 951 (boric acid), seawater and corals. NIST SRM 951 shows a $\delta^{11}B$ value of +0.04 ± 0.13‰ (2σ, n = 11), indicating no isotope fractionation during sublimation. Seawater IAEA-B1 (+39.74 ± 0.03‰, 2σ, n=2) and the laboratory internal seawater standard BSW Susu Knolls (+39.64 ± 0.21‰, 2σ, n=11), overlap within uncertainty with literature values on modern seawater (+ 39.61 ± 0.2‰, $2\sigma_{mean}$(Foster et al., 2010)). An internal laboratory coral reference material from ZMT has a $\delta^{11}B$ value of +25.44 ± 0.12 ‰ (2σ, n = 8) and the GSJ CRM JCp-1 (*Porites* sp.) (+24.30 ± 0.19‰, 2σ, n = 5) agrees with published $\delta^{11}B$ values (e.g. +24.36 ± 0.45 ‰(Gutjahr et al.,

2021)). Repeatability of fully processed samples is within 0.3‰ (2σ). Coral $\delta^{11}B$ measurements were made every 3rd year.

2.2.5.3 Stable isotope measurements

Splits of the homogenous powder sample for stable isotope measurements were also taken for trace element analysis. 500 μg of the coral aragonite powder was digested in 2 mL of 2% ultrapure HNO_3 for 24h. 0.6 mL of the digested coral solution was further diluted with 0.6 mL of 2% ultrapure HNO_3. Samples were measured together with an in-house standard and the international coral standard JCp-1 after every 5 samples and diluted to reach approximately 50 ppm Ca concentration. The measurements were completed on the Plasma Quant ICP-MS from Analytic Jena at Leibniz Centre for Tropical Marine Research in Bremen. Detailed methods for trace elements analysis for these samples using this machine is described elsewhere(Harbott et al., 2023). For single element measurements, every dilution factor was calculated for each sample. Relative standard deviation for B is 2.2% (2σ).

2.2.5.4 Trace element

Splits of the homogenous powder sample for stable isotope measurements were also taken for trace element analysis. 500 μg of the coral aragonite powder was digested in 2 mL of 2% ultrapure HNO_3 for 24h. 0.6 mL of the digested coral solution was further diluted with 0.6 mL of 2% ultrapure HNO_3. Samples were measured together with an in-house standard and JCP-1 after every 5 samples and diluted to reach approximately 50 ppm Ca concentration. The measurements were done on the Plasma Quant ICP-MS from Analytic Jena at Leibniz Centre for Tropical Marine Research in Bremen. Detailed methods for trace elements analysis is described elsewhere(Harbott et al., 2023). For single element measurements, every dilution factor was calculated for each sample. Relative standard deviation for B is 2.2 % (2sd).

2.2.5.5 Carbonate chemistry reconstruction of the calcifying fluid

Boron is dissolved in seawater as boric acid [$B(OH)_3$] and borate ions [$B(OH)_4$]$^-$, where the relative abundances depend on pH (Fowell, Foster, Ries, Castillo, De La Vega, et al., 2018). The predominant boron species at low pH is boric acid while at high pH it is the borate anion (Kowalski & Wunder, 2018; Zeebe & Wolf-Gladrow, 2001). The two stable boron isotopes are ^{11}B (~80% abundance) and ^{10}B (~20% abundance), where borate is enriched in ^{11}B. Corals preferentially incorporate borate-derived boron in their skeleton(Marschall & Foster, 2018).

Thus, both skeletal B/Ca and the relative abundance of ^{11}B (expressed as $\delta^{11}B$, see below) increase with pH. In turn, skeletal B/Ca and $\delta^{11}B$ serve as proxies of pH_{SW}. The boron isotopic ratio in the coral skeleton is commonly expressed as :

$$\delta^{11}B_{coral} = \left(\left[\frac{(\frac{^{11}B}{^{10}B})_{Coral}}{(\frac{^{11}B}{^{10}B})_{NIST}} \right] - 1 \right) \times 1000 \qquad [2]$$

$^{11}B/^{10}B_{Coral}$ is the isotope ratio of the coral skeleton and $^{11}B/^{10}B_{NIST}$ is the isotopic ratio of a boric acid standard(M. T. McCulloch et al., 2017b).

Coral incorporate borate ions into their aragonite skeleton with very little or no isotopic fractioning, making it possible to approximate the pH_{CF} when comparing the borate ion isotopic ratio from the coral to the boron isotopic ratio of seawater(Zeebe & Wolf-Gladrow, 2001).

$$pH_{CF} = log \left[\frac{\delta^{11}B_{SW} - \delta^{11}B_{Coral}}{\alpha_{B3-B4} * \delta^{11}B_{Coral} - \delta^{11}B_{SW} + 1000(\alpha_{B3-B4}) - 1} \right] \qquad [3]$$

pK_B is defined by temperature and salinity(Dickson, 1990) and $\delta^{11}B_{SW}$ is the isotopic composition of seawater (39.61 ‰(Foster et al., 2010)). The B isotopic fractioning factor is 1.0272, as proposed by Klochko et al. (2009). Changes in pH_{CF} parallel changes in pH_{SW}. Currently, there is no species-specific calibration for *S. siderea* for absolute pH_{SW} values. Relative changes in pH_{SW} can however be determined with the calibration equation for *Porites cylindrica* (Fowell, Foster, Ries, Castillo, De La Vega, et al., 2018; M. McCulloch, Falter, et al., 2012b; Trotter et al., 2011) (reconstructed pH_{SW} with other species-specific calibrations can be seen in the supplementary material in figure 2.2.5).

$$pH_{SW} = pH_{CF} - 4.72 / 0.466 \qquad [4]$$

Together with B/Ca as a proxy for $[CO_3^{2-}]_{CF}$, it is possible to reconstruct the carbonate chemistry of the calcifying fluid following the principle that two carbonate system proxies can reconstruct all carbonate system components(Zeebe & Wolf-Gladrow, 2001). Boron is incorporated as $B(OH)_4^-$ and substitutes for $[CO_3^{2-}]_{CF}$ with the partitioning coefficient KD depending on pH (McCulloch et al., 2017). Under the assumption that $[B_{CF}]$ is equal to the boron concentration in seawater, $[CO_3^{2-}]_{CF}$ can be calculation following equation [5](M. T. McCulloch et al., 2017b):

$$[CO_3^{2-}]_{CF} = KD \frac{[B(OH)_4^-]_{CF}}{(B/Ca)_{CaCO_3}}$$ [5]

We used the R code provided by DeCarlo et al. (2018) to calculate $[CO_3^{2-}]_{CF}$ and DIC using the Default settings (for KD from (M. T. McCulloch et al., 2017a), K1 and K2 from (Lueker et al., 2000); and 0.1336*salinity mg/kg after (Lee et al., 2010). With pH_{cf} and $[CO_3^{2-}]_{CF}$ from the calculations and SST and SSS reconstructed from coral Sr/Ca-SST and δ^{18}O-SST, the missing carbonate system components can be calculated(Zeebe & Wolf-Gladrow, 2001). As δ^{11}B was measured at every 3-year resolution, the calcifying fluid of the carbonate chemistry components could only be computed at the same resolution of every 3rd year.

2.2.5.6 Carbonate chemistry reconstruction of seawater

For the reconstruction of the carbonate chemistry of the seawater another carbonate system parameter in addition to pH_{SW} is necessary. TA correlates with SSS for the open ocean and can hence be reconstructed where SSS is known (Brewer & Goldman, 1976; Takahashi et al., 2014; Tarique & Rahaman, 2022). For coastal processes determining TA is more complicated. The western North Atlantic Ocean margins are usually impacted by a dominant river output mixing with ocean water or by alongshore currents (Cai). The Cuban coral core is not located in the vicinity of the Mississippi-Atchafalaya river system and probably along shore current dominated, coming from the Caribbean Sea. The TA-SSS regression presented for the Caribbean Sea from Cai et al. (2010) is quite close to the regression presented in Takahashi et al. (2014) (Lee et al., 2006). TA for seawater was calculated using the linear relationship between potential alkalinity and SSS for the central Atlantic from Takahashi et al (2014). Northern and southern tropical waters were combined in a single regression between 40°N and 40°S. The regression lead to lower TA values than measured from the GLODAPv2 (Olsen et al., 2019) dataset, therefore the intercept was corrected by 40 and agrees with the endmember of the SSS-TA regression from Cai et al. (2019).

TA= 58.5 * SSSC + 230.9 (±12.6) [6]

Equation 6 is adapted from the main Central Atlantic [40°N – 40°S] TA - SSS regression from Takahashi et al (2014), with an initial intercept of 270.9 (Millero et al., 1998).

Currently, there is no in-situ SSS-$\delta^{18}O_{SW}$ data available for the GOM. The Reanalysis of the Simple Ocean Data Assimilation gridded SSS product (SODA2.1.6)(Carton & Giese, 2008) offers SSS data from 1958 to 2008. Regressing $\delta^{18}O_{SW}$ with extracted SSS data (centered at 23.25°N and 82.25°W) yielded following relation for the reconstruction of SSS data:

$$\delta^{18}O_{SW} = 0.25\ (\pm 0.09) \times SSS - 7.18\ (\pm 3.28) \qquad [7]$$

$\delta^{18}O_{SW}$ was calculated following previously established method (Ren et al. (2003)) with additional calculations that can be found in detail in another publication(Harbott et al., 2023). For the reconstruction the method assumes that instantaneous changes in $\delta^{18}O$ of the coral are the sum of two components: changes in SST and instantaneous changes in $\delta^{18}O_{SW}$. The SST component can be expressed by the rate of change of Sr/Ca per °C for the specific coral a shown in Harbott et al. (2023).

All seawater carbonate chemistry parameters were then calculated with the R package Seacarb(J.-P. Gattuso et al., 2021) for the total scale, using reconstructed SST, SSS, and TA values together with pH$_{SW}$ from the δ^{11}B-pH relationship (Lewis & Wallace, 1998). The R package is based on the thermodynamic equilibrium of the carbonate system and can be described by 6 parameters (DIC, TA, pH, $[CO_3^{2-}]$, $[HCO_3^-]$, CO_2) (Zeebe, 2012; Zeebe & Wolf-Gladrow, 2001). Two carbonate system parameters are required next to SST and SSS to calculate the rest. For the calculations we chose for k1 and k2 from Luecker et al. (2000)(Lueker et al., 2000) and for the concentration boron-salinity relationship we went with the one proposed by Lee et al. (2010)(Lee et al., 2010).

2.2.5.7 Error Estimation

To estimate an error for the TA$_{SW}$, pH$_{SW}$, pH$_{CF}$ reconstruction, we used a R script for Monte Carlo error estimates provided by ChatGPT. Random errors (the non-systematic errors for measurements provided the standard deviation frame for the random errors) were added to parameters 30000 times to ensure normal distribution. The standard deviation of the results was used as the error and reported or propagated for further calculations. For an error estimation of pH$_{SW}$ and pH$_{CF}$ the error for δ^{11}B of 0.11 ‰ was propagated. For the error of TA$_{SW}$, we used the SSS error of 0.71 for the standard deviation frame. The Monte Carlo error estimation code for R can be found in the Supplementary Information.

Standard deviation DIC_{CF} of the calcifying fluid 263.05 µmol/kgSW for DIC_{CF}. This error was estimated by a Monte Carlo scheme, provided in the R code by DeCarlo et al. (2018)(DeCarlo et al., 2018). The DIC_{CF} error together with the pH error (0.21) was used in the Seacarb package to calculate the errors of TA_{CF} (569.51µmol/kg), pCO_{2CF} (154.38 µmol/kg), and Ω_{CF} (6.47). The Seacarb package considers the errors for SST, SSS, DIC_{CF}, and pH_{CF}. Error for the carbonate chemistry of seawater were also calculated with the Seacarb package. Errors propagated for the carbonate chemistry of seawater were TA_{SW} (0.1), propagated from SSS reconstruction and pH_{SW} (0.21), as well as SST and SSS. DIC_{SW} has a standard deviation of 150.37 µmol/kg, pCO_{2SW} has a standard deviation of 182.25 ppm and Ω_{SW} has a standard deviation of 1.56.

2.2.6   Data availability

Parts of the cited data this manuscript is based on, is published and accessible in the data repository of Pangaea https://doi.pangaea.de/10.1594/PANGAEA.963278. The carbonate chemistry data, δ11B, and B/Ca can be found on Pangaea
https://doi.pangaea.de/10.1594/PANGAEA.965916
 The SODA SSS v2.1.6 (Carton & Giese, 2008) dataset was accessed through the IRI/LDEO Climate Library, and is publicly available
(http://iridl.ldeo.columbia.edu/SOURCES/.CARTON-GIESE/.SODA/.v2p1p6/, accessed 01.04.2022). The ORA-20C dataset is openly available (https://www.cen.uni-hamburg.de/en/icdc/data/ocean/easy-init-ocean/ecmwf-ensemble-of-ocean-reanalyses-of-the-20th-century-ora-20c.html, accessed 16.11.2023). The historical OCADS surface ocean acidification indicators dataset is publicly accessible
(https://www.ncei.noaa.gov/data/oceans/ncei/ocads/metadata/0259391.html, accessed on 05.05.2023). GLODAPv2 2019 is freely accessible (https://www.ncei.noaa.gov/access/ocean-carbon-acidification-data-system/oceans/GLODAPv2_2019/, accessed on 6.1.2023) and SOCAT is also publicly available (https://www.ncei.noaa.gov/access/metadata/landing-page/bin/iso?id=gov.noaa.nodc:0278913, accessed on 6.11.2023).

2.2.7   Acknowledgments

2.2.8 Authors Contribution

M.H. and H.C.W. designed the research. M.H. completed the sampling, sample analysis, data analysis, and served as primary author. M.H., H.K., S.A.K., and A.M., performed the isotope geochemical analyses. M.H. carried out the trace elements analysis. T.R. provided initial field sampling funding and T.R., C.J., and P.G.-D. recovered the coral core. P.G.-D. was responsible for local logistics, expertise, and permitting. M.H. and T.R. conceptualized the manuscript. All of the authors discussed the results and commented on the manuscript.

2.2.9 Supplementary Information

The supplementary material contains correlation tables for reanalysis products such as SSS SODA(Carton & Giese, 2008) to $\delta^{18}O_{SW}$ and correlation coefficients for TA, DIC, pCO_2, and $\Omega_{Aragonite}$ calculated from the corals skeletal material B/Ca, $\delta^{11}B$, and $\delta^{18}O_{SW}$ compared to the carbonate chemistry parameter from the OCADS dataset (L.-Q. Jiang et al., 2023) and their trends since 1850.

Different species specific calibrations for *Pocillopora damicornis,* and *Acropora youngei* are compared to the calibration used in this manuscript for *Porites cylindrica,* to demonstrate that the best fit for the pH_{SW}-pH_{CF} calibration for the S. siderea is the one used here.

Table 2.2.1: Correlation coefficients of smoothed $\delta^{18}O_{SW}$ data and Indices and gridded data sets.

Dataset $\delta^{18}O_{SW}$	r monthly	p-value	r 10 years	p-value	r 40 years	p-value
AMO	-0.0119956	0.6181	-0.0347558	0.1632	0.217746	<0.001
CMAP	-0.0350396	0.5362	-0.4062348	<0.001	-	-
SSS SODA Carton and Giese, 2007	0.113818	0.006715	0.6586492	<0.001	0.806984	<0.001
SSS SODA detrended	0.05457149	0.1948	0.4376748	<0.001	-0.513564	<0.001

Table 2.2. 2: OCADS carbonate chemistry data and correlation coefficients compared to corresponding carbonate chemistry of SW reconstructed from the coral core of this study.

OCADS	r	p-value	Degrees of freedom
pH$_{SW}$	0.7905937	<0.001	14
TA$_{SW}$	0.2891276	0.2774	14
DIC$_{SW}$	0.7266202	0.001431	14
pCO$_{2SW}$	0.8036892	<0.001	14
Ω$_{SW}$	0.5201512	0.03888	14

Table 2.2.3: Trends for reconstructed carbonate chemistry of SW and CF as well as OCADS.

Coral	Trend over time	p-value	Trend over 160 years
pH$_{SW}$	pH$_{SW}$=-0.0018351 (0.0003) yr + 11.7166126 (0.64)	<0.001	-0.29
TA$_{SW}$	TA$_{SW}$= - 0.08281 (0.02705)yr + 2076 (52.08)	0.002	13.25
DIC$_{SW}$	DIC$_{SW}$=1.1329 (0.22)*yr1+-371.0792 (419.5)	<0.001	181.26
pCO$_{2SW}$	pCO$_{2SW}$= 1.6325 (0.28)*yr-2873.96 (547.69)	<0.001	261.20
Ω$_{SW}$	Ω$_{SW}$= -0.009396 (0.002) yr +22.933750 (3.89)	<0.001	-1.50
pH$_{CF}$	pH$_{CF}$= -0.0008551 (0.00016)yr + 10.1799415 (0.3)	<0.001	-0.14
TA$_{CF}$	TA$_{CF}$= -2.43 (0.57) *yr + 9836.31 (1103.64)	<0.001	-388.42
DIC$_{CF}$	DIC$_{CF}$=-1.05 (0.43)*yr+5837.85 (826.61)	0.01768	-168.34
pCO$_{2CF}$	pCO$_{2CF}$= 0.34 (0.08)*yr-480.89 (153.38)	<0.001	54.54
Ω$_{CF}$	Ω$_{CF}$ = -0.018 (0.004)*yr + 53.58 (7.52)	<0.001	-2.95

OCADS			
pHT	pHT=-5.225e-04 (0.00005) yr+9.147 (0.103)	<0.001	-0.08
TA	TA=0.0276*yr + 2255	<0.001	9.22
DIC	DIC=0.3757 (0.037)*yr1+1247 (0.7)	<0.001	60.11
pCO$_2$	pCO$_2$=0.49118 (0.055)*yr-639.85294 (106.11)	<0.001	78.59
Ω	Ω =-0.0032353 (0.0003) yr+10.6111765 (0.54)	<0.001	-0.52
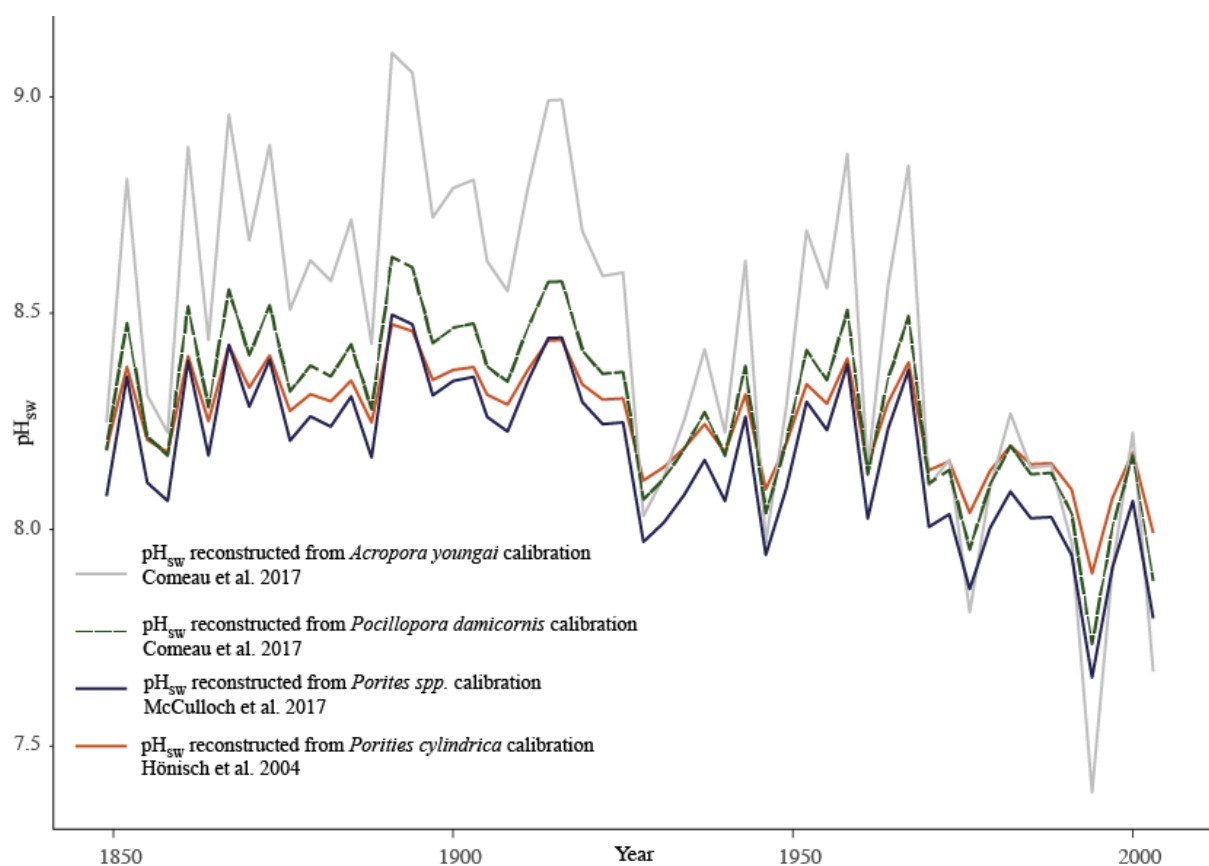
Figure 2.2.5: pH of seawater reconstructed from pH of the calcifying fluid as described in Methods eq. 3 following different species-specific calibrations from Acropora youngei in grey(Comeau, Cornwall, et al., 2017), Pocillopora damicornis in green and as a dashed line(Comeau, Cornwall, et al., 2017), Porites spp.(M. T. McCulloch et al., 2017a) in dark blue and Porities cylindrica(Hönisch et al., 2004) that was used for the reconstruction of the carbonate chemistry. pHSW calibration from the Porities cylindrica shows the lest variability in pHSW and fits well within the accretion model proposed by McCulloch et al. (2012 and 2017)(M. McCulloch, Trotter, et al., 2012; M. T. McCulloch et al., 2017a).
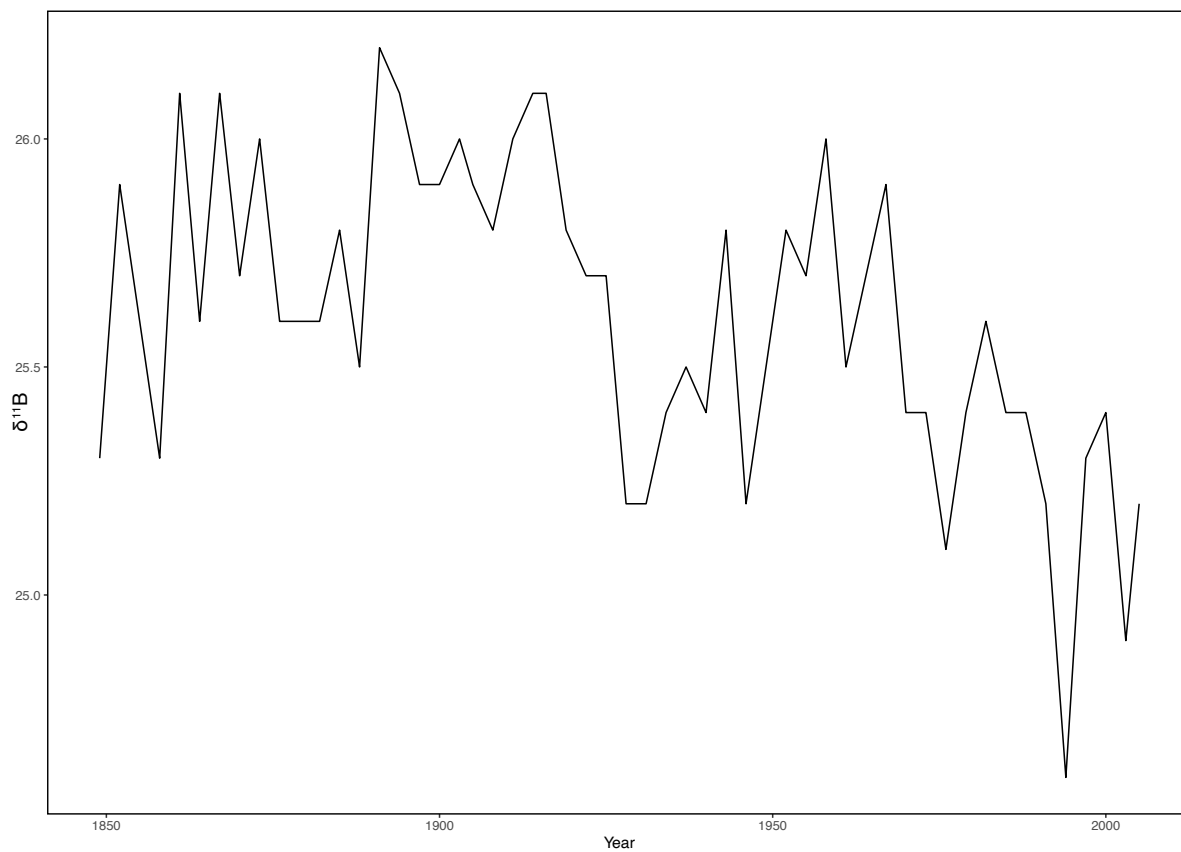
Figure 2.2.6: Measured Boron isotope data for every 3rd year from the *S. siderea* coral core.

2.3 High resolution pH-δ^{11}B calibration for a pristine vs. infested scleractinian coral *Orbicella annularis* from Puerto Rico

Marie Harbott[1], Sara Todorovic[1], Henry Wu[2], Grit Steinhöfel-Sasgen[3], Albert Bentin[3], Sherman Clark[4], Amos Winter[4]

[1] Leibniz Centre for Tropical Marine Research (ZMT) GmbH, Fahrenheitstraße 6, 28359 Bremen, Germany

[2] Institute of Geology, University of Hamburg, Bundesstrasse 55, 20148 Hamburg, Germany

[3] Helmholtz-Zentrum für Polar- und Meeresforschung, Alfred-Wegener-Institut, Bremerhaven, Germany

[4] Department of Earth and Environmental Systems, Indiana University, Terra Haute, Indiana

Department of Marine Sciences, University of Puerto Rico, Mayaguez, Puerto Rico

Corresponding author: Marie Harbott (marie.harbott@leibniz-zmt.de)

Abstract

Coral cores taken from living or fossil cores frequently help decoding changes in our past climate. They incorporate environmental information into their skeleton while growing, such as boron isotopes. The composition of δ11B of the skeletal material depends on the pH of the ambient water. Part of a coral is their microbiome, that when the coral is healthy, can live in symbiosis with the coral. However, stress like warming temperatures and acidification can weaken the coral and make it easier for algae, bacteria, fungi to enter the coral and attack it from the inside. The boreholes, that are left behind can be filled for example with secondary calcite or aragonite leading to a change in the chemical signal and potentially in the interpretation of environmental changes. An Orbicella annularis coral core was chosen from La Parguera, Puerto Rico, due to its proximity to a buoy measuring pH, SST, and SSS. High resolution LA-MC-ICP-MS measurements revealed alterations δ^{11}B ratio due to secondary aragonite. Parts of the skeleton with enhanced boring activity and borehole fillings show higher δ^{11}B values than more pristine coral skeletal parts. δ^{11}B values from the pristine part of the coral served as the calibration ratios for a new pH-δ^{11}B calibration for the Orbicella annularis species.

2.3.1 Introduction

Massive scleractinian corals are frequently used for the reconstruction of the paleoclimate and paleoenvironmental conditions (e.g. DeLong et al., 2014; Hönisch et al., 2004; Maupin et al., 2008; Ren et al., 2003; Tarique & Rahaman, 2022; Wu et al., 2014, 2017, 2018; Wu & Grottoli, 2010). They are an important tool to understand climate variability where there is limited or missing data, especially prior to in situ measurements. The results give us insights into past events and possibly help understand future climate variabilities.

Coral reefs are exposed to several destructive forces, such as physical, chemical and biological threats (Tribollet, 2008). Bioerosion is an important part of the carbonate balance of the reef environment (Tribollet & Golubic, 2011). Microboring and macroboring as well as grazing are part of the bioerosion process. Microborers use mostly chemical forces to penetrate into the carbonate substrate by dissolving the carbonate while macroborers use both, physical and chemical forces (Tribollet & Golubic, 2011). Microborers are also part of the microbiome of the coral and can also benefit the coral by providing alternative energy sources (Ricci et al., 2019). Corals suffering through bleaching events might have higher survival chances due to green algae living just below the coral tissue layer (Ricci et al., 2019). It has been shown that carbohydrates, produced in an algae green band, where translocated and incorporated into the coral skeleton. When symbionts leave the coral hosts, the green algae could help with the recovery of the coral animal (Ricci et al., 2019)
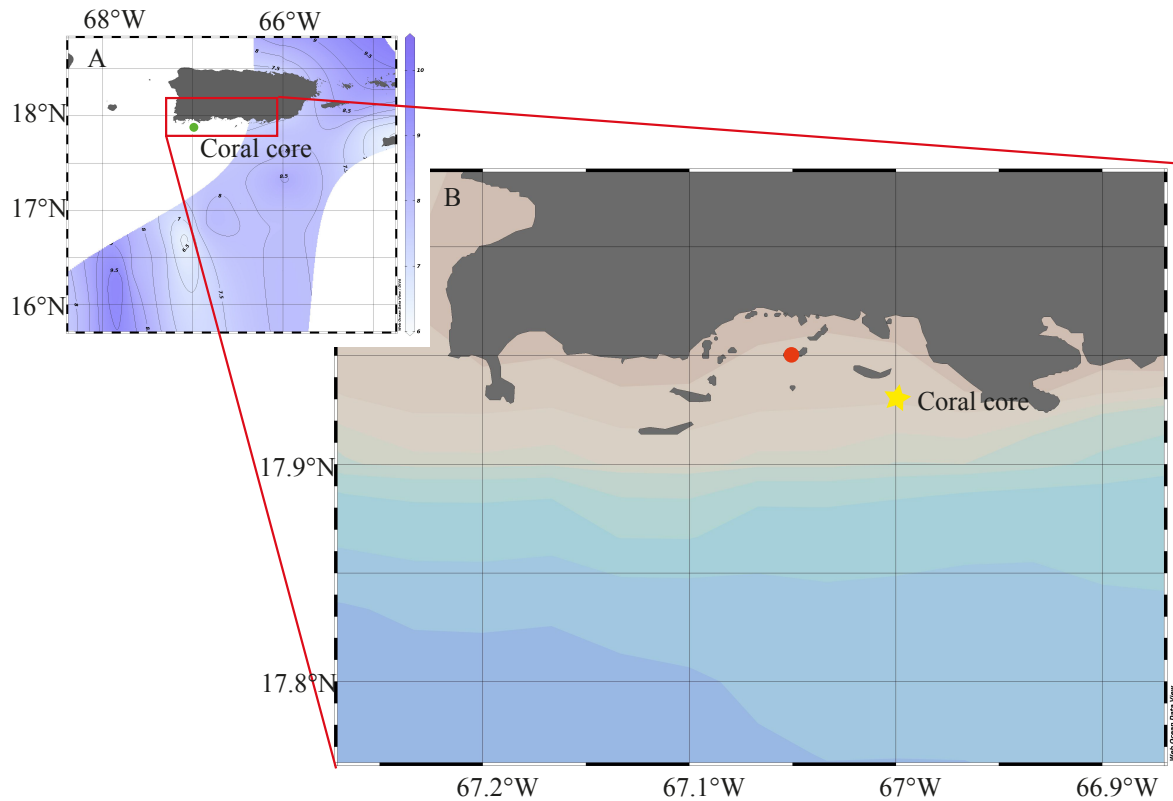
Figure 2.3.1: A- Map of Puerto Rico and GLODAPv2.2023(Lauvset et al., 2022) pH data for this region. Green dot on map represents the location of both buoy and coral core. B- Zoom on Map with more precise locations of the coral core (represented by the yellow star) and a red dot, indicating the location of the buoy.

Biological erosion, due to fungi infestation, on the other hand, is considered the main force of reef degradation (Tribollet & Golubic, 2011). Algae and cyanobacteria are not necessarily parasites and harmful to living corals, as are fungi (Nothdurft et al., 2007; Tribollet, 2008). Secondary diagenesis can happen as early as the first settling of the coral larva and its first skeletal deposition, with fungi attacking the coral from the beginning (Golubic et al., 2005).

2.3.1.1   Green algae

Major endolithic constituents of living corals are the green algae *Ostreobium quekettii* (Le Campion-Alsumard, Golubic, & Priess, 1995) and *Ostreobium constrictum* (Le Campion-Alsumard, Golubic, & Priess, 1995). *Osteobium* has been identified as one of the most common green algae endolith in coral substrate and is responsible for the formation of green bands in the coral skeleton beneath and parallel to the polyp zone (Le Campion-Alsumard, Golubic, & Hutchings, 1995). The green algae *Ostreobium* is responsible for most of the skeletal

deterioration in corals of up to 60-90% (Ricci et al., 2019). The boreholes are between 2 and 50 µm in diameter (Perry, 1998). Green algae bands can usually be found a few millimeters below the living coral tissue (Hartmann et al., 2010; Krause et al., 2019). It does not precipitate secondary aragonite or calcite and there is no knowledge on what happens to the dissolved skeletal material (Hartmann et al., 2010). Green algae are phototrophic organisms, depending on sunlight to perform photosynthesis. The seasonal difference in sunlight can lead to seasonal algae blooms just below the corals tissue layer (Galindo-Martínez et al., 2022).

2.3.1.2 Cyanobacteria

Cyanobacteria are frequently found in living and dead corals and follow the coral growths due to their dependence on light. Their borehole size is between 5 and 20 µm in diameter (Perry, 1998).

To dissolve the skeletal material of the coral, cyanobacteria lower the Ca^{2+} concentration thereby provoking dissolution. The Ca^{2+} is transported intracellular by the cyanobacteria to the end of the filament into the external medium. The excretion will lead to an oversaturation in Ca^{2+} and provoke precipitation in the form of calcite or secondary aragonite (Garcia-Pichel et al., 2010). Cyanophotes are active deeper inside of the coral and may offer another source for organic material for fungi (Bak & Laane, 1987).

2.3.1.3 Fungi

Fungi are part of the endolithic microborers that live in hard substrates such as the corals skeleton. They penetrate into marine carbonates by dissolving them and are between 1-2 µm in diameter (Perry, 1998). Fungi are organotroph (heterotroph) microborers whereas cyanobacteria and algae belong to the microboring phototrophs. Cyanobacteria and algae themselves can be attacked by fungi, which is also found as a microborer in live corals. However, fungi can also coexist in an equilibrium in a healthy coral as part of the coral microbiome (Ricci et al., 2019).

The effect that microborers and secondary precipitation due to microborers have, is not well understood. Secondary precipitation in pore spaces might come from the dissolved aragonite in borings that enter the pore space, when the microboring organisms does, thereby increasing the aragonite saturation state in the pore space. This might also work the other way around, when

pore water enters the boreholes and mixes with the dissolved mix in the borehole (Gaillardet & Allègre, 1995; Ricci et al., 2019). The formation of aragonite by the coral is discussed in the following chapter.

2.3.1.4   Biomineralization

Coral biomineralization happens in a partially isolated extracellular calcifying medium (ECM) (Allemand et al., 2004). The ECM is situated between the skeleton of the coral and coral polyps basal cell layer (Allemand et al., 2004; Marschall & Foster, 2018). Dissolved inorganic carbon (DIC) reaches the ECM through mostly two pathways. Bicarbonate $[HCO]_3^-$ is the most abundant carbonate species in seawater and is supplying the ECM directly. CO2 also reaches the ECM via diffusion, most likely from CO_2 enriched, low pH domains, presumably supplied by zooxanthellae activity(Marschall & Foster, 2018) The coral acidifies the calcifying fluid in the calcifying zone through the CATPase to produce aragonite, by exchanging $[H]^+$ with $[Ca]^{2+}$ from $[HCO]_3^-$ (Zoccola et al., 2015). The following equation shows the formation of the skeleton aragonite in the calcifying medium (Marschall & Foster, 2018; Zoccola et al., 2015):

$$CO_2 + H_2O \xrightarrow{CA} CaCO_3 + 2\,H^+ \qquad [2.3.1]$$
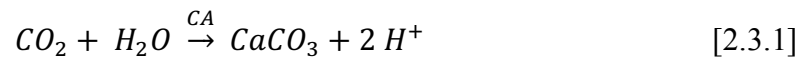
CA stands for carbonic anhydrase (Zoccola et al., 2015). The described mechanisms is lowering the pH thereby shifting the equilibrium composition of DIC towards $[CO]_3^{2-}$ (compared to $[HCO]_3^-$). Thereby, the aragonite saturation state is increased in the calcifying fluid. Boron reaches the ECM probably through the most direct pathway, supplied by seawater (Marschall & Foster, 2018).

2.3.1.5   Boron isotopes in seawater and incorporation into the coral skeleton

Two different molecular species of Boron exist in seawater: Boric acid $[B(OH)]_3$ and Borate $[B(OH)]_4^-$. Their relative abundance depends on pH of seawater. The isotopic ratio of both species is also pH dependent and is expressed in equation (2) (Marschall & Foster, 2018):
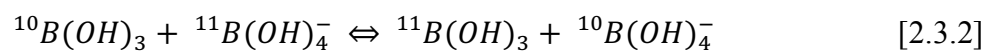
$$^{10}B(OH)_3 + {}^{11}B(OH)_4^- \Leftrightarrow {}^{11}B(OH)_3 + {}^{10}B(OH)_4^- \qquad [2.3.2]$$

Boric acid has a trigonal shape and is slightly smaller than the tetrahedral borate anion (Hershey et al., 1986). The isotopically heavier [11]B prefers the trigonal shape of boric acid, while the isotopically lighter [10]B prefers the borate anion (Marschall & Foster, 2018). Those two aqueous species are in a pH dependent equilibrium, where boric acid is predominant at lower pH of seawater and the borate anion at higher pH in seawater. Their dissociation constant pkB is temperature and salinity dependent and is 8.6 at 25°C and 35 salinity (Dickson, 1990; Marschall & Foster, 2018). The most frequently used fractioning factor for the isotope fractionation was defined by Klochko et al. (2016) and is $\alpha_{(B3-B4)}$ = 1.0272 through experiments (Klochko et al., 2006). However, the fractioning factor cannot describe the isotope fractioning for all marine isotopes. Species specific calibration is needed. Fractioning factor ranges have been reported to be between 1.024 and 1.030 (Klochko et al., 2006; Nir et al., 2015).

Boron is found in marine carbonates as a trace element. Aragonite incorporated 3 to 5 times more Boron than calcite. While calcite mostly incorporates the trigonal boric acid, in aragonite the borate anion is predominantly used (Marschall & Foster, 2018). Studies investigating the growth of synthetic aragonite show that Boron is incorporated straight from the surrounding solution without fractioning. Hence, δ¹¹B values from the aragonite correspond to δ¹¹B$_{[B(OH)4-]}$ values from the solution (Holcomb et al., 2016; Mavromatis et al., 2015; Noireaux et al., 2015). In experiments under controlled conditions aragonite appears to only incorporate the tetrahedral borate anion (Marschall & Foster, 2018) with a very small percentage (<15 %) of the trigonal boric acid, probably transformed in a post crystallization process (Marschall & Foster, 2018). Tropical corals live in a pH environment of typically 8.0 to 8.1 and have a δ¹¹B composition of ca. 22% to 25%.

2.3.1.6   pH reconstruction

Due to the pH dependence of the two aqueous Boron species and the pH dependence of isotope fractioning, pH can be calculated with the isotopic ratio of Boron δ¹¹B, and is expressed as (Marschall & Foster, 2018):

$$\delta^{11}B_{coral} = \left(\left[\frac{\frac{^{11}B}{^{10}B_{Coral}}}{\frac{^{11}B}{^{10}B_{NIST}}}\right] - 1\right) \times 1000 \qquad [2.3.3]$$

The isotopic ratio measured in the coral is expressed as $^{11}B/^{10}B_{Coral}$, while the isotopic ratio of the boric acid standard NIST951 is expressed as $^{11}B/^{10}B_{NIST951}$.
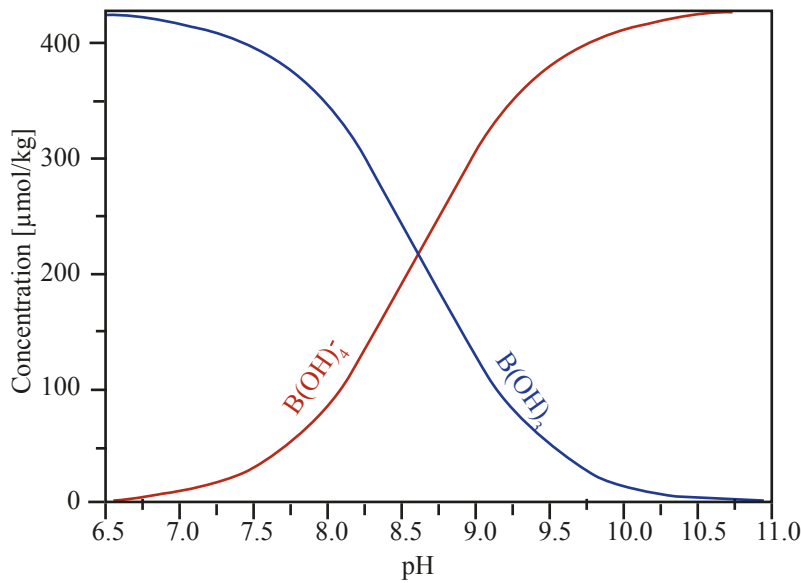
Figure 2.3.2: Borate ion and boric acid concentration in seawater depending on pH.

The relative abundance of both boron species depending on the pH in seawater can be seen in figure 2.3.2 and is expressed as follows (Marschall & Foster, 2018):

$$^{10}B(OH)_3 + {}^{11}B(OH)_4^- \Leftrightarrow {}^{11}B(OH)_3 + {}^{10}B(OH)_4^- \qquad [2.3.4]$$

To calculate pH of the calcifying fluid we follow the equation of Zeebe and Wolf-Gladrow (2001):

$$pH_{CF} = log\left[\frac{\delta^{11}B_{SW} - \delta^{11}B_{Coral}}{\alpha_{B3-B4} * \delta^{11}B_{Coral} - \delta^{11}B_{SW} + 1000(\alpha_{B3-B4}) - 1}\right] \qquad [2.3.5]$$

$\delta^{11}B_{SW}$ is the isotopical ratio of seawater (39.61 ‰) (Foster et al., 2010) and αB3-B4 defines the isotopic fractioning factor 1.0272 (Klochko et al., 2006), while $\delta^{11}B_{Coral}$ is the measured boron isotopic ration of the coral skeleton. For the reconstruction of the pH of seawater (pH_SW), coral species specific δ¹¹B-pH_SW calibrations exist that can be used to reconvert pH_C into pH_SW. The choice of calibration should have no influence on relative change of pH_SW, but only on absolute pH_SW values, therefore the widely used calibration for the massive coral *Porites cylindrica* (Fowell, Foster, Ries, Castillo, Vega, et al., 2018; Hönisch et al., 2004; M. McCulloch, Falter, et al., 2012a; Trotter et al., 2011) was used with following δ¹¹B – pH calibration equation.

$$pH_{SW} = \frac{(pH_C - 4.72)}{0.466} \qquad [2.3.6]$$

Manuscript III: pH - δ¹¹B calibration for an *Orbicella sp.* from Puerto Rico

2.3.1.7 Study and coral site

The coral core was taken from a living coral at the La Parguera Marine Reserve.

There is an approximate coral coverage of ca. 10 % living corals. Reefs are affected by coral bleaching, coral infectious diseases and fishing (Meléndez et al., 2020). Fresh water input comes solely from precipitation and river plumes from the Amazon and Orinoco Rivers (Chérubin & Richardson, 2007). Low precipitation patterns mark this region from January to April, while heavier rains start from May through October (Jury et al., 2007).

In 2009 the NOAA Coral Reef Conservation Program (CRCP) started measuring SST, SSS, pH, and pCO$_2$ in the water column (17.95°N, 67.05°W compared to 17.93°N, 67°W, where the coral core was taken from; on the forereef of the Enrique middle-shelf reef at 3-m depth) (Meléndez et al., 2020) and with that offer a unique perspective on the coral reef, with the coral core taken in the proximity of the buoys location. The close location provides the opportunity for an in-situ pH- δ¹¹B calibration for the coral species *Orbicella annularis*, comparing high resolution pH- with high resolution δ¹¹B measurements (fig. 2.3.1).

This coral shows secondary diagenesis in boreholes and pore spaces, changing the δ¹¹B signature and therefore the pH- δ¹¹B relationship for at least 4 years of the δ¹¹B time measurements. The pristine part of the coral offers the unique opportunity to establish a pH-δ¹¹B calibration for the coral species *Orbicella annularis,* thereby adding to the limited pH calibration pool. Furthermore, we want to investigate the impact on δ¹¹B from secondary aragonite and discuss the reconstruction of pH from the affected coral core.

2.3.2 Method

2.3.2.1 Coral Core retrieval

The coral *Orbicella annularis* was collected on 04.12.2020 Turrumute Reef La Parguera, Puerto Rico (17.93°N, 67°W). The location was chosen due to its proximity to the buoy collecting SST, SSS, and pH of the surrounding seawater since 2009 located at 17.95°N, 67.05°W (Meléndez et al., 2020).

The core was transported to the Leibniz Center for Marine Tropical Research where it was cut in half and cleaned for the δ¹¹B analysis. For the cleaning process we followed the method used

by Krawczyk et al (2020). The core halves were cleaned 3 times in an ultrasonic bath with MilliQ water for 10 minutes. Overnight the core halved were submerged in a bath of sodium hypochlorite (with 6-14% active chlorine) diluted to a 1:1 ratio with distilled water to remove any organics from the core surfaces. The next day the core halves were again cleaned in ultrapure MilliQ water in an ultrasonic bath 3 times for 10 minutes before they were covered and dried at room temperature.

A 7cm long and ca 3 cm wide piece was cut from the top left corner of one coral half for analysis with LA-MC-ICP-MS. The piece was further cut to 4 smaller pieces to fit onto glass slides. The difference pieces where cut to 2.2 mm thick slabs with a Buehler Isomet precision wet saw at 300 rpm. Each piece was then glued to a glass slide and ground down to less than 4mm thickness, so it would fit into the Laser chamber of the UV fs LA system. The coral thick slides were covered with Araldite and once dry, polished with 1200, 2400, and 4000 grit paper.

2.3.2.2   In situ B isotope analysis by femtosecond laser ablation

We measured B isotope ratios at high spatial resolution using the customized UV femtosecond laser ablation system (Solstice, Spectra Physics) connected to a multi-collector inductively coupled plasma mass spectrometer (MC-ICP-MS) (Nu Plasma II, Nu Instruments) at the AWI ICP facility of the Alfred-Wegener Institute in Bremerhaven, Germany. This set-up enables B isotope analysis with a precision of ± 0.9 ‰ (2 SD) independently of the sample matrix and was successfully applied to investigate corals (Steinhoefel et al., 2023).

The laser ablation system consists of a Ti-sapphire regenerative amplifier system (Solstice, Spectra-Physics, USA), an optical unit to convert the fundamental wavelength of 775 nm into deep UV light and a software-controlled sample stage designed by Rapp Opto Electronics, which includes a microscope (Zeiss Axio Scope A1), a charge-coupled device (CCD) camera and an ablation chamber. This system provides an output laser beam with a wavelength of 193 nm and a maximum energy of 0.08 mJ pulse $^{-1}$. A thick section of the coral sample together with standard materials were placed into the ablation chamber, which is flushed by He gas (ca. 0.4 L min-1). After the chamber, the aerosol is mixed with Ar gas (0.8-1.0 L min-1) and transported via Teflon tubing to a Nu Plasma II MC-ICP-MS. Prior each analysis, sample or standard material was pre-ablated to remove potential surface contamination.

Manuscript III: pH - δ¹¹B calibration for an *Orbicella sp.* from Puerto Rico

For B isotope analysis of coral samples, we used the helix-mode scan of the laser ablation system with a laser spot size of 40 µm to ablate a circular area with an approximate diameter of about 150 µm (right?), which integrates over a growth period of approximately two weeks. We positioned LA analysis within the theca wall by avoiding septa, which often show differing geochemical signatures (Jurikova et al., 2019; Robinson et al., 2014; Rollion-Bard & Blamart, 2015; Stewart et al., 2016) (Jurikova et al, 2019; Rollion-Bard et al, 2016, Robinson et al., 2014, Stewart et al, 2016).

Boron isotope ratios were measured on a Nu Plasma MC-ICP-MS equipped with Ni cones for dry plasma conditions and Daly detectors. We applied the standard-sampling-bracketing method using the silicate glass NIST SRM 610 as bracketing standard to correct for mass bias and instrumental drift. On-peak gas blanks were measured for 30 s prior each analysis and subtracted from signal intensities for B10 and B11 obtained for sample or standard material, respectively, which were measured for 150 cycles with an integration time of 1 s. The data were evaluated using a self-created Microsoft Excel spreadsheet macro to calculate δ¹¹B values with propagated errors. Further details on the instrumental set-up and, B isotopic analysis and data evaluation are provided in (Steinhoefel et al., 2023).

Boron isotope ratios are given in delta notion (δ¹¹B) in permil units relative to the standard material NIST SRM 951, which is commonly used for reporting data obtained by solution MC-ICP-MS. We recalculated our LA data by assuming a difference of -0.26‰ between our bracketing standard NIST SRM 610 and NIST SRM 951 (Standish et al., 2019):

$$\delta^{11}B = \left(\frac{^{11}B/^{10}B_{Sample}}{^{11}B/^{10}B_{NIST\ SRM\ 951}} - 1 \right) \times 1000$$

2.3.2.3 Chronology

We established an age model based on annual growth banding of the coral and δ¹¹B values. The continuously daily measured pH values from the La Parguera buoy were summed up to bi-weekly resolution to match the high resolution δ¹¹B measurements. δ¹¹B peaks were matched with pH highs and δ¹¹B lows were matched with pH maxima. Most pH lows occur in July, September and October, while the pH highs are mostly from January to April. As many peaks and dips were matched to the buoy pH- times series as possible, yielding 3 to 4 tie points between the δ¹¹B values and pH measurements. Ages for the remaining measurements were linearly interpolated based on spatial distances between the tie points. This was done with the

Arand Software Ager (Howell et al., 2006). Furthermore, we interpolated the data for equidistant bi-weekly resolution (if that was not already covered by the measurements) with the Timer Software from Arand (Howell et al., 2006), to be able to compare the data to the buoy measurements.

2.3.2.4 Buoy

The buoy measures every 3 hours pCO$_2$ in the atmosphere and at the surface of the ocean, due to its equipment consisting of a seawater-gas equibrilator, reference gas standard, and an infrared gas analyzer. SST and SSS are measured with Seabird conductivity and temperature recorder every 3h as well. A Sunburst^{TM} SAMI pH system records the pH of the water column (Meléndez et al., 2020). The replacement of the buoy in 2014 lead to the longest data gap in the time series. Every year, during buoy maintenance the instruments are not recording the environmental parameters, leading to additional gaps (Meléndez et al., 2020; Sutton et al., 2014). The pH sensor failed more often than SST and SSS measurements and shows therefore more gaps in the time series (fig. 2.3.4).

2.3.3 Results

2.3.3.1 Preservation of coral skeleton

The coral core shows slight green-yellow banding in the upper 4.5 cm. Below that, the banding is light grey. In SEM images the banding, that is visible on a macroscale is reflected in micro boreholes. The upper 5 mm from the youngest part of the coral are pristine with no visible boreholes in any part of the coral skeleton as well as no secondary aragonite or calcite in pore spaces of the skeleton. Below the first 5 mm the first boreholes appear. The last 4 mm of the first slab are again in a pristine state. Some boreholes are filled, with what appears to be aragonite needles. The parts of the skeleton that are infested with boreholes also show conic structures in the pore spaces of the septa (fig. 2.3.3 G). In some of the pore spaces aragonite needles have grown (fig. 2.3.5).
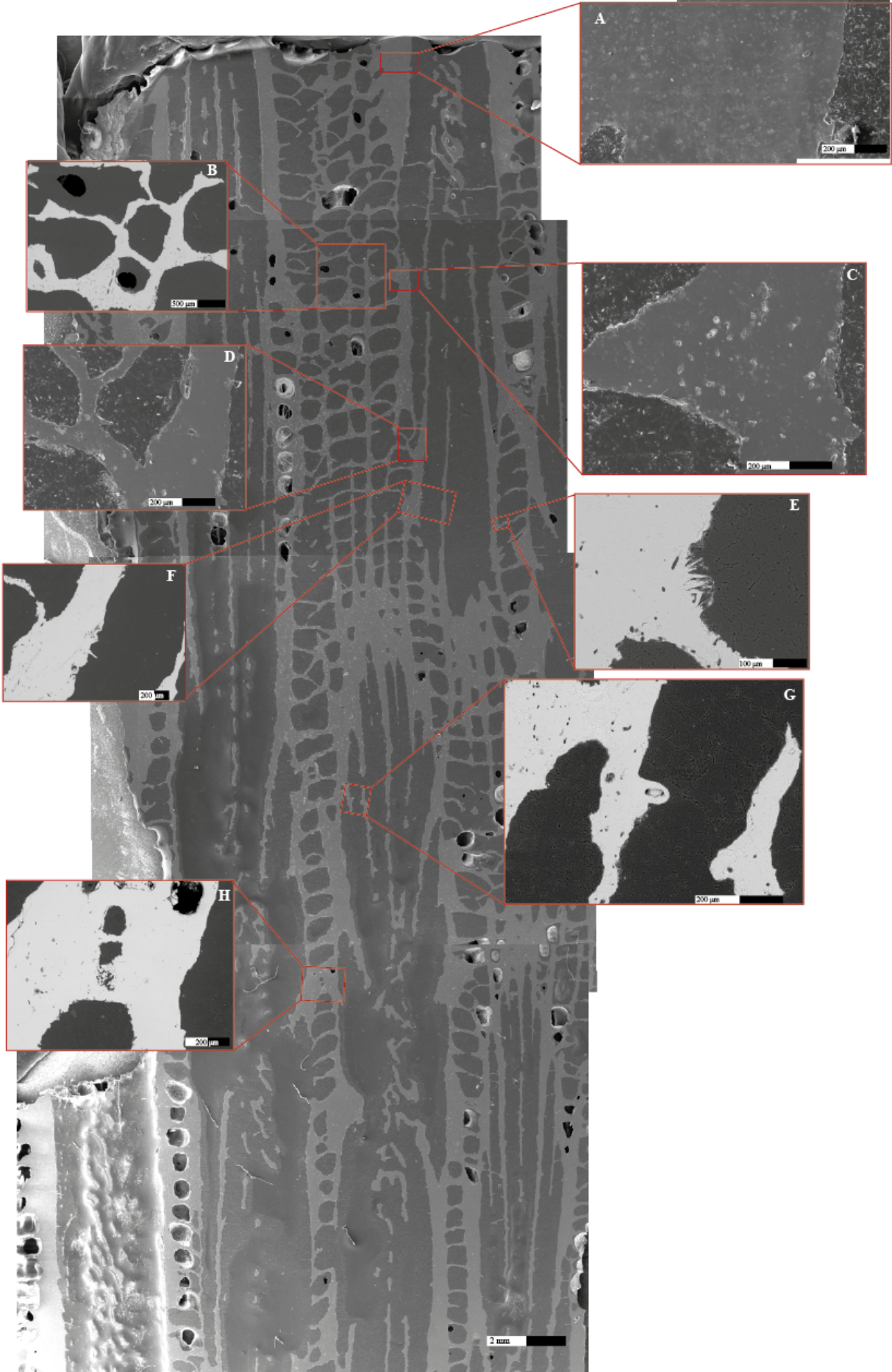
Figure 2.3.3: SEM images of *Orbicella annularis* thick slab, with zoom on pristine skeletal areas and heavily invested skeletal material. A- pristine top of the coral thick slab. B- Transition from pristine infested area of the corals thecal wall. C- mostly empty boreholes of different size. D-bore holes in thecal wall and secondary aragonite in pore space of the skeleton. E- Secondary aragonite needles in pore space of a neighboring thecal wall. F,G- Wavy margin possibly indicating cone like structure as a self defense mechanisms of the coral against fungi attacks. H- less infested part of the coral towards the bottom/older part of the thick slab.

2.3.3.2 pH and carbonate chemistry measurements at La Parguera

The maximum pH value of 8.09 was measured in October 2018 (3.10.2018). The lowest pH value of 7.95 occurred in August 2019 (08.08.2019). For comparison reasons, we averaged the pH measurements to a bi weekly frequency shifting the maximum to 8.06 in the beginning of January 2014 and the minimum to 7.9 in the beginning of October 2018. These correspond to δ^{11}B ratios of 21.44 ‰ and 22.45 ‰ respectively. Minimum values of pH are mostly in July, September and October and have declined from 2013 to 2020 ($p<0.001$) by 0.02. The maximum SST measured was 30.7°C in September 2015, while the coldest temperature between 2013 and 2020 was measured in February 2019 and was 26.4°C.

A maximum in salinity of 36.6 psu was recorded in June 2017, while a minimum of 33.5 psu was measured in November 2018. The lowest measured δ^{11}B ratio is 19.17 ‰ and translates into a pH$_C$ of 7.48 applying equation 6. The corresponding measured pH is missing due to a failure or service of the La Parguera buoy.

The maximum δ^{11}B ratio is 27.09 ‰ translates into a pH$_C$ of 8.76 (eq. 7). The maximum value in δ^{11}B was paired to the measured pH value of 8.05 in the age model. The δ^{11}B timeseries shows relatively low values from 2013 to the end of 2015, when the values shift to heavier ratios. This translates to lower pH$_C$ values from 2013 to 2016 and more basic values for the period of 2017 to 2020. Although we have high resolution δ^{11}B measurements from the coral skeletal material and high resolution pH measurements of the ambient seawater, the Pearson correlation coefficient shows an insignificant correlation of 0.16 (p =0.1). A clear drop in the δ^{11}B data is visible in September of 2015. By increasing the values between 2013 and 2015 by 1 correlation ameliorates to a significant Pearson correlation factor of 0.41 (p<0.001).
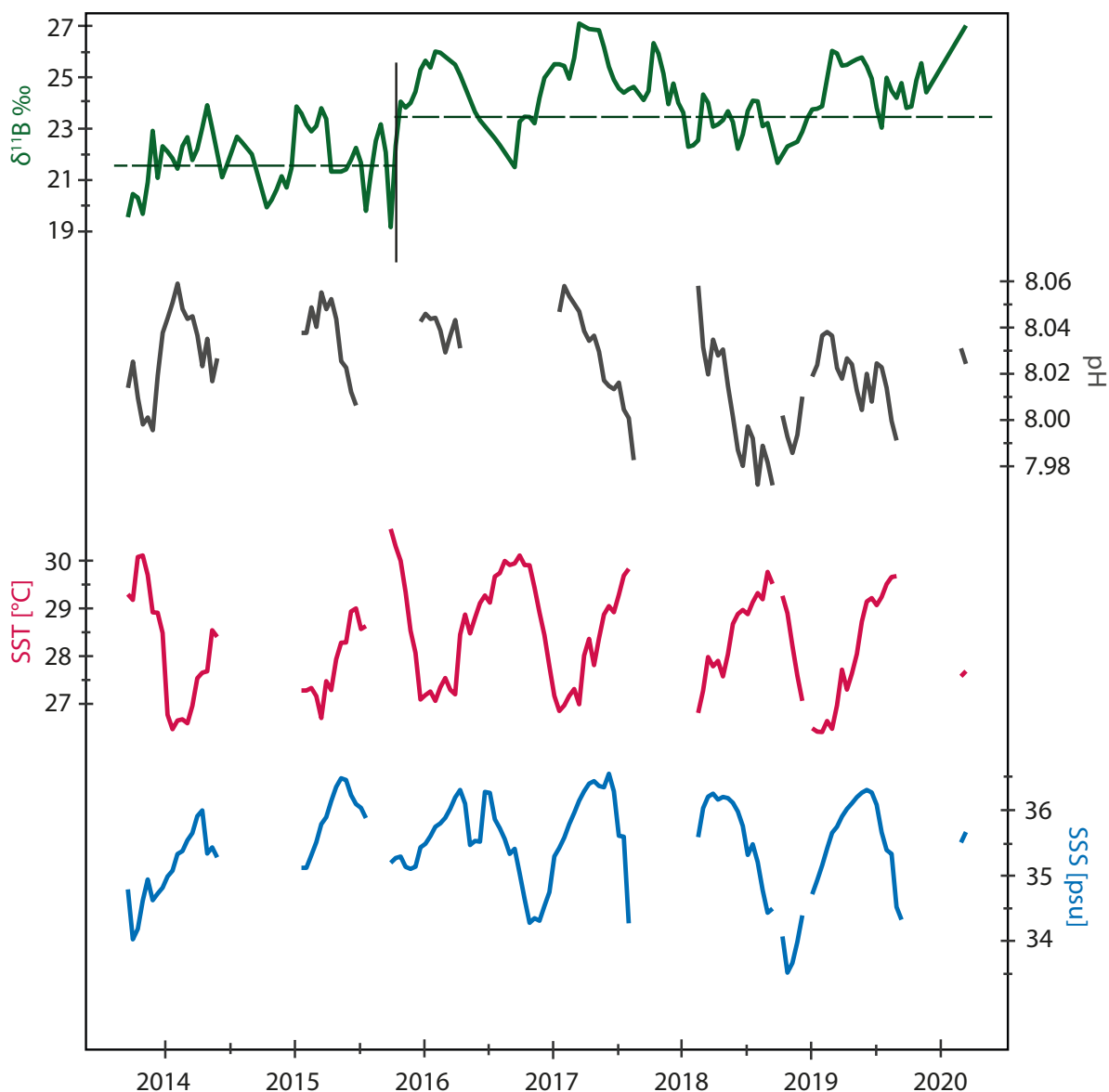
Figure 2.3.4: A- δ¹¹B in ‰ measured with LA-MC-ICP-MS from the coral thick slab of an *Orbicella annularis*. Dashed straight line shows shift in mean from 21.8 ‰ to 24. 2 ‰ in September 2015. B- pH measurement from Buoy installed at La Parguera National Parc. Yearly services and one exchange if the buoy in 2014 have led to multiple data gaps. The pH sensor failed more often than measurements for SST and SSS. C-SST measurements from buoy. D- SSS measurements from buoy.

2.3.4   Discussion

Having a coral grow right underneath a buoy measuring pCO_2 and pH since 2009 is a great opportunity to have a high resolution δ¹¹B to pH calibration for a *Orbicella annularis* and thereby adding to the sparse existing calibrations of e.g. *Porities cylindrica* (Hönisch et al., 2004), *Acropora nobilis* (Hönisch et al., 2004), *Acropora youngei*, and *Porities damicornis*

(Comeau, Cornwall, et al., 2017). Unfortunately, the coral shows green and gray banding, indicating an infestation of endolithic algea and fungi (Priess et al., 2000) on a macroscale and microboring of the skeletal material, as well as secondary aragonite in pore spaces on a microscale. Secondary aragonite and calcite is changing the chemical signal thereby making the environmental signal, reconstructed from skeletal material measurements, unreliably.

2.3.4.1   Algae bands and fungi infestation

From the macro and micro appearance of the coral skeletal material, it is likely that there is a multitude of microborers acting to dissolve and participate the skeleton inside the coral. Due to the preparation of the coral core for LA-MC-ICP-MS measurements the preservation of the endoliths did not take place, the identification of the microborers can therefore only go of the appearance of the boreholes and secondary aragonite left.

The coral core does not show green bands but dark-grey/brown bands. The algae remains can be recognized by their dark coloring as dark bands in the coral skeleton (Priess et al., 2000). An increase in algae density can lead to fungal attacks, ad lead to a change in color from green to brownish/greyish (Le Campion-Alsumard, Golubic, & Priess, 1995; Priess et al., 2000). Some boreholes show secondary aragonite fillings, indicating another organisms filling in the boreholes.

Contrary to algae, fungi can also penetrate skeleton still occupied by the coral's polyp. The polyp detects the fungi as a parasite and reacts with a defense mechanisms (Le Campion-Alsumard, Golubic, & Priess, 1995). At the site of fungi penetration the coral polyp reacts by accreting carbonate around the site of penetration, forming a cone like structure (Le Campion-Alsumard, Golubic, & Priess, 1995). The cone like structure can be recognized in the pore space of the coral in fig. 2.3.3 G, indicating the defense mechanisms taking place against the fungi hyphae, while the space was still occupied by the coral polyp. (Le Campion-Alsumard, Golubic, & Priess, 1995)

The fillings of some boreholes with most probably secondary aragonite indicate another organisms, since fungi and green algae do not precipitate in their borings. Cyanobacteria may be responsible for the secondary aragonite observed in some boreholes (fig. 2.3.5). In test on foraminifera a coccoid cyanobacteria was responsible for secondary aragonite cement in

boreholes, that resembles the filled boreholes found in the *Orbicella* from this study. The filling of boreholes has not been extensively studied, probably due to the resin cast method, that is usually used to form a cast of the boreholes left by microborers. Since filled boreholes will not leave a cast, they are easily overlooked (Golubic et al., 2005; Reid & Macintyre, 2000). Although microboring organisms are part of the coral's microbiome, the effect of secondary aragonite as a borehole filling on the geochemistry of the skeletal material of is poorly researched.
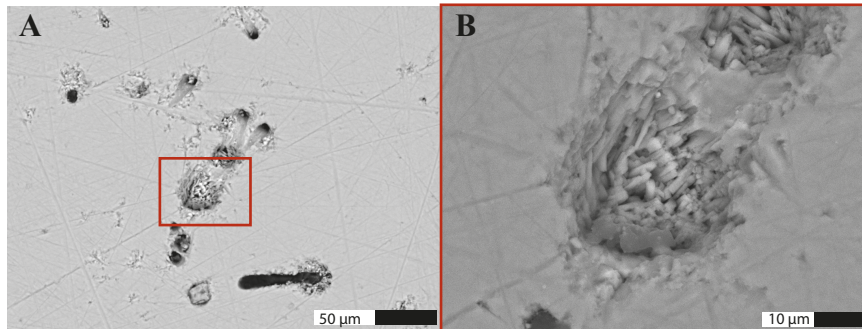
Figure 2.3.5: A- Filled and empty boreholes. Red rectangle location of B image. B- Secondary aragonite filling of borehole.

2.3.4.2   Implications of secondary aragonite for δ¹¹B and pH reconstructions

The signal in δ¹¹B from secondary aragonite consists of a mixture of the signature of the pore fluid (39.8‰) found in the pore spaces of the coral head and the dissolved biogenic aragonite (25‰) (Gaillardet & Allègre, 1995). The pore fluid of massive scleractinian corals is manipulated by the microbiome found in the corals skeleton (Ricci et al., 2019). The green algae situated just below the tissue layer of the coral, is producing a maximum in oxygen due to photosynthesis, that is diffusing into deeper parts of the skeleton. The oxygen is consumed by the microorganisms in the deeper skeleton and about 1 -2 cm below the green algae band, the skeleton is anoxic. Photosynthesis of the green algae happens during daylight leading to more alkaline pore water, due to the removal of CO_2. pH increases and exceeds 8.5. During nighttime, the oxygen is consumed and pH drops sharply (Ricci et al., 2019; Shashar & Stambler, 1992). Calcifying microorganisms boring through the coral skeleton will therefore incorporate the pH signal of the pore fluid depending on the time of the day into the secondary aragonite depositions. The high variability in pore water is most probably reflected in δ¹¹B variability.

Looking at the thecal wall corresponding to the years or, 2013 to 2015 there is very little bore holes visible and the thecal wall appears untouched. δ¹¹B values are relatively low with a mean

of 21.8 ‰. The mean rises to 24.4 ‰ after 2016 in a part of the coral that is heavily altered by microboring organisms and where some boring tunnels were filled with secondary aragonite.

While the first part of the δ^{11}B time series translates to very low pH values for the calcifying fluid, when using the existing δ^{11}B calibration for *Porites cylindrica* (Hönisch et al., 2004; Trotter et al., 2011), values after September 2015 show very high pH values for the region. However, values prior to 2015 are expected to be reflecting the pH of the calcifying fluid since the skeleton seems more pristine with almost no boreholes visible. Transforming values prior to 2015 into pH values of the calcifying fluid with the *Porites sp.* calibration equation (Hönisch et al., 2004; Trotter et al., 2011) results in a high variability in pH values of 7.4 to 8.8. One reason for the high variability could be the measuring method. Laser ablation picks up the heterogeneity of the coral skeletal material. Bulk analysis might yield more robust results with secondary calcite or aragonite, when the amount Is less than 5% (Lazareth et a.). Although the jump in values is most prominent at the end of 2015, with a significant (<0.001) change in mean from 21.8 ‰ to 24.4‰, a change point analysis reveals 3 other change points at the end of 2016, at the end of 2017, and in the beginning of 2019. Each time just before the peak in δ^{11}B and therefore a peak in pH. Usually algae and cyanobacterial blooms will happen when more light is penetrating through the coral tissue and reaching the algae or bacteria, or when the coral is stressed and the symbionts disappear, e.g. during a bleaching event. Both events are more likely to happen during boreal summer (Galindo-Martínez et al., 2022; Ricci et al., 2019). The pH values bouncing back after such a potential bloom occurred in winter could explain the change in mean in 2016, 2017, and 2019, when pH values reconstructed with the *Porites sp.* calibration exceed a pH of 8.5.

Considering other species specific calibrations yield even higher values, reconstructed pH$_{SW}$ exceeding a pH of 9 and 10 (species specific calibration with *P. damicornis* and *A. youngei* (Comeau, Cornwall, et al., 2017)). The species specific calibrations used here are therefore most probably not valuable for the *Orbicella* species of this study, since the reconstructed pH does not reflect values measured by the buoy. If we take the δ^{11}B values only form the pristine part of the coral and calibrate it with the measured pH values from 2013 to 2015, a robust (p<0.001) regression yields a new calibration of:

$$pH_{SW} = pH_C * 0.042\ (\pm 0.015) + 7.61\ (\pm 0.12) \qquad [2.3.7]$$

With this species specific calibration, the reconstructed pH ranges between 8.00 and 8.06, not entirely recording the maxima and minima recorded by the buoy (fig. 2.3.6 C). Values prior to September 2015 fall between the derived calibration curve of Kakihana et al. (1977) and the experimentally calibrated curve of Klochko et al. (2006) (fig. 2.3.6 A). The fractioning factor of 1.0272 from Klochko et. al. (2006) is now widely established as the fractioning factor between boric acid and borate ion for marine carbonates, does however not represent perfectly values in coral aragonite. Large offsets from the Klochko curve in corals are attributed to the upregulation of the internal pH and need to be corrected for by species specific calibrations (Marschall & Foster, 2018). From experiments and other species specific calibration a wider range of pH was either enforced on the corals in experiments, or corals from a high variability pH environment were taken to establish calibration curves covering a wider range (Hönisch et al., 2004; Reynaud et al., 2004; Trotter et al., 2011). The coral from this study grew in a relatively stable pH and SST environment, therefore representing only minor changes. Improving the calibration for *Orbicella* would need a wider range of pH and continuous pH measurements.
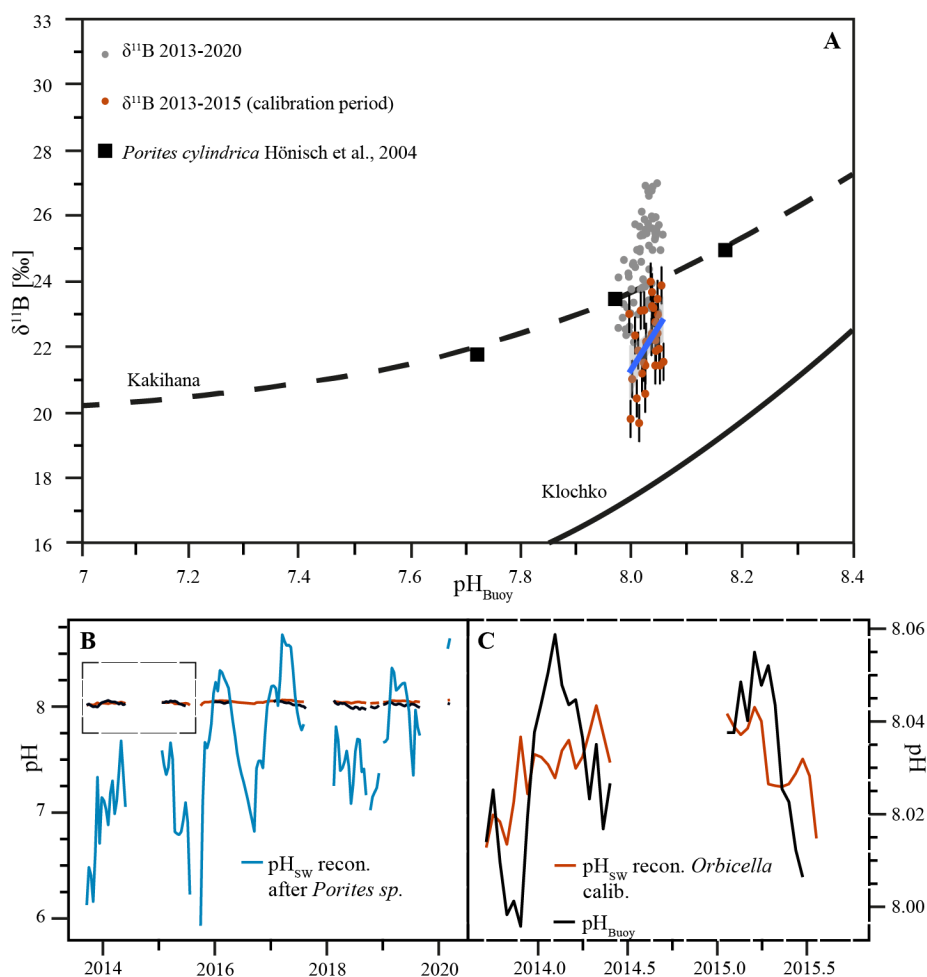
Figure 2.3.6: A- δ11B – pH calibration for Orbicella annularis. δ11B fall between the Kahikana et al. (1977) and Klochko et al. (2006). Also displayed are the values from the δ11B-pH calibration of Porites cylindrica. B- pHSW reconstructed from Porites sp. calibration (blue) and from the Orbicella calibration (orange, eq. 7) as well as pH recorded by the buoy (black) from 2013 to 2020. Dashed rectangle displayed in C- pHSW reconstructed from Orbicella calibration (orange) and recorded by the buoy (black).

While LA-MC-ICP-MS offers the opportunity to reconstruct high resolution changes in δ¹¹B and with that, the chance to reconstruct high resolution pH, it also presents certain caveats. The heterogeneity of the coral skeleton is picked up the laser and adds to the variability in the results. As part of the microbiome, green algae, cyanobacteria, and fungi are always present in the coral skeleton. Those boring organisms will change the porosity and might facilitate secondary precipitation that is picked up by the laser measurements. By performing bulk analysis, small alterations in the coral material will get lost in the overall primary aragonite signal, assuming less than 5% alterations, as observed in a previous study (Lazareth et al., 2016).

2.3.5 Conclusion

The heavily modified parts of the coral skeleton, due to algae and fungi infestation, show heavier $\delta^{11}B$ after September 2015. Secondary aragonite formed in parts of the boreholes, has altered the $\delta^{11}B$ signature of the skeletal material and has been picked up by the fine scale, high resolution measuring method with the LA-MC-ICP-MS. The new calibration for the species *Orbicella* presented here can be a first reference point for further work with this species. Experiments with wider pH ranges and the coral species could help develop a more robust calibration and create new opportunities for pH reconstructions. However, there is still a huge knowledge gap on the influence of boring organisms on high resolution $\delta^{11}B$ data especially on secondary aragonite. As part of the coral microbiome, green algae, fungi, bacteria and viruses can be found in healthy corals and can contribute to the coral's health. Yet, it is still not clear, which organisms is responsible for secondary deposits such as secondary aragonite, although there is more extensive knowledge on secondary calcite.

2.3.6 Data availability

The data is shown in the supplementary materials in section 2.3.8 of this chapter.

2.3.7 Acknowledgements

We thank the following people for their assistance and support: Sebastian Flotow for coral core sample preparation and microstructure analysis, and Gernot Nehrke for his advice and help in thick slide preparation. The OASIS project is funded by the Federal Ministry of Education and Research (BMBF) under the "Make Our Planet Great Again – German Research Initiative", grant number 57429626 to Dr. Henry C. Wu (Junior Research Group Leader), implemented by the German Academic Exchange Service (DAAD).

2.3.8 Supplementary Material

Table 2.3.1: Interpolated results according to the agemodel for the *Orbicella annularis* coral core and buoy measurements from the La Parguera Marine Reserve in Puerto Rico buoy installed by NOAA Reef Conservation Program (at 17.95°N, 67.05°W) adapted to the agemodel of the coral.

Year	d11B	SST	SSS	pco2	pH
2013.7104	19.55906661	29.3019554	34.7786607	424.053571	8.014
2013.7488	20.46003244	29.1829107	34.0167143	417.233036	8.02523375
2013.7872	20.31748699	30.0875446	34.1759196	434.23125	8.00963163

2013.8256	19.68657928	30.1192232	34.6082054	446.624107	7.99827743
2013.864	20.91467533	29.7066607	34.9295	442.200893	8.0012753
2013.9024	22.91668466	28.9200089	34.6129464	451.352679	7.99581146
2013.9408	21.08659103	28.9125179	34.7135804	421.369643	8.01942492
2013.9792	22.31764161	28.4854196	34.8038625	401.076071	8.03764963
2014.0176	22.10758241	26.7608839	34.9748929	394.352883	8.04392052
2014.056	21.84509825	26.4567857	35.0637143	386.82125	8.0506506
2014.0944	21.44456105	26.6394554	35.3175893	376.738878	8.05875254
2014.1328	22.32287552	26.6649375	35.3621786	388.536743	8.04784822
2014.1712	22.67086808	26.5819732	35.5260179	392.786224	8.04359293
2014.2096	21.7806102	26.9482589	35.6363214	390.658988	8.04471779
2014.248	22.20764333	27.5317411	35.8943929	398.289915	8.03647661
2014.2864	23.03207423	27.6477679	26.6391786	399.885238	8.02328571
2014.3248	23.91232379	27.6773929	35.3247946	401.970808	8.03505135
2014.3632	23.01876024	28.543375	35.4184911	422.011828	8.01683187
2014.4016	22.0643972	28.4039821	35.2665	411.082781	8.02664185
2014.44	21.11003417	NAN	NAN	NAN	NAN
2014.4784	21.60740593	NAN	NAN	NAN	NAN
2014.5168	22.14839444	NAN	NAN	NAN	NAN
2014.5552	22.68938295	NAN	NAN	NAN	NAN
2014.5936	22.47534443	NAN	NAN	NAN	NAN
2014.632	22.24122455	NAN	NAN	NAN	NAN
2014.6704	22.00710467	NAN	NAN	NAN	NAN
2014.7088	21.32582967	NAN	NAN	NAN	NAN
2014.7472	20.6341931	NAN	NAN	NAN	NAN
2014.7856	19.94255654	NAN	NAN	NAN	NAN
2014.824	20.2338104	NAN	NAN	NAN	NAN
2014.8624	20.63835763	NAN	NAN	NAN	NAN
2014.9008	21.15099916	NAN	NAN	NAN	NAN
2014.9392	20.71200708	NAN	NAN	NAN	NAN
2014.9776	21.47064476	NAN	NAN	NAN	NAN
2015.016	23.86422581	NAN	NAN	NAN	NAN
2015.0544	23.59091723	27.27275	35.1072946	401.376786	8.03758929
2015.0928	23.15996095	27.27275	35.1072946	401.376786	8.03758929
2015.1312	22.8955694	27.3250583	35.3000708	394.520833	8.04852679
2015.1696	23.10335355	27.154375	35.4975804	405.919643	8.04017857
2015.208	23.79646858	26.6923095	35.7727351	391.71369	8.05495536
2015.2464	23.37926765	27.4694965	35.8789236	394.139931	8.04776786
2015.2848	21.3317485	27.2816696	36.1240179	393.733036	8.05208929
2015.3232	21.3317485	27.9306637	36.3400387	401.139881	8.04354464
2015.3616	21.3317485	28.2804315	36.4724345	422.060119	8.0254375
2015.4	21.41683625	28.2851944	36.4456285	421.175347	8.02264286
2015.4384	21.79043435	28.9389509	36.2165647	435.538839	8.01225893

2015.4768	22.25442945	29.0027222	36.0784826	438.998611	8.0064375
2015.5152	21.67584976	28.5680125	36.0213601	429.296667	NAN
2015.5536	19.80587235	28.6304931	35.8659444	420.251389	NAN
2015.592	21.25165085	NAN	NAN	NAN	NAN
2015.6304	22.52705812	NAN	NAN	NAN	NAN
2015.6688	23.17046958	NAN	NAN	NAN	NAN
2015.7072	22.08039884	NAN	NAN	NAN	NAN
2015.7456	19.17168076	30.678	35.183	457.5	NAN
2015.784	22.33804726	30.3096099	35.2561926	468.913075	NAN
2015.8224	24.05322811	30.0070089	35.2786265	455.734673	NAN
2015.8608	23.82155339	29.3466667	35.1213542	457.363542	NAN
2015.8992	24.00028047	28.5341146	35.0909896	450.936458	NAN
2015.9376	24.44395102	28.0654896	35.1239688	426.23125	NAN
2015.976	25.28873218	27.0828646	35.4185313	399.126042	8.04242708
2016.0144	25.64562397	27.1765833	35.4732917	396.325	8.04577083
2016.0528	25.37780776	27.2513333	35.5897813	369.996875	8.04358333
2016.0912	26.00122044	27.053875	35.7325104	400.463542	8.0440625
2016.1296	25.9561435	27.34025	35.7847083	406.2	8.03861042
2016.168	25.8008713	27.5353333	35.8685417	411.603125	8.02919792
2016.2064	25.64559909	27.2893646	36.0069688	407.44375	8.03646429
2016.2448	25.49032689	27.1920417	36.1798333	371.763542	8.04309375
2016.2832	25.08973909	28.4513259	36.2937247	418.469345	8.031
2016.3216	24.61048971	28.8739792	36.0845	424.6	NAN
2016.36	24.13124033	28.4767083	35.4547083	424.713542	NAN
2016.3984	23.65199096	28.8058854	35.5171042	436.25625	NAN
2016.4368	23.32885185	29.1136667	35.5057083	438.959375	NAN
2016.4752	23.09479544	29.2760729	36.2641042	437.501042	NAN
2016.5136	22.86073903	29.1256146	36.2489792	432.107292	NAN
2016.552	22.62668262	29.6772917	35.84625	434.183333	NAN
2016.5904	22.36541107	29.7476146	35.7104167	431.692708	NAN
2016.6288	22.07862914	30.0042396	35.5442604	452.238542	NAN
2016.6672	21.7918472	29.9191326	35.3189396	455.571944	NAN
2016.7056	21.50506527	29.9513542	35.3964792	444.613542	NAN
2016.744	23.27862996	30.1192604	35.0228125	464.153125	NAN
2016.7824	23.46685666	29.9173958	34.633125	428.959375	NAN
2016.8208	23.45534895	29.9134375	34.2687083	412.128125	NAN
2016.8592	23.21092244	29.4429479	34.3386563	459.421875	NAN
2016.8976	24.19469202	28.9176354	34.3004375	467.446875	NAN
2016.936	24.97968697	28.4379464	34.5251741	425.54747	NAN
2016.9744	25.23964034	27.7813348	34.7366071	417.218452	NAN
2017.0128	25.50891208	27.1598917	35.2811506	400.734167	NAN
2017.0512	25.5058646	26.841287	35.4112477	393.773843	8.04659028
2017.0896	25.44067706	26.9590313	35.5675521	385.826042	8.05770764

2017.128	24.94421172	27.1604167	35.7729271	390.272917	8.05331994
2017.1664	25.75117121	27.3036875	35.9438958	394.5125	8.05007887
2017.2048	27.09171449	26.9826146	36.1299896	400.915625	8.04677282
2017.2432	26.98047688	28.0099688	36.2742039	409.606696	8.03836607
2017.2816	26.87718742	28.3611429	36.3894554	414.161607	8.0341875
2017.32	26.85308835	27.8078661	36.4284375	414.083036	8.03638903
2017.3584	26.82898928	28.3728036	36.3549375	418.665179	8.02951786
2017.3968	26.17710351	28.8740268	36.3345268	431.3625	8.01716437
2017.4352	25.40887987	29.0524337	36.5411215	405.768895	8.01481505
2017.4736	24.90071755	28.9229583	36.2724031	426.369738	8.01344048
2017.512	24.56876273	29.2893107	35.5959571	426.03	8.01623452
2017.5504	24.3993286	29.6941821	35.5811717	436.36398	8.00468265
2017.5888	24.53365209	29.8375633	19.4824364	402.439048	8.00099362
2017.6272	24.62845379	NAN	NAN	NAN	7.98298611
2017.6656	24.37144933	NAN	NAN	NAN	NAN
2017.704	24.11444488	NAN	NAN	NAN	NAN
2017.7424	24.46913905	NAN	NAN	NAN	NAN
2017.7808	26.32764151	NAN	NAN	NAN	NAN
2017.8192	25.9161474	NAN	NAN	NAN	NAN
2017.8576	25.14367672	NAN	NAN	NAN	NAN
2017.896	23.95418789	NAN	NAN	NAN	NAN
2017.9344	24.75668649	NAN	NAN	NAN	NAN
2017.9728	24.00139654	NAN	NAN	NAN	NAN
2018.0112	23.62449291	NAN	NAN	NAN	NAN
2018.0496	22.2968593	NAN	NAN	NAN	NAN
2018.088	22.35322457	NAN	NAN	NAN	NAN
2018.1264	22.54825164	26.7997232	35.574994	384.999107	8.05779677
2018.1648	24.32908179	27.2726071	36.0161786	420.575893	8.03141709
2018.2032	24.00848291	27.9781339	36.1918839	432.708036	8.01976403
2018.2416	23.07993867	27.7828125	36.2377143	400.232143	8.03468878
2018.28	23.16690296	27.8974464	36.1469107	409.114286	8.0278801
2018.3184	23.33207144	27.5705	36.1875625	420.805357	8.03045255
2018.3568	23.67940291	28.0384643	36.1694554	437.991071	8.01480527
2018.3952	23.25930908	28.6755179	36.0979911	453.514286	8.00156293
2018.4336	22.21703947	28.8843571	35.9649464	453.347321	7.98729209
2018.472	22.77462619	28.9709107	35.7445357	472.25625	7.98049617
2018.5104	23.69103821	28.8824821	35.3037143	449.93125	7.99743296
2018.5488	24.08922855	29.1340446	35.4660804	451.666964	7.99231791
2018.5872	24.06637095	29.3267143	35.1942857	479.211607	7.97245193
2018.6256	23.09738497	29.1965461	34.7678348	459.56756	7.98913097
2018.664	23.21865827	29.7727589	34.4219107	469.888393	7.98198533
2018.7024	22.44734044	29.5216488	34.4847857	482.527083	7.97215843
2018.7408	21.66818894	NAN	NAN	NAN	NAN

2018.7792	21.98977813	29.2684286	34.0609821	431.492857	8.00208354
2018.8176	22.31117528	28.9023661	33.5091161	432.671429	7.99295153
2018.856	22.40167348	28.2186696	33.6559911	436.1375	7.98605357
2018.8944	22.49217168	27.5851786	33.9777143	434.724107	7.99382143
2018.9328	22.88401108	27.0541161	34.381625	405.999107	8.01022577
2018.9712	23.41164993	NAN	NAN	NAN	NAN
2019.0096	23.74976288	26.4762768	34.7042946	399.777679	8.01885587
2019.048	23.77582593	26.4052679	34.9164018	403.746429	8.02381633
2019.0864	23.87166488	26.3971161	35.1432946	402.578571	8.03647184
2019.1248	24.94895336	26.6295714	35.4002589	399.596429	8.03797626
2019.1632	26.02624184	26.4648571	35.6399554	400.694643	8.03638172
2019.2016	25.92962273	26.9604485	35.73359	415.956057	8.02249289
2019.24	25.45184145	27.7119821	35.8894732	419.882143	8.01792526
2019.2784	25.48340004	27.2915446	36.0044018	409.591071	8.02664614
2019.3168	25.59997837	27.6303036	36.0904018	411.821429	8.02409792
2019.3552	25.69981133	28.0414107	36.1834821	424.533036	8.01278591
2019.3936	25.77168818	28.723849	36.2515938	438.727188	8.00449021
2019.432	25.42486342	29.1486169	36.2939432	447.982873	8.02001667
2019.4704	24.95010661	29.2209196	36.2552054	448.425893	8.00808546
2019.5088	23.81914676	29.0722679	36.0669018	440.640179	8.0245051
2019.5472	23.03933251	29.2451786	35.6477857	447.980357	8.0228108
2019.5856	24.98110812	29.5163214	35.3777321	466.308929	8.01400017
2019.624	24.48011504	29.6656696	35.3198393	445.358036	7.99978185
2019.6624	24.19774479	29.6838214	34.5101964	435.621429	7.99143878
2019.7008	24.77299709	NAN	34.3166875	NAN	NAN
2019.7392	23.80897236	NAN	NAN	NAN	NAN
2019.7776	23.86300204	NAN	NAN	NAN	NAN
2019.816	24.88059475	NAN	NAN	NAN	NAN
2019.8544	25.547259	NAN	NAN	NAN	NAN
2019.8928	24.41361155	NAN	NAN	NAN	NAN
2019.9312	24.73840184	NAN	NAN	NAN	NAN
2019.9696	25.06319213	NAN	NAN	NAN	NAN
2020.008	25.38798242	NAN	NAN	NAN	NAN
2020.0464	25.71277271	NAN	NAN	NAN	NAN
2020.0848	26.037563	NAN	NAN	NAN	NAN
2020.1232	26.36235329	NAN	NAN	NAN	NAN
2020.1616	26.68714358	27.571586	35.4931534	406.897816	8.03094816
2020.2	27.01193387	27.6802634	35.6521004	413.965323	8.02429628

3 Summary and conclusion

Modern massive reef-building corals have been used to reconstruct environmental parameters for the past 50 years, thereby prolonging the instrumental climate records (e.g. DeLong et al., 2014; Wu et al., 2014, 2018). Reconstruction from recent Atlantic corals of carbonate chemistry parameters and hydroclimate variability have been mostly neglected so far. This thesis aims to establish multidecadal records of seasonal changes in the southern GOM, a region that has been often overlooked when it comes to coral reconstructions. Furthermore, with numerous buoys being installed to monitor the health and carbonate chemistry parameters in coral reefs, there is an opportunity to add to existing pH-δ^{11}B calibration from new coral species. Another aspect that has been overlooked in the reconstruction of geochemical records from coral cores is the effect of microboring organisms on those records. In the second part of this thesis we aimed to shed some light on the latter.

The first manuscript of this thesis established the modern coral *Siderastrea siderea* as a robust climate archive for the southern GOM. In its skeletal material it recorded a bi-monthly seasonality using coral Sr/Ca, δ^{18}O, and Sr-U as SST proxies in a multi proxy approach. All of these SST proxies have shown an increase in SST over 160 years from 1845 to 2005. All proxies also showed a halt in the warming trend starting in the 1980s. This phenomena is also picked up by corals further to the north at Dry Tortugas , USA (DeLong et al., 2014), indicating a slowdown of the Loop Current (DeLong et al., 2014; Y. Liu et al., 2012). The warming trend picks up after 2005, as shown by OI-SST (Huang et al., 2021a) and ER-SST(Huang et al., 2017). Sr/Ca and oxygen isotopes can further be used to reconstruct hydroclimate variability by reconstructing δ^{18}O$_{SW}$. Although, seasonal variability is not well reflected in the δ^{18}O$_{SW}$ record of the Cuban coral, long term trends align well with re-analysis products for this region. Major climatic signals were also picked up by the corals δ^{18}O$_{SW}$ record such as ENSO events and a shift to a positive AMO in the 1990s, underlining the potential of coral archives to prolong records for climate variability and ameliorate their predictability.

The same coral from Cuba is reliably recording carbonate chemistry changes and adaption mechanisms to ocean acidification. In the second manuscript the first ever attempt to reconstruct the carbonate chemistry of seawater from coral skeletal material is demonstrated. The coral shows the clear signature of an acidifying ocean by an increase in DIC and a stable

Summary and Conclusion

TA signature in the surface seawater. At the same time, both carbonate chemistry parameters are declining in the ECM together with the pH and the aragonite saturation state. Nevertheless, the coral manages to keep its linear extension rate stable, probably due to an increased metabolic energy supply. The changing reconstructed carbonate chemistry parameters (DIC, TA, pCO_2, pH, and Ω) for SW agree well with in-situ measurements from GLODAPv2 2023 (Lauvset et al., 2022) and SOCATv2023 (Bakker et al., 2023), as well as data from the ocean carbon data repository (OCADS; Jiang et al., 2023). The reconstructed pCO_2 for SW from skeletal material demonstrated the increased pressure of CO_2. While in the beginning of the record pCO_2 are similar in the ECM and in SW, they diverge more and more from the 1920, when pCO_2 in SW exceeds the pCO_2 in the ECM. The coral keeps controlling its pCO_2 in the ECM to stabilize extension rates, however pCO_2 is increasing in the ECM gradually over time. This is also demonstrated by the $\delta^{13}C$ values from the coral. Over the 160 years of the coral record the carbonate isotope ratio declines by -1.5 ‰, which is confirmed by the Law Dome ice core record (Rubino et al., 2013) as well as multiple other coral records (Quinn et al., 1998; H. C. Wu et al., 2018) and attributed to the Suess Effect. However, considering the varying surface dissolved CO_2 content in coastal waters, models such as HAMOCC (B. Liu et al., 2021) come to a resulting decline in $\delta^{13}C$ values of -0.8 ‰. The decrease of 1.5 ‰ could therefore be explained by a decline due to the Suess Effect and partially because of enhanced diffusion of pCO_2 into the coral.

The coral core from the northern Cuban coast has shown that the ocean surface temperature for the southern GOM has warmed in the last 160 years since 2005. As a reliable environmental recorder, it showed that extreme ENSO events and an AMO signature are reflected in its hydroclimate oxygen record. Reconstructing SSS and pH allowed us to gain insights into the acidifying GOM and a coral capable of adapting to a changing environment. The good agreement to existing data from GLODAPv2 2023, SOCATv2023, and OCADS shows the potential for corals as archives for changes in the carbonate chemistry of seawater. pH reconstructions from coral skeletal material have been restricted by species-specific pH-$\delta^{11}B$ calibrations, that can or cannot be applied to other species. Adding more species-specific calibrations to the pool could not only open up paths to more pH reconstructions but potentially also for carbonate chemistry reconstructions. For this we looked at an *Orbicella annularis* from Puerto Rico in the Caribbean Sea. Ultra-high resolution $\delta^{11}B$ measurements showed that the younger part was infested and altered by the coral's microbiome (green algae, bacteria, and

fungi) and that borehole fillings of secondary aragonite had altered the measured $\delta^{11}B$ signature to higher values. The older and pristine part of the coral yielded a new $\delta^{11}B$-pH species specific calibration, that adds to the existing list calibration and might open up further opportunities to reconstruct pH for coral cores already taken from this species.

4   Outlook for future research

Results from this thesis have shown, that the tropical Atlantic corals *Siderastrea siderea* and *Orbicella annularis* have a great potential as a climate and environmental archive. They can live up to serval hundred years and can be found all over the western tropical Atlantic. Coral cores already drilled in the late 1990 and early 2000s from those corals have the potential of being explored and reanalyzed to apply new methods that have been introduced since.

By adding a new species-specific pH-$\delta^{11}B$ coral calibration, this thesis provides new opportunities for pH reconstruction in the Atlantic. Although the calibration period in chapter 2.3 is short, it is a first foundation for a calibration based on *Orbicella annularis* and could be extended in future for coral cores from this species. More research is needed to confirm the proposed species-specific pH-$\delta^{11}B$ calibration in the future.

The reconstruction of the carbonate chemistry of SW, as presented in the chapter 2.2 could prolong our knowledge of long-term changes in TA, DIC, pH, pCO_2, and aragonite saturation state and help explain the gap we see between the OCADS data and the reconstructed data in chapter 2.2. For the moment the OCADS dataset covers the period from 1750 to today in 10 year increments (L. Jiang et al., 2023; L.-Q. Jiang et al., 2023). Replicating the carbonate chemistry reconstruction method could lead to higher resolution of carbonate chemistry changes over time and a better coverage. The record could be prolonged by coral cores, reaching further back in time, or even be applied to fossil cores and foraminifera. The method proposed in chapter 2.2 should however be tested on different species and different resolutions to confirm the corals recording of long term trend in carbonate chemistry changes in SW. By monitoring carbonate chemistry components in SW with a better global coverage than we have currently and comparing them to the corals ECM chemistry, it is possible to see long term adaption mechanisms of corals to ocean acidification and create a more comprehensive picture of coral reefs in future climate change scenarios.

Summary and Conclusion

This thesis shows furthermore the importance of screening the coral cores, determined for geochemical analysis, for secondary diagenesis. A healthy coral lives in symbiosis with its microbiome (Ricci et al., 2019) and therefore, boreholes in the coral skeleton are common. Geochemical data might however be biased by diagenesis that can either be found in the corals pore space or that can fill the borings. The scale of change in the geochemical record also depends on the type of analysis: bulk or LA; and how much ratio of secondary diagenetic material compared to skeletal material. The LA method picks up on heterogeneities in the skeletal material and will show a high variability in measured values, even without secondary material. Bulk analysis on the other hand, can average out secondary material signals, if it is not overpowering (for calcite for example it should be less than 5%, Lazareth et al., 2016). Finding boreholes is therefore not an excluding criterion but an indication to further examine the core and the parts that are meant to be analyzed.

Extending existing climate variability records is crucial to understanding the changing climate that we are facing. Coral cores are a very suitable climate archive to fill in knowledge gaps enhance the coverage of environmental records. Calibration from modern corals of SST and SSS, but also the carbonate chemistry of SW are further crucial for the development of fossil coral proxies. The important insights gained will help understand future variabilities and adaption to the obstacles we face.

5 References

Allemand, D., Ferrier-Pagès, C., Furla, P., Houlbrèque, F., Puverel, S., Reynaud, S., Tambutté, É., Tambutté, S., & Zoccola, D. (2004). Biomineralisation in reef-building corals: From molecular mechanisms to environmental control. *Comptes Rendus Palevol*, *3*(6–7), 453–467. https://doi.org/10.1016/j.crpv.2004.07.011

Alvarez-Filip, L., Dulvy, N. K., Côté, I. M., Watkinson, A. R., & Gill, J. A. (2011). Coral identity underpins architectural complexity on Caribbean reefs. *Ecological Applications*, *21*(6), 2223–2231. https://doi.org/10.1890/10-1563.1

Bak, R., & Laane, R. (1987). Annual black bands in skeletons of reef corals (Scleractinia). *Marine Ecology Progress Series*, *38*, 169–175. https://doi.org/10.3354/meps038169

Baker, A. C., Glynn, P. W., & Riegl, B. (2008). Climate change and coral reef bleaching: An ecological assessment of long-term impacts, recovery trends and future outlook. *Estuarine,   Coastal   and   Shelf   Science*,   *80*(4),   435–471. https://doi.org/10.1016/j.ecss.2008.09.003

Bakker, D. C. E., Alin, S. R., Bates, N., Becker, M., Feely, R. A., Gkritzalis, T., Jones, S. D., Kozyr, A., Lauvset, S. K., Metzl, N., Munro, D. R., Nakaoka, S.-I., Nojiri, Y., O'Brien, K. M., Olsen, A., Pierrot, D., Rehder, G., Steinhoff, T., Sutton, A. J., … Wimart-Rousseau, C. (2023). *Surface Ocean CO2 Atlas Database Version 2023 (SOCATv2023) (NCEI Accession 0278913)* [Dataset]. NOAA National Centers for Environmental Information. https://doi.org/10.25921/R7XA-BT92

Bakker, D. C. E., Pfeil, B., Landa, C. S., Metzl, N., O'Brien, K. M., Olsen, A., Smith, K., Cosca, C., Harasawa, S., Jones, S. D., Nakaoka, S., Nojiri, Y., Schuster, U., Steinhoff, T., Sweeney, C., Takahashi, T., Tilbrook, B., Wada, C., Wanninkhof, R., … Xu, S. (2016). A multi-decade record of high-quality fCO_2 data in version 3 of the Surface Ocean CO_2 Atlas   (SOCAT).   *Earth   System   Science   Data*,   *8*(2),   383–413. https://doi.org/10.5194/essd-8-383-2016

Banzon, V. F., Reynolds, R. W., Stokes, D., & Xue, Y. (2014). A 1/4°-Spatial-Resolution Daily Sea Surface Temperature Climatology Based on a Blended Satellite and in situ Analysis. *Journal of Climate*, *27*(21), 8221–8228. https://doi.org/10.1175/JCLI-D-14-00293.1

Barker, S., Greaves, M., & Elderfield, H. (2003). A study of cleaning procedures used for foraminiferal Mg/Ca paleothermometry: MG/CA PALEOTHERMOMETRY. *Geochemistry,   Geophysics,   Geosystems*,   *4*(9),   n/a-n/a. https://doi.org/10.1029/2003GC000559

Bates, N. R. (2002). Seasonal variability of the effect of coral reefs on seawater CO2 and air—Sea   CO2   exchange.   *Limnology   and   Oceanography*,   *47*(1),   43–52. https://doi.org/10.4319/lo.2002.47.1.0043

Boisseson, E. de, & Alonso-Balmaseda, M. (2016). An ensemble of 20th century ocean reanalyses for providing ocean initial conditions for CERA-20C coupled streams. In *ERA Report Series*. ECMWF.

Boyer, T., García, H. E., Locarnini, R. A., Zweng, M. M., Mishonov, A. V., Reagan, J. R., Weathers, K. A., Baranova, O. K., Paver, C. R., Seidov, D., & Smolyar, I. V. (2018). *World Ocean Atlas 2018. [Salinity]. NOAA National Centers for Environmental Information* (Version WOA2018) [Dataset].

Bradley, R. S., & Elias, S. A. (2015). PALEOCLIMATOLOGY: Reconstructing Climates of the Quaternary. In *Arctic, Antarctic, and Alpine Research* (Vol. 31, Issue 3). https://doi.org/10.2307/1552264

Brewer, P. G., & Goldman, J. C. (1976). Alkalinity changes generated by phytoplankton growth1.   *Limnology   and   Oceanography*,   *21*(1),   108–117. https://doi.org/10.4319/lo.1976.21.1.0108

Buddemeier, R. W. (2004). *Coral reefs & global climate change: Potential contributions of climate change to stresses on coral reef ecosystems* (Vol. 10). Pew Center on Global Climate Change.

Cai, W.-J., Hu, X., Huang, W.-J., Jiang, L.-Q., Wang, Y., Peng, T.-H., & Zhang, X. (2010). Alkalinity distribution in the western North Atlantic Ocean margins. *Journal of Geophysical Research: Oceans*, *115*(C8). https://doi.org/10.1029/2009JC005482

Cameron, L. P., Reymond, C. E., Bijma, J., Büscher, J. V., De Beer, D., Guillermic, M., Eagle, R. A., Gunnell, J., Müller-Lundin, F., Schmidt-Grieb, G. M., Westfield, I., Westphal, H., & Ries, J. B. (2022). Impacts of Warming and Acidification on Coral Calcification Linked to Photosymbiont Loss and Deregulation of Calcifying Fluid pH. *Journal of Marine Science and Engineering*, *10*(8), Article 8. https://doi.org/10.3390/jmse10081106

Cao, L., Caldeira, K., & Jain, A. K. (2007). Effects of carbon dioxide and climate change on ocean acidification and carbonate mineral saturation: CLIMATE CHANGE ON OCEAN ACIDIFICATION. *Geophysical Research Letters*, *34*(5). https://doi.org/10.1029/2006GL028605

Carton, J. A., & Giese, B. S. (2008). A Reanalysis of Ocean Climate Using Simple Ocean Data Assimilation (SODA). *Monthly Weather Review*, *136*(8), 2999–3017. https://doi.org/10.1175/2007MWR1978.1

Castillo, K. D., Ries, J. B., Bruno, J. F., & Westfield, I. T. (2014a). The reef-building coral *Siderastrea siderea* exhibits parabolic responses to ocean acidification and warming. *Proceedings of the Royal Society B: Biological Sciences*, *281*(1797), 20141856. https://doi.org/10.1098/rspb.2014.1856

Castillo, K. D., Ries, J. B., Bruno, J. F., & Westfield, I. T. (2014b). The reef-building coral *Siderastrea siderea* exhibits parabolic responses to ocean acidification and warming. *Proceedings of the Royal Society B: Biological Sciences*, *281*(1797), 20141856. https://doi.org/10.1098/rspb.2014.1856

Chalk, T. B., Foster, G. L., & Wilson, P. A. (2019). Dynamic storage of glacial CO_2 in the Atlantic Ocean revealed by boron [CO_3^{2-}] and pH records. *Earth and Planetary Science Letters*, *510*, 1–11. https://doi.org/10.1016/j.epsl.2018.12.022

Chan, D., Kent, E. C., Berry, D. I., & Huybers, P. (2019). Correcting datasets leads to more homogeneous early-twentieth-century sea surface warming. *Nature*, *571*(7765), Article 7765. https://doi.org/10.1038/s41586-019-1349-2

Chen, T., Yu, K., Zhao, J., Yan, H., Song, Y., Feng, Y., & Chen, T. (2015). Testing coral paleothermometers (B/Ca, Mg/Ca, Sr/Ca, U/Ca and δ 18O) under impacts of large riverine runoff. *Acta Oceanologica Sinica*. https://doi.org/10.1007/s13131-015-0705-9

Chen, X., Deng, W., Kang, H., Zeng, T., Zhang, L., Zhao, J., & Wei, G. (2021). A Replication Study on Coral δ [11] B and B/Ca and Their Variation in Modern and Fossil *Porites*: Implications for Coral Calcifying Fluid Chemistry and Seawater pH Changes Over the Last Millennium. *Paleoceanography and Paleoclimatology*, *36*(10). https://doi.org/10.1029/2021PA004319

Chérubin, L. M., & Richardson, P. L. (2007). Caribbean current variability and the influence of the Amazon and Orinoco freshwater plumes. *Deep Sea Research Part I: Oceanographic Research Papers*, *54*(9), 1451–1473. https://doi.org/10.1016/j.dsr.2007.04.021

Chollett, I., Müller-Karger, F. E., Heron, S. F., Skirving, W., & Mumby, P. J. (2012). Seasonal and spatial heterogeneity of recent sea surface temperature trends in the Caribbean Sea

and southeast Gulf of Mexico. *Marine Pollution Bulletin, 64*(5), 956–965. https://doi.org/10.1016/j.marpolbul.2012.02.016

Coadic, R., Bassinot, F., Dissard, D., Douville, E., Greaves, M., & Michel, E. (2013). A coretop study of dissolution effect on B/Ca in Globigerinoides sacculifer from the tropical Atlantic: Potential bias for paleo-reconstruction of seawater carbonate chemistry. *Geochemistry, Geophysics, Geosystems, 14*(4), 1053–1068. https://doi.org/10.1029/2012GC004296

Colantonio, A., & Potter, R. B. (2006). Havana. *Cities, 23*(1), 63–78. https://doi.org/10.1016/j.cities.2005.10.001

Collins, M., Sutherland, M., Bouwer, L., Cheong, S.-M., Frölicher, T., Jacots de Combes, H., Koll Roxy, M., Losada, I., McInnes, K., Ratter, B., Rivera-Arriaga, E., Susanto, R. D., Swingedouw, D., & Tibig, L. (2019). *Extremes, Abrupt Changes and Managing Risk. In: IPCC Special Report on the Ocean and Cryosphere in a Changing Climate* (1st ed.). Cambridge University Press. https://doi.org/10.1017/9781009157964

Comeau, S., Cornwall, C. E., DeCarlo, T. M., Krieger, E., & McCulloch, M. T. (2018). Similar controls on calcification under ocean acidification across unrelated coral reef taxa. *Global Change Biology, 24*(10), 4857–4868. https://doi.org/10.1111/gcb.14379

Comeau, S., Cornwall, C. E., & McCulloch, M. T. (2017). Decoupling between the response of coral calcifying fluid pH and calcification to ocean acidification. *Scientific Reports, 7*(1), 7573. https://doi.org/10.1038/s41598-017-08003-z

Comeau, S., Tambutté, E., Carpenter, R. C., Edmunds, P. J., Evensen, N. R., Allemand, D., Ferrier-Pagès, C., Tambutté, S., & Venn, A. A. (2017). Coral calcifying fluid pH is modulated by seawater carbonate chemistry not solely seawater pH. *Proceedings of the Royal Society B: Biological Sciences, 284*(1847), 20161669. https://doi.org/10.1098/rspb.2016.1669

Compo, G. P., Whitaker, J. S., Sardeshmukh, P. D., Matsui, N., Allan, R. J., Yin, X., Gleason, B. E., Vose, R. S., Rutledge, G., Bessemoulin, P., Brönnimann, S., Brunet, M., Crouthamel, R. I., Grant, A. N., Groisman, P. Y., Jones, P. D., Kruk, M. C., Kruger, A. C., Marshall, G. J., … Worley, S. J. (2011). The Twentieth Century Reanalysis Project. *Quarterly Journal of the Royal Meteorological Society, 137*(654), 1–28. https://doi.org/10.1002/qj.776

Cooper, T. F., De'Ath, G., Fabricius, K. E., & Lough, J. M. (2008). Declining coral calcification in massive *Porites* in two nearshore regions of the northern Great Barrier Reef: *PORITES* AND ENVIRONMENTAL CHANGE. *Global Change Biology, 14*(3), 529–538. https://doi.org/10.1111/j.1365-2486.2007.01520.x

Cuny-Guirriec, K., Douville, E., Reynaud, S., Allemand, D., Bordier, L., Canesi, M., Mazzoli, C., Taviani, M., Canese, S., McCulloch, M., Trotter, J., Rico-Esenaro, S. D., Sanchez-Cabeza, J.-A., Ruiz-Fernández, A. C., Carricart-Ganivet, J. P., Scott, P. M., Sadekov, A., & Montagna, P. (2019). Coral Li/Mg thermometry: Caveats and constraints. *Chemical Geology, 523*, 162–178. https://doi.org/10.1016/j.chemgeo.2019.03.038

Dassié, E. P., Hasson, A., Khodri, M., Lebas, N., & Linsley, B. K. (2018). Spatiotemporal Variability of the South Pacific Convergence Zone Fresh Pool Eastern Front from Coral-Derived Surface Salinity Data. *Journal of Climate, 31*(8), 3265–3288. https://doi.org/10.1175/JCLI-D-17-0071.1

de Villiers, S., Nelson, B. K., & Chivas, A. R. (1995). Biological Controls on Coral Sr/Ca and δ ^{18} O Reconstructions of Sea Surface Temperatures. *Science, 269*(5228), 1247–1249. https://doi.org/10.1126/science.269.5228.1247

de Villiers, S., Shen, G. T., & Nelson, B. K. (1994). The Sr Ca-temperature relationship in coralline aragonite: Influence of variability in (Sr Ca)seawater and skeletal growth

parameters. *Geochimica et Cosmochimica Acta*. https://doi.org/10.1016/0016-7037(94)90457-X

DeCarlo, T. M., Gaetani, G. A., Cohen, A. L., Foster, G. L., Alpert, A. E., & Stewart, J. A. (2016). Coral Sr-U thermometry. *Paleoceanography*, *31*(6), 626–638. https://doi.org/10.1002/2015PA002908

DeCarlo, T. M., Gaetani, G. A., Holcomb, M., & Cohen, A. L. (2015). Experimental determination of factors controlling U/Ca of aragonite precipitated from seawater: Implications for interpreting coral skeleton. *Geochimica et Cosmochimica Acta*, *162*, 151–165. https://doi.org/10.1016/j.gca.2015.04.016

DeCarlo, T. M., Holcomb, M., & McCulloch, M. T. (2018). Reviews and syntheses: Revisiting the boron systematics of aragonite and their application to coral calcification. *Biogeosciences*, *15*(9), 2819–2834. https://doi.org/10.5194/bg-15-2819-2018

DeLong, K. L., Flannery, J. A., Maupin, C. R., Poore, R. Z., & Quinn, T. M. (2011). A coral Sr/Ca calibration and replication study of two massive corals from the Gulf of Mexico. *Palaeogeography, Palaeoclimatology, Palaeoecology*, *307*(1–4), 117–128. https://doi.org/10.1016/j.palaeo.2011.05.005

DeLong, K. L., Flannery, J. A., Poore, R. Z., Quinn, T. M., Maupin, C. R., Lin, K., & Shen, C.-C. (2014). A reconstruction of sea surface temperature variability in the southeastern Gulf of Mexico from 1734 to 2008 C.E. using cross-dated Sr/Ca records from the coral *Siderastrea siderea*. *Paleoceanography*, *29*(5), 403–422. https://doi.org/10.1002/2013PA002524

Díaz-Asencio, M., Alvarado, J. A. C., Alonso-Hernández, C., Quejido-Cabezas, A., Ruiz-Fernández, A. C., Sanchez-Sanchez, M., Gómez-Mancebo, M. B., Froidevaux, P., & Sanchez-Cabeza, J. A. (2011). Reconstruction of metal pollution and recent sedimentation processes in Havana Bay (Cuba): A tool for coastal ecosystem management. *Journal of Hazardous Materials*, *196*, 402–411. https://doi.org/10.1016/j.jhazmat.2011.09.037

Dickson, A. G. (1990). Thermodynamics of the dissociation of boric acid in synthetic seawater from 273.15 to 318.15 K. *Deep Sea Research Part A. Oceanographic Research Papers*, *37*(5), 755–766. https://doi.org/10.1016/0198-0149(90)90004-F

Dima, M., Nichita, D. R., Lohmann, G., Ionita, M., & Voiculescu, M. (2021). Early-onset of Atlantic Meridional Overturning Circulation weakening in response to atmospheric CO2 concentration. *Npj Climate and Atmospheric Science*, *4*(1), 27. https://doi.org/10.1038/s41612-021-00182-x

Dissard, D., Reichart, G. J., Menkes, C., Mangeas, M., Frickenhaus, S., & Bijma, J. (2021). Mg∕Ca, Sr∕Ca and stable isotopes from the planktonic foraminifera *T. sacculifer*: Testing a multi-proxy approach for inferring paleotemperature and paleosalinity. *Biogeosciences*, *18*(2), 423–439. https://doi.org/10.5194/bg-18-423-2021

D'Olivo, J. P., Ellwood, G., DeCarlo, T. M., & McCulloch, M. T. (2019). Deconvolving the long-term impacts of ocean acidification and warming on coral biomineralisation. *Earth and Planetary Science Letters*, *526*, 115785. https://doi.org/10.1016/j.epsl.2019.115785

Doney, S. C., Fabry, V. J., Feely, R. A., & Kleypas, J. A. (2009). Ocean Acidification: The Other CO$_2$ Problem. *Annual Review of Marine Science*, *1*(1), 169–192. https://doi.org/10.1146/annurev.marine.010908.163834

Drake, J. L., Mass, T., Stolarski, J., Von Euw, S., van de Schootbrugge, B., & Falkowski, P. G. (2020). How corals made rocks through the ages. *Global Change Biology*, *26*(1), 31–53. https://doi.org/10.1111/gcb.14912

Duran, A., Shantz, A. A., Burkepile, D. E., Collado-Vides, L., Ferrer, V. M., Palma, L., Ramos, A., & Gonzalez-Díaz, S. P. (2017). Fishing, pollution, climate change, and the long-

term decline of coral reefs off Havana, Cuba. *Bulletin of Marine Science*. https://doi.org/10.5343/bms.2017.1061

Evans, M. N., Kaplan, A., & Cane, M. A. (2000). Intercomparison of coral oxygen isotope data and historical sea surface temperature (SST): Potential for coral-based SST field reconstructions. *Paleoceanography*, *15*(5), 551–563. https://doi.org/10.1029/2000PA000498

Fairbanks, R. G., & Dodge, R. E. (1979). Annual periodicity of the '*O/16O and 13C/12C ratios in the coral Montastrea annularis. *Geochimica et Cosmochimica Acta, 43*, 1009–1020. https://doi.org/DOI:OOl6-7037/79/0701-1009102.00/0

Falini, G., Fermani, S., & Goffredo, S. (2015). Coral biomineralization: A focus on intra-skeletal organic matrix and calcification. *Seminars in Cell & Developmental Biology*, *46*, 17–26. https://doi.org/10.1016/j.semcdb.2015.09.005

Falter, J. L., Lowe, R. J., Zhang, Z., & McCulloch, M. (2013). Physical and Biological Controls on the Carbonate Chemistry of Coral Reef Waters: Effects of Metabolism, Wave Forcing, Sea Level, and Geomorphology. *PLoS ONE*, *8*(1), e53303. https://doi.org/10.1371/journal.pone.0053303

Finch, A. A., & Allison, N. (2003). Strontium in coral aragonite: 2. Sr coordination and the long-term stability of coral environmental records. *Geochimica et Cosmochimica Acta*, *67*(23), 4519–4527. https://doi.org/10.1016/S0016-7037(03)00410-1

Foster, G. L., Pogge von Strandmann, P. a. E., & Rae, J. W. B. (2010). Boron and magnesium isotopic composition of seawater. *Geochemistry, Geophysics, Geosystems*, *11*(8). https://doi.org/10.1029/2010GC003201

Foster, G. L., & Rae, J. W. B. (2016). Reconstructing Ocean pH with Boron Isotopes in Foraminifera. *Annual Review of Earth and Planetary Sciences*, *44*(1), 207–237. https://doi.org/10.1146/annurev-earth-060115-012226

Fowell, S. E., Foster, G. L., Ries, J. B., Castillo, K. D., De La Vega, E., Tyrrell, T., Donald, H. K., & Chalk, T. B. (2018). Historical Trends in pH and Carbonate Biogeochemistry on the Belize Mesoamerican Barrier Reef System. *Geophysical Research Letters*, *45*(7), 3228–3237. https://doi.org/10.1002/2017gl076496

Fowell, S. E., Foster, G. L., Ries, J. B., Castillo, K. D., Vega, E., Tyrrell, T., Donald, H. K., & Chalk, T. B. (2018). Historical Trends in pH and Carbonate Biogeochemistry on the Belize Mesoamerican Barrier Reef System. *Geophysical Research Letters*, *45*(7), 3228–3237. https://doi.org/10.1002/2017GL076496

Fowell, S. E., Sandford, K., Stewart, J. A., Castillo, K. D., Ries, J. B., & Foster, G. L. (2016). Intrareef variations in Li/Mg and Sr/Ca sea surface temperature proxies in the Caribbean reef-building coral *Siderastrea siderea*. *Paleoceanography*, *31*(10), 1315–1329. https://doi.org/10.1002/2016PA002968

Fox-Kemper, B., Hewitt, H. T., Xiao, C., Aoalgeirsdóttir, G., Drijhout, S. S., Edwards, T. L., Golledge, N. R., Hemer, M., Kopp, R. E., Krinner, G., Mix, A., Notz, D., Nowicki, S., Nurhati, I. S., Ruiz, L., Sallée, J.-B., Slangen, A. B. A., & Yu, Y. (2021). Ocean, Cryosphere and Sea Level Change. In Climate Change 2021: The Physical Science Basis. Contribution of Working Group I to the Sixth Assessment Report of the Intergovernmental Panel on Climate Change. In *Climate Change 2021 – The Physical Science Basis: Working Group I Contribution to the Sixth Assessment Report of the Intergovernmental Panel on Climate Change* (pp. 1211–1362). Cambridge University Press. https://doi.org/10.1017/9781009157896.011

Gagan, M. K., Ayliffe, L. K., Hopley, D., Cali, J. A., Mortimer, G. E., Chappell, J., McCulloch, M. T., & Head, M. J. (1998). Temperature and Surface-Ocean Water Balance of the Mid-Holocene Tropical Western Pacific. *Science*, *279*(5353), 1014–1018. https://doi.org/10.1126/science.279.5353.1014

Summary and Conclusion

Gagan, M. K., Dunbar, G. B., & Suzuki, A. (2012). The effect of skeletal mass accumulation in *Porites* on coral Sr/Ca and δ^{18}O paleothermometry: SKELETOGENESIS AND CORAL THERMOMETRY. *Paleoceanography*, *27*(1), n/a-n/a. https://doi.org/10.1029/2011PA002215

Gaillardet, J., & Allègre, C. J. (1995). Boron isotopic compositions of corals: Seawater or diagenesis record? *Earth and Planetary Science Letters*, *136*(3–4), 665–676. https://doi.org/10.1016/0012-821X(95)00180-K

Galindo-Martínez, C. T., Weber, M., Avila-Magaña, V., Enríquez, S., Kitano, H., Medina, M., & Iglesias-Prieto, R. (2022). The role of the endolithic alga Ostreobium spp. During coral bleaching recovery. *Scientific Reports*, *12*(1), 2977. https://doi.org/10.1038/s41598-022-07017-6

Galochkina, M., Cohen, A. L., Oppo, D. W., Mollica, N., & Horton, F. (2023). Coral Sr-U Thermometry Tracks Ocean Temperature and Reconciles Sr/Ca Discrepancies Caused by Rayleigh Fractionation. *Paleoceanography and Paleoclimatology*, *38*(7), e2022PA004541. https://doi.org/10.1029/2022PA004541

Garcia-Pichel, F., Ramírez-Reinat, E., & Gao, Q. (2010). Microbial excavation of solid carbonates powered by P-type ATPase-mediated transcellular Ca^{2+} transport. *Proceedings of the National Academy of Sciences*, *107*(50), 21749–21754. https://doi.org/10.1073/pnas.1011884108

Gattuso, J. P., Pichon, M., & Frankignoulle, M. (1995). Biological control of air-sea CO2 fluxes: Effect of photosynthetic and calcifying marine organisms and ecosystems. *Marine Ecology Progress Series*, *129*, 307–312. https://doi.org/10.3354/meps129307

Gattuso, J.-P., Orr, J., epitalon, jean marie, Baldry, K., Hoshijima, U., & Abulos. (2021). *jpgattuso/seacarb-git: Numerous updates since first release* (Version v3.2.16) [Computer software]. Zenodo. https://doi.org/10.5281/zenodo.4600014

Giannini, A., Cane, M. A., & Kushnir, Y. (2001). Interdecadal changes in the ENSO Teleconnection to the Caribbean Region and the North Atlantic Oscillation. *Journal of Climate*, *14*(13), 2867–2879. https://doi.org/10.1175/1520-0442(2001)014<2867:ICITET>2.0.CO;2

Giannini, A. (Lamont-doherty E. O., Kushnir, Y. (Lamont-doherty E. O., & Cane, M. A. (Lamont-doherty E. O. (2000). Interannual Variability of Caribbean Rainfall, ENSO, and the Atlantic Ocean. *Journal of Climate*, *13*, 297–311.

Giry, C., Felis, T., Scheffers, S., & Fensterer, C. (2010). Assessing the potential of Southern Caribbean corals for reconstructions of Holocene temperature variability. *IOP Conference Series: Earth and Environmental Science*, *9*(1). https://doi.org/10.1088/1755-1315/9/1/012021

Goldstein, A. H., & Galbally, I. E. (n.d.). *In the Earth's Atmosphere*.

Goldstein, A. H., & Galbally, I. E. (2007). Known and Unexplored Organic Constituents in the Earth's Atmosphere. *Environmental Science & Technology*, *41*(5), 1514–1521. https://doi.org/10.1021/es072476p

Golubic, S., Radtke, G., & Campion-Alsumard, T. L. (2005). Endolithic fungi in marine ecosystems. *Trends in Microbiology*, *13*(5), 229–235. https://doi.org/10.1016/j.tim.2005.03.007

Goodkin, N. F., Wang, B.-S., You, C.-F., Hughen, K. A., Grumet-Prouty, N., Bates, N. R., & Doney, S. C. (2015). Ocean circulation and biogeochemistry moderate interannual and decadal surface water pH changes in the Sargasso Sea: pH Variability in the Sargasso Sea. *Geophysical Research Letters*, *42*(12), 4931–4939. https://doi.org/10.1002/2015GL064431

Gordon, A. L. (1967). Circulation of the Caribbean Sea. *Journal of Geophysical Research*, *72*(24), 6207–6223. https://doi.org/10.1029/jz072i024p06207

Summary and Conclusion

Grinsted, A., Moore, J. C., & Jevrejeva, S. (2013). Projected Atlantic hurricane surge threat from rising temperatures. *Proceedings of the National Academy of Sciences*, *110*(14), 5369–5373. https://doi.org/10.1073/pnas.1209980110

Grottoli, A. G. (1999). Variability of stable isotopes and maximum linear extension in reef-coral skeletons at Kaneohe Bay, Hawaii. *Marine Biology*, *135*(3), 437–449. https://doi.org/10.1007/s002270050644

Grottoli, A. G. (2000). Stable Carbon Isotopes (δ^{13}C) in Coral Skeletons. *Oceanography*, *13*(2), 93–97.

Grottoli, A. G., & Eakin, C. M. (2007). A review of modern coral δ18O and Δ14C proxy records. *Earth-Science Reviews*, *81*(1–2), 67–91. https://doi.org/10.1016/j.earscirev.2006.10.001

Grove, C. A., Kasper, S., Zinke, J., Pfeiffer, M., Garbe-Schönberg, D., & Brummer, G.-J. A. (2013). Confounding effects of coral growth and high SST variability on skeletal Sr/Ca: Implications for coral paleothermometry: CORAL GROWTH EFFECT ON Sr/Ca VARIABILITY. *Geochemistry, Geophysics, Geosystems*, *14*(4), 1277–1293. https://doi.org/10.1002/ggge.20095

Gulev, S. K., Thorne, P. W., Ahn, J., Dentener, F. J., Domingues, C. M., Gerland, S., Gong, S., Kaufman, D. S., Nnamchi, H. C., Quaas, J., Rivera, J. A., Sathyendranath, S., Smith, S. L., Trewin, B., & von Schuckmann, K. (2021). *Changing State of the Climate System. In Climate Change 2021: The Physical Science Basis. Contribution of Working Group I to the Sixth Assessment Report of the Intergovernmental Panel on Climate Change.* 287–422. https://doi.org/doi:10.1017/9781009157896.004.

Gutjahr, M., Bordier, L., Douville, E., Farmer, J., Foster, G. L., Hathorne, E. C., Hönisch, B., Lemarchand, D., Louvat, P., McCulloch, M., Noireaux, J., Pallavicini, N., Rae, J. W. B., Rodushkin, I., Roux, P., Stewart, J. A., Thil, F., & You, C. (2021). Sub-Permil Interlaboratory Consistency for Solution-Based Boron Isotope Analyses on Marine Carbonates. *Geostandards and Geoanalytical Research*, *45*(1), 59–75. https://doi.org/10.1111/ggr.12364

Harbott, M., Wu, H. C., Kuhnert, H., Jimenez, C., González-Díaz, P., & Rixen, T. (2023). A Warming Southern Gulf of Mexico: Reconstruction of Anthropogenic Environmental Changes From a *Siderastrea siderea* Coral on the Northern Coast of Cuba. *Paleoceanography and Paleoclimatology*, *38*(12), e2023PA004717. https://doi.org/10.1029/2023PA004717

Hartmann, A. C., Carilli, J. E., Norris, R. D., Charles, C. D., & Deheyn, D. D. (2010). Stable isotopic records of bleaching and endolithic algae blooms in the skeleton of the boulder forming coral Montastraea faveolata. *Coral Reefs*, *29*(4), 1079–1089. https://doi.org/10.1007/s00338-010-0667-5

Hathorne, E. C., Felis, T., Suzuki, A., Kawahata, H., & Cabioch, G. (2013). Lithium in the aragonite skeletons of massive Porites corals: A new tool to reconstruct tropical sea surface temperatures. *Paleoceanography*, *28*(1), 143–152. https://doi.org/10.1029/2012PA002311

Hemming, N. G., & Hanson, G. N. (1992). Boron isotopic composition and concentration in modern marine carbonates. *Geochimica et Cosmochimica Acta*, *56*(1), 537–543. https://doi.org/10.1016/0016-7037(92)90151-8

Hershey, J. P., Fernandez, M., Milne, P. J., & Millero, F. J. (1986). The ionization of boric acid in NaCl, NaCaCl and NaMgCl solutions at 25°C. *Geochimica et Cosmochimica Acta*, *50*, 143–148.

Hillaire-Marcel, C., & de Vernal, A. (2007). Proxies in Late Cenozoic Paleoceanography. In *Developments in Marine Geology*. https://doi.org/10.1016/S1572-5480(07)01005-6

Summary and Conclusion

Hoegh-Guldberg, O. (1999). Climate change, coral bleaching and the future of the world's coral reefs. *Marine and Freshwater Research*, *50*(8), 839–866. https://doi.org/10.1071/mf99078

Hoegh-Guldberg, O., Poloczanska, E. S., Skirving, W., & Dove, S. (2017). Coral Reef Ecosystems under Climate Change and Ocean Acidification. *Frontiers in Marine Science*, *4*, 158. https://doi.org/10.3389/fmars.2017.00158

Hohn, S., & Merico, A. (2012). Modelling coral polyp calcification in relation to ocean acidification. *Biogeosciences*, *9*(11), 4441–4454. https://doi.org/10.5194/bg-9-4441-2012

Holcomb, M., DeCarlo, T. M., Gaetani, G. A., & McCulloch, M. (2016). Factors affecting B/Ca ratios in synthetic aragonite. *Chemical Geology*, *437*, 67–76. https://doi.org/10.1016/j.chemgeo.2016.05.007

Hönisch, B., Hemming, N. G., Grottoli, A. G., Amat, A., Hanson, G. N., & Bijma, J. (2004). Assessing scleractinian corals as recorders for paleo-pH: Empirical calibration and vital effects. *Geochimica et Cosmochimica Acta*, *68*(18), 3675–3685. https://doi.org/10.1016/j.gca.2004.03.002

Hönisch, B., Ridgwell, A., Schmidt, D. N., Thomas, E., Gibbs, S. J., Sluijs, A., Zeebe, R., Kump, L., Martindale, R. C., Greene, S. E., Kiessling, W., Ries, J., Zachos, J. C., Royer, D. L., Barker, S., Marchitto, T. M., Moyer, R., Pelejero, C., Ziveri, P., … Williams, B. (2012). The Geological Record of Ocean Acidification. *Science*, *335*(6072), 1058–1063. https://doi.org/10.1126/science.1208277

Howell, P., Pisias, N., Ballance, J., Baughman, J., & Ochs, L. (2006). ARAND time-series analysis software. *Brown University, Providence RI*, *685*.

Huang, B., Liu, C., Banzon, V. F., Freeman, E., Graham, G., Hankins, W., Smith, T. M., & Zhang, H.-M. (2021a). *NOAA 0.25-degree Daily Optimum Interpolation Sea Surface Temperature (OISST), Version 2.1* [Dataset]. NOAA National Centers for Environmental Information. https://doi.org/10.25921/RE9P-PT57

Huang, B., Liu, C., Banzon, V., Freeman, E., Graham, G., Hankins, B., Smith, T., & Zhang, H.-M. (2021b). Improvements of the Daily Optimum Interpolation Sea Surface Temperature (DOISST) Version 2.1. *Journal of Climate*, *34*(8), 2923–2939. https://doi.org/10.1175/JCLI-D-20-0166.1

Huang, B., Thorne, P. W., Banzon, V. F., Boyer, T., Chepurin, G., Lawrimore, J. H., Menne, M. J., Smith, T. M., Vose, R. S., & Zhang, H.-M. (2017). Extended Reconstructed Sea Surface Temperature, Version 5 (ERSSTv5): Upgrades, Validations, and Intercomparisons. *Journal of Climate*, *30*(20), 8179–8205. https://doi.org/10.1175/JCLI-D-16-0836.1

Hurrell, J. W. (1995). Decadal Trends in the North Atlantic Oscillation: Regional Temperatures and Precipitation. *Science*, *269*(5224), 676–679. https://doi.org/10.1126/science.269.5224.676

Intergouvernemental panel on climate change (Ed.). (2007). *Climate change 2007: The physical science basis*. Cambridge university press.

Jiang, L., Dunne, J., Carter, B. R., Tjiputra, J. F., Terhaar, J., Sharp, J. D., Olsen, A., Alin, S., Bakker, D. C. E., Feely, R. A., Gattuso, J., Hogan, P., Ilyina, T., Lange, N., Lauvset, S. K., Lewis, E. R., Lovato, T., Palmieri, J., Santana-Falcón, Y., … Ziehn, T. (2023). Global Surface Ocean Acidification Indicators From 1750 to 2100. *Journal of Advances in Modeling Earth Systems*, *15*(3), e2022MS003563. https://doi.org/10.1029/2022MS003563

Jiang, L.-Q., Feely, R. A., Wanninkhof, R., Greeley, D., Barbero, L., Alin, S., Carter, B. R., Pierrot, D., Featherstone, C., Hooper, J., Melrose, C., Monacci, N., Sharp, J. D., Shellito, S., Xu, Y.-Y., Kozyr, A., Byrne, R. H., Cai, W.-J., Cross, J., … Townsend, D. W.

133

(2021). Coastal Ocean Data Analysis Product in North America (CODAP-NA) – an internally consistent data product for discrete inorganic carbon, oxygen, and nutrients on the North American ocean margins. *Earth System Science Data*, *13*(6), 2777–2799. https://doi.org/10.5194/essd-13-2777-2021

Jiang, L.-Q., Kozyr, A., Relph, J. M., Ronje, E. I., Kamb, L., Burger, E., Myer, J., Nguyen, L., Arzayus, K. M., Boyer, T., Cross, S., Garcia, H., Hogan, P., Larsen, K., & Parsons, A. R. (2023). The Ocean Carbon and Acidification Data System. *Scientific Data*, *10*(1), 136. https://doi.org/10.1038/s41597-023-02042-0

Jiang, Z.-P., Tyrrell, T., Hydes, D. J., Dai, M., & Hartman, S. E. (2014). Variability of alkalinity and the alkalinity-salinity relationship in the tropical and subtropical surface ocean. *Global Biogeochemical Cycles*, *28*(7), 729–742. https://doi.org/10.1002/2013GB004678

Jurikova, H., Liebetrau, V., Raddatz, J., Fietzke, J., Trotter, J., Rocholl, A., Krause, S., McCulloch, M., Rüggeberg, A., & Eisenhauer, A. (2019). Boron isotope composition of the cold-water coral Lophelia pertusa along the Norwegian margin: Zooming into a potential pH-proxy by combining bulk and high-resolution approaches. *Chemical Geology*, *513*, 143–152. https://doi.org/10.1016/j.chemgeo.2019.01.005

Jury, M., Malmgren, B. A., & Winter, A. (2007). Subregional precipitation climate of the Caribbean and relationships with ENSO and NAO. *Journal of Geophysical Research*, *112*(D16), D16107. https://doi.org/10.1029/2006JD007541

Keeling, C. D. (1979). The Suess effect: 13Carbon-14Carbon interrelations. *Environment International*, *2*(4), 229–300. https://doi.org/10.1016/0160-4120(79)90005-9

Kennedy, J. J., Rayner, N. A., Atkinson, C. P., & Killick, R. E. (2019). An Ensemble Data Set of Sea Surface Temperature Change From 1850: The Met Office Hadley Centre HadSST.4.0.0.0 Data Set. *Journal of Geophysical Research: Atmospheres*, *124*(14), 7719–7763. https://doi.org/10.1029/2018JD029867

Kilbourne, K. H., Quinn, T. M., Taylor, F. W., Delcroix, T., & Gouriou, Y. (2004). El Niño-Southern Oscillation-related salinity variations recorded in the skeletal geochemistry of a *Porites* coral from Espiritu Santo, Vanuatu: CORAL RECORD OF SALINITY VARIATIONS. *Paleoceanography*, *19*(4), n/a-n/a. https://doi.org/10.1029/2004PA001033

Kline, D. I., Teneva, L., Hauri, C., Schneider, K., Miard, T., Chai, A., Marker, M., Dunbar, R., Caldeira, K., Lazar, B., Rivlin, T., Mitchell, B. G., Dove, S., & Hoegh-Guldberg, O. (2015). Six Month In Situ High-Resolution Carbonate Chemistry and Temperature Study on a Coral Reef Flat Reveals Asynchronous pH and Temperature Anomalies. *PLOS ONE*, *10*(6), e0127648. https://doi.org/10.1371/journal.pone.0127648

Klochko, K., Cody, G. D., Tossell, J. A., Dera, P., & Kaufman, A. J. (2009). Re-evaluating boron speciation in biogenic calcite and aragonite using 11B MAS NMR. *Geochimica et Cosmochimica Acta*, *73*(7), 1890–1900. https://doi.org/10.1016/j.gca.2009.01.002

Klochko, K., Kaufman, A. J., Yao, W., Byrne, R. H., & Tossell, J. A. (2006). Experimental measurement of boron isotope fractionation in seawater. *Earth and Planetary Science Letters*, *248*(1–2), 276–285. https://doi.org/10.1016/j.epsl.2006.05.034

Knight, J. R., Folland, C. K., & Scaife, A. A. (2006). Climate impacts of the Atlantic Multidecadal Oscillation. *Geophysical Research Letters*, *33*(17), L17706. https://doi.org/10.1029/2006GL026242

Knutson, T. R., McBride, J. L., Chan, J., Emanuel, K., Holland, G., Landsea, C., Held, I., Kossin, J. P., Srivastava, A. K., & Sugi, M. (2010). Tropical cyclones and climate change. *Nature Geoscience*, *3*(3), Article 3. https://doi.org/10.1038/ngeo779

Kowalski, P. M., & Wunder, B. (2018). Boron Isotope Fractionation Among Vapor–Liquids–Solids–Melts: Experiments and Atomistic Modeling. In H. Marschall & G. Foster

(Eds.), *Boron Isotopes: The Fifth Element* (pp. 33–69). Springer International Publishing. https://doi.org/10.1007/978-3-319-64666-4_3

Krause, S., Liebetrau, V., Nehrke, G., Damm, T., Büsse, S., Leipe, T., Vogts, A., Gorb, S. N., & Eisenhauer, A. (2019). Endolithic Algae Affect Modern Coral Carbonate Morphology and Chemistry. *Frontiers in Earth Science*, 7, 304. https://doi.org/10.3389/feart.2019.00304

Lan, X., Tans, P., Thoning, K., & NOAA Global Monitoring Laboratory. (2023). *Trends in globally-averaged CO2 determined from NOAA Global Monitoring Laboratory measurements.* [Dataset]. NOAA GML. https://doi.org/10.15138/9N0H-ZH07

Langdon, C., & Atkinson, M. J. (2005). Effect of elevated pCO2 on photosynthesis and calcification of corals and interactions with seasonal change in temperature/irradiance and nutrient enrichment. *Journal of Geophysical Research: Oceans*, 110(C9). https://doi.org/10.1029/2004JC002576

Lauvset, S. K., Lange, N., Tanhua, T., Bittig, H. C., Olsen, A., Kozyr, A., Alin, S., Álvarez, M., Azetsu-Scott, K., Barbero, L., Becker, S., Brown, P. J., Carter, B. R., Da Cunha, L. C., Feely, R. A., Hoppema, M., Humphreys, M. P., Ishii, M., Jeansson, E., … Key, R. M. (2022). GLODAPv2.2022: The latest version of the global interior ocean biogeochemical data product. *Earth System Science Data*, 14(12), 5543–5572. https://doi.org/10.5194/essd-14-5543-2022

Lazareth, C. E., Soares-Pereira, C., Douville, E., Brahmi, C., Dissard, D., Le Cornec, F., Thil, F., Gonzalez-Roubaud, C., Caquineau, S., & Cabioch, G. (2016). Intra-skeletal calcite in a live-collected Porites sp.: Impact on environmental proxies and potential formation process. *Geochimica et Cosmochimica Acta*, 176, 279–294. https://doi.org/10.1016/j.gca.2015.12.020

Le Bec, N., Julliet-Leclerc, A., Corrège, T., Blamart, D., & Delcroix, T. (2000). A coral δ18O record of ENSO driven sea surface salinity variability in Fiji (south -western tropical Pacific). *Geophysical Research Letters*, 27(23), 3897–3900. https://doi.org/10.1029/2000GL011843

Le Campion-Alsumard, T., Golubic, S., & Hutchings, P. (1995). Microbial endoliths in skeletons of live and dead corals: Porites lobata (Moorea, French Polynesia). *Marine Ecology Progress Series*, 117, 149–157. https://doi.org/10.3354/meps117149

Le Campion-Alsumard, T., Golubic, S., & Priess, K. (1995). Fungi in corals: Symbiosis or disease? Interaction between polyps and fungi causes pearl-like skeleton biomineralization. *Marine Ecology Progress Series*, 137–147.

Leder, J. J., Szmant, A. M., & Swart, P. K. (1991). The effect of prolonged ?bleaching? On skeletal banding and stable isotopic composition in Montastrea annularis: Preliminary observations. *Coral Reefs*, 10(1), 19–27. https://doi.org/10.1007/BF00301902

Lee, K., Kim, T.-W., Byrne, R. H., Millero, F. J., Feely, R. A., & Liu, Y.-M. (2010). The universal ratio of boron to chlorinity for the North Pacific and North Atlantic oceans. *Geochimica et Cosmochimica Acta*, 74(6), 1801–1811. https://doi.org/10.1016/j.gca.2009.12.027

Lee, K., Tong, L. T., Millero, F. J., Sabine, C. L., Dickson, A. G., Goyet, C., Park, G.-H., Wanninkhof, R., Feely, R. A., & Key, R. M. (2006). Global relationships of total alkalinity with salinity and temperature in surface waters of the world's oceans. *Geophysical Research Letters*, 33(19), L19605. https://doi.org/10.1029/2006GL027207

Lewis, E., & Wallace, D. (1998). CO2SYS-Program developed for the CO2 system calculations, Carbon Dioxide Inf. Anal. Center. *Oak Ridge National Laboratory, US Department of Energy, Oak Ridge, TN, USA.*

Summary and Conclusion

Linsley, B. K., Messier, R. G., & Dunbar, R. B. (1999). Assessing between-colony oxygen isotope variability in the coral Porites lobata at Clipperton Atoll. *Coral Reefs*, *18*(1), 13–27. https://doi.org/10.1007/s003380050148

Liu, B., Six, K. D., & Ilyina, T. (2021). Incorporating the stable carbon isotope <sup>13</sup>C in the ocean biogeochemical component of the Max Planck Institute Earth System Model. *Biogeosciences*, *18*(14), 4389–4429. https://doi.org/10.5194/bg-18-4389-2021

Liu, H., Wang, C., Lee, S.-K., & Enfield, D. (2012). Atlantic Warm-Pool Variability in the IPCC AR4 CGCM Simulations. *Journal of Climate*, *25*(16), 5612–5628. https://doi.org/10.1175/JCLI-D-11-00376.1

Liu, Y., Lee, S.-K., Muhling, B. A., Lamkin, J. T., & Enfield, D. B. (2012). Significant reduction of the Loop Current in the 21st century and its impact on the Gulf of Mexico: FUTURE WARMING OF THE GOM. *Journal of Geophysical Research: Oceans*, *117*(C5), n/a-n/a. https://doi.org/10.1029/2011JC007555

Livingston, H. D., & Thompson, G. (1971). TRACE ELEMENT CONCENTRATIONS IN SOME MODERN CORALS1: TRACE ELEMENTS IN CORALS. *Limnology and Oceanography*, *16*(5), 786–796. https://doi.org/10.4319/lo.1971.16.5.0786

Lueker, T. J., Dickson, A. G., & Keeling, C. D. (2000). Ocean pCO2 calculated from dissolved inorganic carbon, alkalinity, and equations for K1 and K2: Validation based on laboratory measurements of CO2 in gas and seawater at equilibrium. *Marine Chemistry*, *70*(1–3), 105–119. https://doi.org/10.1016/S0304-4203(00)00022-0

Manzello, D. P. (2010). Ocean acidification hotspots: Spatiotemporal dynamics of the seawater CO2 system of eastern Pacific coral reefs. *Limnology and Oceanography*, *55*(1), 239–248. https://doi.org/10.4319/lo.2010.55.1.0239

Marchitto, T. M., Bryan, S. P., Doss, W., McCulloch, M. T., & Montagna, P. (2018). A simple biomineralization model to explain Li, Mg, and Sr incorporation into aragonitic foraminifera and corals. *Earth and Planetary Science Letters*, *481*, 20–29. https://doi.org/10.1016/j.epsl.2017.10.022

Marschall, H., & Foster, G. (Eds.). (2018). *Boron Isotopes*. Springer International Publishing. https://doi.org/10.1007/978-3-319-64666-4

Martinez, A., Crook, E. D., Barshis, D. J., Potts, D. C., Rebolledo-Vieyra, M., Hernandez, L., & Paytan, A. (2019). Species-specific calcification response of Caribbean corals after 2-year transplantation to a low aragonite saturation submarine spring. *Proceedings of the Royal Society B: Biological Sciences*, *286*(1905), 20190572. https://doi.org/10.1098/rspb.2019.0572

Marubini, F., Ferrier-Pagès, C., Furla, P., & Allemand, D. (2008). Coral calcification responds to seawater acidification: A working hypothesis towards a physiological mechanism. *Coral Reefs*, *27*(3), 491–499. https://doi.org/10.1007/s00338-008-0375-6

Maupin, C. R., Quinn, T. M., & Halley, R. B. (2008). Extracting a climate signal from the skeletal geochemistry of the Caribbean coral *Siderastrea siderea*: CLIMATE SIGNAL FROM CORAL *S. SIDEREA*. *Geochemistry, Geophysics, Geosystems*, *9*(12), n/a-n/a. https://doi.org/10.1029/2008GC002106

Mavromatis, V., Montouillout, V., Noireaux, J., Gaillardet, J., & Schott, J. (2015). Characterization of boron incorporation and speciation in calcite and aragonite from co-precipitation experiments under controlled pH, temperature and precipitation rate. *Geochimica et Cosmochimica Acta*, *150*, 299–313. https://doi.org/10.1016/j.gca.2014.10.024

McCulloch, M., Falter, J., Trotter, J., & Montagna, P. (2012a). Coral resilience to ocean acidification and global warming through pH up-regulation. *Nature Climate Change*, *2*(8), 623–627. https://doi.org/10.1038/nclimate1473

Summary and Conclusion

McCulloch, M., Falter, J., Trotter, J., & Montagna, P. (2012b). Coral resilience to ocean acidification and global warming through pH up-regulation. *Nature Climate Change*, *2*(8), 623–627. https://doi.org/10.1038/nclimate1473

McCulloch, M. T., D'Olivo, J. P., Falter, J., Holcomb, M., & Trotter, J. A. (2017a). Coral calcification in a changing World and the interactive dynamics of pH and DIC upregulation. *Nature Communications*, *8*(1), 15686. https://doi.org/10.1038/ncomms15686

McCulloch, M. T., D'Olivo, J. P., Falter, J., Holcomb, M., & Trotter, J. A. (2017b). Coral calcification in a changing World and the interactive dynamics of pH and DIC upregulation. *Nature Communications*, *8*(1), 15686. https://doi.org/10.1038/ncomms15686

McCulloch, M. T., Gagan, M. K., Mortimer, G. E., Chivas, A. R., & Isdale, P. J. (1994). A high-resolution Sr/Ca and δ18O coral record from the Great Barrier Reef, Australia, and the 1982–1983 El Niño. *Geochimica et Cosmochimica Acta*, *58*(12), 2747–2754. https://doi.org/10.1016/0016-7037(94)90142-2

McCulloch, M., Trotter, J., Montagna, P., Falter, J., Dunbar, R., Freiwald, A., Försterra, G., López Correa, M., Maier, C., Rüggeberg, A., & Taviani, M. (2012). Resilience of cold-water scleractinian corals to ocean acidification: Boron isotopic systematics of pH and saturation state up-regulation. *Geochimica et Cosmochimica Acta*, *87*, 21–34. https://doi.org/10.1016/j.gca.2012.03.027

Meléndez, M., Salisbury, J., Gledhill, D., Langdon, C., Morell, J. M., Manzello, D., Rodriguez-Abudo, S., Musielewicz, S., & Sutton, A. (2020). Seasonal Variations of Carbonate Chemistry at Two Western Atlantic Coral Reefs. *Journal of Geophysical Research: Oceans*, *125*(8), e2020JC016108. https://doi.org/10.1029/2020JC016108

Millero, F. J., Lee, K., & Roche, M. (1998). Distribution of alkalinity in the surface waters of the major oceans. *Marine Chemistry*, *60*(1), 111–130. https://doi.org/10.1016/S0304-4203(97)00084-4

Mitsuguchi, T., Matsumoto, E., Abe, O., Uchida, T., & Isdale, P. J. (1996). Mg/Ca thermometry in coral skeletons. *Science*, *274*(5289), 961–963. https://doi.org/10.1126/science.274.5289.961

Mollica, N. R., Cohen, A. L., Horton, F., Oppo, D. W., Solow, A. S., & McGee, D. (2023). Capturing Equatorial Pacific Variability With Multivariate Sr-U Coral Thermometry. *Paleoceanography and Paleoclimatology*, *38*(10), e2022PA004508. https://doi.org/10.1029/2022PA004508

Montagna, P., McCulloch, M., Douville, E., López Correa, M., Trotter, J., Rodolfo-Metalpa, R., Dissard, D., Ferrier-Pagès, C., Frank, N., Freiwald, A., Goldstein, S., Mazzoli, C., Reynaud, S., Rüggeberg, A., Russo, S., & Taviani, M. (2014a). Li/Mg systematics in scleractinian corals: Calibration of the thermometer. *Geochimica et Cosmochimica Acta*, *132*, 288–310. https://doi.org/10.1016/j.gca.2014.02.005

Montagna, P., McCulloch, M., Douville, E., López Correa, M., Trotter, J., Rodolfo-Metalpa, R., Dissard, D., Ferrier-Pagès, C., Frank, N., Freiwald, A., Goldstein, S., Mazzoli, C., Reynaud, S., Rüggeberg, A., Russo, S., & Taviani, M. (2014b). Li/Mg systematics in scleractinian corals: Calibration of the thermometer. *Geochimica et Cosmochimica Acta*, *132*, 288–310. https://doi.org/10.1016/j.gca.2014.02.005

Nir, O., Vengosh, A., Harkness, J. S., Dwyer, G. S., & Lahav, O. (2015). Direct measurement of the boron isotope fractionation factor: Reducing the uncertainty in reconstructing ocean paleo-pH. *Earth and Planetary Science Letters*, *414*, 1–5. https://doi.org/10.1016/j.epsl.2015.01.006

Noireaux, J., Mavromatis, V., Gaillardet, J., Schott, J., Montouillout, V., Louvat, P., Rollion-Bard, C., & Neuville, D. R. (2015). Crystallographic control on the boron isotope paleo-

137

pH proxy. *Earth and Planetary Science Letters*, *430*, 398–407. https://doi.org/10.1016/j.epsl.2015.07.063

Nothdurft, L. D., Webb, G. E., Bostrom, T., & Rintoul, L. (2007). Calcite-filled borings in the most recently deposited skeleton in live-collected Porites (Scleractinia): Implications for trace element archives. *Geochimica et Cosmochimica Acta*, *71*(22), 5423–5438. https://doi.org/10.1016/j.gca.2007.09.025

Nurhati, I. S., Cobb, K. M., & Di Lorenzo, E. (2011). Decadal-Scale SST and Salinity Variations in the Central Tropical Pacific: Signatures of Natural and Anthropogenic Climate Change. *Journal of Climate*, *24*(13), 3294–3308. https://doi.org/10.1175/2011JCLI3852.1

Olsen, A., Lange, N., Key, R. M., Tanhua, T., Álvarez, M., Becker, S., Bittig, H. C., Carter, B. R., Cotrim Da Cunha, L., Feely, R. A., Van Heuven, S., Hoppema, M., Ishii, M., Jeansson, E., Jones, S. D., Jutterström, S., Karlsen, M. K., Kozyr, A., Lauvset, S. K., … Wanninkhof, R. (2019). GLODAPv2.2019 – an update of GLODAPv2. *Earth System Science Data*, *11*(3), 1437–1461. https://doi.org/10.5194/essd-11-1437-2019

Orr, J. C., Epitalon, J.-M., & Gattuso, J.-P. (2015). Comparison of ten packages that compute ocean carbonate chemistry. *Biogeosciences*, *12*(5), 1483–1510. https://doi.org/10.5194/bg-12-1483-2015

Orr, J. C., Fabry, V. J., Aumont, O., Bopp, L., Doney, S. C., Feely, R. A., Gnanadesikan, A., Gruber, N., Ishida, A., Joos, F., Key, R. M., Lindsay, K., Maier-Reimer, E., Matear, R., Monfray, P., Mouchet, A., Najjar, R. G., Plattner, G.-K., Rodgers, K. B., … Yool, A. (2005). Anthropogenic ocean acidification over the twenty-first century and its impact on calcifying organisms. *Nature*, *437*(7059), Article 7059. https://doi.org/10.1038/nature04095

Osborne, E., Hu, X., Hall, E. R., Yates, K., Vreeland-Dawson, J., Shamberger, K., Barbero, L., Martin Hernandez-Ayon, J., Gomez, F. A., Hicks, T., Xu, Y.-Y., McCutcheon, M. R., Acquafredda, M., Chapa-Balcorta, C., Norzagaray, O., Pierrot, D., Munoz-Caravaca, A., Dobson, K. L., Williams, N., … Dash, P. (2022). Ocean acidification in the Gulf of Mexico: Drivers, impacts, and unknowns. *Progress in Oceanography*, *209*, 102882. https://doi.org/10.1016/j.pocean.2022.102882

Pandolfi, John M., Connolly, Sean R., (second), Marshall, Dustin J., (third), & Cohen, Anne L., (fourth). (2011). Projecting Coral Reef Futures Under Global Warming and Ocean Acidification. *Science Review*, *333*, 418–422. https://doi.org/DOI: 10.1126/science.1204794

Pelejero, C., Calvo, E., McCulloch, M. T., Marshall, J. F., Gagan, M. K., Lough, J. M., & Opdyke, B. N. (2005). Preindustrial to Modern Interdecadal Variability in Coral Reef pH. *Science*, *309*(5744), 2204–2207. https://doi.org/10.1126/science.1113692

Perry, C. T. (1998). Grain susceptibility to the effects of microboring: Implications for the preservation of skeletal carbonates. *Sedimentology*, *45*(1), 39–51. https://doi.org/10.1046/j.1365-3091.1998.00134.x

Popp, B. N., Takigiku, R., Hayes, J. M., Louda, J. W., & Baker, E. W. (1989). The post-Paleozoic chronology and mechanism of 13 C depletion in primary marine organic matter. *American Journal of Science*, *289*(4), 436–454. https://doi.org/10.2475/ajs.289.4.436

Priess, K., Le Campion-Alsumard, T., Golubic, S., Gadel, F., & Thomassin, B. A. (2000). Fungi in corals: Black bands and density-banding of Porites lutea and P. lobata skeleton. *Marine Biology*, *136*(1), 19–27. https://doi.org/10.1007/s002270050003

Quinn, T. M., Crowley, T. J., Taylor, F. W., Henin, C., Joannot, P., & Join, Y. (1998). A multicentury stable isotope record from a New Caledonia coral: Interannual and decadal

sea surface temperature variability in the southwest Pacific since 1657 A.D. *Paleoceanography*, *13*(4), 412–426. https://doi.org/10.1029/98PA00401

Reid, R. P., & Macintyre, I. G. (2000). Microboring Versus Recrystallization: Further Insight into the Micritization Process. *Journal of Sedimentary Research*, *70*(1), 24–28. https://doi.org/10.1306/2DC408FA-0E47-11D7-8643000102C1865D

Ren, L., Linsley, B. K., Wellington, G. M., Schrag, D. P., & Hoegh-guldberg, O. (2003). Deconvolving the δ18O seawater component from subseasonal coral δ18O and Sr/Ca at Rarotonga in the southwestern subtropical Pacific for the period 1726 to 1997. *Geochimica et Cosmochimica Acta*, *67*(9), 1609–1621. https://doi.org/10.1016/S0016-7037(02)00917-1

Reynaud, S., Hemming, N. G., Juillet-Leclerc, A., & Gattuso, J.-P. (2004). Effect of pCO2 and temperature on the boron isotopic composition of the zooxanthellate coral Acropora sp. *Coral Reefs*. https://doi.org/10.1007/s00338-004-0399-5

Reynolds, R. W., Smith, T. M., Liu, C., Chelton, D. B., Casey, K. S., & Schlax, M. G. (2007). Daily High-Resolution-Blended Analyses for Sea Surface Temperature. *Journal of Climate*, *20*(22), 5473–5496. https://doi.org/10.1175/2007JCLI1824.1

Ricci, F., Rossetto Marcelino, V., Blackall, L. L., Kühl, M., Medina, M., & Verbruggen, H. (2019). Beneath the surface: Community assembly and functions of the coral skeleton microbiome. *Microbiome*, *7*(1), 159. https://doi.org/10.1186/s40168-019-0762-y

Rippe, J. P., Baumann, J. H., De Leener, D. N., Aichelman, H. E., Friedlander, E. B., Davies, S. W., & Castillo, K. D. (2018). Corals sustain growth but not skeletal density across the Florida Keys Reef Tract despite ongoing warming. *Global Change Biology*, *24*(11), 5205–5217. https://doi.org/10.1111/gcb.14422

Rixen, T. (2023). Past changes in and present status of the coastal carbon cycle. *Cambridge Prisms: Coastal Futures*, *1*, e34. https://doi.org/10.1017/cft.2023.20

Robinson, L. F., Adkins, J. F., Frank, N., Gagnon, A. C., Prouty, N. G., Brendan Roark, E., & De Flierdt, T. V. (2014). The geochemistry of deep-sea coral skeletons: A review of vital effects and applications for palaeoceanography. *Deep Sea Research Part II: Topical Studies in Oceanography*, *99*, 184–198. https://doi.org/10.1016/j.dsr2.2013.06.005

Rollion-Bard, C., & Blamart, D. (2015). Possible controls on Li, Na, and Mg incorporation into aragonite coral skeletons. *Chemical Geology*, *396*, 98–111. https://doi.org/10.1016/j.chemgeo.2014.12.011

Ross, C. L., DeCarlo, T. M., & McCulloch, M. T. (2019). Calibration of Sr/Ca, Li/Mg and Sr-U Paleothermometry in Branching and Foliose Corals. *Paleoceanography and Paleoclimatology*, *34*(8), 1271–1291. https://doi.org/10.1029/2018PA003426

Ross, C. L., Falter, J. L., & McCulloch, M. T. (2017). Active modulation of the calcifying fluid carbonate chemistry (δ11B, B/Ca) and seasonally invariant coral calcification at sub-tropical limits. *Scientific Reports*, *7*(1), 13830. https://doi.org/10.1038/s41598-017-14066-9

Rubino, M., Etheridge, D. M., Trudinger, C. M., Allison, C. E., Battle, M. O., Langenfelds, R. L., Steele, L. P., Curran, M., Bender, M., White, J. W. C., Jenk, T. M., Blunier, T., & Francey, R. J. (2013). A revised 1000 year atmospheric δ13C-CO2 record from Law Dome and South Pole, Antarctica. *Journal of Geophysical Research: Atmospheres*, *118*(15), 8482–8499. https://doi.org/10.1002/jgrd.50668

Santos, I. R., Glud, R. N., Maher, D., Erler, D., & Eyre, B. D. (2011). Diel coral reef acidification driven by porewater advection in permeable carbonate sands, Heron Island, Great Barrier Reef. *Geophysical Research Letters*, *38*(3). https://doi.org/10.1029/2010GL046053

Summary and Conclusion

Sanyal, A., Bijma, J., Spero, H., & Lea, D. W. (2001). Empirical relationship between pH and the boron isotopic composition of *Globigerinoides sacculifer*: Implications for the boron isotope paleo-pH proxy. *Paleoceanography*, *16*(5), 515–519. https://doi.org/10.1029/2000PA000547

Schulz, K. G. (2009). *CO2 perturbation experiments: Similarities and differences between dissolved inorganic carbon and total alkalinity manipulations*.

Seneviratne, S. I., Zhang, X., Adnan, M., Badi, W., Dereczynski, C., Di Luca, A., Ghosh, S., Iskandar, I., Kossin, J., Lewis, S., Otto, F., Pinto, I., Satoh, M., Vincente-Serrano, S. M., Wehner, M., & Zhou, B. (2021). Weather and Climate Extreme Events in a Changing Climate. In Climate Change 2021: The Physical Science Basis. Contribution of Working Group I to the Sixth Assessment Report of the Intergovernmental Panel on Climate Change. In *Climate Change 2021 – The Physical Science Basis: Working Group I Contribution to the Sixth Assessment Report of the Intergovernmental Panel on Climate Change* (pp. 1513–1766). Cambridge University Press. https://doi.org/10.1017/9781009157896.013

Shashar, N., & Stambler, N. (1992). Endolithic algae within corals—Life in an extreme environment. *Journal of Experimental Marine Biology and Ecology*, *163*(2), 277–286. https://doi.org/10.1016/0022-0981(92)90055-F

Shaw, E. C., McNeil, B. I., & Tilbrook, B. (2012). Impacts of ocean acidification in naturally variable coral reef flat ecosystems. *Journal of Geophysical Research: Oceans*, *117*(C3), 2011JC007655. https://doi.org/10.1029/2011JC007655

Smith, S. V., Buddemeier, R. W., Redalje, R. C., & Houck, J. E. (1979a). Strontium-Calcium Thermometry in Coral Skeletons. *Science*, *204*(4391), 404–407. https://doi.org/10.1126/science.204.4391.404

Smith, S. V., Buddemeier, R. W., Redalje, R. C., & Houck, J. E. (1979b). Strontium-calcium thermometry in coral skeletons. *Science*, *204*(4391), 404–407. https://doi.org/10.1126/science.204.4391.404

Spalding, M. D., & Brown, B. E. (2015). Warm-water coral reefs and climate change. *Science*, *350*(6262), 769–771. https://doi.org/10.1126/science.aad0349

Standish, C. D., Chalk, T. B., Babila, T. L., Milton, J. A., Palmer, M. R., & Foster, G. L. (2019). The effect of matrix interferences on *in situ* boron isotope analysis by laser ablation multi-collector inductively coupled plasma mass spectrometry. *Rapid Communications in Mass Spectrometry*, *33*(10), 959–968. https://doi.org/10.1002/rcm.8432

Steinhoefel, G., Beck, K. K., Benthien, A., Richter, K., Schmidt-Grieb, G. M., & Bijma, J. (2023). Matrix-independent boron isotope analysis of silicate and carbonate reference materials by ultraviolet femtosecond laser ablation multi-collector inductively coupled plasma mass spectrometry with application to the cold-water coral DESMOPHYLLUM DIANTHUS . *Rapid Communications in Mass Spectrometry*, *37*(13), e9508. https://doi.org/10.1002/rcm.9508

Stewart, J. A., Anagnostou, E., & Foster, G. L. (2016). An improved boron isotope pH proxy calibration for the deep-sea coral Desmophyllum dianthus through sub-sampling of fibrous aragonite. *Chemical Geology*, *447*, 148–160. https://doi.org/10.1016/j.chemgeo.2016.10.029

Sutton, A. J., Sabine, C. L., Morell, J. M., Musielewicz, S., Maenner Jones, S., Dietrich, C., Bott, R., & Osborne, J. (2014). *High-resolution ocean and atmosphere pCO2 time-series measurements from mooring La_Parguera_67W_18N in the Caribbean Sea (NCEI Accession 0117354)* [Dataset]. NOAA National Centers for Environmental Information. https://doi.org/10.3334/CDIAC/OTG.TSM_LA_PARGUERA_67W_18N

Summary and Conclusion

Swart, P. K., Elderfield, H., & Greaves, M. J. (2002). A high-resolution calibration of Sr/Ca thermometry using the Caribbean coral *Montastraea annularis*: CALIBRATION OF SR/CA THERMOMETRY. *Geochemistry, Geophysics, Geosystems*, *3*(11), 1–11. https://doi.org/10.1029/2002GC000306

Swart, P. K., Greer, L., Rosenheim, B. E., Moses, C. S., Waite, A. J., Winter, A., Dodge, R. E., & Helmle, K. (2010). The [13]C Suess effect in scleractinian corals mirror changes in the anthropogenic CO_2 inventory of the surface oceans: THE ^{13}C SUESS EFFECT IN SCLERACTINIAN CORALS. *Geophysical Research Letters*, *37*(5), n/a-n/a. https://doi.org/10.1029/2009GL041397

Szmant, A. M., & Gassman, N. J. (1990). The effects of prolonged ?bleaching? On the tissue biomass and reproduction of the reef coral Montastrea annularis. *Coral Reefs*, *8*(4), 217–224. https://doi.org/10.1007/BF00265014

Takahashi, T., Sutherland, S. C., Chipman, D. W., Goddard, J. G., Ho, C., Newberger, T., Sweeney, C., & Munro, D. R. (2014). Climatological distributions of pH, pCO2, total CO2, alkalinity, and CaCO3 saturation in the global surface ocean, and temporal changes at selected locations. *Marine Chemistry*, *164*, 95–125. https://doi.org/10.1016/j.marchem.2014.06.004

Tarique, M., & Rahaman, W. (2022). Recent ocean acidification trends from boron isotope (δ11B) records of coral: Role of oceanographic processes and anthropogenic CO2 forcing. *Journal of Earth System Science*, *131*(3), 165. https://doi.org/10.1007/s12040-022-01907-z

Thompson, D. M. (2022). Environmental records from coral skeletons: A decade of novel insights and innovation. *WIREs Climate Change*, *13*(1), e745. https://doi.org/10.1002/wcc.745

Tribollet, A. (2008). The boring microflora in modern coral reef ecosystems: A review of its roles. In M. Wisshak & L. Tapanila (Eds.), *Current Developments in Bioerosion* (pp. 67–94). Springer Berlin Heidelberg. https://doi.org/10.1007/978-3-540-77598-0_4

Tribollet, A., & Golubic, S. (2011). Reef Bioerosion: Agents and Processes. In Z. Dubinsky & N. Stambler (Eds.), *Coral Reefs: An Ecosystem in Transition* (pp. 435–449). Springer Netherlands. https://doi.org/10.1007/978-94-007-0114-4_25

Trotter, J., Montagna, P., McCulloch, M., Silenzi, S., Reynaud, S., Mortimer, G., Martin, S., Ferrier-Pagès, C., Gattuso, J.-P., & Rodolfo-Metalpa, R. (2011). Quantifying the pH 'vital effect' in the temperate zooxanthellate coral Cladocora caespitosa: Validation of the boron seawater pH proxy. *Earth and Planetary Science Letters*, *303*(3–4), 163–173. https://doi.org/10.1016/j.epsl.2011.01.030

Turner, R. E., & Rabalais, N. N. (2019). The Gulf of Mexico. In *World Seas: An Environmental Evaluation* (pp. 445–464). Elsevier. https://doi.org/10.1016/B978-0-12-805068-2.00022-X

van Hooidonk, R., Maynard, J., Tamelander, J., Gove, J., Ahmadia, G., Raymundo, L., Williams, G., Heron, S. F., & Planes, S. (2016). Local-scale projections of coral reef futures and implications of the Paris Agreement. *Scientific Reports*, *6*(1), Article 1. https://doi.org/10.1038/srep39666

Villiers, S. De, Nelson, B. K., & Chivas, A. R. (1994). Biological Controls on Coral Sr / Ca and 5180 Reconstructions of Sea Surface Temperatures which. *Science*, *269*(September), 1247–1250.

Watanabe, T. K., Watanabe, T., Ohmori, K., & Yamazaki, A. (2020). Improving analytical method of SR/CA ratios in coral skeletons for paleo- SST reconstructions using ICP-OES. *Limnology and Oceanography: Methods*, *18*(6), 297–310. https://doi.org/10.1002/lom3.10357

Weber, J. N., & Woodhead, P. M. J. (1972). Temperature dependence of oxygen-18 concentration in reef coral carbonates. *Journal of Geophysical Research (1896-1977)*, *77*(3), 463–473. https://doi.org/10.1029/JC077i003p00463

Wu, H. C., Dissard, D., Douville, E., Blamart, D., Bordier, L., Tribollet, A., Le Cornec, F., Pons-Branchu, E., Dapoigny, A., & Lazareth, C. E. (2018). Surface ocean pH variations since 1689 CE and recent ocean acidification in the tropical South Pacific. *Nature Communications*, *9*(1), 2543. https://doi.org/10.1038/s41467-018-04922-1

Wu, H. C., Dissard, D., Le Cornec, F., Thil, F., Tribollet, A., Moya, A., & Douville, E. (2017). Primary Life Stage Boron Isotope and Trace Elements Incorporation in Aposymbiotic Acropora millepora Coral under Ocean Acidification and Warming. *Frontiers in Marine Science*, *4*, 129. https://doi.org/10.3389/fmars.2017.00129

Wu, H. C., Felis, T., Scholz, D., Giry, C., Kölling, M., Jochum, K. P., & Scheffers, S. R. (2017). Changes to Yucatán Peninsula precipitation associated with salinity and temperature extremes of the Caribbean Sea during the Maya civilization collapse. *Scientific Reports*, *7*(1), 15825. https://doi.org/10.1038/s41598-017-15942-0

Wu, H. C., & Grottoli, A. G. (2010). Stable oxygen isotope records of corals and a sclerosponge in the Western Pacific warm pool. *Coral Reefs*, *29*(2), 413–418. https://doi.org/10.1007/s00338-009-0576-7

Wu, H. C., Moreau, M., Linsley, B. K., Schrag, D. P., & Corrège, T. (2014). Investigation of sea surface temperature changes from replicated coral Sr/Ca variations in the eastern equatorial Pacific (Clipperton Atoll) since 1874. *Palaeogeography, Palaeoclimatology, Palaeoecology*, *412*, 208–222. https://doi.org/10.1016/j.palaeo.2014.07.039

Wu, Y., Fallon, S. J., Cantin, N. E., & Lough, J. M. (2021). Assessing multiproxy approaches (Sr/Ca, U/Ca, Li/Mg, and B/Mg) to reconstruct sea surface temperature from coral skeletons throughout the Great Barrier Reef. *Science of The Total Environment*, *786*, 147393. https://doi.org/10.1016/j.scitotenv.2021.147393

Xu, Y.-Y., Pearson, S., & Halimeda Kilbourne, K. (2015). Assessing coral Sr/Ca–SST calibration techniques using the species Diploria strigosa. *Palaeogeography, Palaeoclimatology, Palaeoecology*, *440*, 353–362. https://doi.org/10.1016/j.palaeo.2015.09.016

Zeebe, R. E. (2012). History of Seawater Carbonate Chemistry, Atmospheric CO_2, and Ocean Acidification. *Annual Review of Earth and Planetary Sciences*, *40*(1), 141–165. https://doi.org/10.1146/annurev-earth-042711-105521

Zeebe, R. E., & Wolf-Gladrow, D. (2001). *CO2 in Seawater: Equilibrium, Kinetics, Isotopes*. Gulf Professional Publishing.

Zoccola, D., Ganot, P., Bertucci, A., Caminiti-Segonds, N., Techer, N., Voolstra, C. R., Aranda, M., Tambutté, E., Allemand, D., Casey, J. R., & Tambutté, S. (2015). Bicarbonate transporters in corals point towards a key step in the evolution of cnidarian calcification. *Scientific Reports*, *5*(1), 9983. https://doi.org/10.1038/srep09983

Zweng, M. M., Reagan, J. R., Seidov, D., Boyer, T., Locarnini, R. A., García, H. E., Mishonov, A. V., Baranova, O. K., Weathers, K. A., Paver, C. R., & Smolyar, I. V. (2019). *World Ocean Atlas 2018, Volume 2: Salinity.* (A. Mishonov Technical Ed.; NOAA Atlas NESDIS 82, 50 pp.) [Dataset].